Eastern Snow Conference

Proceedings of the

1990

Annual Meeting

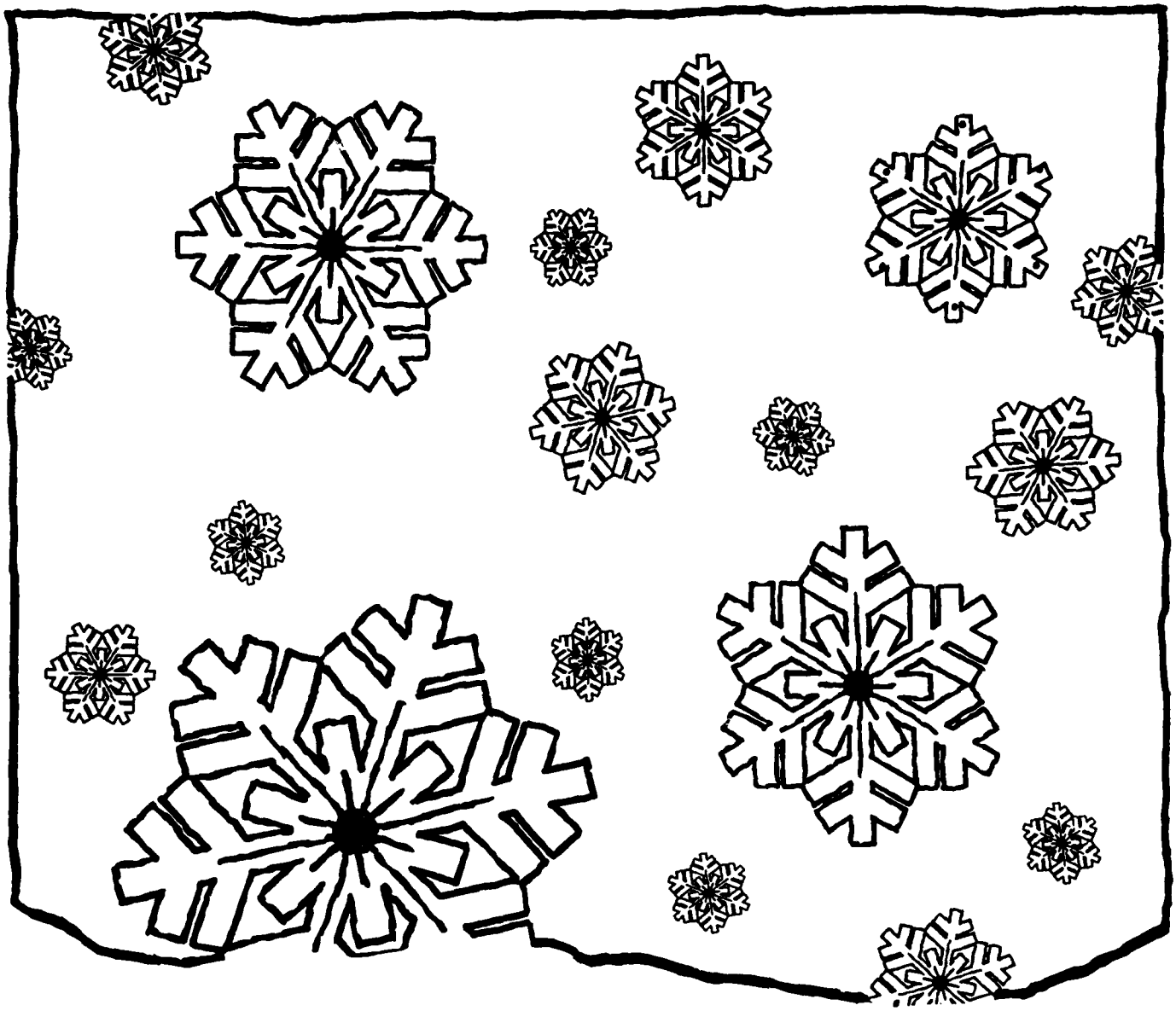

Proceedings of the FORTY-SEVENTH ANNUAL

EASTERN SNOW CONFERENCE

JUNE 7-8, 1990
BANGOR, MAINE

CRREL Special Report 90-44

ISBN 0-920081-12-6

ISSN 0424-1932

Proceedings of the Eastern Snow Conference

Printed and Bound in United States of America

FOREWORD

The 47th annual Eastern Snow Conference (ESC) was held in Bangor, Maine on June 7th and 8th, 1990. The program included oral and poster presentations, and displays of scientific equipment. Almost all of the papers and the advertisements from the equipment companies are published in these proceedings.

For the first time, all of the oral papers at the conference were reviewed, and the revised papers appear in these proceedings. The officers of the ESC hope that the newly instituted review process and Honor Paper Award will assist the authors in improving their papers, upgrade the quality of the proceedings and make the ESC an even more valuable forum for discussion of both practical and scientific issues related to snow and ice.

In order to permit the timely reporting of recent results, we collected draft manuscripts at the meeting. The chairman of each session coordinated the review of papers in his/her session. If the chairman was also an author of a paper in the session, the responsibility for review of that paper was shifted to another chairman. At least two reviews were obtained for each paper and returned to the authors. Final camera-ready manuscripts were submitted by the authors in September. Comments received from the authors concerning the review process were almost entirely favorable. The clear majority thought that their final manuscripts represented a significant improvement from the draft, and we agree.

In addition to the review process, the 1990 proceedings include the initial designation of an Honor Paper Award by the ESC. During the review process the referees nominated papers that they considered worthy of consideration for this award. The criteria that were included in this judgement included:

1. Clarity of the written presentation,
2. Originality of the contribution, and
3. Importance of the work in practice or in basic understanding of snow and ice related processes.

Five papers received unanimous nominations by the reviewers for consideration as 1990 Honor Paper. The final camera-ready version of each of these papers was reviewed by a 5-person panel having a broad range of backgrounds and interests. The authors and co-authors of the nominated papers are not eligible for membership on this panel. The nominated papers were all of high quality, as indicated in the point totals assigned by the reviewers. The 1990 Honor Paper Award was presented to A. Hogan and M. Ferrick for their paper entitled "Air temperature variation over snow-covered terrain."

Publication of this year's proceedings was accomplished with the assistance of the U.S. Army Cold Regions Research and Engineering Laboratory (Technical Communication Branch, Information Management Division). Stephen L. Bowen, David W. Cate and Thomas Vaughan are gratefully acknowledged for their assistance. The editors especially thank Sandra Smith for her exceptional effort in the final production of this document.

Membership in the ESC is open to all interested individuals and corporations. Additional copies of the current proceedings and all back issues can be obtained from the Secretary. The annual meeting of the Eastern Snow Conference is co-sponsored by the American Geophysical Union and the American Water Resources Association. Publication of these proceedings is made possible in part by Corporate Memberships in the Conference held by:

Hydro Québec
Place Dupuis
855 est, rue St. Catherine
Montréal, Québec
CANADA H2l 4M4

Province of New Brunswick
Department of the Environment—
Water Resources
P.O. Box 6000
Fredericton, New Brunswick,
CANADA E3B 5H1

Ontario Hydro
700 University Ave.
Toronto, Ontario
CANADA M5G 1X6

Niagara Mohawk Power Corp.
300 Erie Blvd. West
Syracuse, N.Y., USA 13202

We look forward to another outstanding meeting in Guelph—June 1991.

Michael Ferrick
Editor

Timothy Pangburn
Associate Editor

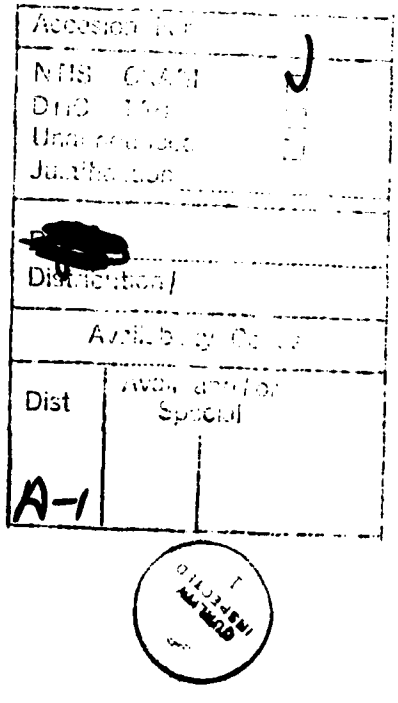

FORTY-SEVENTH ANNUAL MEETING, JUNE 7–8 , 1990, BANGOR, MAINE, U.S.A.

TABLE OF CONTENTS

THE EASTERN SNOW CONFERENCE

The Eastern Snow Conference (ESC) is a joint U.S./Canadian organization which was founded in the 1940's. It is an association of people interested in research and applied aspects of the study of ice in all its forms, especially snow. The principal activities of the ESC are the organization of an annual meeting, in the U.S. or Canada in alternate years, and the production of the annual Proceedings of the Eastern Snow Conference, which now form more than forty volumes deposited in libraries throughout North America and Europe. The annual meetings are sometimes held in major cities such as Washington, Montreal, Toronto or Boston and sometimes in smaller cities such as Peterborough, Oswego, Portland or Fredericton.

The members of the ESC are a very diverse and, over the years, fluctuating, group. They include professional snow surveyors, engineers and technologists (of various stripes), professors and students, hydrologists and biologists, people responsible for keeping roads clear of snow and rivers free of ice, and others interested in snow and agriculture. The members are drawn from all parts of eastern North America, they live and work in places which extend from Maryland to the high Arctic. The line between the territory of the ESC and its counterpart in the other half of the continent, the equally venerable Western Snow Conference, is not a precise one. Residents of the Mid-west and of the Prairie provinces seem to join one or the other organization on the basis of personal whim such as a preference for Reno, Nevada, over Bangor, Maine, as a desirable meeting place.

In recent years, the annual ESC meetings have included sessions on snow and small mammals, snow and buildings, river ice, permafrost, remote sensing of snow and ice, biology of sea ice, snow and ice on lakes, measuring snow and ice, hydroelectricity and snow and ice, glaciers, icebergs, snow and farming, etc.

Eastern Snow Conference est une organisation internationale canado-américaine fondée dans les années '40. Elle regroupe des gens qui ont des intérêts communs dans l'étude théorique et pratique de la glace sous toutes ses formes, en particulier sous la forme de neige. Eastern Snow Conference a comme activités principales d'organiser sa réunion annuelle en alternant le site du Canada aux États-Unis, d'en produire les comptes-rendus qui se montent maintenant à plus de quarante volumes que l'on peut trouver dans les bibliothèques de l'Amérique du Nord et d'Europe. La réunion annuelle peut se tenir tout aussi bien dans des villes importantes comme Washington, Montréal, Toronto ou Boston comme dans des plus petites comme Peterborough, Oswego, Portland ou Frédéricton.

Les membres d' Eastern Snow Conference représentent un grand nombre de domaines reliés à la neige et la glace. On y retrouve des spécialistes des relevés de neige, des ingénieurs et des techniciens, des professeurs et des étudiants, des hydrologues et des biologistes, des gens ayant la responsabilité d'entretenir les chemins en hiver ou de contrôler la glace en riviére, d'autres ayant quelqu'intérêt dans la neige et l'agriculture. Tous ces membres viennent de l'est de l'Amérique du Nord et peuvent y habiter de Maryland, U.S.A., à l'Arctique. D'ailleurs la ligne qui sépare le territoire d' Eastern Snow Conference à son pendant de l'ouest la vénérable Western Snow Conference est assez diffuse. Les habitants du centre-ouest américain ou des Prairies peuvent choisir de rallier une ou l'autre organisation sur une base très personnelle comme de préférer d'aller à Reno, Nevada, plutôt que Bangor, Maine, pour leur colloque annuel.

Dans les derniéres années, aux réunions annuelles d' Eastern Snow Conference on a tenu des sessions sur la neige et les petits mammifères, la neige et le bâtiment, la glace de riviére, le pergélisol, la télédétection de la neige et de la glace, la biologie de la glace marine, la neige et la glace lacustres, la mesure de la glace et de la neige, l'hydroélectricité et la glace et la neige, les glaciers, les icebergs, la neige et l'agriculture, etc.

EASTERN SNOW CONFERENCE OFFICERS
1989–1990

PRESIDENT
H. Gerald Jones
INRS-EAU
Université du Québec
Ste. Foy, Québec G1V 4C7

VICE-PRESIDENT
Nabil Elhadi
Department of the Environment—Water Resources
P.O. Box 6000
Fredericton, New Brunswick E3B 5H1

PAST-PRESIDENT
James Foster
NASA/Goddard Space Flight Center
Greenbelt, Maryland 20771

SECRETARY/TREASURER
John Metcalfe
161 London Road
Newmarket, Ontario L3Y 7A7

ASSISTANT SECRETARY
Donald V. Duncan
12 Seaman Street
New Brunswick, New Jersey 08901

EDITORS
Michael Ferrick and Timothy Pangburn
U.S. Army—CRREL
72 Lyme Road
Hanover, New Hampshire 03755-1290

STEERING COMMITTEE
Timothy Pangburn
Derrill Cowing
Terry Prowse

RESEARCH COMMITTEE
Rick Fontaine, Chairman
Michael Ferrick
Brian Day
Grady Moore

EQUIPMENT COMMITTEE
Stan Zeccolo, Chairman
Robert Fox
Cuyler Onclin
John Govoni

SNOW SURVEY COMMITTEE
Paul Lamb, Chairman
Thomas Brewer

LOCAL ARRANGEMENTS COMMITTEE
Derrill Cowing
Rick Fontaine

CORPORATE MEMBERS
Hydro Québec, New Brunswick Department of Environment, Ontario Hydro, and
Niagara Mohawk Power Corporation

THE PRESIDENT'S PAGE

General Activities

In addition to the ongoing activity for the preparation of the 47th annual meeting of the Eastern Snow Conference (ESC) at Bangor, Maine, in the spring of 1990, the major effort that took part during the year was the Editor's definition of a refereeing procedure for the papers submitted at the annual meeting. The precise description of the procedure may be found in the Foreword; it suffices to note here, however, that the decision to introduce the review process into the preparation of the proceedings was not taken lightly. I will not elaborate on the reasons which led to the adoption of the review proposal, except to say that it was taken after two years of thoughtful, and sometimes vigorous!, discussion, and on the pertinence of refereeing papers relative to the context of ESC activities and interest. It was ultimately felt, however, that a review process could be worked out which respected both the need for continuity in the ESC traditional activities, and the desire to attract new blood by offering the equivalent of a recognized refereed journal for the publication of peer-assured quality papers. The review procedure is, itself, under review and the Editor would welcome any comments and suggestions from the members on this matter.

Committees

1. Research Committee.

   It was decided that the status requirements for students wishing to submit a paper for the Student Paper Competition be made more flexible; the competition is now open to both full-time and part-time students.

   The awards for the competition are currently:

   Winning paper; a one year free membership in ESC, the Weisnet medal, $250.00 cash prize, and up to $500.00 travel and associated expenses.

   Runner-up papers; a one-year free membership in ESC, an ESC President's certificate and a $100.00 cash prize.

   This year the Research Committee judged that A.K. Abdel-Zaher of the University of New Brunswick, Canada, should be the recipient of the award for his paper "Numerical investigation of border ice failure."

2. Snow Survey Committee.

   The Snow Survey Committee carries out its regular program of data acquisition from the satellite Landsat overpasses and snow surveys reported by the five regional centers in Canada (Atlantic provinces, New Brunswick, Quebec) and the United States (Maine, New England States). The committee is always alert to technological advances in the field and is also presently considering the development of a training video on both the sampling of snow and the measurement of snow-cover properties.

3. Equipment Committee

   The task to put together a snow equipment reference manual has turned out to be significant in both time and effort. It has, in effect, led to an alternative proposal which will be examined in the coming year.

The suggestion is that a section in the proceedings would be devoted to one type of equipment only; the articles would be published at a rate of approximately one per year.

Final Thoughts

"Another good one come and gone" an old, but well-worn cliche often heard at the end of a successful meeting (yet again) of the Eastern Snow Conference; and the 47th annual meeting at Bangor, Maine, was no exception. The turnout was excellent and the diverse nature of the program made for the exchange of knowledge and ideas between attendees from many different backgrounds and expertise. A quick glance at the Table of Contents in this proceedings shows clearly the wide scope of interests of the members, ranging from the microphysics of snow crystals to animal behavior during the winter season. For many years this multidisciplinary facet of the ESC has evolved to the point where each meeting finds academics, operational personnel, and management under the same roof discussing the same materials, snow and ice, in, however, so many different ways.

This diversity of the ESC can be fragile; each member wishes to find himself in the familiar surroundings of his own expertise while expecting a profitable input of ideas and new techniques from other disciplines. Maintaining multidisciplinary meetings which can stimulate the interest and interactive participation of a wide range of professions is, thus, not always an easy task. However, as David Daugharty concluded in his 1988 President's page message on the need to maintain close ties between academics and operators in the ESC, we must keep working at it and we must have patience. Patience in the knowledge that the solution to large-scale environmental problems just cannot be tackled without the interdisciplinary approach. And so the ESC continues to act as a forum for the teachers and the students, the theorists and the operators, for all who have an open mind and a desire to further the multidisciplinary practice of snow/ice science and technology.

Finally, and on a personal note, my thanks to one and all, the stalwarts of the executive, the committee chairmen, members, and the local arrangements committee who made everything tick along so easily during the year. See you in Guelph, Ontario for the 48th—it looks like it's going to be a corker!

H. G. Jones
President
Eastern Snow Conference

Honor Paper Award:

Air Temperature Variation Over Snow-Covered Terrain

A. HOGAN AND M. FERRICK

U.S. Army Cold Regions Research and Engineering Laboratory
72 Lyme Road
Hanover, New Hampshire 03755-1290 U.S.A.

ABSTRACT

December 1989 was not only one of the coldest months for which instrumental records exist in the Northeastern United States, but was also unusual in that the air temperature remained continuously below freezing during all but the last day of the month. This prolonged cold period provided relatively homogeneous meteorological conditions in which to study the relationship among complex terrain variables and early morning air temperatures. An experiment was conducted in the Connecticut River Valley near 43°N latitude, based on the hypothesis that the river pool above Wilder Dam would provide a homogeneous surface reference for comparison of air temperatures observed nearby in differing geographic settings. Temperatures were measured 1.5 m above the surface at 92 relocatable points along a 33-km north-south transect and a 12-km east-west transect. Morning twilight temperatures measured on five days prior to a 30-cm snowfall on 16 December were compared with temperatures at the same locations on the five following days. Prior to the snowfall, the temperatures near the river were higher than those immediately upslope by more than 2°C. This trend was reversed following the snowfall, with colder air near the river. An analysis is presented to demonstrate that the heat rejected from river ice growth would be sufficient to provide the observed local warming. The quantity of heat available from this source decreased by an order of magnitude coincident with the observed reversal in temperature trends near the river. The influences of terrain slope, vegetation and the "heat island" of a village are also discussed.

INTRODUCTION

The nature of atmospheric flow, exchange and plume dispersion over complex terrain is of current interest in environmental impact studies and air pollution research (Clements, 1989). Local variations in temperature are of continuing interest in agriculture and in the construction, energy and utility industries, as are rural/urban temperature differences. Terrain-induced and rural/urban temperature differences seem to be enhanced by snow cover, which amplifies the problem of identifying climatic fluctuations in temperature records (Karl et al., 1988; Jones et al., 1989; Landsberg, 1981; Robinson and Kukla, 1988), and complicates long-range weather forecasting (Walsh and Ross, 1988). Most specifically, these small-distance scale variations in near-surface atmospheric conditions prohibit conclusive extrapolation of single-point meteorological observations and interpretation of remotely sensed surface data.

Local variation in near-surface air temperature, initially a function of radiation, is complicated by considerations of air/surface energy exchange and thermal storage (Miller, 1956 a,b). Overnight radiation deficits alter the structure of the boundary layer (Sasamori, 1968; Yu, 1978; Yamada, 1979; Nieustadt, 1980; Arya, 1981; Andre and Marht, 1982), often decoupling the surface from larger scale and more vigorous circulation above, but coupling the near-surface air and cold snow surface (Miller, 1956b). The relatively dense air formed near the surface tends to flow downslope, but this flow may be accelerated or retarded by terrain (Baines, 1979) and vegetation features (Li et al., 1990).

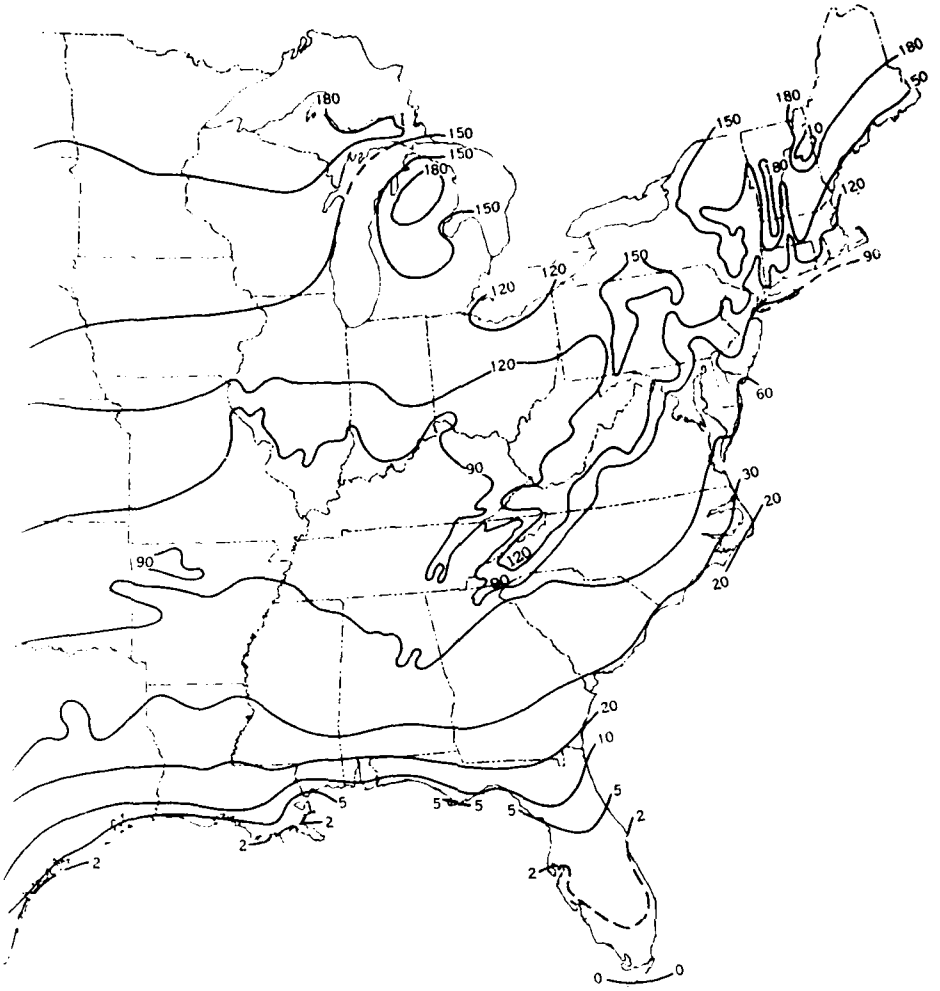

Figure 1. Climatic map of the eastern United States showing the number of days the minimum air temperature is below 0°C [from the National Climatic Atlas, NOAA (1977)].

Maki et al. (1986) and Maki and Harimaya (1988) studied and modeled the heat budget in a basin in volcanic terrain on Hokkaido Island, Japan. The model predicts nocturnal winter cooling to be greater in basins than in flat terrain, and greater at the bases than at the tops of mountains. This is due to the drainage of denser air down slopes and pooling in basins. Mountaintops are not as frequently decoupled from tropospheric flow, as they may remain above the inversion. Air entrained to replace that draining down the mountain may be much warmer than that in the decoupled surface layer below.

The Connecticut River Valley between Vermont and New Hampshire is anecdotally cooler than regions at equal latitude 100 km to the east or west. Later blooming of plants, later and earlier frosts, and absence of some particular types of vegetation native to nearby areas characterize many places in the region. The climatic map in Figure 1 indicates the complexity of the temperature conditions in the northeastern United States. As the observation station spacing is comparable to that of the isotherms in this region, the actual spatial variation of temperatures may not be accurately represented. This paper describes experimental measurements of near-dawn surface air temperatures in the Connecticut River Valley near 43°N as part of an investigation of the influence of nocturnal inversions, drainage winds, basin effects and settlement on local minimum air temperatures.

EXPERIMENT DESIGN

A shielded, relatively rapid response thermistor (YSI 400, response 10 s in air) and its digital readout (repeatable to ± 0.1°C) were adapted for convenient mounting on a car or

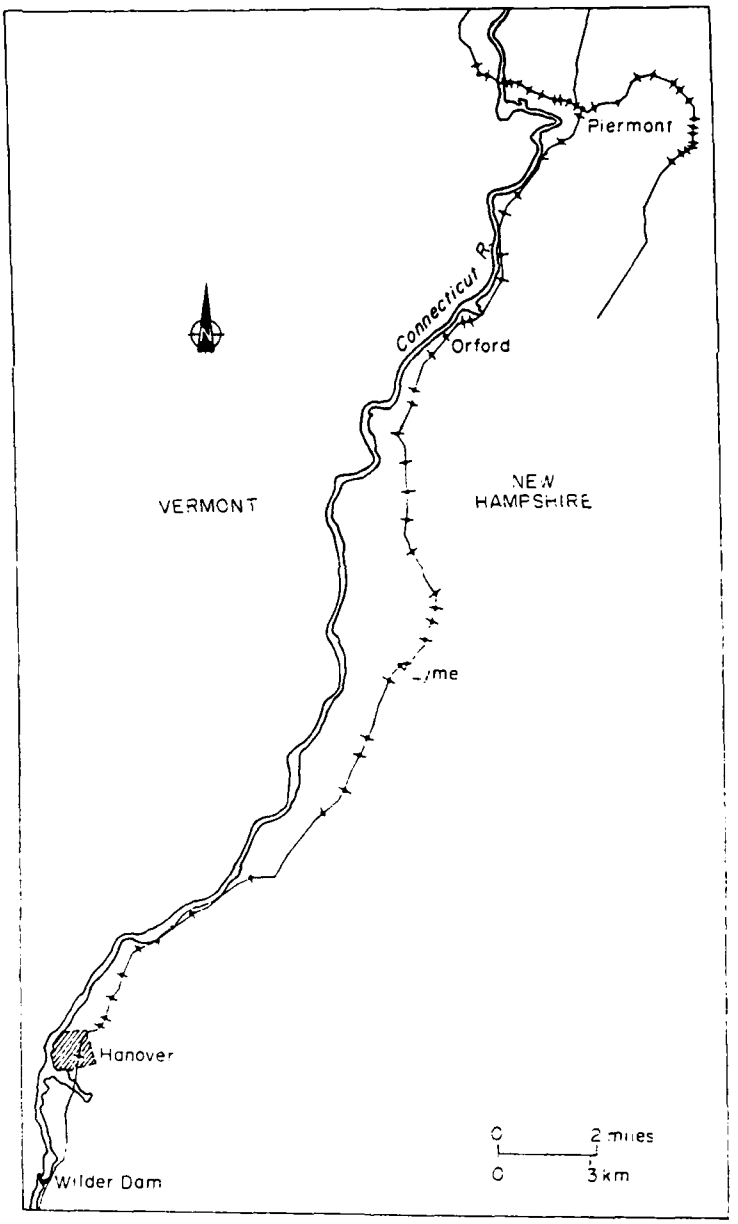

Figure 2. The section of the Connecticut River Valley where the experiment was conducted, including the longitudinal and transverse data transects.

truck. Some experimentation was necessary to select mountings 1.25 to 1.5 m above ground level that were not influenced by radiation or advection of heat from the vehicle. The door-top mount finally selected was found to reflect the free-stream temperature whenever the vehicle was in motion. Experiment and calculation show that the temperature indicated while in motion is representative of an integration of 150 m of horizontal path through the air. This limits the spatial resolution of temperatures to this distance.

Preliminary experiments were attempted during the winters of 1987-88 and 1988-89, and on days when late or early frosts were expected during the spring or fall of those years. The results of these experiments demonstrated that a wide range of temperatures could occur in a 10- by 30-km rectangle with less than 330 m total variation in elevation. A precisely defined measurement protocol was considered essential to subsequent experiments. Observation points which could be precisely located on the USGS topographic maps of the area were selected along an east-west (transverse) transect of the valley at Piermont, N.H., and along a north-south (longitudinal) transect extending from Piermont to Hanover, N.H. A total of 96 observing points (Fig. 2) were defined and noted by landmark on a standardized data

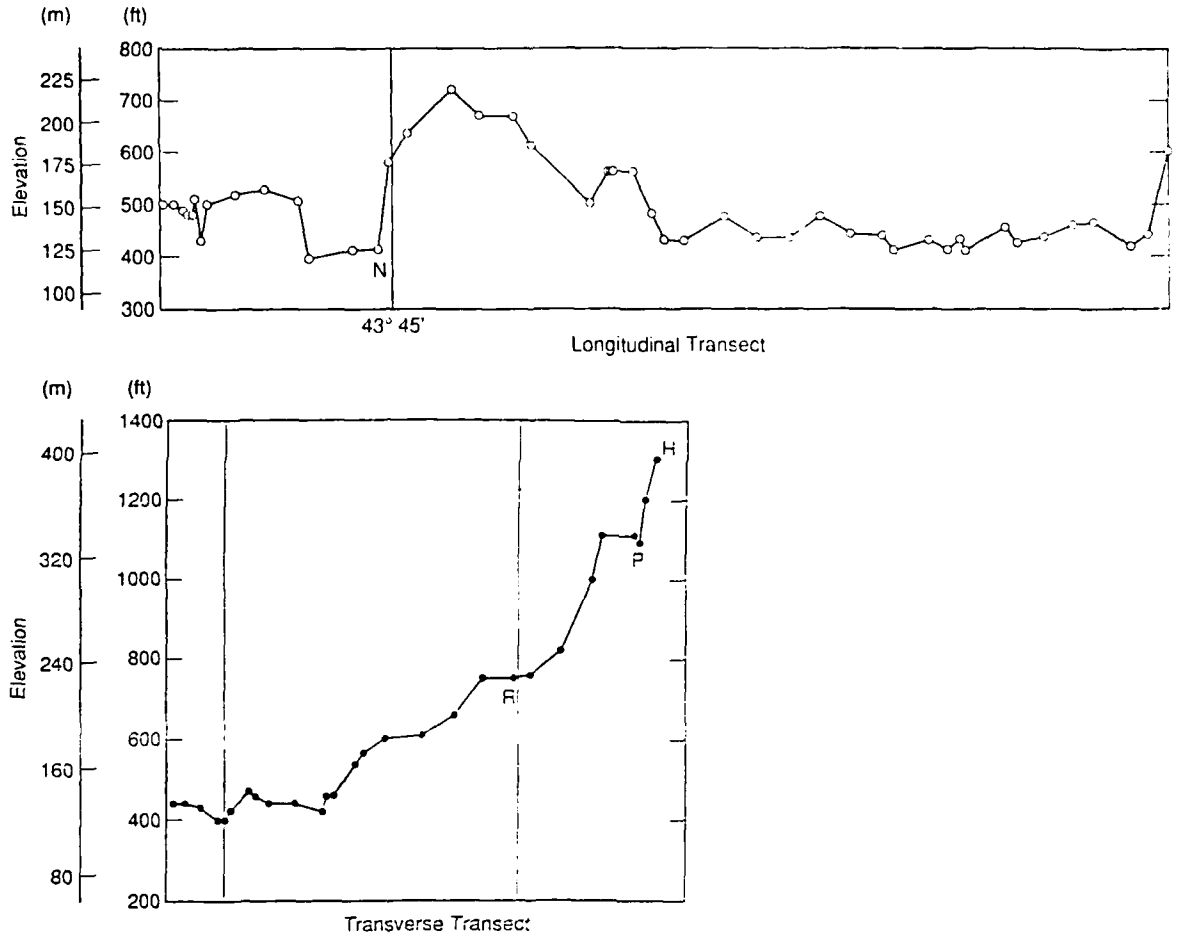

Figure 3. Elevation and location of observation points projected to a north-south line for the longitudinal transect and an east-west line for the transverse transect.

sheet. The analysis was conducted by projecting the terrain cross-sections to east-west and north-south transect lines and entering observed temperatures above the projection. The cross-section projections are shown in Figures 3a and b.

Air temperature measurements were made while in motion between the hours of 0615 and 0730 EST during the period 1 Dec 1989 to 30 Mar 1990. This time was prior to sunrise during most of the period and in the shadow of the hills during March. Only days with relatively uniform sky conditions throughout the experiment area are considered in the analysis. Three days were deleted from the analysis due to fog or precipitation in a fraction of the area. A total of 60 days of observations were obtained that yield some whole winter generalizations. This paper focuses on the results obtained during the relatively homogeneous cold period of December 1989.

We propose two hypotheses as the basis for our analysis of minimum local air temperatures. First, if decoupling of the air in the valley from the lower tropospheric flow is occurring, a discontinuity will be present, and the surface temperature will not be isentropically related to that of the free air above. Second, a conservative plane of reference that is level and homogeneous and extends throughout the experiment area is necessary to compare air temperatures in adjacent environments with variable topography, vegetation or population, within the decoupled layer. The Connecticut River is dammed south of Hanover and presents a level pond throughout the experiment area. The water in this pond is exchanged frequently, preventing stagnation and development of warm or cool pools. We propose that this frequent water exchange will provide a relatively stable heat source or sink to the air at the lowest point in our experiment area and provide a homogeneous reference plane for comparison of temperatures measured in other environments within a reasonable distance

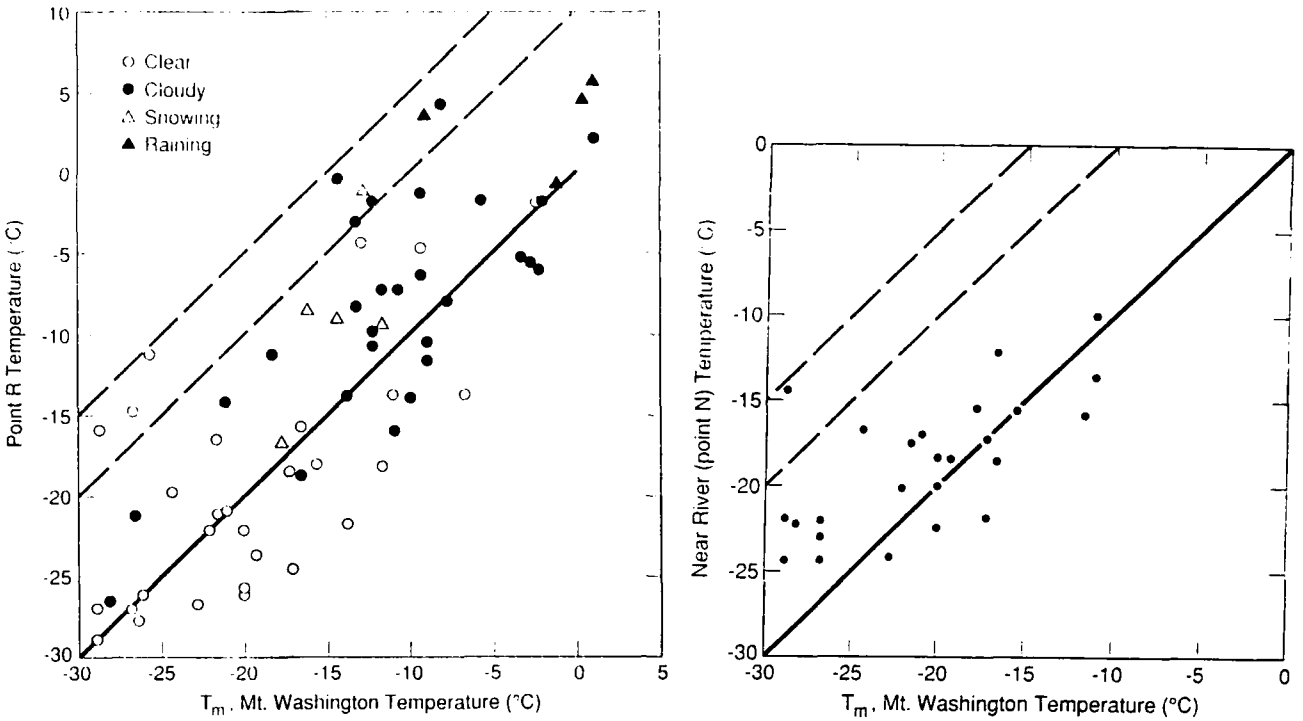

Figure 4. Temperature comparisons of data at points R and N with data recorded at the summit of Mount Washington.

of the river. The river was frozen and snow-covered during most of the period reported, providing an even more stable reference plane.

RESULTS OF EXPERIMENTS

A comparison of temperatures measured at river level, 4 km north of the CRREL recording thermometer (point N), another point in a tributary valley (point R), and the 0700 LCL [12 UT] observation made at the summit of Mt. Washington (80 km east) is shown in Figure 4. The summit of Mt. Washington is nearly 2 km above sea level, and several hundred meters higher than surrounding terrain. The temperature observed there is representative of the lower tropospheric potential temperature over inland New England. The 12 UT observation is synoptic with upper air observations to allow further analysis of the deviation of the mountain temperatures from free-stream temperatures. If no inversion or decoupling were present, adiabatic exchange would provide surface air temperatures in the Connecticut Valley about 20°C higher than Mt. Washington (T_M) in dry air, and 10 to 15°C higher in cloudy air. Figure 4 shows the valley to be always colder than (T_M +15°C), and generally colder than (T_M +10°C). On many occasions the valley temperatures are less than the temperature at the summit of Mt. Washington. Comparison of the temperatures observed at these basin points with nearby hilltop points shown in Figures 5 and 6 indicates the presence of a warmer layer above the valley floor but below the altitude of Mt. Washington. These temperature relations are indicative of one or more temperature inversions between the levels of the experiment points and Mt. Washington. Visual observations showed that near-surface flow was very weak and usually easterly or northerly and occasionally southerly in the valley, while Mt. Washington winds were strong and westerly. The lower mountains between the valley and Mt. Washington apparently interact with the upper winds to produce a weak eddy flow east of the river. The nocturnal inversion decouples the lowest layers from tropospheric circulation. The presence of colder air at the surface than atop Mt. Washington, and a reversal of the near-surface wind direction, supports the hypothesis that the Connecticut Valley is decoupled from the flow above, but definitive proof would require tethersonde or airsonde temperature profiles.

Point N, about 4 km north of the CRREL temperature shelter, was chosen as the basis for comparison of temperatures observed at several points near river level in Dec 1989. The road is immediately adjacent to the river bank for at least 300 m at point N, and a hill immediately east of the road confines circulation, limiting admixture of air from other than

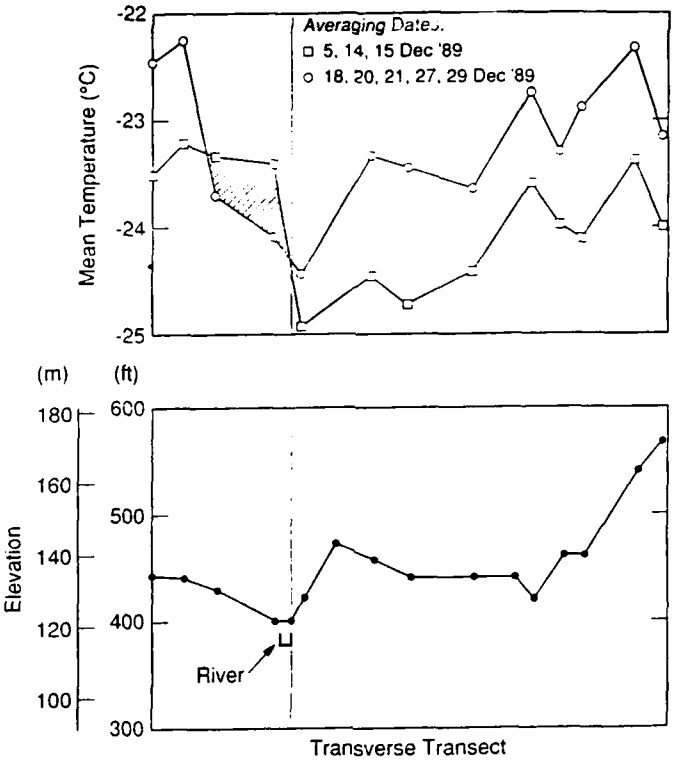

Figure 5. Mean temperatures along the transverse transect near the river before and after the 16 December snowfall.

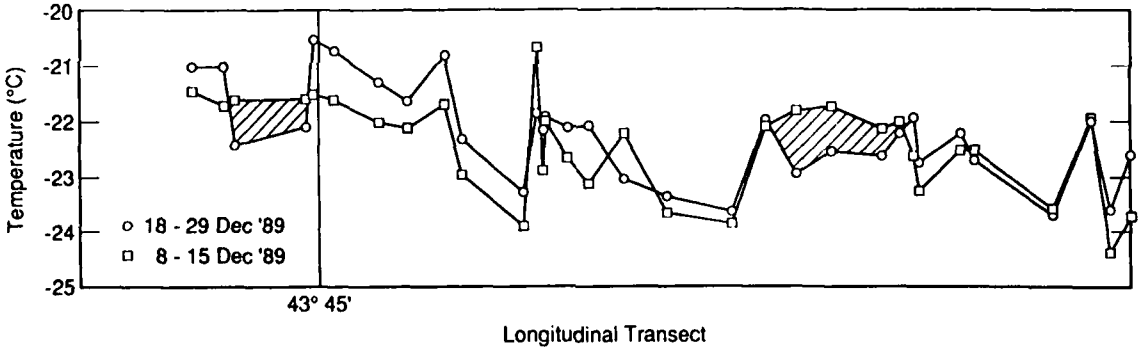

Figure 6. Mean temperatures along the longitudinal transect before and after the 16 December snowfall.

the river direction during still conditions. The temperatures observed at six points near or over the river, displaced in distance by 1.5 to 22 km from point N, are compared with those observed at point N in Figure 7. Examination of Figure 7 shows that 99 of 114 comparison points correspond to within ± 1.5°C; this is considered a tentative verification of the second hypothesis, allowing use of the near-river temperature as reference to examine terrain influence on other nearby temperatures.

Temperatures during December 1989 as observed at the CRREL temperature shelter (about 300 m from the river and 35 m above river level) were less than -15°C on all but four days, and on only one day did the daily maximum exceed freezing. Grease ice was observed on the Connecticut on 1 Dec, and an initial ice cover formed by 4 Dec. A light (5 cm) snowfall on 6 Dec produced a thin snow cover on the river ice throughout the experiment area, which verified that the ice cover was continuous. An additional 25 to 35 cm was deposited in the experimental area on 16-17 Dec. A comparison of temperatures observed prior to 16 Dec and following 17 Dec along north-south and east-west transects of the Connecticut Valley is

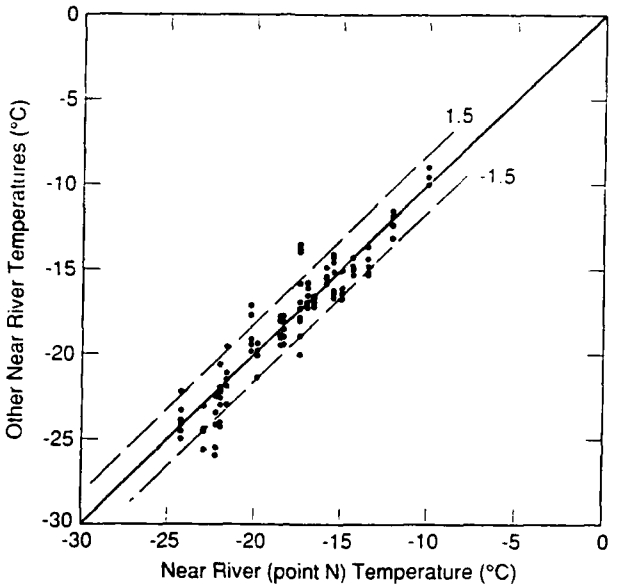

Figure 7. Comparison of temperatures at several locations adjacent to the river with those at point N.

presented in Figures 5 and 6. It is quite apparent that temperatures observed adjacent to or over the river prior to the snowfall are greater than those observed nearby, while temperatures observed at these places following the snow of 16 Dec are less than those observed nearby.

Consistent with our observations we will assume that the river ice growth from zero thickness began on 3 December. Ashton (1989) presented an equation for thin ice growth as

$$\frac{dh}{dt} = \frac{1}{\rho L} \frac{(T_m - T_a)}{\left(\frac{h}{k} + \frac{1}{H_{ia}}\right)} \qquad (1)$$

and in integrated form as

$$h = \left[\frac{2k}{\rho L}(T_m - T_a)\, t + \left(\frac{k}{H_{ia}}\right)^2\right]^{1/2} - \frac{k}{H_{ia}} \qquad (2)$$

where

- h is ice thickness (m)
- k is thermal conductivity of ice (2.24 W/m °C)
- L is latent heat of fusion (3.34×10^5 J/kg)
- ρ is density of ice (917 kg/m^3)
- H_{ia} is the heat transfer coefficient between ice and air (20 W/m^2 °C)
- T_m is the melting point temperature (0°C)
- T_a is air temperature (°C)
- t is time (s)

The temperature data presented in Figure 8 indicate significant warming near the river on 6 December. The heat source is probably the rapid growth of river ice. Therefore, we neglect the insulating effect of the light snowfall in the ice growth calculations. Then, equation (2) yields a mean ice growth of 2.9 cm/day for the period 3-15 December 1989. The Connecticut River has an average width of approximately 150 m in this reach, and ice growth of 2.9 cm/day will produce a daily heat release of 1.33×10^9 J/m of river length. Large snowfalls on well-established ice covers provide insulation that resists heat flow and greatly reduces subsequent ice growth. The denominator of equation (1) must then expand to include a term that represents the thermal resistance of the snow layer ($h/k + 1/H_{ia} + h_s/k_s$), where h_s and k_s are thickness and thermal conductivity of the snow, respectively. The thermal conductivity of a snow layer increases with the density of the snow (Ashton, 1986). We will assume that the snowfall of 16 December compacted to a thickness of 15 cm

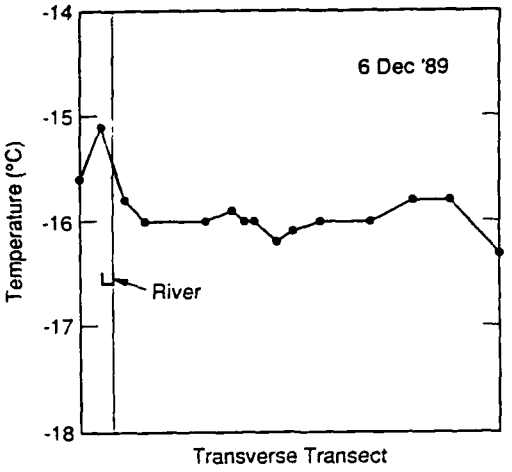

Figure 8. Temperature data from 6 December along the transverse transect near the river concurrent with total freeze-up, verified by continuous snow cover from a light snowfall.

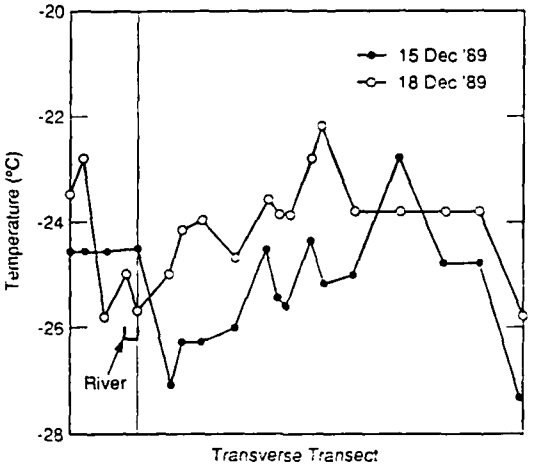

Figure 9. Temperature data along the transverse transect near the river before (15 Dec) and after (18 Dec) the 16 December snowfall.

with a density of 200 kg/m^3 and thermal conductivity 0.12 W/m °C. For an initial ice thickness of 0.38 m, we obtain 0.25 cm of ice growth for 17 December with a corresponding heat release of 1.15 x 10^8 J/m of river length. A comparison with the heat release prior to the snowfall indicates an order of magnitude reduction as a result of the snow cover on the ice.

On 15 December and 18 December the near-river temperatures are approximately equal (Fig. 9). However, the temperature immediately adjacent to the river is about 2°C higher on the 15th, prior to the snowfall. The average temperatures presented in Figures 5 and 6 also indicate relative temperature reductions following snowfall in areas adjacent to the river. We propose that a reduction in local heating resulting from a diminished rate of river ice growth beneath new snow cover was responsible for the observed temperature behavior adjacent to the river. An estimate of the local volume of air that received heat from the river is needed to determine whether differential heat output could cause the observed temperature differences. Observations of smoke plumes from chimneys indicated an inversion at about 25 m above the surface near the river. The temperature data from the valley profiles indicated elevated temperatures, before 16 December, in a band near the river extending through the entire study area with a total width of about 15 river widths. The total volume of air in this band is then about 56,000 m^3/m of river length.

The heat transfer to a system in a constant pressure quasi-equilibrium process corresponds to a change in enthalpy of the volume:

$$_1Q_2 = dH = m\ C_p\ dT \qquad (3)$$

where C_p is the specific heat of air at constant pressure, m is the mass of the air and dT is the change in air temperature. At a temperature of -22.5°C and pressure of 1000 mb (100 kPa) the density of air is 1.39 kg/m^3 (List, 1950), and the total mass of air in our system is 77800 kg per unit length. The specific heat of air at constant pressure is 1002.3 J/kg K at -23°C (Keenan and Kaye, 1948). Then from equation (3) the quantity of heat required to raise the temperature of the air in the system by 2°C is about 1.56 x 10^8 J. The difference between the daily heat release from river ice growth prior to and following the snowfall provides about eight times the quantity of heat needed to account for this temperature increase. We conclude that rapid ice growth can cause a significant temperature increase adjacent to a river when this air mass is isolated from large scale exchange. However, a snow cover on the ice can greatly reduce ice production so that the local increase in air temperature becomes negligible.

RESULTS OF EXPERIMENTS: TERRAIN-INDUCED TEMPERATURE VARIATION

Mather and Miller (1967) and Bromwich et al. (1990) have described major terrain-induced air flows over large areas of snow-covered ground in Antarctica. Maki et al. (1986) and Maki and Harimaya (1988) described temperature variation in a smaller basin due to radiation and drainage-induced air flows and showed examples of temperature difference relative to idealized terrain features. Comparing the slope and elevation features of Figure 3 with the temperature features of Figures 5 and 6 shows the importance of terrain considerations in a diverse environment. Slope is a dominant temperature predictor on this scale. Small, flat areas are consistently colder than adjacent slopes; the lowest air temperatures were consistently found above small, flat areas interrupting a slope. Apparently an additional inversion forms above these flats, allowing continuing radiational cooling to occur there, while drainage flow proceeds along the slope and above this additional nocturnal inversion. The flat terrain surrounding point P was just 150 m along the transect, and actual temperatures there may be slightly less than those observed, due to the integration time of the thermistor.

The barriers to flow described by Raynor (1971), Baines (1979) and Li et al. (1990) are present in the form of narrowing or widening of tributary valleys, small ridges, woods and forests. Temperature differences near these barriers were quite pronounced on individual days, but a consistent pattern of significant magnitude is not apparent in the total record. The relative change of slope seems to be the dominant factor which influenced near surface air temperatures during this experiment.

RESULTS OF EXPERIMENTS: THE URBAN HEAT ISLAND

Additional to the temperature differences attributable to terrain, urban/rural temperature differences are well known. Landsberg (1981) showed an immediate effect accompanying the initial development of Columbia, Maryland, when the population was below 10,000 persons. It was immediately apparent in our experiment that the village of Hanover was somewhat warmer than the surrounding areas. The greatest temperature observed on each day was in the downtown area. Perhaps some old New England towns were settled in more climatically benign areas, and are naturally somewhat warmer in winter than the surroundings. Temperatures observed along a golf course near the northern edge of the settled area and those measured between three-story brick buildings on Main Street are plotted in Figure 10 against the temperatures observed adjacent to the river less than 10 minutes earlier. The temperature observed near the golf course is about 1°C less than that observed near the river on half of the coldest mornings when temperatures were less than -15°C; on other occasions the temperatures are generally nearly equal. The temperatures observed in the settled areas are, in all but two cases greater than the nearby river temperature. Twenty-six of the forty-six observations found the settled area more than 1°C warmer than near-river temperatures, and the difference increased as temperature decreased. When temperatures were near freezing, in-town snow removal apparently reduced heat loss, as found in Arctic settlements by Woo and Dubreuil (1983). It appears that a small, non-industrial village can produce a measurable heat island even in complex surroundings.

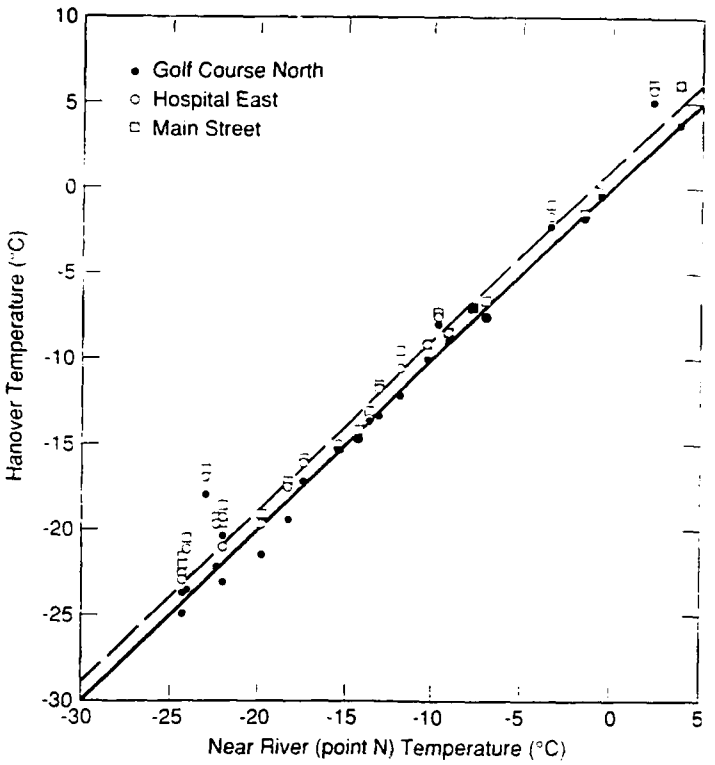

Figure 10. Comparison of temperature data recorded in Hanover with those at point N.

Two additional analyses were performed on hamlets within the experiment area. In these cases, temperatures observed near the center of activity in the settlements and the temperature observed in a sparsely settled flat of similar elevation within a few hundred meters of the hamlet were compared with near-river temperatures. There was no apparent heat island associated with either hamlet, even in the cases when area temperature was less than -20°C.

DISCUSSION

The Connecticut River above Wilder Dam hypothetically provides a temperature reference plane when the adjacent valley is snow-covered. Temperature measurements near and over the river along 30 km of the impoundment, made about the time of sunrise each morning, were used to test and preliminarily verify this hypothesis, when the valley is decoupled from lower tropospheric flow. As the river ice cover is thickening in early winter, the heat released causes the air above and immediately adjacent to the river to be warmed; after the river ice becomes well snow-covered, the air above becomes colder than that nearby in the valley. Although the relative temperature of air over the river when compared to adjacent air varies with ice thickness and snow cover on the ice, the above-river air temperature is quite constant along a 30-km reach, allowing it to serve as a temperature reference plane.

Comparing the temperatures observed in Hanover to nearby over-river air temperatures shows that even a small non-industrial community produces an "urban heat island" on winter nights. Similar comparisons involving hamlets in the vicinity show no systematic temperature difference. This does not eliminate the possibility that heat islands exist at these locations, but indicates that the magnitude is less than that of the terrain-induced temperature variation.

The basin and hilltop variation in temperature presented by Maki and Kikuchi (1986) is apparently amplified over snow-covered ground, due to the decoupling afforded by the multiple inversions present over variably sloped terrain. Relative slope and change in slope appear to produce large changes in early morning air temperature over small distances. Some of these variations may be attributable to vegetation-induced surface roughness and the trapping of air within forests, preventing strong downslope drainage of cold air or promot-

ing eddy circulation of warmer air from above; these variations are not as easily isolated as the heat island and river plane influences and may require a much greater number of measurements to verify or reject.

It appears that the relative coolness of the Connecticut River Valley is due to the decoupling of the air circulation of the valley floor, and of many of the smaller branch basins above, from lower tropospheric flow by combinations of inversions and eddies caused by the north-south axis of the White Mountains. This allows cool pools of dense cold air to form in the valley bottom and in small basins above, and provides "oases" on some hillsides where exchange occurs more freely above local inversions.

Research on this phenomenon is far from complete, and we have only isolated the most apparent terrain/temperature relations thus far. Some practical applications exist, relative to examining the influence of microclimate on historic settlement and abandonment, and perhaps isolating a "rural cold island" that may be generated by extensive cleared fields which are relatively cooler than the antecedent forest.

CONCLUSIONS

A hypothesis has been proposed and preliminarily verified, that a level ice-covered river pool can be used as an air temperature reference when studying elevation-, slope-, and population-induced temperature variation in snow-covered terrain. Changes in the terrain slope and the presence of a non-industrial village both produced significant variations in the local temperature. A research challenge remains, relative to application of this hypothesis to vegetation-induced temperature variation over snow-covered ground.

The presence of colder air, greatly diminished winds and a reversal of the wind direction in a valley relative to conditions aloft has preliminarily verified the hypothesis of a decoupled air mass in the valley during cold, clear early morning conditions with snow-covered ground. The heat released from formation of ice on a river during freeze-up is sufficient to produce 2°C of warming within a band of several river widths in a valley bottom that is decoupled. This heat release diminished to below the level of detection when 15 cm of snow covered the ice.

ACKNOWLEDGEMENTS

We would like to thank D.H. Miller for helpful discussions at the conference, and several members of IMD at CRREL for the production of the final paper.

REFERENCES

Andre, J.C. and L. Marht (1982) The Nocturnal Surface Inversion and Influence of Clear Air Radiative Cooling. J. Atmos. Sci., 39, pp. 864-878.

Arya, S.P.S. (1981) Parameterizing the Height of the Stable Atmospheric Boundary Layer. J. Appl. Meteorol., 20, pp. 1192-1202.

Ashton, G.D. (1989) Thin Ice Growth. Water Resources Research, 25(3), pp. 564-566.

Ashton, G.D., Editor (1986) River and Lake Ice Engineering. Water Resources Publications, Littleton, Colorado, p. 235.

Baines, P.G. (1979) Observations of Stratified Flow Past Three-Dimensional Barriers. J. Geophys. Res., 84, pp. 7834-7838.

Bromwich, D.H., T.R. Parish and C.A. Zorman (1990) The Confluence Zone of the Intense Katabatic Winds at Terra Nova Bay, Antarctica, as Derived from Airborne Sastrugi Surveys and Mesoscale Numerical Modeling. J. Geophys. Res., 95, pp. 5495-5509.

Clements, W.E. (1989) Organizer, Atmospheric Studies in Complex Terrain: Part I and Part II. J. Appl. Meteorol., 28, pp. 405-542 and pp. 545-689.

Jones, P.D., P.M. Kelly, C.M. Goodess and T. Karl (1989) The Effect of Urban Warming on the Northern Hemisphere Temperature Average. J. Climate, 2, pp. 285-290.

Karl, T.R., H.F. Diaz and G. Kukla (1988) Urbanization: Its Detection and Effect in the United States Climatic Record. J. Climate, 1, pp. 1099-1123.

Keenan, J.H. and J. Kaye (1948) Gas Tables. John Wiley & Sons, Inc., New York, p. 34.

Landsberg, H.E. (1981) The Urban Climate. Academic Press, 285 pp.

Li, Z., Lin, J.D. and Miller, D.R. (1990) Air Flow Through A Forest Edge: A Steady State Numerical Simulation. Bound. Layer Met., 51, pp. 179-197.

List, R.J., Editor (1950) Smithsonian Meteorological Tables. Smithsonian Misc. Collections Vol. 114, Smithsonian Institution, Washington, D.C.

Maki, M. and T. Harimaya (1988) The Effect of Advection and Accumulation of Downslope Cold Air on Nocturnal Cooling of Basins. J. Met. Soc. Japan, 66, pp. 581-597.

Maki, M., T. Harimaya and K. Kikuchi (1986) Heat Budget Studies on Nocturnal Cooling in a Basin. J. Met. Soc. Japan, 64, pp. 727-741.

Mather, K.B. and G.S. Miller (1967) Notes on the Topographic Factors Affecting the Surface Wind in Antarctica, with Special Reference to Katabatic Winds and Bibliography. REP UAG R 189, Geophysical Institute, University of Alaska, Fairbanks, pp. 864-878.

Miller, D.H. (1956a), The Influence of Snow Cover on Local Climate in Greenland. J. Meteorol., 13, pp. 112-120.

Miller, D.H. (1956b) The Influence of Open Pine Forest on Daytime Temperature in the Sierra Nevada. Geog. Rev., 46, pp. 209-218.

Nieustadt, F.T.M. (1980) A Rate Equation for the Inversion Height in a Nocturnal Boundary Layer. J. Appl. Meteorol., 19, pp. 1445-1447.

Rayner, G.S. (1971) Wind and Temperature Structure in a Coniferous Forest and a Contiguous Field. For. Sci., 17, pp. 351-363.

Robinson, D.A. and G. Kukla (1988) Comments on "Comparison of Northern Hemisphere Snow Cover Datasets." J. Climate, 1, pp. 435-440.

Sasamori, T. (1968) The Radiative Cooling Calculation for Application to General Circulation Experiments. J. Appl. Meteorol., 7, pp. 721-729.

Walsh, J.E. and B. Ross (1988) Sensitivity of 30 Day Dynamical Forecasts to Continental Snow Cover. J. Climate, 1, pp. 739-754.

Woo, M.K. and Dubreuil, M.-A., (1983) Effects of an Arctic Settlement on the Snow Pack. Proc. Eastern Snow Conf., pp. 143-155.

Yamada, T. (1979) Prediction of the Nocturnal Surface Inversion Height. J. Appl. Meteorol., 18, pp. 526-531.

Yu, T.-W. (1978) Determination Height of the Nocturnal Boundary Layer. J. Appl. Meteorol., 17, pp. 28-33.

Student Paper Prize:

Numerical Investigation of Border Ice Failure

A.K. ABDEL-ZAHER

Department of Civil Engineering
University of New Brunswick
P.O. Box 4400
Fredericton, New Brunswick E3B 5A3, Canada

ABSTRACT

Border ice commonly occurs in small rivers and brooks with rapid flow; it grows slowly until a complete ice cover is formed. Border ice may be subjected to rapid changes in water level leading to its failure.

An analytical approach has been developed for modelling the hydrodynamic-structural interaction of border ice and its failure. The analysis considers the possibility of failure of border ice due to rapid changes in water level. The modelling process assumes elastic behavior of the ice and is based on a finite element technique which has been used to develop the FEMI Model presented herein. The analogy of a beam on an elastic foundation has been used in the formulation the FEMI Model.

The paper investigates the possibility of failure of border ice with different variations in slope of the undersurface and hinged or fixed boundary conditions at the river bank, employing principal stress theory as a criterion for failure.

The results of this investigation are presented in a dimensionless form to enable examining the border ice for small rivers with different geometries and ice properties.

1. INTRODUCTION

The phenomenon of border ice formation in small rivers has been investigated numerically and experimentally by many researchers, Devik (1964), Hanley and Michel (1975 and 1977), Hirayama (1986), Matousek (1984), and Michel (1971). These investigations thoroughly examined air temperature, wind velocity, stream discharge, etc. and their effects on the rate of formation of border ice. The border ice may be subjected to rapid changes in water level. To the author's knowledge, these changes in water level and their effects on the cracking of the border ice, its failure and separation from the river bank have not been examined.

This paper presents a numerical model called FEMI which has been developed based on the finite element technique. The paper investigates the hydrodynamic-structural interaction for border ice and its failure. The analogy of a beam on an elastic

foundation has been used in the formulation of the FEM1 Model. The possibility of border ice failure is predicted on the basis of a combination of bending moments and shearing forces in the ice employing principal stress theory as a criterion for failure.

Many cases of border ice have been examined with different variations in slope of the undersurface, lengths, thicknesses, ice properties, and end conditions at the river bank. The variation in border ice geometries in different rivers and its properties in different cold regions at the time of the failure does not permit effective presentation of results for specific geometry and ice properties. Therefore, the model results have been generalized by presenting them in a dimensionless form. The solution stability and validity of the dimensionless results have been examined along with different combinations of input variables such as number of ice beam elements, thickness, length, uplift pressure, and elastic modulus. These variables have been used to obtain the relative stiffnesses and corresponding dimensionless deflections, bending moments, and shearing forces. It is submitted that the presented results will enable examining many small rivers with different widths, border ice geometry, and ice properties. Numerical examples are given at the end to demonstrate the use of the developed dimensionless formulation.

2. STATEMENT OF THE PROBLEM OF BORDER ICE

The border ice is initially buoyantly supported on the water and attached at the river bank. The application of the uplift pressure due to rapid changes in water level can be followed by cracking in the border ice and separation from the bank. The vertical structural equilibrium of an element of the border ice in such a case considers its own weight, the buoyant force, decrease on buoyant force due to deflection, and uplift pressure as shown in Fig. (1) and represented by the following equations:

$$P = p + \gamma\ (S_i\ H_i - Y) - \gamma_i\ H_i\ , \tag{1}$$

or

$$P = p - \gamma\ Y. \tag{2}$$

Here, P is net upward pressure, p is uplift pressure, γ, and γ_i are unit weights of water and ice, S_i is specific gravity of ice, Y, and H_i are the deflection and the border ice thickness.

The form of equation (2) implies that the uplift pressure is directly proportional to the deflection. This suggests that a unit length of the border ice in the direction of flow may be treated as a beam on an elastic foundation with modulus of foundation reaction equal to γ, the unit weight of water. Hetenyi (1946) examined the behaviour of a beam on an elastic foundation; he presented his solutions for the general differential equation governing the deflected shape of a uniform beam resting on a Winkler medium; such a medium was defined as one for which "the pressure in the foundation is proportional at every point to the deflection occurring at that point and independent of pressures or deflections elsewhere in the foundation". The differential equation can be written as follows:

$$EI\ \frac{d^4Y}{dX^4} + \gamma\ Y = p, \tag{3}$$

or

$$EI\ \frac{d^4Y}{dX^4} + 4\ \lambda^4\ Y = \frac{p}{EI}\ . \tag{4}$$

Here, $\lambda = \sqrt[4]{\gamma/4EI}$ is the characteristic of the system or the damping factor, EI is the flexural rigidity of the border ice for unit length, and X is the distance from the shore.

It should be noted that γ, the modulus of foundation reaction, is specified for the

length border ice in the direction of flow. It will only be numerically equal to the unit weight of the water if the border ice is of unit length in the direction of flow which is true in this analysis in which γ = 9.81 kPa.

In Hetenyi's solution, it has been indicated that λ, the characteristic of the system, controls the distributions of deflection, rotation, bending moment, and shearing force for any particular case of loading.

Some researchers, Beltaos (1984 and 1985) and Billfalk (1981 and 1982) have employed Hetenyi's solutions for analysis of river ice covers. Their work considered a finite complete ice cover with symmetrical boundaries (hinged-hinged and fixed-fixed) and an infinite river ice cover. In both cases a uniform thickness for the ice cover was considered.

3. FEMI MODEL FORMULATION AND COMPUTER IMPLEMENTATION

The formulation of the FEMI Model for border ice is based on the finite element stiffness methodology for structures. In this method, the border ice is divided into a finite number of ice beam elements on an 'elastic foundation'. These elements are interconnected at nodal points which have a sequential numbering system to minimize the memory required during the computer calculations. It should be noted that it is important to have a considerable number of elements especially for varied thickness as is the case in border ice analysis.

All forces and displacements for an element of the border ice are shown in Fig. (2). Considering border ice with a finite number of beam elements, the external and internal forces can be related as follows:

$$\{P\} = [A]\ \{F\}; \tag{5}$$

where $\{P\}$ is an external forces vector, $[A]$ is a statics matrix, and $\{F\}$ is an internal forces vector.

Wang (1970) indicated, by using the reciprocal theory, that the internal and external displacements can be related as follows:

$$\{e\} = [A]^T\ \{X\}; \tag{6}$$

where $\{e\}$ is an internal deformations vector and $\{X\}$ is an external displacements vector.

The internal forces can be related to the internal deformations as follows:

$$\{F\} = [S]\ \{e\}; \tag{7}$$

where, $[S]$ is a local stiffness matrix of the border ice.

Equilibrium, compatibility, and force-deformation requirements are satisfied by equation (5) through (7) which are the fundamental equations in the finite element analysis of border ice.

By substituting equation (6) into equation (7) the following equation can be written:

$$\{F\} = [SA^T]\ \{X\}; \tag{8}$$

and substituting equation (8) into equation (5) the following equation can be written:

$$\{P\} = [ASA^T]\ \{X\} \tag{9}$$

where, $[ASA^T]$ is the global stiffness matrix of the border ice.

Equation (9) represents a system of simultaneous equations which can be solved to

obtain the displacements {X} after imposing boundary conditions. Then using equation (8), the forces induced in the border ice at the nodal points can be obtained. Imposing the fixed boundary conditions in the stiffness method has been made by considering very high stiffness for the rotational and vertical springs at the fixed boundary (i.e. no rotation and no vertical translation), and for the hinged boundary very high stiffness for the vertical spring and zero stiffness for the rotational spring (i.e. free to rotate and no vertical translation).

In the analogy of border ice with beam on an elastic foundation a provision has to be made to update the results especially for deflection. There is a subroutine named ICDISP in the FEM1 Model which solves the simultaneous equations and calculates the dimensionless deflections and rotations, and has a provision to stop the calculations if $Y_{max} > S_1 H_i$ (the maximum allowable deflection) and continue if $Y_{max} \leq S_1 H_i$. If FEM1 Model stops the calculations, it means that the free edge emerges from the water and the theory of beam on an elastic foundation is no longer valid. Also, to satisfy the analogy of a beam on an elastic foundation the border ice should not be flooded from the top.

The assumption of elastic response for the ice is valid for rapid changes in the water level as considered in this analysis. There is no universal agreement on the elastic limits for ice but some figures have been given by Sinha (1977), he suggested that for stresses less than 2 MPa and time less than 1 second or stress less than 0.5 MPa and time less than 100 seconds elastic behaviour can be assumed. Also, Ashton (1986) has reported limits in which the ice responds elastically to stresses less than 1 MPa and time less than 100 second or if ice is loaded to fail within 2 seconds based on Traetteberg et al. (1975).

4. DIMENSIONLESS DEFLECTION, BENDING MOMENT, AND SHEARING FORCE

Since the results are presented in a dimensionless form, it is found from equation (2) that a dimensionless group for the deflection can be written as follows:

$$\text{Dimensionless deflection} = \frac{\gamma Y}{p} . \tag{10}$$

Equation (10) represents the proportionality between the deflection and pressure due to changes in water level.

The bending moment, M, and shearing force, Q, distributed along the border ice for ice length, L, are governed by the characteristic of the system, λ. If L, λ, M, Q, and p are considered variables for a dimensional analysis, the following dimensionless groups can be formed:

$$\text{Relative stiffness} = \lambda L; \tag{11}$$

The characteristic of the system λ, is calculated based on the minimum thickness of the border ice at the free edge.

$$\text{Dimensionless shearing force} = \frac{\lambda^2 M}{p} , \tag{12}$$

$$\text{Dimensionless shearing force} = \frac{\lambda Q}{p} . \tag{13}$$

All results are presented in the next section referring to these dimensionless groups in equations (10) through (13). Also, the shore distance is considered in a dimensionless form (X/L).

5. RESULTS AND DISCUSSION

The dimensionless bending moment and deflections for border ice with uniform thickness and hinged ends at the river bank are presented in Fig. (3) and Fig. (4). In establishing these relationships and all others, different combinations of the input parameters such as Himin, E, L, and p, were used in obtaining different values of λL from 1 to 6. All dimensionless relationships have been checked by using different element sizes until a stable solution was obtained. Also, the solutions obtained by the FEMI Model have been verified by comparing them with the available solutions by Hetenyi (1946) for uniform thickness. This confirmed the validity and the stability of the results. It can be seen that the position of the maximum dimensionless bending moment tends to move toward the shore with increasing relative stiffness λL (Fig. (3)). The maximum dimensionless deflection occurs at the free edge of the border ice for $\lambda L \leq 3$ as shown in Fig. (4). It tends to move toward the centre of the border ice for $\lambda L \geq 4$. The dimensionless bending moment for uniform thickness of border ice with fixed ends is shown in Fig. (5). It can be seen that the value of the maximum dimensionless bending moment always occurs close to the bank. The dimensionless deflection which tends to behave similar to the hinged end case is presented in Fig. (6).

In the case of variable thickness, four different slopes of the under surface (2.5°, 5°, 7.5°, and 10°) have been assumed. This range is assumed to cover most of the border ice formed in small rivers.

The dimensionless bending moments for the four slopes, a range of λL from 1 to 6, and hinged ends are shown in Fig. (7), Fig. (9), Fig. (11), and Fig. (13). These figures show an insignificant change in the dimensionless bending moment with increasing slope of the undersurface for each λL from 1 to 6. Such change vanishes for slopes greater than 5°. The corresponding dimensionless deflections are presented in Fig. (8), Fig. (10), Fig. (12), and Fig. (14). These figures show an insignificant change in the dimensionless deflection with increasing slope of the undersurface and the relative stiffness λL. Such change vanishes for slopes greater than 5°.

It should be pointed out that all dimensionless relationships for nonuniform thickness have been established based on the characteristic of the system at the free edge (i.e. at H_{imin}). Also, the border ice with slopes 2.5° and more has a large increase in flexural rigidity toward the bank for all relative stiffnesses; this explains the decrease in deflection and the behavior of border ice as a highly stiffened beam in all cases. Undersurface slopes from 0.5° to 2.0° are to be investigated for future applications of FEMI Model to examine the changes in the dimensionless relationships, especially for deflections.

In case of border ice with uniform thickness, the predicted position of cracking is the same as the position of maximum dimensionless bending moment and maximum bending stress as well as the position of maximum principal stresses. The predicted position of cracking tends to move toward the bank with increasing the relative stiffness as shown in Fig. (15). However, for border ice with uniform thickness and a fixed end, the predicted position of cracking is always close to the bank which represents the position of maximum dimensionless bending moment, maximum bending stress, and maximum principal stress. Such cracking positions for both cases indicates that the shear stress has a negligiable effect.

The flexural rigidity was found to be the major factor affecting the predicted position of cracking for varied thickness of border ice with a hinged end. The flexural rigidity caused the predicted position of cracking to shift toward the free edge from the position of maximum dimensionless bending moment. However, the predicted positions of cracking, maximum bending stress, and maximum principal stress coincided. The predicted position of cracking tends to move toward the free edge with increasing slope of the undersurface for any given relative stiffness from 1 to 6 as shown in Fig. (15).

The predicted position of cracking for fixed end border ice with varied thickness is close to the bank. In this paper, due to the limitation of space. The results for only one slope (2.5°) are presented for three different relative stiffnesses from 1 to 3. The

dimensionless bending moment for these cases is presented in Fig. (16). It shows that the maximum dimensionless bending moment is close to the bank. Furthermore, it was found that the predicted cracking, maximum bending stress, and maximum principal stress coincided and were close to the bank. Figure (17) shows the dimensionless deflection; from which it can be seen that the position of maximum dimensionless deflection occurs at the free edge of the border ice.

The present formulation is also applicable to the case of border ice subjected to a drop in water levels with the undersurface in contact with the water everywhere.

6. NUMERICAL EXAMPLES

Example (1): Examine the failure of uniform thickness border ice for H_i = 0.16 m, L = 10.0 m, E = 4600 MPa, p = 0.5 kN/m, and flexural strength = 700 kPa for (a) hinged end and (b) fixed end.

(a) Hinged end case

These data give $S_i H_i$ = 0.147 m, λ = 0.2 hence λL = 2. Using results in Fig. (4) gives Y_{max} = 0.068 m < 0.147 m, Fig. (15) gives X_c/L = 0.3. Also using results in Fig. (3). and Fig. (18). M = 1.5 kN.m, and Q = -0.035 kN. The principal stresses $\sigma_{1,2}$ can be obtained from

$$\sigma_{1,2} = 0.5\ \sigma_b \pm 0.5\ \sqrt{\sigma_b^2 + 4\ \tau^2}$$

($\sigma_{1,2}$ are principal stresses, σ_b is bending stress, and τ is average shear stress). Hence, maximum principal tensile stress at top ≈ maximum bending stress at top = 353.5 kPa. Therefore, p = 0.5 kN/m is not suffient to cause cracking. However, if p = 1.0 kN/m by similar calculations it can be shown that cracking will occur at 3.0 m from the bank.

(b) Fixed end case

From the results in Fig. (6) gives Y_{max} = 0.062 m < 0.147 m, also using the results in Fig. (5) and Fig. (18) M = -6.25 kN.m, and Q = -2.33 kN.

Hence maximum principal tensile stress at bottom ≈ maximum bending stress at bottom = 1465 KPa. Therefore, p = 0.5 kN/m or less is enough to cause cracking close to the bank. This implies that the uplift pressure due to change in water level which is required to cause cracking for fixed end is less than that required for a hinged end.

Example (2): Examine the failure of border ice with variable thickness for H_{imin} = 0.05 m, L = 4.0 m, θ = 2.5°, E = 4600 MPa, p = 1 kN/m, and flexural strength = 700 kPa for (a) hinged end and (b) fixed end.

(a) Hinged end case

These data give $S_i H_{imin}$ = 0.046 m, λ = 0.5 hence λL = 2. From the results in Fig. (8) Y_{max} = 0.152 m > 0.046 m and therefore the free edge emerges from the water level, and hence the methodology is not applicable.

(b) Fixed end case

From the results in Fig. (17) gives Ymax = 0.026 m < 0.046 m, also from Fig. (16), and Fig. (18) M = -6.95 kN.m, and Q = -3.6 kN. Hence, maximum principal tensile stress at bottom ≈ maximum bending stress at bottom = 830 KPa. Therefore, p = 1.0 kN/m which is sufficient to cause cracking close to the bank.

The limitation criterion built into FEM1 for the maximum deflection implies that for flooding from the top these calculations will be automatically stopped and so indicated in the output.

7. CONCLUSIONS

A FEM1 Model based on the finite element method coupled with the analogy of a beam on an elastic foundation has been developed to analyze the possibility of border ice cracking at the bank under rapid changes in water level.

It has been found that the predicted position of cracking for fixed end border ice with uniform and varied thickness of border ice is close to the bank. The hinged end border ice with uniform thickness has a predicted cracking position which tends to move toward the bank with increasing relative stiffnesses from 1 to 6. In these three cases the predicted position of cracking occurred at the position of maximum bending moment, which coincided with the location maximum bending stress and maximum principal stress. In case of variable thickness of border ice with hinged end, the predicted cracking position tends to move toward the free edge from the position of maximum bending moment with increasing slope of the undersurface for any given relative stiffness from 1 to 6. This displayed the importance of flexural rigidity. However the predicted cracking position coincided with the position of maximum bending stress and maximum principal stress in all cases. These results suggest that the shear stress has no effect on the predicted position of cracking. It was found that the changes in dimensionless bending moment for hinged border ice with varied thickness insignificant with increasing slopes between 2.5° to 10°, for each relative stiffness from 1 to 6. However, these changes vanish for slopes greater than 5°. It was also found that the changes in the corresponding dimensionless deflection are insignificant with increasing slopes and relative stiffnesses. Such changes vanish for slopes greater than 5°.

The numerical examples imply that the uplift pressures required to cause cracking in case of fixed end border ice are less than those required for a hinged end case with the same geometries, strength, and properties. This was found to be the case for border ice with uniform or variable thickness.

The developed dimensionless formulation can also apply for border ice subjected to a rapid drop in the water levels with the undersurface still in contact with the water everywhere. The border ice must be free from flooding at the top to satisfy the analogy of beam on an elastic foundation.

8. ACKNOWLEDGEMENTS

The author wishes to express his appreciation to Dr. S. Beltaos (NWRI) Burlington, Dr. K.S. Davar, Dr. A.J. Valsangkar, and Dr. J.L. Dawe for their encouragement and guidance during this investigation. The financial support for this work was from a grant awarded by National Sciences and Engineering Research Council of Canada to Dr. K.S. Davar, Department of Civil Engineering, University of New Brunswick.

9. REFERENCES

1. Abdel-Zaher, A.K., K.S. Davar and J.L. Dawe (1989). "The Initiation of the Premature Breakup of River Ice Cover: Existing Methodologies and Approaches to Integral Analysis" Proceedings, ESC, June 8-9, Quebec City, Canada.

2. Ashton, G.D./Editor (1986). "River and Lake Ice Engineering" Water Resources Publications, Littleton, Colorado, USA.

3. Beltaos, S. (1984) "A Conceptual Model of River Ice Breakup" Canadian Journal of Civil Engineering, Vol. 1, No. 3

4. Beltaos, S. (1985) "Initial Fracture Patterns of River Ice Cover" NWRI Contribution #85-139, National Water Research Institute, Burlington, Ontario.

5. Billfalk, L. (1981) "Formation of Shore Cracks in Ice Covers due to Changes in the Water Level", Proceedings, IAHR International Symposium on Ice, Quebec City.

6. Billfalk, L. (1982) "Break-up of Solid Ice Covers due to Rapid Water Level Variations" Report no. 82-3, CRREL, Hanover, New Hampshire, USA.

7. Christensen, F.T. and Tryde, P. (1986) "Uplifting Forces on Long Vertical Walls" Proceedings, IAHR International Symposium on Ice, Iowa City, USA.

8. Cook, R.D. (1974) "Concepts and Applications of Finite Element Analysis" second edition, John Wiley & Sons, Inc., New York USA.

9. Devik, O. (1964) "Present Experience on Ice Problems Connected with The Utilization of Water Power in Norway" Journal IAHR, Vol. 2, No. 1.

10. Frederking, R. and F.U. Hausler (1978) "The Flexural Behaviour of Ice From in Situ Cantillever Beam Tests" Proceedings, IAHR International Symposium on Ice, Lulea, Sweden.

11. Hanley, T.O'D and Michel, B. (1975) "Temperature Patterns During The Formation of Border Ice and Frazil in A Laboratory Tank" Proceedings, IAHR International symposium on Ice, Hanover, New Hampshire, USA.

12. Hanley, T.O'D and Michel, B. (1977) "Laboratory Formation of Border Ice and Frazil Slush" Canadian Journal of Civil Engineering, Vol. 4, No. 2.

13. Hearn, E.J. (1985) "Mechanics of Materials" second edition, Pergamon Press.

14. Hetenyi, M. (1946) "Beams on Elastic Foundation" Ann Arbor, The University of Michigan Press.

15. Hirayama, K. (1986) "Growth of Ice Cover in Steep and Small Rivers" Proceedings, IAHR International Symposium on Ice, Iowa, USA.

16. Kozitskiy, I.YE. (1982) "The Mechanism of Breakup of the Ice Cover of Rivers and Canals" Fluid Mechanics-Soviet Research, Vol. 11, No. 5.

17. Matousek, V. (1984) "Regularity of the Freezing Up of Water Surface and Heat Exchange Between Water Body and Water Surface" Proceedings, IAHR International Symposium on Ice, Hamburg.

18. Michel, B. (1971) "Winter Regime of Rivers and Lakes" Crops of Engineers, U.S. Army, Hanover, New Hampshire, USA.

19. Shulyakvskii, L.G./Editor (1963) "Manual of Forecasting Ice Formation for Rivers and Inland Lakes" Israel Program for Scientific Translations, Jerualem, 1966.

20. Sinha, N.K. (1977). "Effective Elasticity of Ice" Workshop on the Mechanical Properties of Ice , 24-25 January, Calgary, Alberta.

21. Timoshenko, S.P. (1956) "Strength of Materials" Part II, D. Van Nostrand Company, Inc.

22. Wang, C.K. (1970) "Matrix Methods of Structural Analysis" second edition, International Textbook Company, USA.

23. Yang, T.Y. (1986) "Finite Element Structural Analysis", Prentice-Hall, Inc., Englewood Cliffs, N.J. 07632, USA.

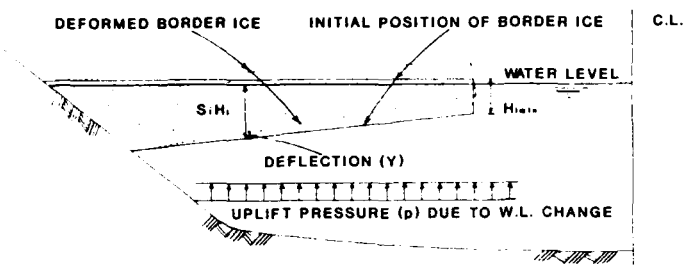

FIG. 1. DEFINITION SKETCH FOR THE PROBLEM

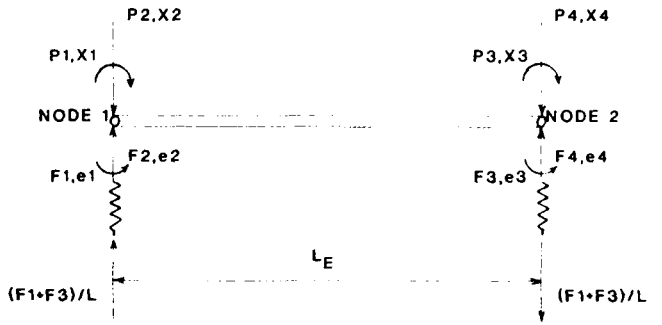

FIG. 2. IDEALIZATION FOR ICE BEAM ELEMENT (P & F FORCES AND X & e DISPLACEMENTS)

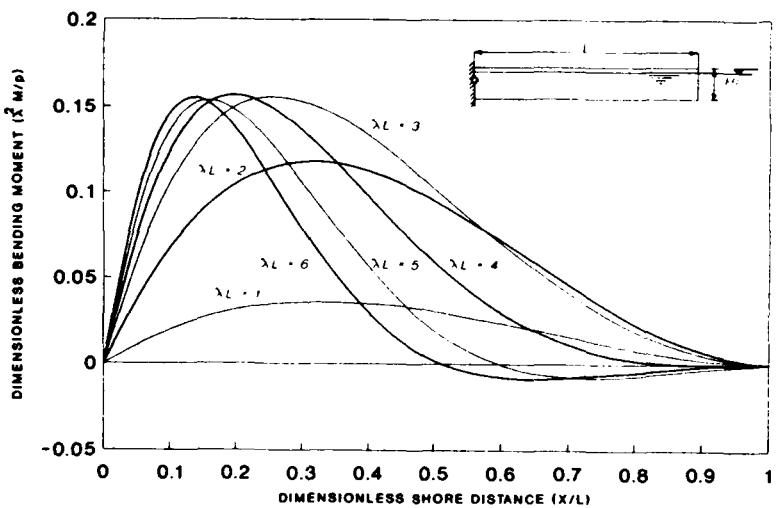

FIG. 3. DIMENSIONLESS BENDING MOMENT FOR HINGED BORDER ICE WITH UNIFORM THICKNESS

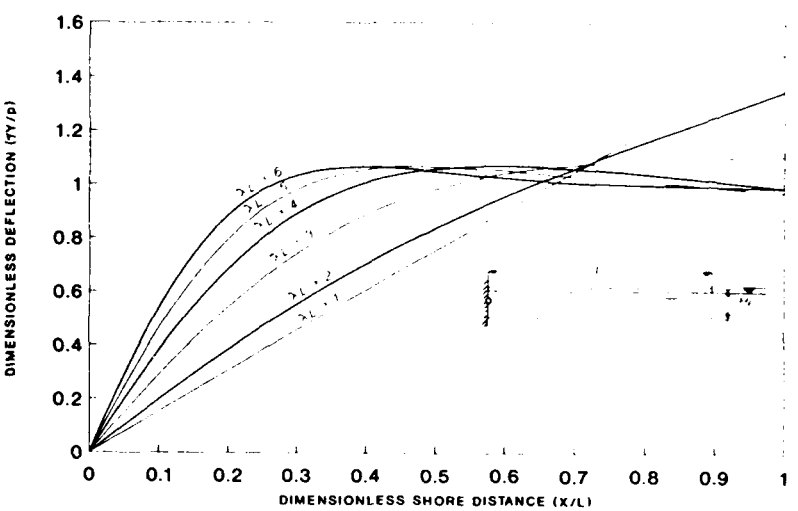

FIG. 4. DIMENSIONLESS DEFLECTION FOR HINGED BORDER ICE WITH UNIFORM THICKNESS

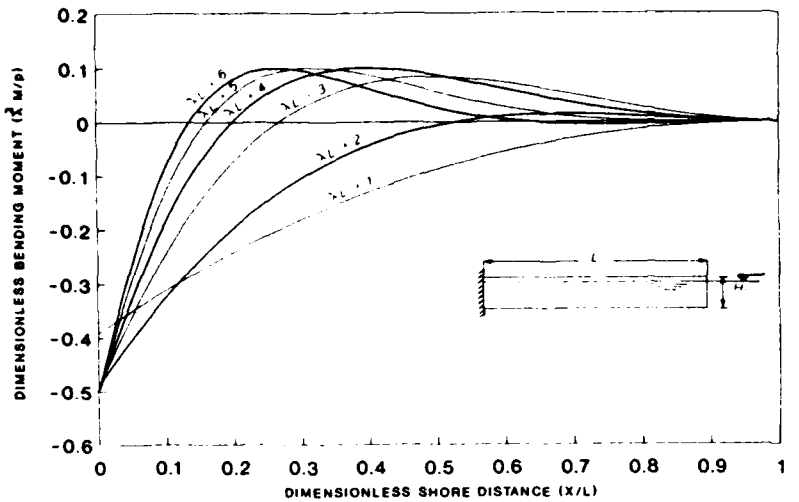

FIG. 5. DIMENSIONLESS BENDING MOMENT FOR FIXED BORDER ICE WITH UNIFORM THICKNESS

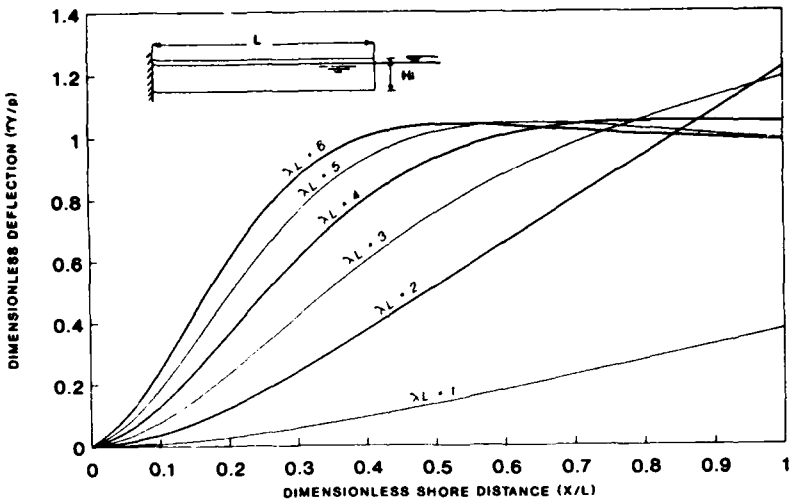

FIG. 6. DIMENSIONLESS DEFLECTION FOR FIXED BORDER ICE WITH UNIFORM THICKNESS

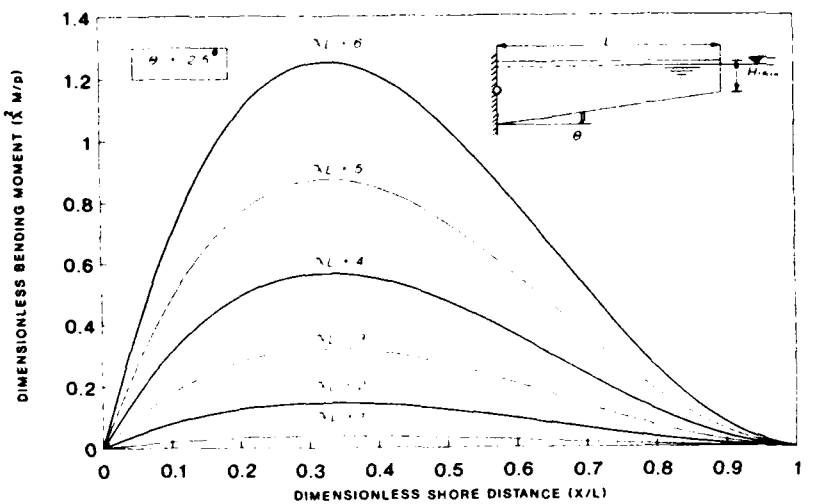

FIG. 7. DIMENSIONLESS BENDING MOMENT FOR HINGED BORDER ICE THICKENED UNIFORMLY

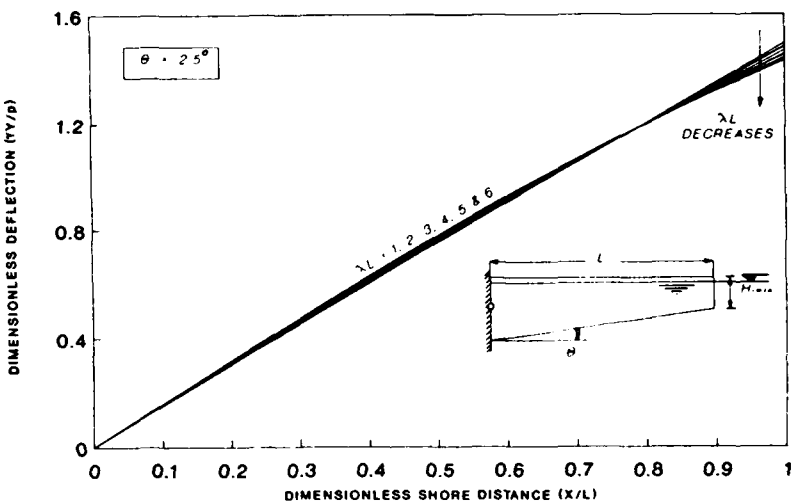

FIG. 8. DIMENSIONLESS DEFLECTION FOR HINGED BORDER ICE THICKENED UNIFORMLY

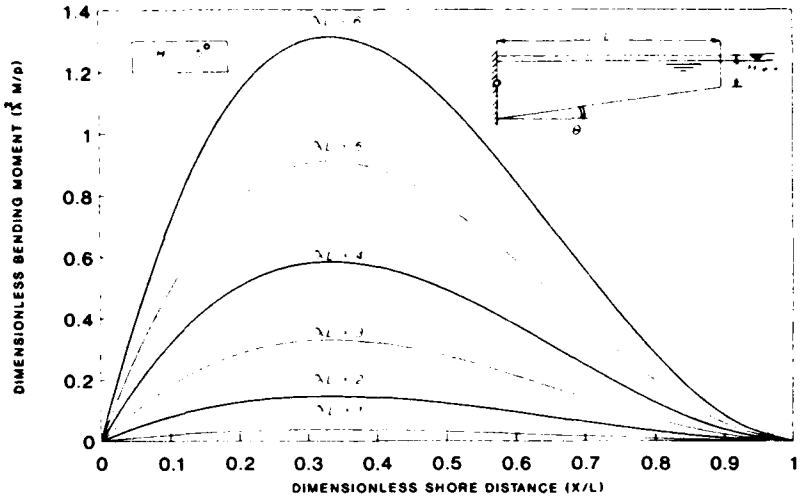

FIG. 9. DIMENSIONLESS BENDING MOMENT FOR HINGED BORDER ICE THICKENED UNIFORMLY

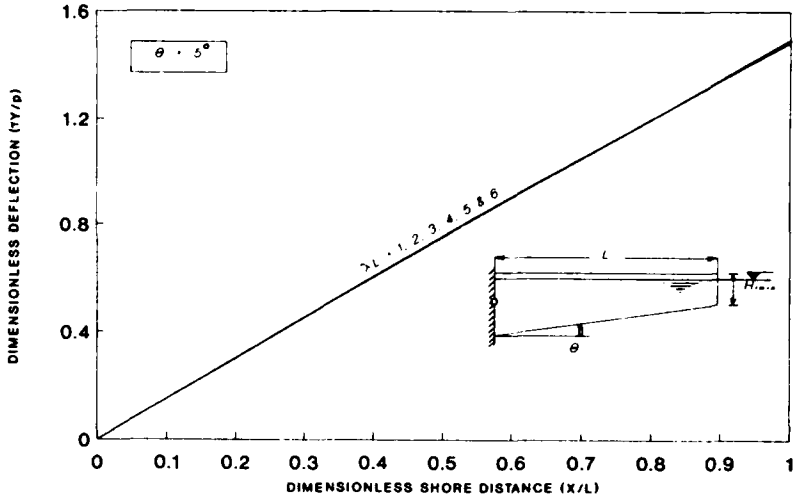

FIG. 10. DIMENSIONLESS DEFLECTION FOR HINGED BORDER ICE THICKENED UNIFORMLY

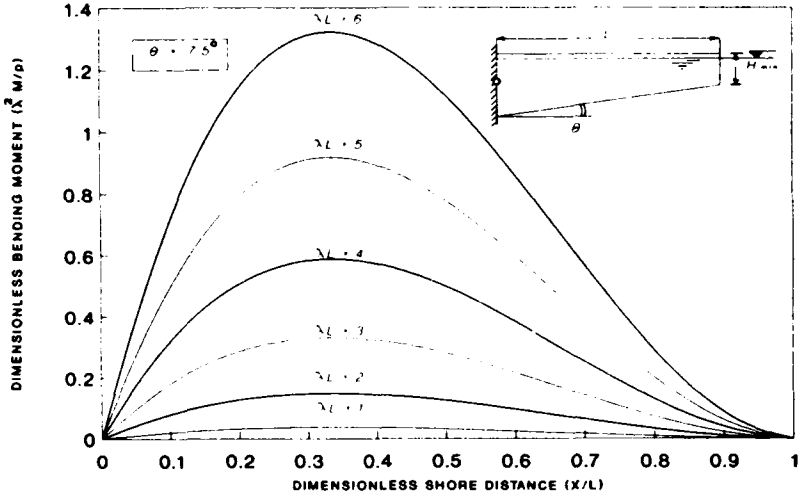

FIG. 11 DIMENSIONLESS BENDING MOMENT FOR HINGED BORDER ICE THICKENED UNIFORMLY

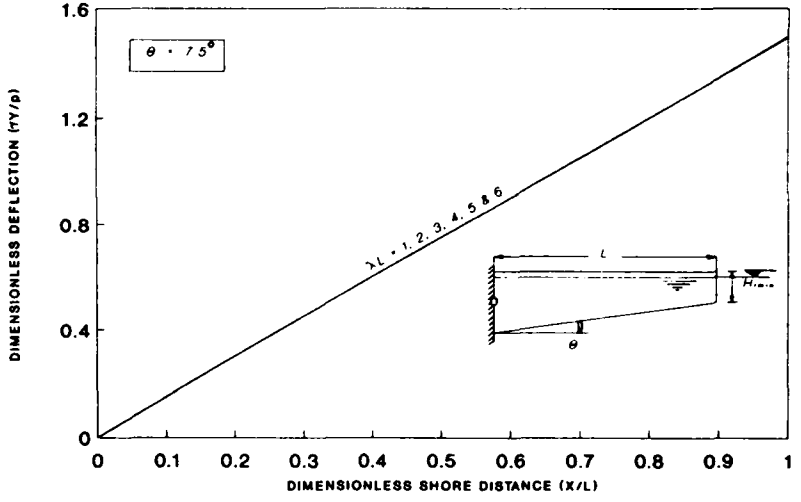

FIG. 12. DIMENSIONLESS DEFLECTION FOR HINGED BORDER ICE THICKENED UNIFORMLY

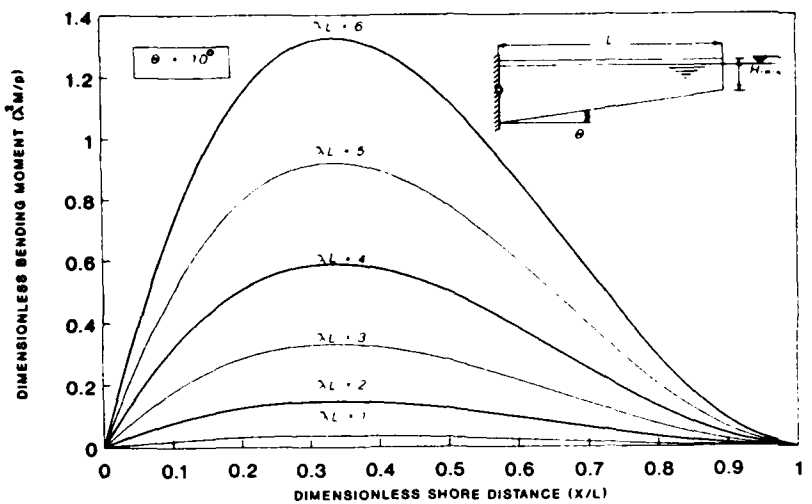

FIG. 13 DIMENSIONLESS BENDING MOMENT FOR HINGED BORDER ICE THICKENED UNIFORMLY

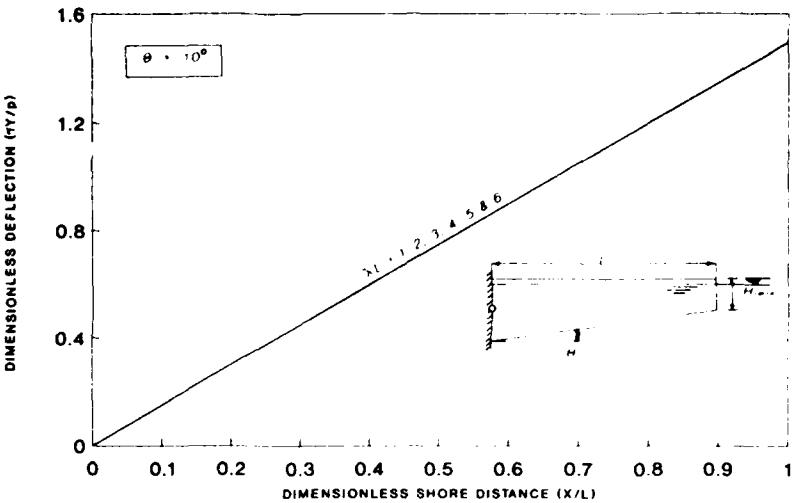

FIG. 14. DIMENSIONLESS DEFLECTION FOR HINGED BORDER ICE THICKENED UNIFORMLY

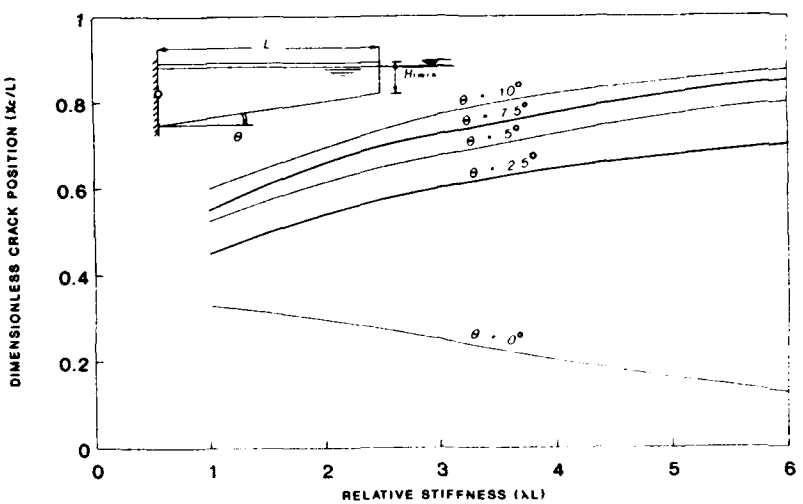

FIG. 15. DIMENSIONLESS PREDICTED CRACK POSITION FOR HINGED BORDER ICE

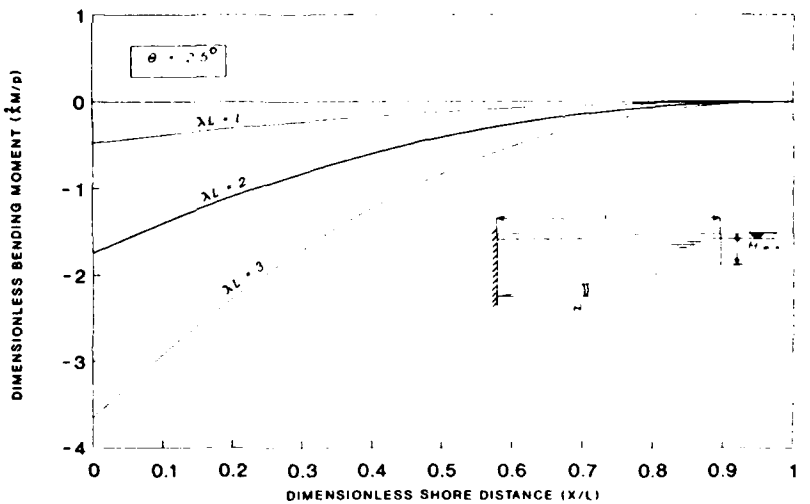

FIG. 16 DIMENSIONLESS BENDING MOMENT FOR FIXED BORDER ICE THICKENED UNIFORMLY

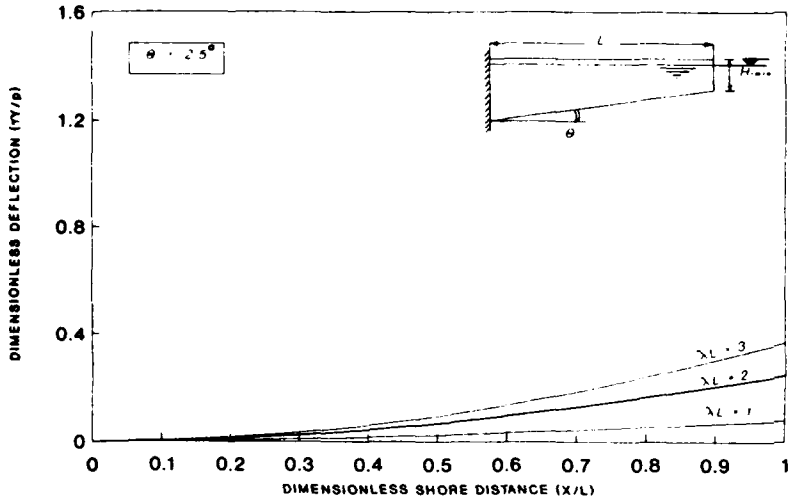

FIG. 17. DIMENSIONLESS DEFLECTION FOR FIXED BORDER ICE THICKENED UNIFORMLY

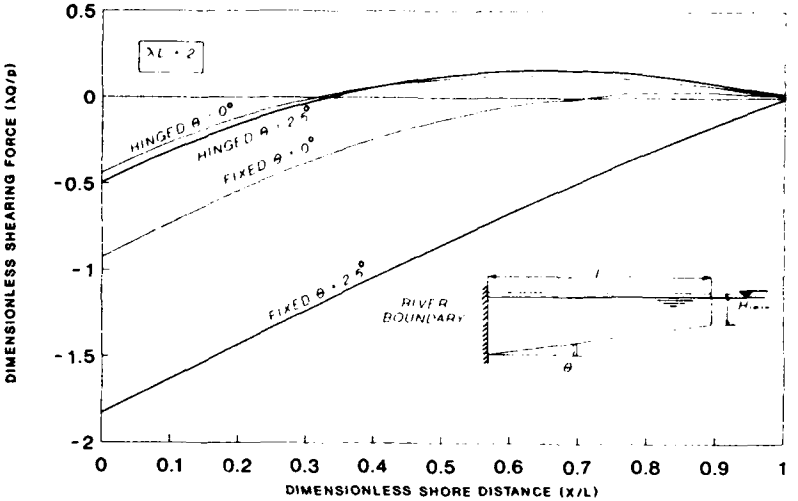

FIG. 18. DIMENSIONLESS SHEARING FORCE FOR BORDER ICE

Microscopic Observations of Snow Deformation

S. SHOOP AND S. TAYLOR

U.S. Army Cold Regions Research and Engineering Laboratory
72 Lyme Road
Hanover, New Hampshire 03755-1290 U.S.A.

ABSTRACT

Snow grains subjected to shearing or compressive forces, or both, were examined with a microscope to explore the conditions that cause melting of grains during snow deformation. Researchers have studied the deformation of snow, caused by wheels, tracks, sliders and skis, but little work has been done on snow deformation at a microscopic scale. This information is useful in defining the processes involved in snow deformation and is applicable to research on vehicle mobility and construction on snow, skiing and avalanches.

Snow samples were deformed using a variety of instruments and studied via thin sections and single grain observations. In general, the sheared zones contained broken grains, crushed material and aggregates of crushed material. Evidence of melting was observed immediately adjacent to sheared surfaces, and when the pressure and temperature conditions were conducive to pressure melting. Snow with large, rounded grains showed changes from deformation most clearly.

INTRODUCTION

Studies on the compressibility of snow (Bader, 1962; Abele, 1967; Colbeck et al., 1978) and on vehicle mobility in snow (Richmond and Blaisdell, 1981) describe the microscopic compression of snow. Compression has also been observed on a microscopic scale by Abele and Gow (1975, 1976). Shearing of snow and ice has also been studied in an attempt to explain the low friction of skis and sliders and how friction changes as a function of temperature and pressure (McClung, 1977; de Montmollin, 1982; Colbeck, 1988; Warren et al., 1989). Water films, generated by frictional heating, are thought to be responsible for the low friction of skis and sliders. Because of the energy expended in melting the snow and the subsequent changes in snow properties, we wanted to see what kinds of conditions and deformations caused melting. We studied the deformation of snow particles, caused by shearing or compression, or both, on a microscopic scale. The results of this research are applicable to studies of the construction of snow roads, vehicle mobility on snow and the interaction between snow and machines.

EXPERIMENTAL METHOD

Our experimental program explored different methods of deforming and observing the snow samples to determine whether melting had occurred during deformation. In addition, to see the results of the deformation more clearly, we tried to produce a snow having round grains of uniform size. Three snow types were thermally cycled at temperatures close to, but below, freezing to produce rounded snow grains through metamorphosis. The first snow type used was tested using a variety on instruments at three coldroom temperatures, –2.2, –3.3 and –4.4°C. Because the more interesting results were observed at the higher temperatures, tests on the next snow type, collected during the spring, were performed primarily between –1 and –2°C. This snow was the best for observing the results of deformation; therefore, most of the testing was done on this snow. Limited tests were performed on the final snow type because of the angularity of the snow grains. The following section describes the preparation of the snow samples, the observational techniques used and the way that the samples were deformed.

Sample Preparation

Using snow with rounded, uniform grains would make it easier for us to distinguish changes in snow grains caused by deformation of the sample from those features present in the undeformed snow. Three types of snow, a dry snow composed of small angular grains, a wet spring snow with rounded grains and grain aggregates, and a drained slush, were placed under conditions designed to cause metamorphosis and produce samples having rounded, uniform grains. All snow was sieved to obtain grain sizes between 0.48 and 2 mm and then placed in plastic or plexiglas sample containers. We found that by gently shaking and tapping the sample containers while adding snow we could regulate the sample densities to within 2%. The samples were then covered and left in a coldroom to metamorphose.

During metamorphism, under low temperature gradients, differences in vapor pressure cause water molecules to evaporate from convex areas of a snow grain and condense on concave areas, thereby producing rounded grains and minimizing the surface area (Bader, 1962; Colbeck, personal communication). In addition, the contact points between snow grains also grow and the snow becomes stronger; in this state it is said to be sintered or age hardened. As the rate at which evaporation/condensation takes place is related to the temperature; the closer the temperature is to freezing the more rapidly this process occurs. Therefore, we tried to create conditions where the snow was near the melting temperature and was subjected to a thermal gradient. The coldroom thermostat was set at either –2.2 or –3.9°C and fluctuated ±1.5°C. Except for tests where the deformation equipment was deliberately set at a temperature different from that of the snow (samples 5, 7, and 10a), all the test equipment and test samples remained in the same coldroom.

Snow 1, a dry snow composed of small angular grains, had been stored in a deep freeze (–29°C) for several years. It was age hardened and had to be broken apart before sieving. Snow 2, a wet spring snow, was collected locally and was composed of rounded grains and grain aggregates. The disadvantage of snow 2 was that it had been thermally cycled in nature and initially contained some aggregate grains and melt features.

Snow 3 was made by adding water to either snow 1 or 2 and placing the resulting slush in a container surrounded by an ice-water bath. In this way the sample was held at a constant 0°C and metamorphism would occur at an accelerated rate. Although this snow was previously sieved and stored, any sintering or aggregate grains formed during storage would break apart in the ice-water bath. After a day, the slush was dewatered by drawing the water through a porous membrane, leaving the grains. As the dewatered slush still had angular grains, it was placed in a sample container and allowed to metamorphose. In general, this snow was not greatly improved over snow 2 and, therefore, was not tested extensively. Examples of the undeformed snow grains for each snow type are shown in Figure 1; the springtime snow has the most uniform and rounded grains.

The snow samples were sized to avoid edge effects during the deformation tests. Although some of the samples had to be quite large (12.6-cm diameter), the majority of the tests were conducted on samples that were between 7 and 8 cm wide (either square or circular in cross section).

a. Snow 1—from old, dry snow stored in a deep freeze for several years.

b. Snow 2—collected during a spring snowfall.

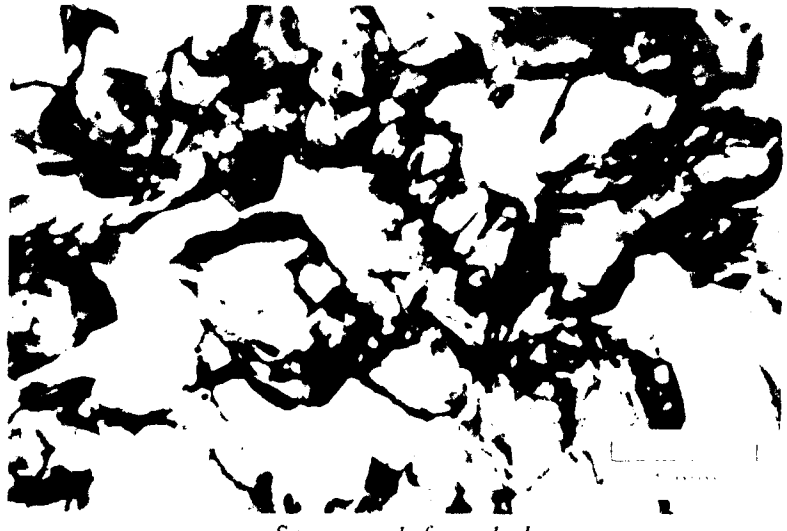

c. Snow—made from slush.

Figure 1. Examples of the three snow types after metamorphosis.

Observational Techniques

Two methods were used to study the snow microscopically. Individual snow grains were examined with a Zeiss monocular microscope and thin sections of the snow were made following the procedures outlined by Watanabe (1974). Thin sections of the deformed snow sample were made by saturating the sample with a mixture of caprylic acid and ethyl cinnamate, which is liquid at temperatures above –8°C. The samples were then placed in a room set at –10°C, allowing the mixture to solidify. After the sample hardened, it was fastened to a glass plate, and sectioned using a microtome. Progressively thinner layers (the last 100 μm were removed a micrometer at a time) were removed until it was thin enough to view the grains under a microscope (50 μm). This was done to avoid disturbing the structure of the snow grains. A few drops of cinnamic aldehyde, added to the thin section, melted the solidified caprylic acid mixture and allowed the structure of the snow to be seen under both plane and polarized light. (Later in this paper, Figure 7 shows one of the sections before the final thinning.) Because it was difficult to maintain the snow structure during the sectioning process, most observations were not made by thin sections, but rather by single grain observations.

For the single grain observations, particles of snow from the deformed area were carefully removed, placed in a small amount of iso-octane and viewed under the microscope. Iso-octane is liquid at low temperatures, immiscible in water, and keeps the small grains from subliming. Snow grains from an undeformed part of the sample were also observed and served as a control. The single grain observations caused less disturbance of the snow grains, were quicker, and the individual grain changes were easier to see.

Deformation Equipment and Procedures

Several instruments were used to produce different kinds of deformation of the snow. A 5-cm-diameter steel cylinder was used to penetrate the snow, creating compression below the piston and shear along the sides of the piston. For the majority of tests, we used a hand-held cone penetrometer because it was easier to use and, as the largest cone was 2 cm in diameter, it required proportionally smaller samples. The penetrometer was used in several configurations (different sized cones, a rubber attachment and the rod with no cone) to produce different types of deformation. Lastly, to produce shear only, samples were held lightly against the side of an operating band saw. A description of each of the test types is given below. Table 1 lists the test conditions and the type of test carried out on each of the samples.

CBR Apparatus

A standard California Bearing Ratio (CBR) apparatus, commonly used in soil mechanics (ASTM, 1989), was used to drive the 5-cm-diameter solid steel cylinder (with a cross-sectional area of 19.4 cm^2) into the sample at a constant speed (Fig. 2). This produces both compression beneath the cylinder and shear along the sides of the cylinder. The piston travel and corresponding load were measured with a proving ring and a dial gauge respectively. The load was recorded at displacement intervals of 25 mm. The piston was lowered until the maximum load on the proving ring was obtained. The entire test (2.54- to 5-cm displacement) was completed in approximately 1 minute.

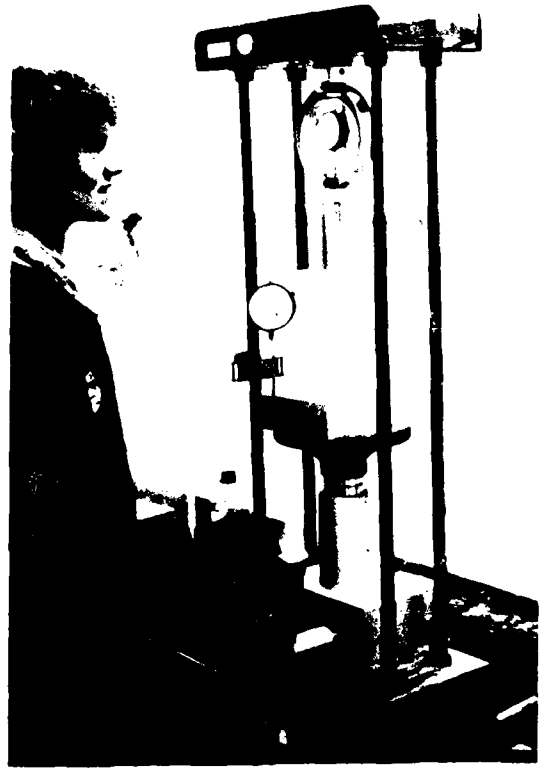

Figure 2. The California Bearing Ratio equipment used to deform snow samples. A steel cylinder is lowered into the sample using a hand crank while the corresponding snow displacement and load are measured.

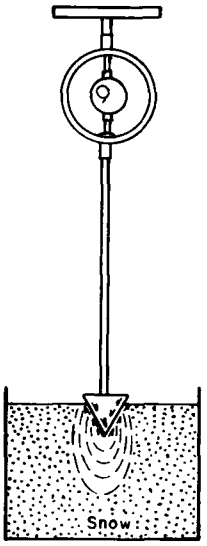

Figure 3. Sketch of hand-held cone penetrometer as used on a snow sample. The device shears the snow along the sides of the cone and compresses the snow beneath the cone.

Cone Penetrometer

Because of its ease of use and the various ways it could be configured, we did most of the deformation tests using a cone penetrometer. The cone penetrometer is also a standard piece of equipment, used for testing soils in the field (ASAE, 1985). The standard cone is 0° and either 1.28- or 2.02-mm in diameter. Penetration is measured along the rod and the corresponding load is measured with a proving ring. When the cone was pressed into the snow sample as shown in Figure 3, it caused both compression beneath the cone and shear along the cone surface. To better examine the effects of shearing alone, we sometimes conducted the tests using the rod without the cone, observing the grains along the side of the rod. The test was further modified to observe the effects of changing 1) the thermal conductivity and 2) the temperature of the penetration instrument. Sample 5 was deformed using a rubber attachment on the rod to see what effect a material with lower thermal conductivity had on the deformation (compared to the standard metal cone). Sample 7 was deformed using a warm cone to see the effects of thermal melting. The temperature and type of test are listed in Table 1.

Table 1. Snow sample specifications and type of test performed on each sample.

Sample ID	*Sample cross section (cm)*	*Sample vol. (cm^3)*	*Initial density (g/cm^3)*	*Length of metamorphosis (days)*	*Final density (g/m^3)*	*Temperature (°C)*			*Test type*
						Room	*Snow*	*Instrument*	
Old Snow (Snow 1)									
1	12.6 dia	1889	0.519	14	0.526	–2.2	—	—	CBR
2	12.6 dia	1889	0.524	18	0.542	–2.2	—	—	CBR
2a	12.6 dia	—	0.524	40	0.542	–3.3	–6.3	–4.2	Penetration (rod only)
3	8.2×8.2	375	0.514	21	0.527	–4.4	–4.3	–4.2	CBR
4	8.2×8.2	381	0.506	21	0.505	–4.4	–4.3	—	Cone penetration
5	8.2×8.2	380	0.483	21	0.476	–4.4	–4.3	+4.2	Rubber attachment on rod
6	8.2×8.2	379	0.476	23	0.474	–3.3	–6.3	–4.2	Penetration (rod only)
7	8.2×8.2	382	0.455	81	0.460	–2.1	–8.3	+9.4	Cone penetration (warm)
Spring Snow (Snow 2)									
10	8 dia	461	0.576	34	0.572	–1.4	—	—	Penetration (rod only)
10a	8 dia	—	0.576	70	0.572	–9.9	–9.5	–10.0	Band saw (short)
10a	8 dia	—	0.576	70	0.572	–9.9	–9.5	–9.3	Band saw (long)
11	8 dia	447	0.594	38	0.588	–1.8	—	–1.9	Penetration (rod only)
12	6.9 dia	285	0.594	42	0.623	–0.7	—	–1.3	Cone penetration
13	7.3 dia	318	0.586	42	0.636	–1.4	—	–1.4	Cone penetration
13a	7.3 dia	209	0.586	70	0.636	–1.5	–1.4	–1.5	CBR
14	7.3 dia	316	0.613	51	0.615	–1.5	–1.4	–1.6	Cone penetration
15	7.3 dia	319	0.587	51	0.575	–1.4	–1.9	–1.7	Cone penetration

Band Saw

To shear the snow sample with a minimum of compressional force (unlike the CBR and the cone penetrometer), a flat sample surface was lightly held against a band saw for a short test (1–5 seconds) or a long test (1 minute). The results of these tests were observed by single grain observations in the area of interest. For comparison, many grains were observed from the deformed areas as well as from an undisturbed area.

RESULTS AND DISCUSSION

CBR Deformation

The load and displacement curves for samples 1 and 2, deformed using the CBR, are shown in Figure 4. Sample 1 was loaded to 1254 N, near the limit of the proving ring, and sample 2 was loaded to 703 N, at which point the sample container broke. Sample 3 was tested at a lower temperature and because the snow was well sintered, the cylinder did not measurably penetrate the sample. Similarly, sample 13a, the undisturbed portion of sample 13, was also impenetrable using the CBR apparatus.

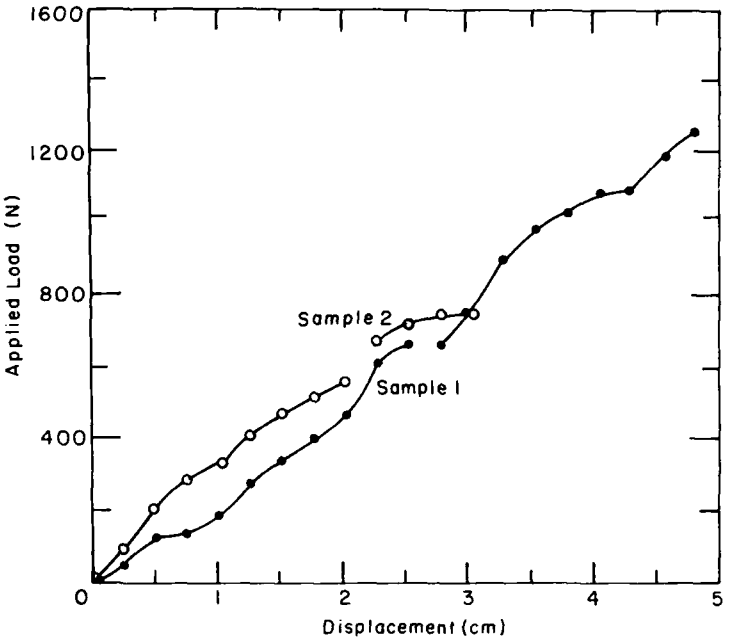

Figure 4. Displacement vs corresponding load generated using the CBR device on snow samples 1 and 2. While sample 2 was being deformed, the sample container broke prematurely.

Samples 1 and 2 were both tested when the snow and the equipment were close to –2.2°C. The deformation of sample 1 resulted in the formation of an ice bulb directly below the piston. The sample was cut in half and sectioned so that the geometry of the ice could be seen (Fig. 5). Because a lower load was applied to sample 2, the snow under the piston did not turn into ice, but was compacted under the piston. For both samples 1 and 2, the geometry of the ice bulb (sample 1) and compacted zone (sample 2) closely resemble the stress contours created by the load applied by the CBR device. Figure 6 shows the nature of the stress distribution caused by a load ap-

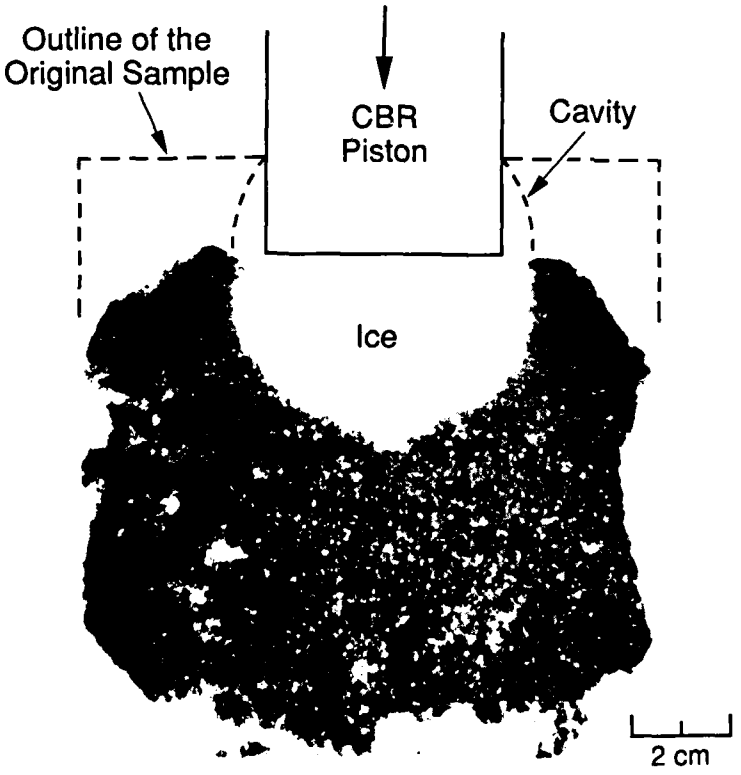

Figure 5. Section of sample 1 before final thinning, showing the ice bulb formed below the CBR piston. The upper part of the sample was destroyed during the sectioning process but is drawn in for reference.

plied by a plate as calculated using the Boussinesq equations for soil, and as measured in snow by Stehle (1970).

The ice bulb, which extended roughly 3.75 cm below the piston, was caused by the effect of pressure on the melting temperature of ice (Hobbs, 1974). The decrease in the melting temperature of ice δT (°C), caused by pressure P (kPa), can be calculated from the Clausius–Clapeyron equation:

$$\delta T = P\ (0.0000738\ ^{\circ}\text{C/kPa})\ .$$

To cause a 2.2°C decrease in melting temperature for these experiments would require a pressure of 29,810 kPa. In sample 1, the applied stress was 646 kPa so, using Figure 6, the stress at the base of the ice bulb would be approximately 23 kPa. If we assume the grain contact area is very small (100^{th} of the grain surface area), then the applied stress is adequate for melting the snow grains. This may be one of the processes involved in the ice bulb formation.

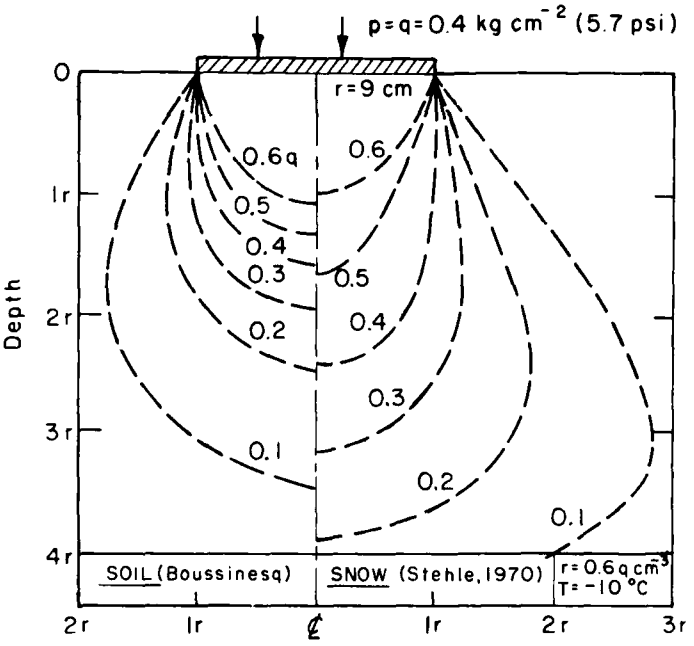

Figure 6. Measured stress distribution generated below a rigid plate on 0.6-g/cm³ snow as compared with that calculated using the Boussinesq equations for soil (after Abele, 1990).

A cavity was formed around the piston in both samples 1 and 2, as seen in Figure 7 and sketched in Figure 5. We think that the snow grains within the spherically shaped pressure zone, as indicated by the stress distribution pattern (Fig. 6) and our experiments, are compressed and adhere together. As the cylinder is driven further into the snow, the entire bulb-shaped compressed zone moves with it, leaving the curious void around the cylinder.

On both samples 1 and 2, there was some melting around the lip of the cavity (near the sample surface) and the sample refroze to the metal piston. This melting was very localized and the snow just a few grain diameters away appeared unaffected by the deformation.

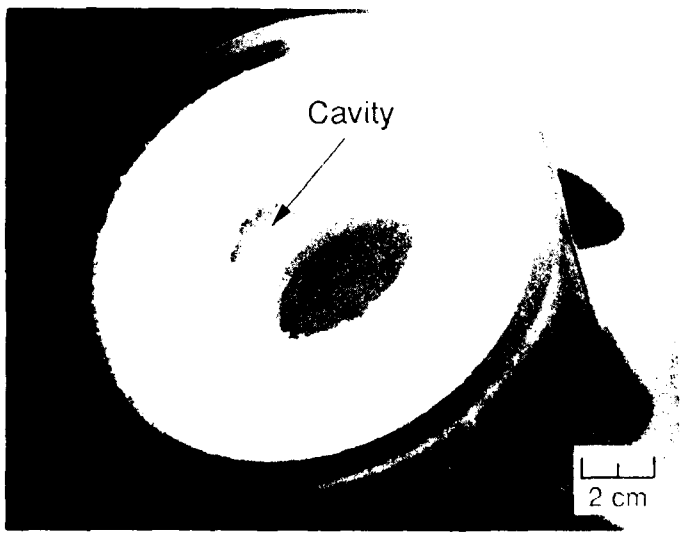

Figure 7. The deformation of samples 1 and 2 generated a cavity along the side of the CBR piston that was thought to have formed as the bulb of compressed snow was pushed further down into the snow sample.

Cone Penetrometer

The cone penetrometer both sheared and compressed the snow grains. Those grains removed from the side wall next to the cone were found to be smaller and more angular than those grains removed from undisturbed sections (Fig. 8). The large number of small angular particles, often adhering to large grains, are thought to be the result of mechanical crushing of the grains. The compressional force exerted on the snow by the cone attachment on the penetrometer also tended to produce aggregates of melted and

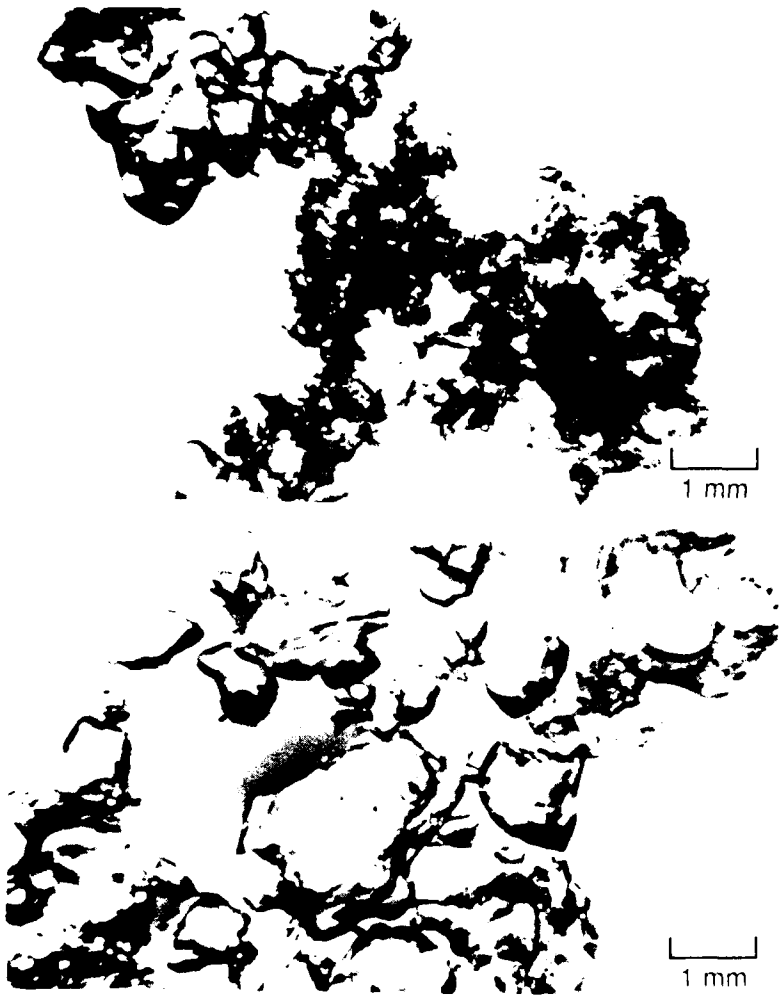

a. Grains from the shear zone.

b. Snow grains from an undisturbed part.

Figure 8. Sample 13.

Figure 9. A grain from a shear/compressional zone (sample 13). The flat side was next to the penetrometer. The grain is made up of small fragments that have been frozen together.

crushed material (Fig. 9). In general, grains taken from this shear/compressional zone tended to be melt aggregates with incorporated crushed material, not the delicate melt structures mentioned below. We saw no additional evidence of melting when the cone was rotated in the snow rather than simply pushed into the sample.

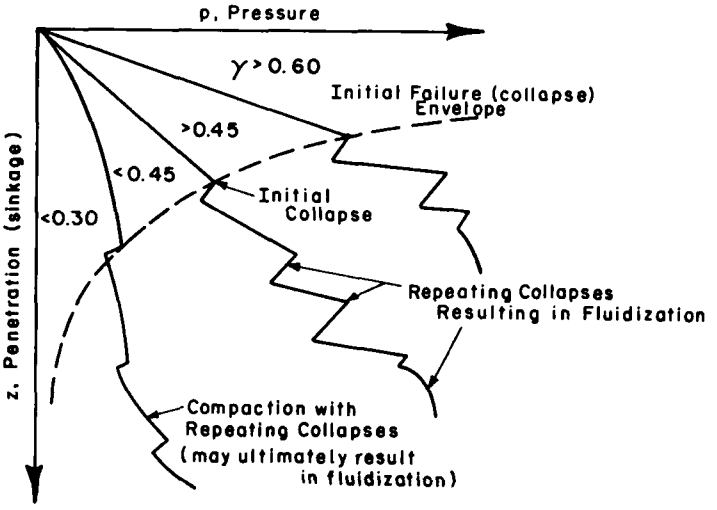

Figure 10. Progressive collapse response of snow to an applied load (after Abele, 1967).

Although the cone is equipped with a proving ring so that the applied load could be monitored (similar to the CBR tests), most of the samples failed in a progressive collapse mode, as is often the case in snow (Abele, 1967). In progressive collapse failure, the stress in the sample increases without failure until, suddenly, the snow collapses. The stress again increases until another collapse, and so on, as shown in Figure 10. This progressive collapse behavior interfered with observing the sheared surface along the penetrometer since much of the shear zone is destroyed during the collapse. To alleviate some of the compressional forces, and the destruction of the sheared particles, the cone was removed from the penetrometer rod and only the rod was pushed into the sample. This way, although progressive collapse occurred, the snow being sheared along the side of the rod was still intact. The grains found adhering to the metal penetrometer rod had flat surfaces with "lips" (Fig. 11), indicating that there was melting immediately adjacent to the rod, probably caused by friction or slight differences in the temperature between the rod and the snow, or both.

A rubber stopper was attached to the rod to determine if a material with a lower thermal conductivity would change the results. The snow grains deformed by the stopper were not noticeably different from those deformed with the metal penetrometer. This may be because of the the short duration of the test and the rapid collapse failure of the snow. To assure thermal melting, sample 7 was deformed with a warm cone. The result was a 1-mm thick, welded, conical snow structure formed around the cone.

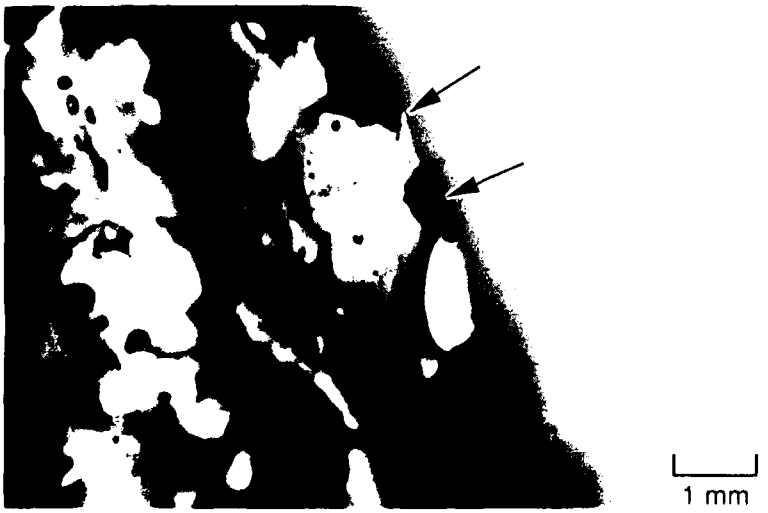

Figure 11. Grains adhering to the penetrometer rod showed delicate melt features such as these "lips" (sample 10).

Figure 12. The disc shaped "hat" found in an undeformed part of sample 12 may have been formed during the storage of the snow, which was collected wet.

Although crushing was seen in all the deformed samples, unambiguous evidence of melting was difficult to find except immediately adjacent to the device. In addition, delicate melt-like structures termed "hats" (Fig. 12) were found in the undeformed portion of the samples and confounded our search for melt features produced by deformation. These "hats" may have formed during the storage of the snow, which was wet when collected.

Band Saw

To create shearing while minimizing compressional forces and to avoid the collapse type of failure, sample 10a was held lightly against a running band saw blade. Two tests were made, one for approximately 5 seconds and one for 1 minute. Both tests generated very flat, shinny surfaces with asymmetrical "hats" or "lips" bridging grains together (Fig. 13). These features indicate that melting took place. The band saw was located in a room set at –10°C and the temperature of the saw blade was measured immediately after each test (Table 1). Since the

Figure 13. Flat surfaces and asymmetrical overhanging lips were seen when snow grains were subjected to shear forces from a band saw (sample 10a).

temperature was below –9°C, melting would be caused by heat of friction rather than the temperature of the device or pressure melting. The microscopic observations of the grains from the long and the short test looked essentially the same. To the eye, however, the surface exposed during the long test appeared smoother and shinier, indicating more melting.

SUMMARY AND CONCLUSIONS

Snow samples were deformed using a variety of instruments and methods at different temperatures to assess what type of deformation and conditions cause melting of the snow grains. After each deformation test, the samples were examined under a microscope, either in thin section or using individual grains taken from the sample. Of the observational techniques tried, looking at individual grains removed from the sheared surface proved the easiest and also the most informative. Of the three snow types tested, the snow that was collected during a spring snowfall (snow 2) had the most uniform, rounded grains.

In all of our tests, we found evidence for mechanical crushing of grains. A compressional force, like that exerted on the snow by a cone attachment on the penetrometer, tended to produce aggregates of crushed and melted material (Fig. 8 and 9). Immediately adjacent to the deformation instrument there is evidence of melting of the grains, and sometimes the snow would melt and refreeze on the equipment. Shearing in the absence of compressive forces was found to make very flat surfaces with melt "lips" (Fig. 11 and 13). Such localized melting would not have a great influence on the performance of machinery on snow unless the snow refroze to the equipment, as it sometimes did on our equipment, causing it to accumulate and clog.

Substantial melting occurred when large compressional forces were applied (in samples 1 and 2) or when the equipment was above freezing (sample 7). The cavity and ice bulb formed during the CBR tests at temperatures near –2°C may illustrate what happens when warm snow is compacted by vehicles or machinery. This process can be tested in the field by observing the deformation pattern as a vehicle passes and by taking samples of the deformed snow for microscopic observation. On the other hand, when older snow was tested at lower temperature (using the CBR device), no substantial deformation resulted. What was observed in the lab, although of a preliminary nature, indicates that substantial differences in vehicle and machine performance may occur, depending on whether the snow is warm (above –2°C) or cold.

Our greatest difficulty was obtaining a snow consisting of well-rounded and uniform, single grains. Snow 1 remained angular and nonuniform, even after having been left to metamorphose for months, at temperatures hovering just below 0°C. The angular and irregular nature of the snow grains made it difficult to see the effects of the deformation on the grains of snow 1. The spring snow (snow 2), because of its large, round grains, most clearly showed changes that occurred along the shear zone. However, the presence of "hats," which look like melt structures, in undeformed sections of the sample confounded our search for melt features produced by deformation. The origin of the very delicate "hat" structures seen in the undeformed parts of the spring snow sample is not understood but may have resulted from storing the wet snow. In general, however, grains taken from the shear zone tend to be melt aggregates with incorporated crushed material and not these more delicate structures. Future work should include devising a reproducible test snow.

ACKNOWLEDGMENTS

We thank Mr. Paul Richmond and Dr. Sam Colbeck for their helpful suggestions and three unknown reviewers for their comments.

REFERENCES

Abele, G., 1967, Deformation of Snow under Rigid Plates at a Constant Rate of Penetration. Masters Thesis for Michigan Technological University. Also USA Cold Regions Research and Engineering Laboratory, Research Report 273 (1970).

Abele, G., 1990, Snow Roads and Airfields. USA Cold Regions Research and Engineering Laboratory Monograph 90-3.

Abele, G. and A.J. Gow, 1976, Compressibility Characteristics of Compacted Snow. USA Cold Regions Research and Engineering Laboratory, CRREL Report 76-21.

Abele, G. and A.J. Gow, 1975, Compressibility Characteristics of Undisturbed Snow. USA Cold Regions Research and Engineering Laboratory, Research Report 336.

ASAE, 1985, Soil Cone Penetrometer. ASAE Standard: ASAE 313.2, American Society of Agricultural Engineers, St. Joseph, Michigan.

ASTM, 1989, Standard Test Method for CBR (California Bearing Ratio) of Laboratory-Compacted Soils, ASTM Designation 1883-87, Annual Book of ASTM Standards, Section 4, volume 04.08, p. 241–248, American Society for Testing and Materials, Philadelphia, Pennsylvania..

Bader, H., 1962, The Physics and Mechanics of Snow as a Material. In Cold Regions Science and Engineering (F.J. Sanger, Ed.). USA Cold Regions Research and Engineering Laboratory, Cold Regions Science and Engineering Monograph IIB.

Colbeck, S.C., A. Shaw and G. Lemieux, 1978, The Compression of Snow. USA Cold Regions Research and Engineering Laboratory, CRREL Report 78-10.

Colbeck, S.C., 1988, The Kinetic Friction of Snow. *Journal of Glaciology*, **4**(116): 78–86.

de Montmollin, 1982, Shear Tests on Snow Explained by Fast Metamorphism. *Journal of Glaciology*, **28**(98): 187–198.

Hobbs, P.V., 1974, *Ice Physics*. Clarendon Press, Oxford, 837 p.

McClung, M., 1977, Direct Simple Shear Tests on Snow and Their Relation to Slab Avalanche Formation. *Journal of Glaciology*, **19**(81): 101–109.

Richmond, P.W. and G.L. Blaisdell, 1981, A Macroscopic View of Snow Deformation under a Vehicle. USA Cold Regions Research and Engineering Laboratory, Special Report 81-17.

Stehle, 1970, Snow Compaction—Investigation of Metamorphosis of Snow. NCEL Technical Report 706.

Warren, G.C, S.C. Colbeck and F.E.Kennedy, 1989, Thermal Response of Downhill Skis. USA Cold Regions Research and Engineering Laboratory, CRREL Report 89-23.

Watanabe, 1974, A Method of Making Thin Sections of Deposited Snow by Mixed Solution. *Journal of the Japanese Society of Snow and Ice*, **36**(3).

What Makes a Good Snow Fence?
Results From 12 Years of Testing at the Ontario Ministry of Transportation

M. S. PERCHANOK

Ontario Ministry of Transportation
1201 Wilson Avenue
Downsview, Ontario M3M 1J8, Canada

ABSTRACT
A variety of new types of snow fences were introduced in the late 1970's and early 1980's, providing more possible ways to effectively and economically control drifting snow on highways. The Ontario Ministry of Transportation (MTO) began investigations in 1978 to determine whether the new products offered advantages over the standard wood slat fence and ought to be considered as alternatives to it.

Seventeen products were tested including vertical slats (wood and metal), polyethylene lattices, polyethylene, polyester and nylon nets, and horizontal straps of polyester and fabric.

No significant differences were seen among the fence types in the proportion of drifting which they intercepted nor the maximum volume of snow which they trapped. The vertical wood slat fence was superior to the other fences in terms of overall handling and installation properties and annual cost of use, and both the wood and metal slat fences performed best in the overall evaluation of durability.

The analysis also identified a minimum value of tensile strength (450 kg) and a maximum elongation (0.6% per kg of applied load) which should be met by snow fence materials.

INTRODUCTION
The Ontario Ministry of Transportation (MTO) has used snow fences for many decades to minimize localized visibility problems and snow accumulation due to drifting on highways. MTO typically erects snow fences on private land because the standard highway right of way is too narrow to permit accumulation of a snow drift without impinging on the road shoulder and pavement. The private land in most cases is used for agriculture, dictating that fences must be removed during the short period between spring snowmelt and crop planting, and reinstalled between harvesting and the first expected snowfall. This requires a large expenditure in labour as well as increasing the handling and consequent wear of fence materials.

A variety of synthetic snow fences were introduced to the market in the late 1970's and early 1980's which were believed to offer more effective and economic snow control. MTO began a testing program to determine whether any of the new types had advantages over the standard wood slat fence. Advantages would be accrued if alternative fences lasted longer, could be installed with less manpower, trapped more snow or stored the same volume of snow in a shorter drift which does not encroach on the road.

This paper reports on the findings of investigations over the period 1978-90 into the snow trapping capabilities, handling and durability properties, and the cost of a variety of new snow fence products.

TEST MATERIALS AND SITES

Fence types included in the MTO test program fall into four categories (Table 1):

* vertical slat (wood, metal)
* horizontal slat (polyester, impregnated fabric)
* lattice (polyethylene)
* net (polyester, polyethylene, nylon).

This includes the standard snow fence used at MTO (MTO, 1977) which is a vertical picket made from 3.8 cm (1.5 in) wide by 1.2 m (4 ft) long wood slats joined together by twisted wire. For comparative purposes the products are identified in Table 1 using a letter code.

MTO's tests were conducted at five locations in central Ontario: Cookstown, Barrie, Mount Forest, Horning's Mills, and Stayner. Fences were erected on private land outside of the highway right of way as part of the normal winter maintenance program. Site selection criteria included flat, featureless land with consistent ground cover and unobstructed wind fetch.

At each site, wood slat fences were installed adjacent to the test fences to provide a standard for comparison. All test fences were erected with a 20 cm bottom gap on steel T-posts or U-flange, following manufacturer's instructions for attaching the fence to the posts.

Table 1/ Snow Fence Evaluation Program

Type	I.D. Code	Height (m)	Material	Years Tested	Total
Vertical Slat	a	1.2	wood	all	12
	b	1.8	metal	81	1
Lattice	c	1.2	polyethylene	86, 87, 88	3
	d	1.2	polyethylene	81, 84, 85, 86, 87, 88, 89	7
	e	1.8	polyethylene	84, 85, 86, 88, 89	5
	f	1.2	polyethylene	86, 87, 88	3
	g	1.2	polyethylene	89	1
	h	1.0	polyethylene	79, 81, 84, 88	4
	i	1.2	polyethylene	86, 87, 88, 89	4
	j	1.2	polyethylene	81	1
Net	k	1.2	polyethylene	89	1
	l	1.2	nylon	78, 79	2
	m	1.2	polyester	83	1
Horizontal Slat	n	1.2	polyester	86, 87, 88	3
	o	1.8	polyester	88	1
	p	1.2	impregnated fabric	88	1
	q	1.8	impregnated fabric	88	1

APPROACH

The fences were evaluated using five general factors: installation and handling, durability, drift capacity, fence efficiency, and overall cost. The following sections describe the specific approaches used in the comparisons.

Installation, Handling and Durability

The first procedure was to identify the qualitative factors which affect the ease of fence erection and susceptibility to material damage from operational and environmental loads. These were identified through discussions with snow erection crews and direct experience. The factors relating to installation and handling include unrolling, joining sections, tensioning, alignment, attaching, bending and handling safety. Stretching, sagging, abrasion and breaking were used to evaluate overall durability. The factors are described in detail in a later section. The fences were given a positive or negative score on each of the factors based on operational experience during the trials, and the scores were summed to give an overall product comparison.

The second procedure was used to provide a quantitative measure of fence tensile strength requirements during installation procedures. Experience showed that certain lattice-type fences broke while being tensioned for installation. As shown

in Figure 1, one end of a section of fence was fixed to a post. The other end was fastened to a proving ring and then tensioned using a truck or loader. The load was increased in steps and read from a dial gauge on the proving ring until the fence failed. The rate of load application was not measured but corresponded with typical operating conditions at MTO.

The third procedure of the installation and handling evaluation was a task analysis, comparing the manpower required to install a standard, 60 m section of each fence. Fence installation was divided into identifiable manual tasks and the time and number of persons required to perform each one was estimated. Manpower loadings were not directly measured but were estimated after observation of several installations, making adjustments for unrelated logistical delays.

Stretching and sagging were observed to impact strongly on the durability of a fence and material elongation was used as a quantitative measure of durability. This involved measuring the length of the top and bottom edges of the fence with a steel tape during the tensile strength tests as lateral tension was increased (Figure 1). Elongation was calculated as the vertically averaged percent increase in fence length per kilogram of applied load.

Finally, observed fence performance was used to estimate the expected useable lifespan of each type.

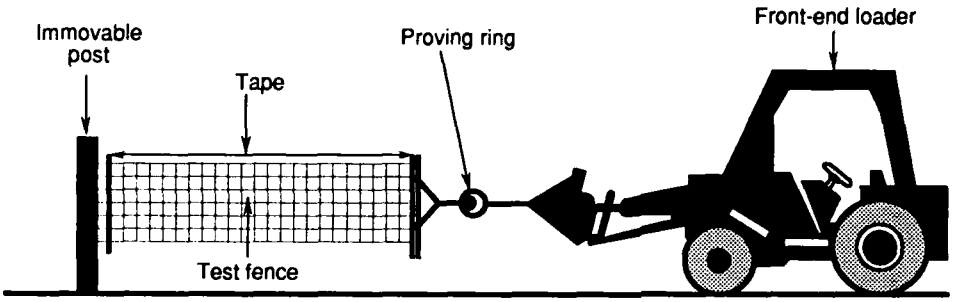

Figure 1/ Set-up for tensile strength and elongation tests

Drift Capacity

Previous studies suggest that snow drifts reach a stable maximum volume determined by the height, porosity and geometry of the snow fence or barrier (Tabler, 1980; 1990). These effects were investigated by measuring the cross-sectional area of the maximum drift attained in each season. Area was measured either by repeated level surveys or by measuring snow height against graduated rods which were driven into the ground at set distances perpendicular to the fence.

Fence Efficiency

Fence efficiency refers to the proportion of the total snow flux between the ground surface and the fence height which is captured by the fence and thus prevented from drifting onto the highway.

It was not possible to measure the actual snow flux at the test sites. Instead, snow captured by each test fence was compared with that captured by adjacent wood slat fences. It was assumed that all wood slat fences have a similar efficiency and provide a suitable standard for comparison. This approach minimizes differences arising from variations in snow flux between sites.

Prior to 1988, data were obtained only for the winter maximum snow drift, but in the 1988/89 and 1989/90 seasons, measurements were obtained on a snow drifting event basis when possible and at least weekly through the winter period. Prior to analysis of the latter seasons, periods having adverse weather conditions in which snow drifts melted or snow was redistributed along the fence rows were removed from the record.

Cost
The overall cost of the fences was compared by calculating a Total Annual Cost (TAC) which includes the purchase cost, the expected longevity and the annual installation cost, as

$$TAC=AIC+ACC,$$

where the annual installation cost (AIC) is the estimated manpower requirement to install a 60 metre (100 foot) section of fence multiplied by the labour rate, and the annual capital cost (ACC) is the purchase price per 60 metre section divided by the fence lifespan (L). L was estimated from the results of the durability analysis as described below.

RESULTS
Installation and Handling
The first part of this analysis involved developing a list of the qualitative factors which impact on the skill, dexterity or time taken to install a fence.

These are described below.

Unrolling: A positive score on this factor indicates that the fence lay flat on the ground after unrolling and prior to lifting against the fence posts. A negative score indicates that the ends of the fence tended to re-roll unless weights or extra people were used to hold them down.

Stiffness: A positive score on this factor indicates that the material stood on its own when raised against the fence posts prior to tensioning. A negative score indicates that it collapsed unless held against the posts. This required additional people to position the fence during tensioning.

Joining: A positive score on this factor indicates that adjacent sections of fence material could be joined either with wire ties or by weaving a 2.5 x 5 cm (1x2 in) wooden slat through the voids of overlapped sections. A negative score indicates that the voids were too small or the fence too stiff to do this easily. This size slat was found by experience to be the smallest which will not break under tensioning load.

Tensioning: A positive score on this factor indicates that a 30 metre section of fence could be tensioned laterally to the point that there was no visible catenary. A negative score indicates that the fence ribs broke before full tensioning of a 30 metre section. In such cases either the fence could not be fully tensioned or it had to be tensioned in shorter sections, which was more time consuming.

Alignment: A positive score on this factor indicates that wire-ties could be inserted through voids in the fence and around the fence post without having to align the post to the voids. A negative score indicates that fence and posts had to be carefully aligned for wire-ties to be inserted without damaging the fence. This was typical of fences with small voids.

Attachment: A positive score on this factor indicates that the fence could be attached to the post with simple wire-ties. A negative score indicates that the fence had first to be sandwiched between wooden slats to avoid the fence being cut by the ties. This was true for all fences of synthetic material.

Bending: A positive score on this factor indicates that the fence material would bend along its length, conforming with rolling topography. A negative score indicates that it did not bend and this resulted in variations in the gap between the fence and the ground.

Handling Safety: A positive score on this factor indicates that the fence edges would not easily cut bare hands, and a negative score indicates that they would.

The scores attained by each fence are shown on Table 2. The wood slat fence (a) ranked highest on the installation and handling factors, followed by horizontal slat and net materials. A metal slat fence (b) had similar properties to the wood fence except for handling safety. All but two (h) and (i) of the lattice type fences

Table 2/ Snow Fence Handling and Durability Characteristics

Fence	Installation and Handling Characteristics																		Score	Rank	Durability Characteristics								Score	Rank
	1		2		3		4		5		6		7		8		9				10		11		12		13			
	+	-	+	-	+	-	+	-	+	-	+	-	+	-	+	-	+	-			+	-	+	-	+	-	+	-		
a	√		√		√		√		√		√		√		√		√		9	1	√		√		√		√		4	1
b	√		√		√		√		√		√		√			√	√		8	2	√		√		√		√		4	1
c		√		√		√		√		√		√		√	√			√	1	7		√		√		√		√	0	4
d		√		√	√		√			√		√		√	√			√	3	5		√		√		√		√	0	4
e		√		√	√		√			√		√		√	√			√	3	5		√		√		√		√	0	4
f		√		√	√			√		√		√		√	√			√	2	6		√		√		√		√	0	4
g		√		√		√		√		√		√		√	√			√	1	7		√		√		√		√	0	4
h		√	√		√		√			√		√		√	√			√	4	4	√		√			√	√		3	2
i		√	√		√		√			√		√		√	√			√	4	4	√		√			√	√		3	2
j		√	√			√	√		√			√		√		√		√	3	5		√		√		√		√	0	4
k	√			√	√		√		√			√	√		√			√	6	3		√	√			√		√	1	3
l	√			√	√		√		√			√	√		√			√	6	3	—	—	—	—	—	—	—	—	—	—
m	√			√	√		√			√		√		√	√			√	4	4	√			√		√		√	1	3
n	√		√			√	√		√			√		√	√		√		6	3	√		√		√			√	3	2
o	√		√			√	√		√			√		√	√		√		6	3	√		√		√			√	3	2
p	√		√			√	√		√		√		√		√		√		8	2		√	√			√		√	1	3
q	√		√			√	√		√		√		√		√		√		8	2		√	√			√		√	1	3

— *indicates data not available*

List of Characteristics:

1. Unrolling
2. Stiffness
3. Joining
4. Tensioning
5. Alignment
6. Attachment
7. Bending
8. Safety
9. Wind
10. Stretching
11. Sagging
12. Abrasion
13. Cutting

scored poorly on the installation factors, and several were particularly difficult to install because they could not be properly tensioned.

The strength tests shown in Figure 2 corroborate the qualitative evaluation of tensioning. The lattice fences which broke during the tensioning operation, (c), (f), and (g), failed at tensile loads of less than 450 kg, while those that did not break, (a), (i), and (d), had tensile strengths of 450 kg or greater.

It should be noted that the tensile strength and elongation of polyester and polyethylene are temperature sensitive, and tests were performed at only one temperature (30°C). Additional testing should be conducted to extend the results to the range of snow fence operating temperatures.

Results of the task analysis are summarized in Table 3. No distinction in manpower requirements could be made among the different lattice type fences, and with one exception, differences among the other types were minor. Manpower requirements for all of these ranged from 5.1 to 6.6 hours. One brand (n,o) of horizontal strap fence was exceptional, requiring 11.9 hours for installation of a 60 metre section.

Table 3/ Manpower Requirements for Snow Fence Installation *

Fence Type	Total Manhours	%
Vertical Slat		
-wood, metal	6.5	100
Horizontal Slat		
-polyester	11.9	183
-impregnated fabric	6.6	102
Lattice		
-polyethylene	6.2	96
Net		
-polyester, polyethylene	5.1	72

* 1.2 m high, 60 m long section including posts, joins, and braces.

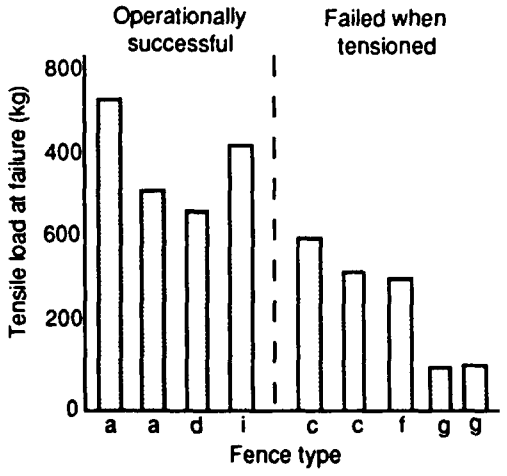

Figure 2/ Snow fence strength limits during tensioning (Ambient temp. 30 °C)

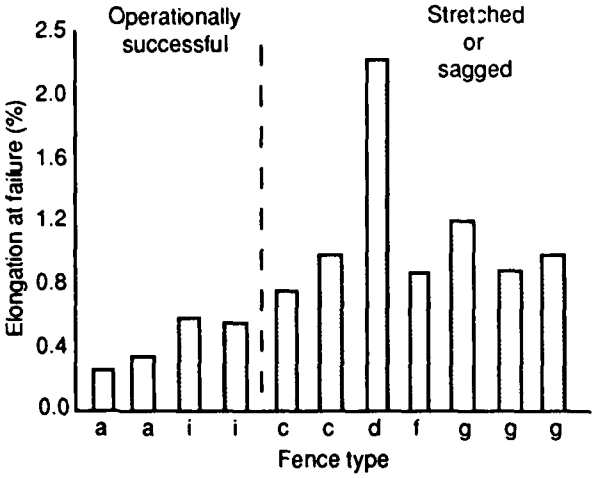

Figure 3/ Snow fence elongation at tensile failure (Ambient temp. 30 °C)

DURABILITY

Four qualitative factors were identified which affect the rate at which fences are damaged by environmental forces or operational incidents (and are assumed to be surrogates for fence longevity under operational use). They are explained below.

Stretching Due to Wind Pressure: A positive score on this factor indicates that the fence was not stretched by wind pressure. A negative score indicates that pressure from the wind stretched the fence, creating a down-wind bulge between posts. This resulted in uneven drifts and in some cases allowed the fence to work loose from the posts, causing permanent deformation and reducing the utility of the fence in subsequent years.

Sagging Due to Snow: A positive score on this factor indicates that the fence shape was not distorted by burying in deep snow. A negative score indicates that it sagged under the weight of overlying snow. The consequences of sagging are similar to those for stretching. In addition, sagging reduced the fence's snow-trapping performance.

Abrasion: A positive score on this factor indicates that the fence material was not affected by winter-long vibrating against the posts or wood slats. A negative score indicates that the fence material was worn thin or roughened where it contacted with fence posts or wooden slats. Synthetic fences frequently failed at points of abrasion and therefore, signs of abrasion were taken as an indicator of a reduced useful lifespan.

Breaking: A positive score on this factor indicates that the fence did not break over the winter season. A negative score indicates that the fence broke due to abrasion or failure in tension.

Table 3 shows the scores attained by each fence. Vertical slat fences ranked highest on the durability factors. The second rank included two lattice fences (h,i) and two horizontal straps (n, o). Most of the lattice fences (c,d,e,f,g,j) were prone to all types of material damage and ranked lowest on durability.

Quantitative measures of fence material elongation corroborated the results of the qualitative evaluations, as shown in Figure 3. Fences which did not stretch or sag, (a) and (i), had measured elongations at tensile failure of 0.6 percent or less per kg of applied load, while those which did sag or stretch, (c) and (d) and (g), had higher elongations.

As noted in the description of tensile testing, properties of the tested materials are temperature sensitive and the tests should be extended to the range of snow fence operating temperatures.

No direct measure of fence longevity could be made because not all fences had the same long-term environmental exposure; however, subjective estimates can be derived from the performances observed during the tests. Patrol personnel observed that wood slat fences last an average of 7 years. Most of the synthetic fences broke and all were abraded during each year they were tested; their performance was unacceptably degraded. Fences which broke in service (c-g,j,k,m-q) were classified as having a useful life of 1 year. Use of fence (b) was also discontinued after one year because of excessive rusting and bending. Fences (h) and (i) have been used for 4 years to date without failing and fences (n) and (o) were used for 3 years before failing: this provided a measure of their minimum useful lifespan. Insufficient data are available to categorize fence (i).

DRIFT CAPACITY

The maximum measured cross-sectional area of drifts of each test fence are compared in Table 4 with the capacity of similar fence types estimated from empirical models by Tabler (1990;1980). While two cases, wood slat (a) and lattice fence (h), show drift volumes close to or exceeding the estimates of drift capacity, no conclusions can be drawn from the data because the values are within the experimental error which is estimated to be +/-10%. In addition, repeated measurements in 1988/89 and 1989/90 suggest that drifts did not fill to capacity during the test program.

Table 4/ Snow Drift Capacity*

Fence Type	Estimated Capacity[1] (m^2)	Maximum Measured[2] (m^2)	(year)	Difference (m^2)
a	29	27.8	1981	-1.2
b	66	26.0	1981	-40.0
c	29	23.0	1986	-6.0
d	29	22.5	1986	-8.1
e	66	26.3	1986	-39.7
f	29	26.0	1986	-3.0
g	29	13.3	1989	-15.7
h	20	22.3	1981	2.3
i	29	23.11	1986	-5.9
j	29	25.4	1981	-3.6
k	X	12.38	1989	X
l	X	21.9	1978	X
n	X	20.9	1987	X
o	X	30.0	1986	X
p	X	11.9	1988	X

1. Tabler, 1980, 1990
2. M.T.O., 1978-1989
X. Unknown

*m2 of drift cross-sectional area per metre of fence length

FENCE EFFICIENCY

Fence efficiency was measured by comparing the volume of snow captured by test fences with that captured by wood slat fences, on both an annual basis and a sample period basis. Annual efficiency is shown in Table 5. One brand of lattice fence (i) had consistently larger drifts than the wood slat fence, averaging 11 percent greater over four years. While data points show other fences which accumulated more snow than wood fence, the inter-annual variability and small number of samples does not permit sound conclusions to be drawn from the annual data.

Trends may also be masked in the annual data by differential snow melt or redistribution prior to drift measurement, and the comparison was therefore repeated using only data from time periods which experienced weather conditions conducive to drift accumulation. Seven or eight sample periods, depending on fence location, were available for comparison in each of 1988/89 and 1989/90 (Table 6).

A Student's 't' test was used to compare the snow accumulation between test fences and wood slat fences on a sample period basis. In both years, the data do not show a significant difference between accumulation at the test fences and adjacent wood slat fences. This conclusion is also true for fence (i) which did have a larger accumulation on an annual basis.

Table 5/ Snow Fence Catch Efficiency

Maximum Drift Cross-Sectional Area as % of Area at 1.2 m Wood Slat Fence

	Fence Type														
Year	**b**	**c**	**d**	**e**	**f**	**g**	**h**	**i**	**j**	**k**	**l**	**n**	**o**	**p**	**q**
1978											124				
1979											52				
1981	115						124		117						
1985			110	113											
1986		95	98		103			102				102			
1987		97	98	112	92			124				96			
1988		98	87	69	90		82	113				87	84	61	71
1989			107	90		83		105		84					
Mean	115	97	100	96	95	83	103	111	117	84	88	95	84	61	71

Note: Fences not necessarily filled to capacity.

Table 6/ Sample Statistics for Snow Drift Cross-Sectional Area

Fence Type (1.2 m)	Year	#. of Samples	Drift X-Section Growth (m^2) Mean		Variance		Student's 't'
			Test Fence	Wood Fence	Test Fence	Wood Fence	
c	1988/89	7	2.8	2.9	4.4	4.2	.07
d	1988/89	7	2.6	2.9	1.4	4.2	.29
d	1989/90	8	1.9	2.9	5.1	22.7	.28
f	1988/89	7	2.6	2.4	2.6	1.7	.23
g	1989/90	8	2.1	2.4	15.6	22.7	.07
h	1988/89	7	1.9	2.2	1.2	1.1	.53
i	1989/90	7	2.6	2.1	19.8	18.3	.12
k	1989/90	8	2.9	2.3	19.0	8.6	.23
n	1988/89	8	2.5	2.4	1.9	1.6	.15
p	1988/89	8	2.0	2.4	2.0	1.6	.57

Notes:
1. Sample periods with adverse weather conditions are excluded.
2. Variance is the best estimate of population variance based on the sample (Gregory, 1963).
3. Student's 't' statistic:

$$t = \frac{|\bar{a} - \bar{b}|}{\sqrt{\frac{\hat{\sigma}^2}{n_a} + \frac{\hat{\sigma}^2}{n_b}}}$$

4. The difference between samples is statistically significant at 95% confidence level if the 't' statistic exceeds 2.365 for 8 samples or 2.447 for 7 samples (Cangelasi, Taylor, and Rice, 1976).

COST

The cost analysis shown in Table 7 used the manpower requirement for installation (Table 3), the purchase price and the estimated lifespan (see above) to estimate a Total Annual Cost for each fence, where data were available.

Table 7/ Snow Fence Life Cycle Cost*

Fence	a	b	c	d,e	f	g	h,i	j	k	l	m	n,o	p,q
AIC	100	100	96	96	96	96	96	96	72	72	72	183	102
L	7	1	1	1	1	1	4	1	1	1	1	3	1
ACC	100	-	1094	1465	1394	-	380	1794	776	-	-	439	-
TAC	100	-	273	340	327	-	146	399	203	-	-	229	-

* Costs in each row are expressed as a percent of the cost for fence (a) per 60 m section of 1.2 m tall fence, installed

AIC = Annual Installation Cost, proportional to Manpower Requirements (Table 3)
L = Expected Lifespan (years)
ACC = Annual Capital Cost; Cost / Lifespan
TAC = Total Annual Cost; sum of AIC and ACC

- data not available

Total annual cost varied by a factor of 4 among the fences. The wood slat fence (a) provided the lowest TAC and the lattice fence (j) the highest. Type (h,i) lattice fence was significantly lower than others in its class because of its greater estimated lifespan. The analysis clearly shows the importance of durability in determining the cost of using different types of snow fence.

CONCLUSIONS AND DISCUSSION

Nine factors were identified which affect the ease of installation and handling of snow fences. Overall, the standard wood slat fence was easier and safer to install than the other fence types. This conflicts with manufacturers' claims that synthetic fences, being lighter, are easier to handle and install. Field experience has shown that this benefit is countered by sharper edges, lower tensile strength, additional installation materials and other factors. In addition, typical MTO practice of trucking the materials to the installation site negates the benefit of reduced material weight. Synthetic fence would, however, rank higher in situations where the materials must be carried by hand.

One of the installation factors, tensioning performance, was related to a measurable material property. The measurements indicate that fence materials which can withstand a tensile load of 450 kg or greater will withstand the tensile force typically exerted during installation procedures used by MTO. Only one of the lattice type fences tested met this criteria.

The effort required to erect snow fences averaged about 6 person-hours for all but one fence type. The exception, type (n) horizontal strap, required twice the effort of the other types.

Four factors were identified which affect the durability of snow fence. According to these factors only the metal fence (b) was as durable as wood slat.

Measurements of fence elongation at tensile failure corroborated the observed performance of sagging or stretching. Fences which had elongation of less than 0.6 percent per kg of applied load at tensile failure did not experience sagging or stretching due to environmental forces. Only one of the synthetic materials tested (h,i) achieved this performance.

High incidences of abrasion and breaking were observed on most of the synthetic fences and as a consequence their estimated lifespan was very low. This is in conflict with the manufacturers' estimate that the fence's longevity exceeds that of wood fences. The primary reason for the short lifespan shown in this study was either abrasion to the point that the fence failed during tensioning or cutting by wire-ties or sharp post edges during the winter season. This indicates that even if the material is immune from chemical weathering or deterioration, its useful life is

governed by its susceptibility to cutting or tearing. Synthetic fences cannot be easily repaired after installation, and a break or tear during the field season creates an unacceptable highway safety hazard.

Insufficient data were collected to compare the drift capacity of the fences tested. Information in the literature suggests that fences with similar height and void ratio have similar capacities. It is concluded that so long as porosity is similar, similar total drift capacity can be expected for wood slats and the other fences tested.

Statistical comparisons of fence efficiency also showed no significant differences between wood slat and the various fences tested and it can be concluded that similar efficiency can be expected of wood slats and other fences which have similar height and porosity.

Annual costs varied widely among fences, but all were greater than the standard wood-slat fence.

Considering all the factors investigated, none of the alternative fences provided a clear advantage over the wood slat fence and many of them exhibited significant disadvantages in terms of handling, durability and cost. Two types of synthetic fences (h,i) had similar performances to the wood slat fence on these factors. In terms of snow-trapping capacity and efficiency, the data suggest that wood slat and alternative fences of similar height and porosity perform equally well.

ACKNOWLEDGEMENTS
Data collection and analysis prior to 1988/89 was directed by J. Gruspier, P.Eng. (ret), assisted by D. Wong, P.Eng.. Data were collected with assistance from M.T.O. Patrolmen at Barrie, Cookstown North, Mount Forest, Shelburne and Stayner, and field assistants S. McFarlane, D. Beach, A. Murray, W. Platt and D. Robertson. Dr. D. Manning and Mr. J.J. Armstrong critically reviewed a draft of this paper.

REFERENCES
Cangelasi, P.H., H. Taylor and P.F. Rice, 1983. Basic Statistics: A Real World Approach. West Publishing Company, New York.

Gregory, S., 1973. Statistical Methods and the Geographer. Longham Group Limited, London.

M.T.O., 1977. Standard J2244, Snow Fence. Purchasing, Sales and Distribution Office, Ontario Ministry of Transportation.

Tabler, R.D., 1990. Snow Control Course Notes. Tabler and Associates, Niwot, Colorado.

Tabler, R.D., 1980. Geometry and Density of Drifts Formed by Snow Fences. Journal of Glaciology 26(94), 405-419.

Ice Detector Measurements of Atmospheric Icing on a Cable

P. MCCOMBER
Ecole de Technologie Supérieure
4750, Henri-Julien
Montréal, Québec H2T 2C8, Canada

J. DRUEZ
Université du Québec à Chicoutimi
555, boulevard de l'Université
Chicoutimi, Québec G7H 2B1, Canada

M. ST-LOUIS
Hydro-Québec
855 est, Sainte-Catherine
Montréal, Québec H2L 4P5, Canada

ABSTRACT

Atmospheric icing is an important cause of damages to structures and power transmission lines in northern Quebec. An icing test line was set up on Mt. Valin (alt. 902 m) near Chicoutimi to measure icing loads on the type of stranded cables used on transmission lines. Measurements of icing loads on a 100 m span stranded cable are obtained from the cable end tension. An ice detector which counts icing detection alarm cycles per unit time is used to measure the icing intensity. Average wind speeds, directions and temperatures at the study site were also recorded.

A detailed study of a few icing events was made in order to relate the icing rate, as measured by the ice detector, with the cable icing rate. Two types of icing events can be distinguished from the range of the ice detector data. Freezing precipitation is associated with significantly higher icing intensities than cases in which only in-cloud icing occurs. Different calibration curves for icing rates of the ice detector were developed to predict cable icing for these two types of events.

The cable icing rate is derived by taking into consideration the accretion size, wind direction and collection efficiency. Results indicate that in most events, the ice detector data can be used to predict ice loads on transmission line cables with an average error of only 2.6 percent per hour. Predictions are generally more accurate at lower icing rates.

INTRODUCTION

Atmospheric icing is an important cause of damages to stuctures and power transmission lines in northern Québec. Due to the topography, it is not possible for the power transmission lines to reach the southern markets without going through mountains for substantial distances. In these mountains, clouds are frequently found above a altitude of 300 m (984 ft) and in-cloud icing will occur with increasing frequency above that altitude and is therefore a hazard for the transmission lines.

Measurements of atmospheric icing on power transmission lines have been made to study the frequency and severity of rime loads (Diem, 1956). Field measurements have been obtained by instrumenting experimental cables located in areas where icing is frequent (Govoni and Ackley, 1983; McComber and Govoni, 1985; Smith and Barker, 1983; Druez et al., 1988).

In order to study in-cloud icing, a test cable was set up on Mt. Valin at an altitude of 902 m (2959 ft), in the Laurentian mountains near Chicoutimi. This test facility consists of a 96.5 m (316.5 ft) cable which was designed and built in collaboration with Hydro-Québec to investigate icing of power line cables. This installation provided the opportunity to gather cable icing data for complete winter seasons. At the Mt. Valin test site, as long as the temperature remains below 0°C, rime accretes and a significant portion stays on the line during the winter season until it melts in the spring. However, it is difficult to relate cable icing measurements to a standard icing meteorological parameter. Icing has never been systematically measured, as precipitation for example, by the meteorological services. Tattelman (1982) has shown that an ice detector can fill that need at least until a better instrument can be marketed.

The purpose of this study is to analyze icing data collected on a test cable and correlate the accreted mass of ice with measured ice detector signals in order to better understand this complicated phenomenon, to contribute to the development of an improved icing model for power transmission line cables, and to verify the possibility of using the ice detector to predict cable icing.

TYPES OF ATMOSPHERIC ICING AFFECTING STRUCTURES

Three basic kinds of ice are formed by accretion in the atmosphere: glaze, hard rime and soft rime. Glaze is transparent and it has a density with respect to water of approximately 0.9 (the density of pure ice is 0.917). Hard rime is white and sometimes opaque, depending on the quantity of air trapped inside the ice. Its density varies from 0.6 to 0.9. Soft rime is white and opaque. It is feathery or granular in appearance with a density less than 0.6. The density will increase with increasing drop size, temperature, windspeed and liquid water content.

Cloud or fog droplets have diameters smaller than 200 μm. Cloud droplet sizes measured experimentally indicate that low level clouds, which can affect a structure on a mountain summit, have droplet sizes in the 1-45 μm range. Consequently, exposure to supercooled clouds or fog will usually result in soft rime. On the Mt. Valin summit in-cloud icing is frequent from December through March. However freezing precipitations, which have droplets larger than 200 μm, also occur and are most frequent in early winter. The higher liquid water content associated with the precipitations can produce hard rime. The boundary between in-cloud and freezing precipitation icing is difficult to establish on a mountain icing site where clouds and precipitations are often mixed and where the icing obtained varies in density, covering the range from soft to hard rime.

EXPERIMENTAL INSTALLATION

The cable icing site is located at the summit of Mt. Valin, in proximity to a Radio-Québec communication antenna which serves the Saguenay-Lac St-Jean area. The presence of the Radio-Québec antenna and its associated access and services combine to make this particular well-exposed summit in the Laurentian mountain range an excellent location for this study.

The experimental installation is composed of a test cable, a thermistor, a de-iced anemometer and an ice detector. A 96.5 m (316.5 ft) span test line supports the 35 mm (1.38 in.) diameter stranded cable which was used to collect the icing data analyzed in this report. A schematic diagram of this cable is shown in Fig. 1. The stranded cable has one of its ends 0.37 m lower than the other. This difference was found when accurate level measurements were made after cable installation. However this difference is only 0.4 % of the span and therefore does not significantly change the equal distribution of weight between the supports.

Load cells measure the cable end tension (N) which is then converted to icing mass per unit length (kg/m), after accounting for the geometry of the cable and line (McComber et al., 1987). Data is collected by an acquisition system installed with signal conditioners in a building close to the experimental test line. The ice is assumed to be

uniformly distributed on the cable span and the icing mass per unit length is obtained from the vertical component of the measured tension using the initial cable angle at the support. This angle, shown in Fig. 1 for the test cable, was measured accurately with surveying instrumentation.

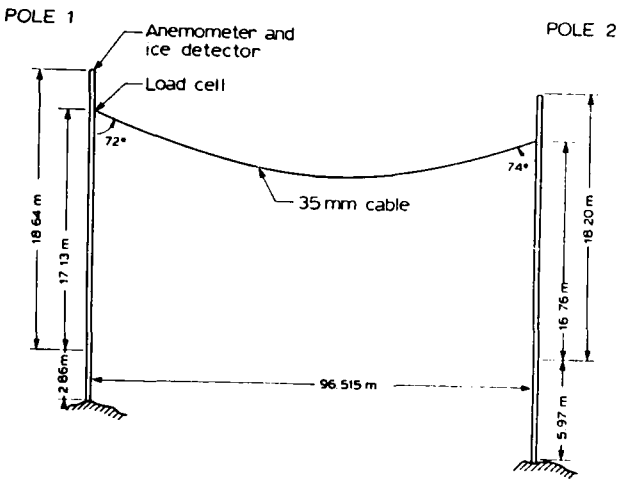

Fig. 1. Schematic diagram showing dimensions of the test cable.

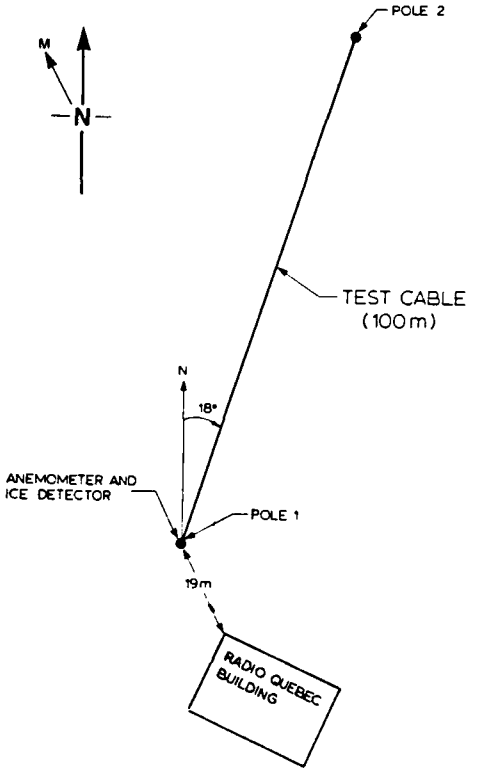

Fig. 2. Direction of the test cable.

Data are collected at 30 min intervals and include the computed average of 180 samples, i.e. every 10 s, for the load cells, 50 samples for the wind velocity and one sample for the temperature and the ice detector. During the icing season, data are transmitted via a telephone line to a computer in the university laboratory and are verified to prevent transmission errors. Each month, curves of the measured icing parameters are plotted. From the measured end tension in the cable, an equivalent average ice load M expressed as a mass per unit length (kg/m), is calculated.

An equivalent ice-covered cable diameter D in meters is often used to describe ice accretion size. The average ice load M can be converted to equivalent diameter by:

$$D = 2\left[\frac{M}{\rho\,\pi} + \frac{D_b^2}{4}\right]^{1/2} \qquad [1]$$

where D_b is the bare cable diameter and ρ is the accretion density (kg/m^3)

In Figure 2, the orientation of the test cable is shown. This orientation is important when determining the effect of the wind speed on ice accretion.

INSTRUMENTATION AND MEASUREMENTS

The ice detector

An ice detector (GENEQ, IREQ-1000) records the occurence and duration of icing conditions. This type of ice detector was originally developed to detect ice formation in the intake portion of turbomachinery. These detectors were aerodynamically designed for use on aircraft, but they have also been used to detect icing on towers. The ice detector's operation is based on the magnetostriction principle. An oscillator forces a small closed cylinder (the sensing probe) to vibrate longitudinally, parallel to its axis. It is driven at its resonant frequency when dry, but accretion of ice will cause a shift in resonance corresponding to the increase in ice adhering to the probe. After a small preset thickness of ice has accumulated, the sensor is de-iced by heating. The sensing probe used by GENEQ is a Rosemount 871 cylinder, 6.2 mm in diameter and 25.5 mm long. Tattelman (1982) has concluded that such a detector has presently the greatest potential as a meteorological instrument for the detection of icing. However, he had also pointed out that the major hindrance to utilization of the detector "off the shelf" for making icing observations, is the problem of retention of melt water on the flat surface area on top of the strut on which the sensor is located. This retained water can cause erroneous cycling upon refreezing. This problem has been alleviated, at least partly, for the GENEQ instrument in use on Mt. Valin by a redesign of the supporting strut made by Hydro-Québec IREQ. The strut is bent sideways by mechanical action permitting any melt water to be removed from the instrument between cycles. A photograph of the ice detector is shown in Fig. 3.

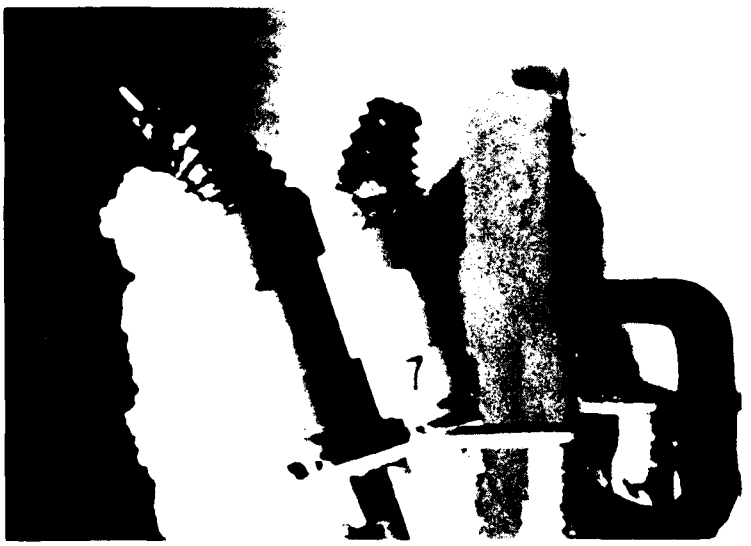

Fig. 3. Photograph of the ice detector.

De-iced anemometer

The wind velocity magnitude and direction are measured with a de-iced anemometer (HYDROTECH). The anemometer has a heated rotor (WS-3) and a heated direction vane (WD-3). Knowing the line orientation, the wind velocity component normal to the test cable is computed.

ATMOSPHERIC IN-CLOUD ICING OF STRANDED CABLES

Ice detector calibration

Tattelman (1982) has made an extensive study on the calibration of the ice detector. In his calibration, the distinction is made between freezing rain and in-cloud icing. Since there is a significant difference in droplet size and therefore in the collection efficiency of the obstacle, this distinction will be retained in the present work.

In the case of in-cloud, icing his results were obtained for cylinders of various diameters and 300 mm in length, and summarized in interpolated curves giving the mass of ice, M (kg/m), as a function of the number of detector alarms, x. This calibration curve can be interpolated for the Mt. Valin 35 mm cable, and divided by 0.3 to obtain icing on a 1 m cable:

$$M = 0.0377 + 0.0075\ x \qquad [2]$$

In Eq. (2) there is a small ordinate (0.0377), such that repeated use of this curve for a small number of alarms would result in an unacceptable multiplication of an error. This is not appropriate, if this equation is to be used, to find an icing rate from a small alarm cycle rate. To obtain the same accuracy using repeatedly a small number of cycles, a curve with a zero ordinate was derived:

$$M = .00867\ x \qquad [3]$$

Eq. (3) was obtained by minimizing the surface between the straight line given by Eq. (2) and a line of unknown slope passing through the origin. The minimization of the error was done between 0 and 50 cycles. The original calibration curve corresponding to Eq. (2) and the curve passing through the origin are shown in Fig. 4.

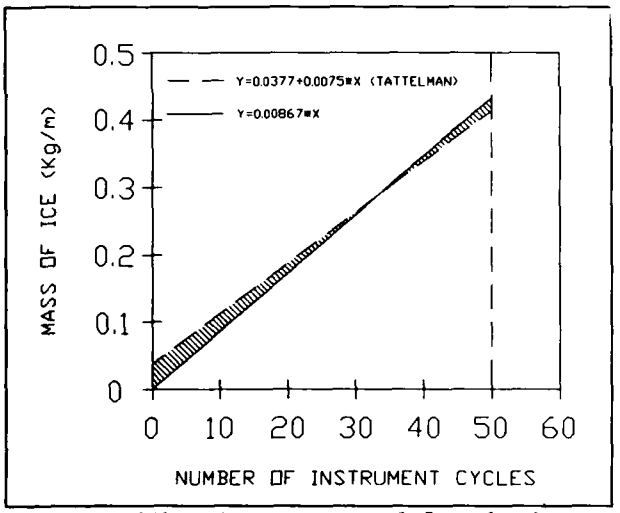

Fig. 4. Calibration curve used for the ice detector, in-cloud icing.

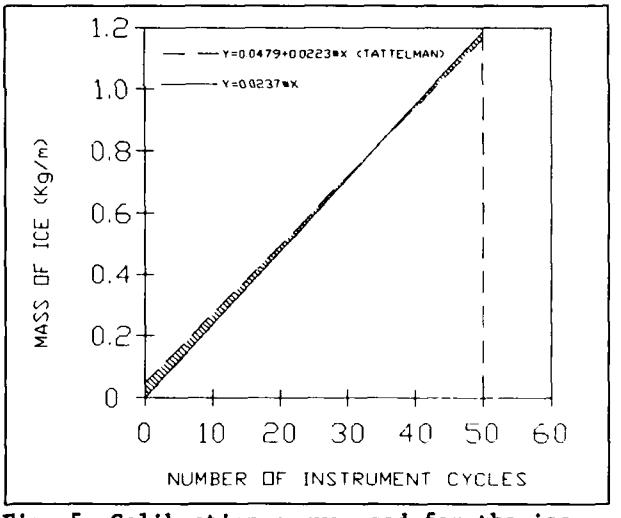

Fig. 5. Calibration curve used for the ice detector, freezing rain.

This equation can also be applied to find the icing rate from the detector cycle rate:

$$\delta M = .00867\ \delta x \qquad [4]$$

The calibration curve given by Tattelman (1982) for freezing rain, multiplied by the appropriate constants for a 35 mm cable and 1 meter in length:

$$M = 0.0479 + 0.0223\ x \qquad [5]$$

and the optimum straight line passing through the origin and obtained by the same method, is:

$$M = .0237\ x \qquad [6]$$

Figure 5 shows these two calibration lines given by Eqs. (5) and (6). Equation (6) will be used below to predict cable icing in the case of freezing precipitation.

Cable icing rate

The icing intensity expressed as mass per unit area and unit time is given by (Makkonen, 1984; Horjen,1983) :

$$R = E\ w\ V_n \qquad (\ kg/m^2s) \qquad [7]$$

where E is the dimensionless collection efficiency, w is the liquid water content (kg/m^3) in the air flow and V_n is the normal wind velocity (m/s). The collection efficiency is defined as the ratio of the mass of drops impinging on an object in unit time to the mass of drops that would have impinged in the same time if there were no deflection resulting from moving air around the cable.

To obtain the accreted mass in 1/2 hour at time t_i, δM_i, the icing intensity is multiplied by the obstacle cross-section normal to the flow direction and the time interval δt. For a cable, if D (m) is the equivalent cable diameter, Eq. (1):

$$\delta M_i = E\ w\ V_n\ D\ \delta t \qquad [8]$$

In order to be able to use the ice detector calibration curves to predict the icing rate of the cable, the effect of three variables must be considered. These are the normal wind speed, V_n, which will have the same effect for in-cloud icing and freezing precipitations, the collection efficiency, E, and the equivalent accretion diameter D.

In-cloud icing

For in-cloud icing, the droplets are small and the collection efficiency can influence the icing rate. However, at low wind speed, experimental data has shown that the calculated collection efficiency is unreliable. McComber et Govoni (1985) and Personne (1988) have shown that a modified collection efficiency has to be used in order to take into account the effect of the accretion surface roughness on the collection efficiency. The value of the calculated collection efficiency E_{oc} has therefore to be corrected using an expression suggested by Personne (1988) and based on experimental results:

$$E_o = E_{oc} + 2.03\ (1 - E_{oc})\ D_o \qquad [9]$$

where E_{oc} is the initial calculated collection efficiency and D_o the initial equivalent diameter of the accretion. Using this value, the icing rate was corrected both for the collection efficiency and the initial accretion size:

$$\delta M_i = 0.0867\ \delta x\ C_E \quad \text{where} \quad C_E = E_o\ D_o\ /\ E_b\ D_b \qquad [10]$$

E_b and D_b are the collection efficiency and diameter of the bare cable respectively.

The following expression was used to find the resulting ice mass as a function of time:

$$M_i = M_{i-1} + \delta M_i \qquad [11]$$

Freezing precipitations

For freezing precipitations, i.e. for droplet with d > 200 μm, which is the case for freezing rain, the collection efficiency E is equal to 1 even for low wind speed , and hence is not considered in the calculations. The icing rate, δM_i, is given by:

$$\delta M_i = 0.0237\ \delta x\ (D_{i-1}/D_b) \qquad [12]$$

The equivalent diameter D_{i-1} is found using Eq. (1), assuming a cylindrical ice accretion shape and an accretion density of $\rho = 900\ kg/m^3$. In this case the higher icing rate justifies a calculation of the equivalent diameter D_{i-1} at every time step.

Wind intensity and direction

The wind velocity is measured by an anemometer located on top of pole 1 of the test line (Fig. 1). Wind velocities vary with height from ground level. This variation is usually assumed to be in the form of a power law (Blevins, 1977):

$$\frac{V(z)}{V(L)} = \left[\frac{z}{L}\right]^{\alpha} \qquad [13]$$

where the velocities at different heights from ground z are compared with the velocity at a reference height L. For the type of terrain where the test line is located, the exponent α should be approximately 0.28 (Blevins, 1977). The ratio of velocities of cable heigth to ice detector height is 0.975 which is approximately unity and has not been taken into consideration for the computation of cable icing.

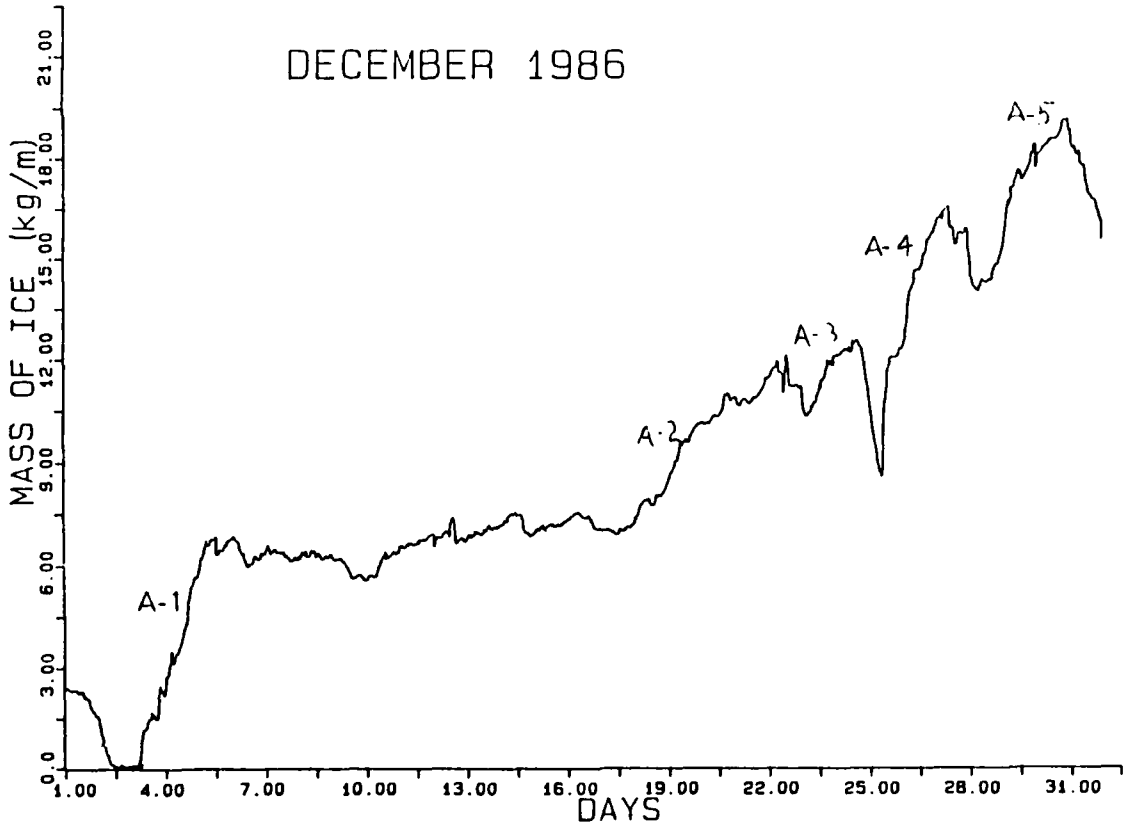

Fig. 6. Mass of ice accreted on the 35 mm cable in December 1986.

Equations (10) and (12) are for a cylinder or cable perpendicular to the wind direction. If the are not perpendicular, the icing rate, δM_{ic}, must be corrected by:

$$\delta M_{ic} = \delta M_i \cdot \cos \Theta \qquad [14]$$

where Θ is the angle between the wind direction and the direction normal to the cable.

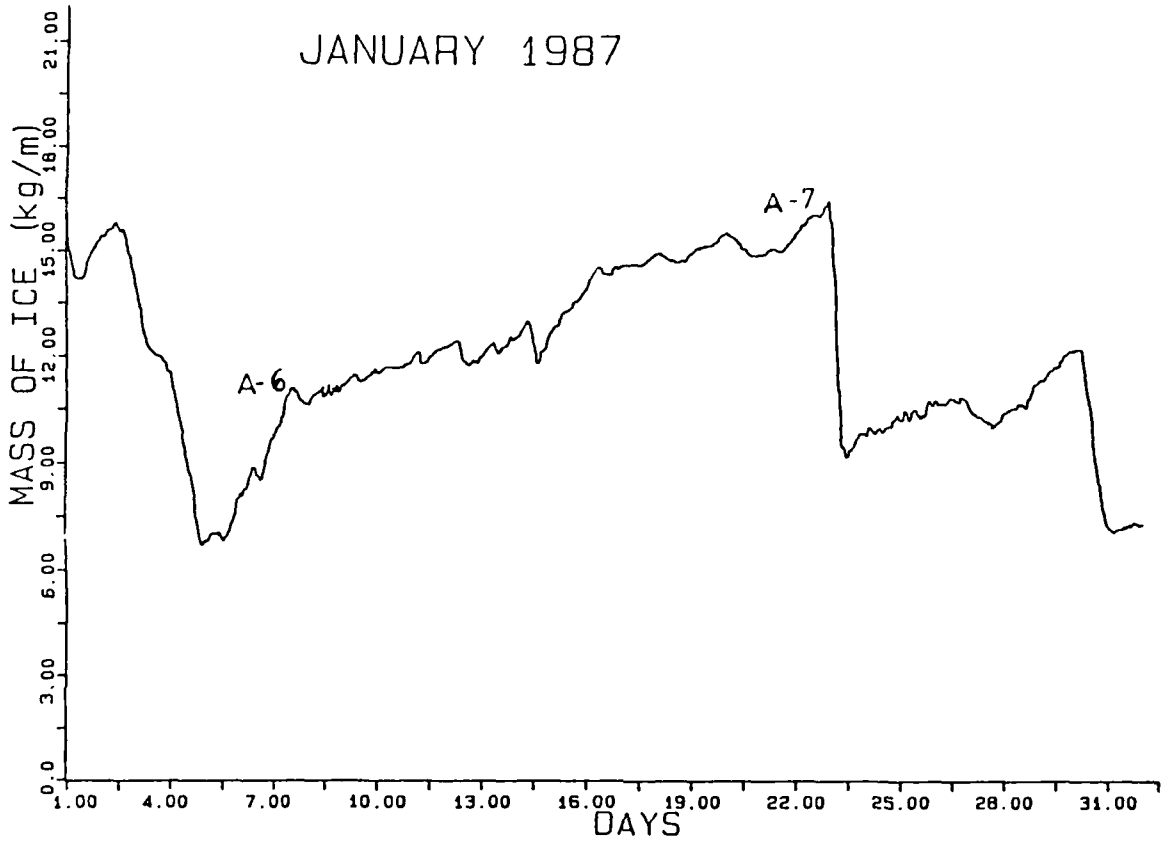

Fig. 7. Mass of ice accreted on the 35 mm cable in January 1987.

RESULTS AND DISCUSSION

Icing measurements

Icing data from the 1986-87 icing season were analyzed. This data period was chosen because important icing events were recorded and the instruments performed adequately. A certain number of accretion events have been chosen in December and January on the basis of the number of icing alarms in an hour and are indicated in Figs. 6 and 7. Whenever the icing alarm rate was more than two or three alarms per hour for four consecutive hours, the icing period was considered as a separate event.

The seven (7) accretion events studied are summarized in Table 1 and are shown in Figs. 8 to 14. From the measurements taken it is not as easy to make the distinction between freezing rain, where precipitation and large droplets are present, from in-cloud icing where only smaller droplets are involved. Freezing precipitations are recognized when an icing rate of approximately 0.4 kg/m.h is obtained for the cable during an event. However this icing rate is not usually sustained for the complete event. In Table 1 the average icing rate during each event is shown and the events classified as freezing rain have approximately twice the icing rate (0.19 kg/m.h) measured for in-cloud icing events (0.099 kg/m.h).

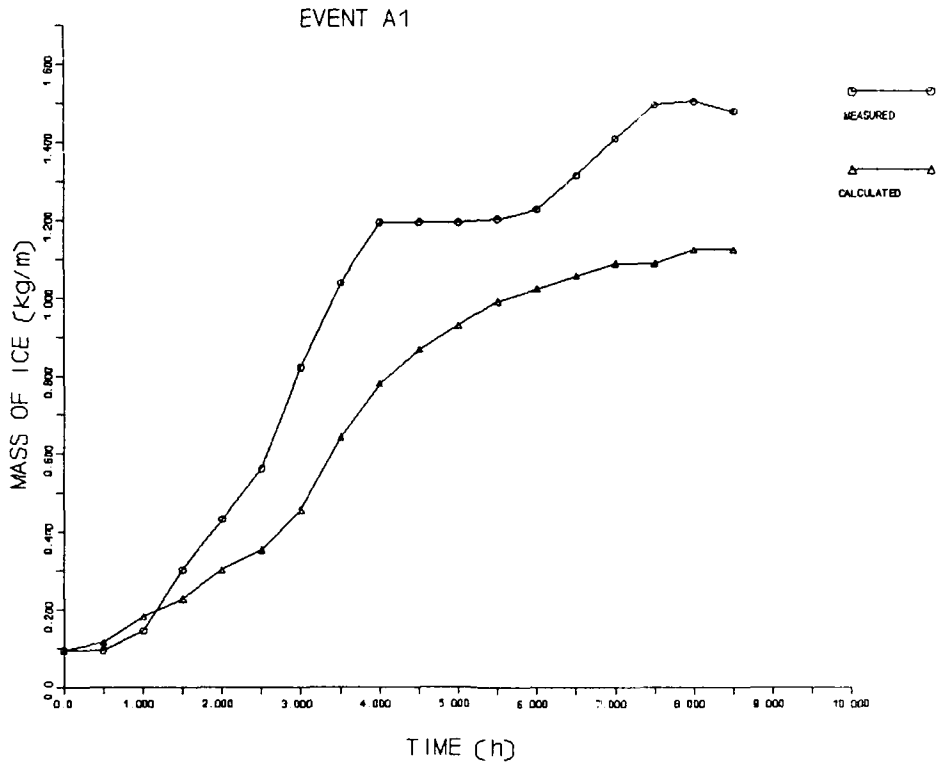

Fig. 8. Comparison of the mass of ice measured on a cable with the mass predicted by the ice detector, event A-1.

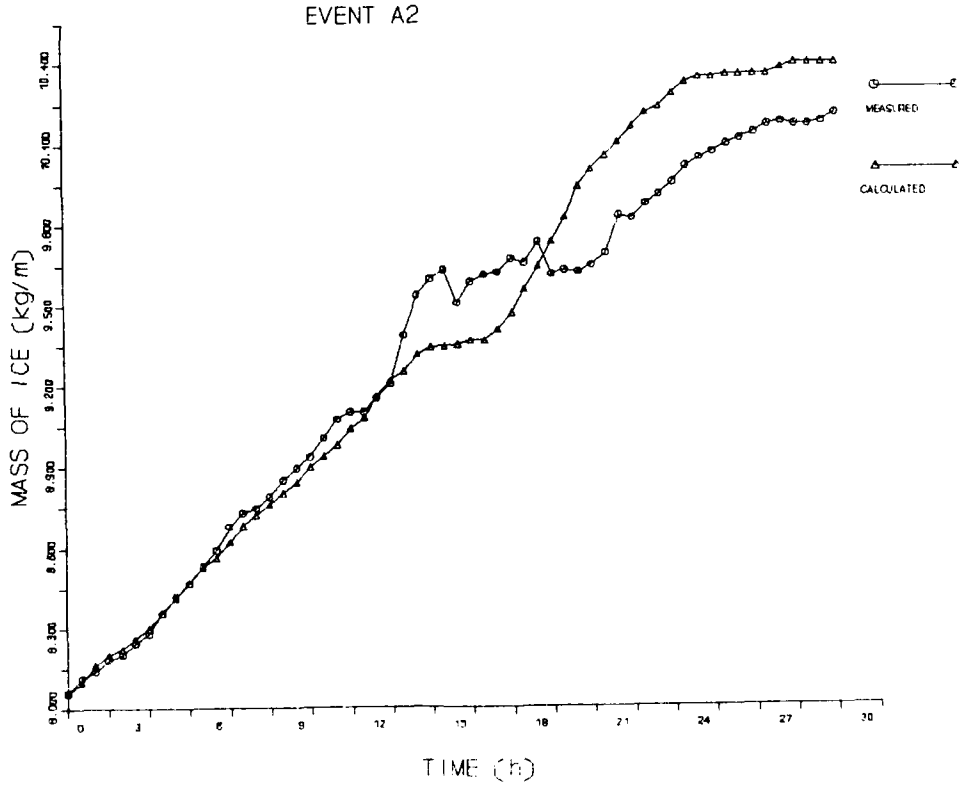

Fig. 9. Comparison of the mass of ice measured on a cable with the mass predicted by the ice detector, event A-2.

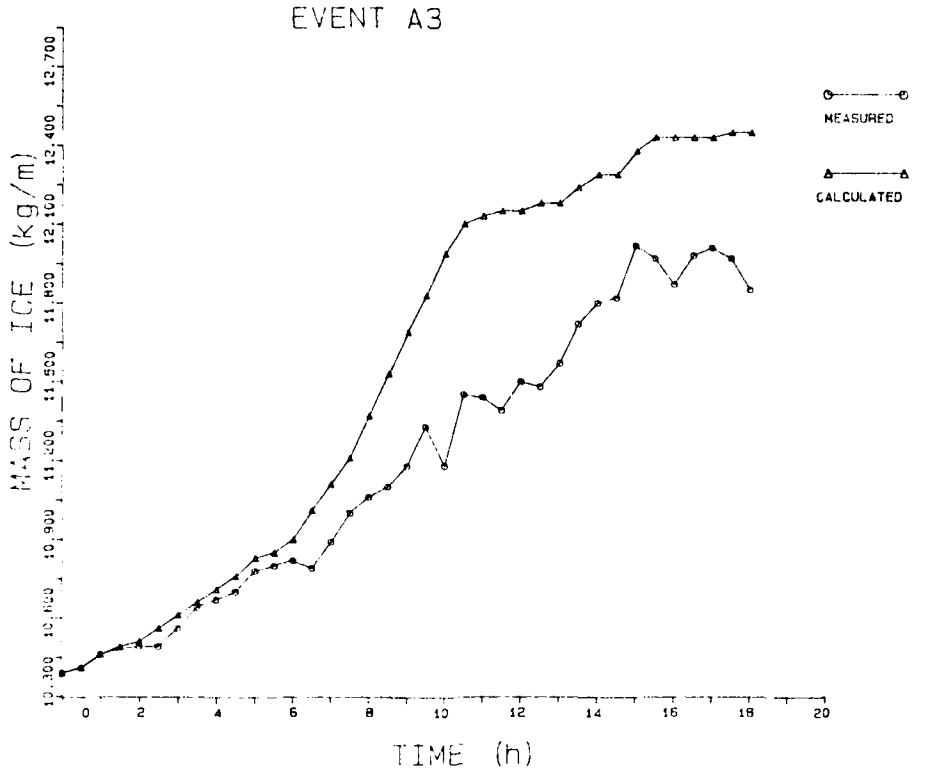

Fig. 10. Comparison of the mass of ice measured on a cable with the mass predicted by the ice detector, event A-3.

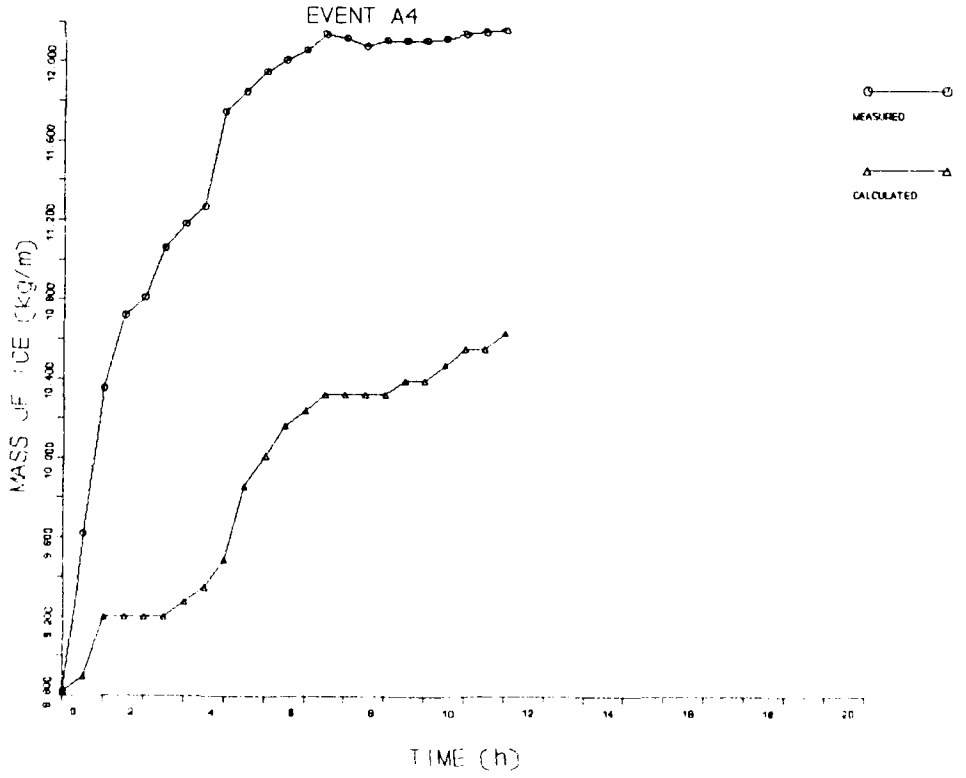

Fig. 11. Comparison of the mass of ice measured on a cable with the mass predicted by the ice detector, event A-4.

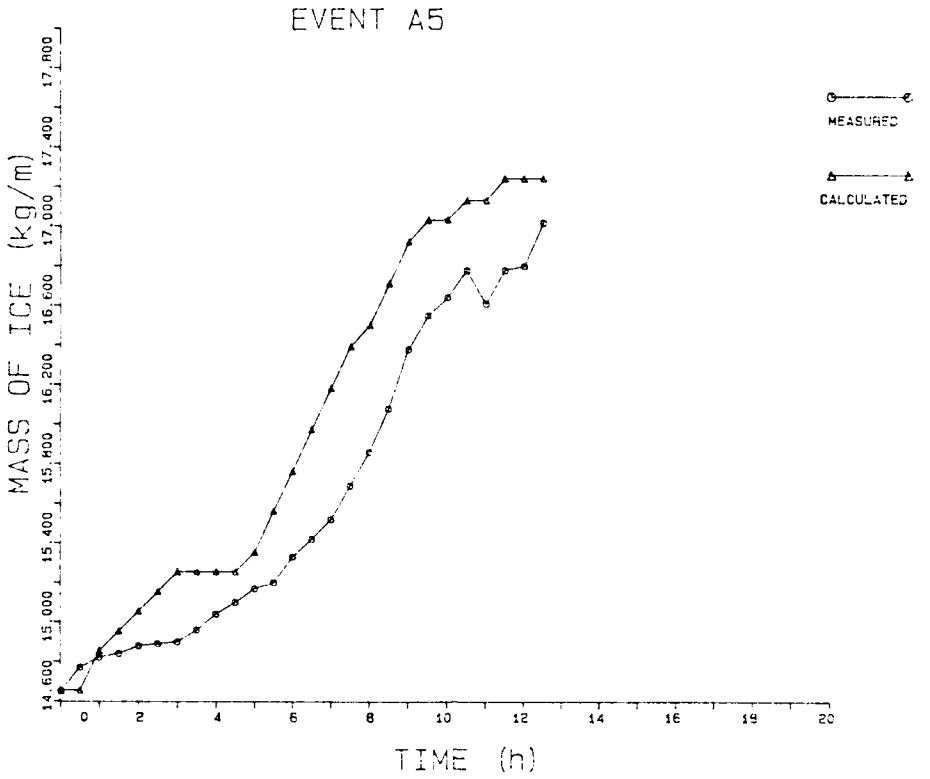

Fig. 12. Comparison of the mass of ice measured on a cable with the mass predicted by the ice detector, event A-5.

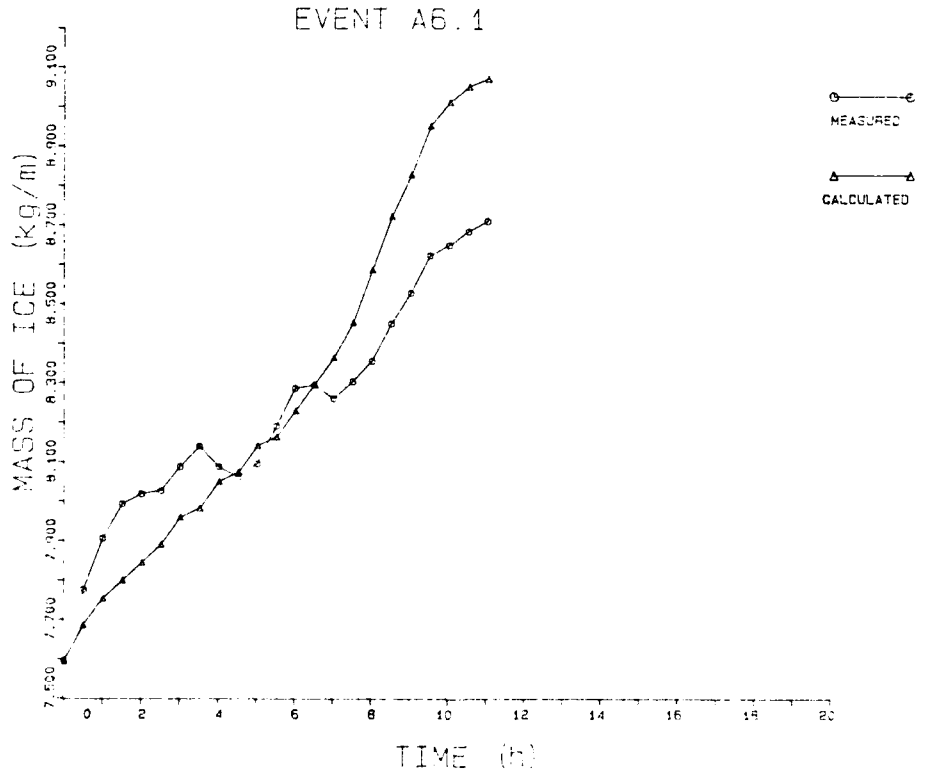

Fig. 13. Comparison of the mass of ice measured on a cable with the mass predicted by the ice detector, event A-6.1.

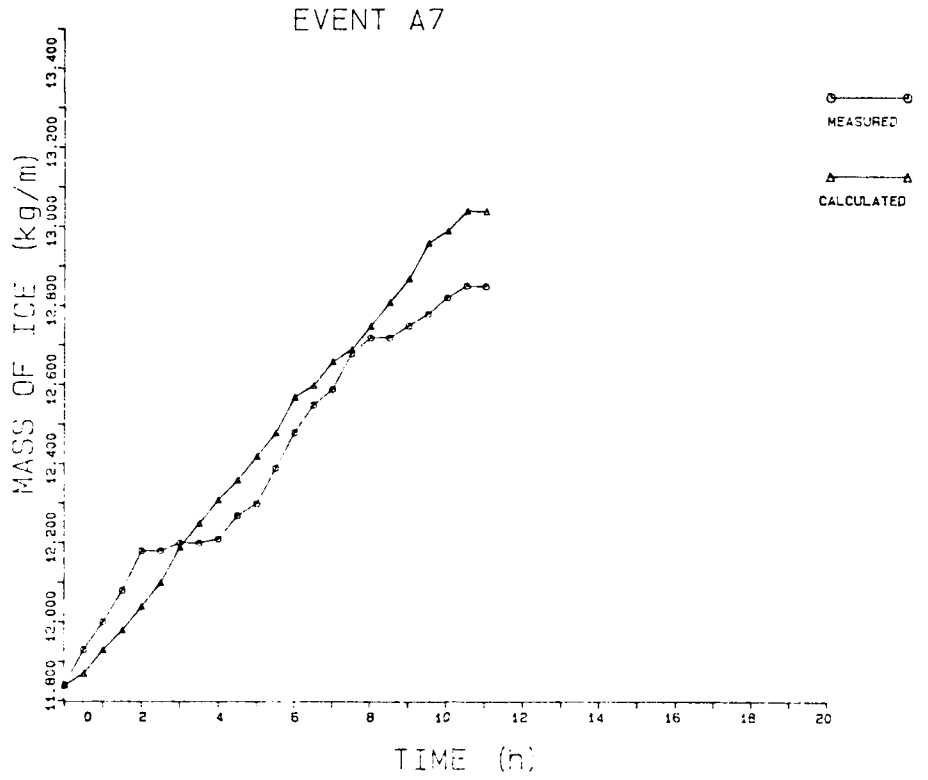

Fig. 14. Comparison of the mass of ice measured on a cable with the mass predicted by the ice detector, event A-7.

Table 1

Summary of icing events

Event number	Date and time	Duration (h)	Average icing rate (kg/m.h)	Average error(%/h)
A-1	3 Dec 4:30	8.5	0.14 (FR)	- 2.5
A-2	18 Dec 19:30	28	0.078	+ 0.3
A-3	23 Dec 3:30	18	0.098	+ 1.9
A-4	25 Dec 9:30	11	0.23 (FR)	- 5.4
A-5	28 Dec 17:30	12.5	0.20 (FR)	+ 0.7
A-6.1	5 Jan 22:00	11	0.12	+ 2.5
A-6.2	6 Jan 15:00	8	0.1	- 9.9
A-7	14 Jan 15:30	11	0.1	+ 1.6
		Average absolute error (%/h):		2.6

In-cloud icing

In Table 1 events A-2, A-3, A-6 and A-7 are classified as in-cloud icing. During event A-6 a significant amount of ice was shedded over a short period of a few hours. Hence that period was removed from the analysis and the remaining time separated in two parts: A-6.1 and A-6.2. Not including event A-6.2, the average absolute difference between the accretion mass predicted and measured is 1.6 %/h. In the case of event A-6.2, the predicted ice mass falls well below the mass collected by the cable. There are two possible explanations for this difference. The first cause could be the change in weather conditions during the analysis period. The change from supercooled droplets to wet snow particles would increase the accretion mass even though the ice detector would not react

to wet snow. The second possibility could well be a temporary failure of the detector, as observed in the case of freezing rain and explained below in the discussion of these events. Indeed the high average icing rate measured in event A-6.2 (0.12 kg/m.h) is the highest among events classified as in-cloud icing and could have been responsible for a partial failure of the ice detector.

Results also show that the ice detector signal increases regularly whereas the accretion mass signal shows more irregularities. The ice detector signal measures a number of icing alarms in a given time period and must always be increasing whereas the measured ice mass on the cable can be affected by ice shedding that most probably occurs in certain wind conditions but that the detector is unable to predict.

In summary, there is a fairly good agreement between the icing rate predicted by the ice detector and the icing rate measured. The average error for the four events studied is 1.6 %/h. However, since the total mass is obtained by an integration over the event period, a small error in the icing rate predicted will result in a large difference in mass over a long period. The longest event, A-3, has a difference of 34 % between the calculated and measured mass for the 28.5 h period.

Freezing rain event

Events A-1, A-4 and A-7 are classified as freezing rain, based on their higher icing rate. This is to be interpreted as the probable presence of freezing precipitations during part of the event. However in-cloud icing is likely to occur simultaneously, and precipitations can also be absent in part of the period studied. Results for these three events show a larger error, an average of 2.9 %/h difference between calculated and measured average icing rate.

At these higher icing rates, the detector has failed at least during part of each event. In the case of event A.1 the ice detector became completely surrounded by the accretion and failed to record icing after 8.5 h. Only the initial period of the event, when the detector was working was considered for the comparison. In the case of events A-4 and A-5 the ice detector recorded no alarms for a pediod of two hours and then seemed slow to record strong icing in the recovery period. It has been observed in the field that the mechanical movement of the ice detector which was intended to remove water from melted ice on the probe is also effective in breaking some of the ice forming on the strut. However, this is not equally effective depending on the wind direction. If the wind is at 180° with the inclining angle, then the movement is less effective in breaking the ice forming in the opposite direction on the strut and hard rime can accrete in the back of the instrument up to a point where the droplets are prevented from reaching the probe. This is the type of failure observed in event A-1, and this is most probably what happened during events A-4 and A-5. Indeed even if the detector probe operates in the vertical direction in order to be insensitive to the wind direction, its mechanical movement, in a preset direction, makes the response of the instrument dependent on the wind direction for high icing rates.

In summary, the analysis of these icing events shows that the number of ice detector alarm cycles per unit of time can be used with appropriate calibration curves to predict the cable icing rate with reasonable accuracy. However, additional factors will affect the total icing rates on the cables. Improvement in modeling cable icing should include the effect of cable diameter (McComber et al., 1987) which controls torsional stiffness of the cable and finally dynamics of the cable during icing. The ability of the ice detector to predict icing rate is therefore dependent on the continued improvements of cable icing modeling. Also since the atmospheric icing phenomenon is highly history dependent, ice shedding appears to be a variable which has to be included in order to make an accurate prediction of cable icing in mountains. Because of the many time dependent variables involved and the complexity of cable icing, more data for different cable sizes and heights, must be collected and analyzed to establish an adequate empirical model. The cable icing model will in turn permit the narrowing of the gap between the icing intensity as measured by the ice detector and the ice mass actually accreting on the cable.

CONCLUSIONS

A relationship was established between ice load measurements obtained on a single cable and an ice detector signals for December 1986 and January 1987, at Mt. Valin. The ice detector number of alarm cycles was counted for half hour periods and used as a measure of icing rate on the instrument, leading to a prediction of the ice mass accreting on the cables. The effects of the wind direction, collection efficiency and accretion size are included in the calculations of the predicted cable icing. The events analyzed indicate that the ice detector performed adequately when the icing rate was less than 0.2 kg/m.h for which an average error of 2.6 %/h was verified. Future improvements in the modeling of cable icing will increase further the accuracy of cable icing prediction with the ice detector.

ACKNOWLEDGMENTS

The Mt. Valin test line was built and instrumented as part of a contract from Hydro-Québec (HO 924345). This work was also supported by the Natural Sciences and Engineering Research Council of Canada. The authors thank Radio-Québec for the permission to use the Mt. Valin building and Hydro-Québec for their help in reaching the site during the winter months. The following people have contributed to the testing: Bernard Desbiens, Serge Gauthier and Alain Royal.

REFERENCES

Blevins, R. D. 1977. " Flow-Induced Vibration", Van Nostrand Reinhold, Co., New-York, pp. 164-182. Reprinted in 1986, Robert E. Krieger, Malabar, Florida.

Diem, M. 1956. "Ice Loads on High Voltage Conductors in the Mountains", Archiv fur Meteor., Geophys. und Bioklim., Vol B7, pp. 84-95. (in German)

Druez, J., McComber, P., Félin, B. 1988." Icing rate Measurements made for different cable configurations on an icing Test Line at Mt. Valin", 4th International Workshop on Atmospheric icing of Structures, Paris, Electricité de France, special Report, pp. 124-128.

Govoni, J.W., Ackley, S. F. 1983. " Field Measurements of Combined Icing and Wind Loads on Wires". Proceedings of First International Workshop on Atmospheric Icing of Structures, CRREL Special Report 83-17, pp 205-215.

Horjen, I. 1983, "Icing on Offshore Structures- Atmospheric Icing", Norwegian Marine Research No 3, pp. 9-22.

Makkonen L., 1984. " Modelling of Ice Accretion on Wires", J. of Appl. Meteor, Vol 23, pp. 929-939.

McComber, P., Druez, J., Bouchard, D., Falgueyret, A. 1987. "Atmospheric Icing Load Measurements on a Cable Using the End Tension", Cold Reg. Sc. and Techn., Vol 13, pp. 131-141.

McComber, P., Govoni, J.W. 1985. "An Analysis of Selected ice Accretion Measurements on a Wire at Mt. Washington", Proceedings of the 42nd Eastern Snow Conference, pp. 34-43.

Personne P., 1988, " Effet de la rugosité sur la croissance du givre à faible vitesse: Résultats expérimentaux et modèlisation ", Thèse de doctorat, Université Blaise Pascal, Clermont-Ferrand, 231 pp.

Smith, B.W., Barker, C.P. 1983. "Icing of Cables", CRREL Special Report 83-17, pp 41-49.

Tattelman, P. 1982. "An Objective Method for Measuring Surface Ice Accretion", J. of Applied Meteor., Vol 21, no 4, pp. 600-612.

Snowmelt Runoff Modeling Using GIS Parameter Estimation in a Western Adirondack Watershed

M.K. MELLANDER AND A.R. ESCHNER

State University of New York
College of Environmental Science and Forestry
Syracuse, New York 13201, U.S.A.

ABSTRACT

Difficulties in obtaining satellite imagery and aerial photography to determine snowcovered area for use in snowmelt runoff models raise the need for other methods of estimation. A raster geographic information system (GIS) and a digital elevation model constructed for this project were used to model the basin topography in a heavily forested, western Adirondack watershed. The calculated daily snowmelt (from daily degree-day data and the degree-day factor) was multiplied by an irradiance index to yield distributed values of snowmelt for each elevation zone on each day. These values were then subtracted from the previous day's snow water equivalent. By calculating the area of cells with water equivalent greater than .1 inches (.25 cm), a daily estimate of snowcovered area was obtained, and entered into the Snowmelt Runoff Model (SRM; Martinec, Rango and Major,1983). Initial results are promising, with r2 (Nash-Sutcliffe)values of .8141 for predicted and measured streamflow for the 1987 season.

INTRODUCTION

Some of the most successful snowmelt-runoff models have been designed for high mountain basins, with few terrestrial factors such as forest cover or land use affecting the model, and with aerial or satellite overviews possible on a regular basis. Areas in the eastern United States or Canada have heavily forested basins with (frequently) dense cloud cover during the snowmelt season. This and infrequent satellite overflights during the short term of snowmelt in these eastern watersheds limit the availability of data for estimates of snowcovered area, snow depletion rates, and other snowpack parameters affecting snowmelt. In addition, the spatial and spectral resolution of imagery is currently not adequate for determination of snow under heavy forest cover (Eschner et al, 1977). Finally, timely acquisition of expensive imagery and photography is a problem for many public and private agencies involved in water resource management.

Geographic information systems (GIS) are promising tools in modeling hydrologic processes. The structure of a GIS allows analysis of basin topography and other physical characteristics, and is also capable of spatially distributing variables affecting snowmelt and subsequent runoff. Energy inputs to the snowpack from solar radiation can be differentially assigned as functions of local elevation and inclination of the local topographic surface.

This study attempts to estimate snowcovered area using a GIS produced distribution of daily snowmelt, by developing an index of potential direct beam irradiance with values dependent upon the geometry of each local topographic facet in relation to the sun. This index,

which assigns an irradiance value for each cell in the basin according to its slope and azimuth direction, was derived from the Cosine Law of Irradiance as presented by Reifsnyder and Lull (1965), Lee (1962) and Kaufmann and Wetherred (1982); with modifications for aspect and slope factors effectively calculating the "equivalent slope"(Lee, 1962) for each cell's local topographic facet. The index was not modified by other spatially variable factors such as forest cover in order to test the method with as operationally simple a method as possible.

STUDY AREA

The Independence River is one of only two uncontrolled major tributaries of the Black River, which drains the western Adirondack Mountains and eastern Tug Hill upland in northern New York State. The Independence watershed is an elongated, east-west oriented basin lying on the western flank of the Adirondacks, and largely within the Adirondack Park (See Figure 1). The drainage is young and poorly defined in many places. Soils are glacial outwash and till, varying from thin layers over Precambrian bedrock to a deep,coarse sandy deposit under most of the river's main channel. Topography ranges from the Adirondack foothills on the eastern end of the watershed (maximum elevation 2340 ft/702 m), to flat, largely wetland areas of glacial outwash interspersed with kames, kettle lakes and drumlins in the central portion of the basin. The river flows with a steeper gradient in the lower reaches of the watershed, emptying into the Black River at an elevation of 840 feet(261 m). (Waller and Ayer, 1975)

The 98 square miles (254 km2) of the watershed to its mouth are approximately 80 percent forested, largely with hardwoods. The major portion of annual runoff is from snowmelt. As one of two uncontrolled subbasins of the Black River, the Independence is of particular interest in studies seeking to control annual flooding of agricultural areas in the Black River flats downstream of the Independence outlet. (US Army Corps of Engineers, 1988)

Available runoff and climatological data is of long term and good quality. The Black River Regulating District is the administrative agency for the basin, collecting hydrologic and climatological data from the contributing agencies (USGS, USWS). The flow at the Donnattsburg gauge(91.7 mi2/238km2 of drainage area) has been recorded since 1942, with telemetry installed since the summer of 1989. Climatological stations used (Figure 1) fairly well represent the basin, although there is poor correlation between temperature and elevation among them, perhaps due to recent rapid development in some of the stations' immediate vicinity.

Snow courses, although none exist within the Independence basin boundaries, are well distributed around the watershed. Water equivalent and snow depth data are available on an approximately 15 day periodic basis during the snowmelt season from the Eastern Snow Conference. See Figure 1 for the distribution of data sources used in this project.

METHODOLOGY

Construction of the DEM

The digital elevation model (DEM) was constructed by overlay of a square grid (ground cell size 868 feet/265 m on a side) on a set of 1:62500 USGS quadrangle maps. A single elevation value was assigned to each of the cells in the 126 by 51 grid. Streams were "channeled" into the DEM according to their placement on the base topographic maps. Average elevations were assigned to cells not containing water, unless the cell contained a local topographic high or low, in order to preserve local surface features in the very flat areas of the watershed. This method of elevation assignment was judged to best represent the area as a hydrologic unit and as topographic modeling surface.

Surface Modeling in IDRISI

IDRISI is a non-commercial, raster GIS constructed with an open architecture which facilitates customizing for specific purposes. It was chosen for this study because of its surface modeling capabilities (including a watershed function) and for its preservation of data

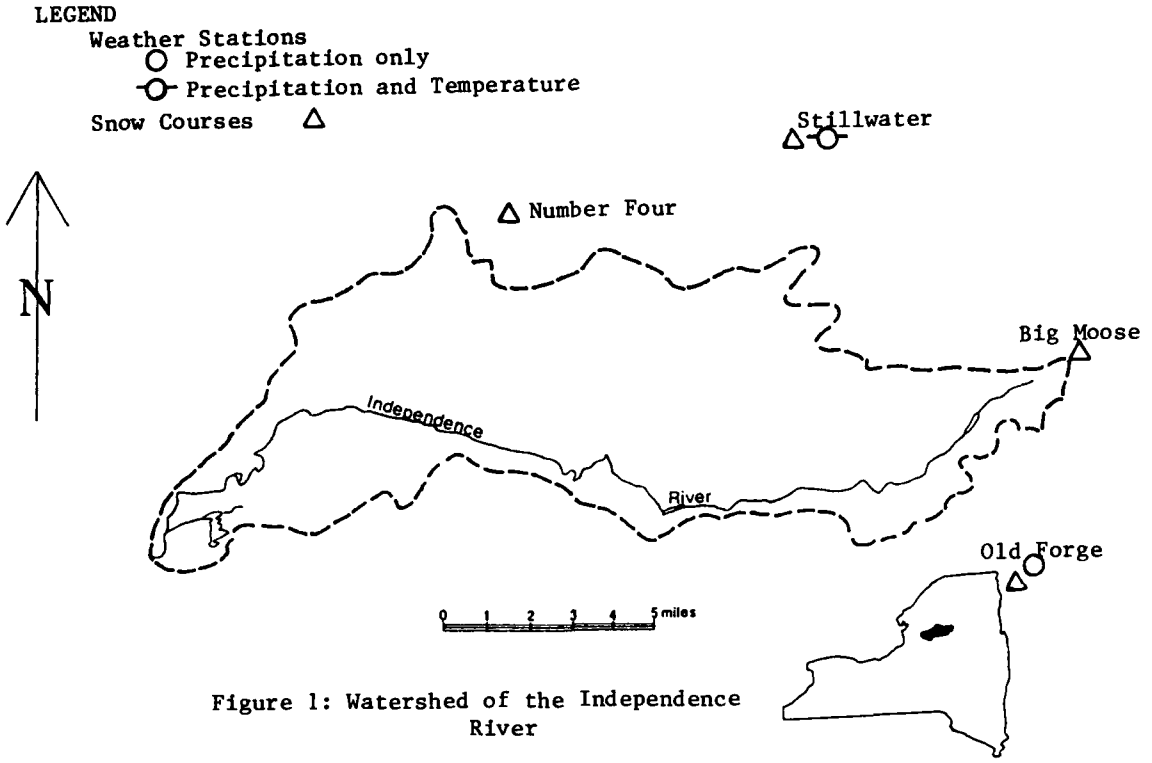

Figure 1: Watershed of the Independence River

layers in distinct data files at each stage of manipulation and analysis.

IDRISI was used in the study not only to model the topographic surface from the DEM through creation of slope and aspect maps, but also for areal analysis (including hypsometric analyses of basin and snowcovered areas) and regionalization of climatic variables.

The surface of the DEM was modeled using the SURFACE function in IDRISI, with both slopes (in degrees) and aspects calculated using a maximum-slope algorithm on neighboring cells. Areal analysis of aspects and slopes using the HISTO and AREA functions allowed classification of slopes and aspects into representative groupings, and for visual analysis of the basin topography.

Development of a spatial index of irradiance

Aspects were classified into four categories based on similarity of potential irradiance values in tests of the Cosine Law adaptations for tilted surfaces (Kaufmann and Wetherred, 1982). These four aspect classes, when further tested in combination with three slope classes of two, five, and ten degrees of slope (derived from analysis of the slopes on the watershed as the mean values of representative slope classes), yielded twelve distinct classes of irradiance values.

The equivalent surface, hour angle correction factor (two hours past solar noon, the time of maximum direct beam solar radiation effect on the snow surface), and "irradiance multiplier" (Kaufmann and Wetherred, 1982) were calculated using 43 degrees north latitude as the mean watershed latitude, for each cell in the basin. Index values were then expressed as the ratio of the cell's potential instantaneous irradiance to that of a horizontal surface. Resulting index values ranged from .80 to 1.20 for the 12 combinations of slope and aspect used in the initial tests.

Snowmelt from irradiance index

The resulting image file of cell values differentiated by each cell's slope and aspect was used to distribute daily snowmelt. The daily melt, S_m, in inches (cm), was derived from the equation

$$S_m = a(sumT),$$

calculated daily for each of the four elevation zones in the watershed, where:

a = the degree-day factor, re-calculated every 15 days , and
sumT = the total degree-days for each day, taken from average temperature minus the critical temperature for each elevation zone

(Martinec and Rango, 1981)

The daily melt value was then multiplied over the irradiance index map, resulting in a range of melt values varying with the potential irradiance on the topographic facets in the watershed. This "melt" image was created for each day and each elevation zone. Beginning with the initial snow water equivalent data from the snow survey measurements extrapolated to each elevation zone and for every 15 day period, the day's melt image was subtracted from the snow water equivalent left from the previous day. Histograms and summary area statistics were generated by IDRISI to calculate the remaining percent of snowcovered area, taken to be all cells with greater than .1 inches (.25 cm) of water equivalent. Additional precipitation (snow and rain) during each period was added to the water equivalent daily, until snowpack conditions seemed to be such that liquid precipitation would become immediately available for runoff. After this, only precipiation occurring as snow (that is, below the designated critical temperature for each zone) was added to the water equivalent.

Snow depletion tables were constructed from the daily snowcovered area values derived by this method, and entered into the SRM for each elevation zone as the snowcovered area factor, S_n. Location of each day's snowcovered and snow free areas were also available for verification and analysis from the water equivalent IDRISI image file for the corresponding day.

After the snow depletion data was entered for the test year, SRM was run using the sequence and procedures of parameter tests suggested in the User's Manual (Martinec, Rango and Major, 1983). No manipulation of parameters was attempted (other than correction of gross input or calculation errors) for the 1987 model calibration season, in order to judge the GIS parameter estimation method as objectively as possible. Other SRM parameters and variables were calculated according to instructions in the manual, which requires several decisions based upon interpretation of the data and a knowledge of basin response. A short discussion of the SRM itself, including its applicability to the lower elevation and relief of basins such as the Independence River, and how the decisions required in calculating basin parameters, follows.

THE SNOWMELT RUNOFF MODEL (SRM)

The Martinec-Rango Snowmelt Runoff Model (1983) is a proven degree-day model developed for high mountain basins "with significant snow accumulation". (Martinec, Rango, Major, 1983) It has been tested successfully on basins with widely differing areas, but tests on lower elevation, forested mountain basins remain scarce. The basic flow equation used in the model is as follows:

$$Q_{n+1} = c_n\left[a_n(T_n + \Delta T_n)S_n + P_n A\right] * 0.01/86400(1 - k_{n+1}) + Q_n k_{n+1}$$

where Q = average daily discharge in cfs(cms)
c = runoff coefficient (c = runoff/precipitation)
a = degree-day factor (in/F/d or cm/C/d), a function of snow density
T = number of degree-days (degF*d or degC*d)
ΔT = adjustment by temperature lapse rate for each elevation zone
S = ratio of the snowcovered area to the total area

P = precipitation contributing to runoff(in/cm). A designated critical temperature (T_{crit}) determines whether precipitation is read as rain or snow.
A = area of the basin or zone in mi2/km2
k = recession coefficient, calculated daily by the model, from seasonally calculated x and y coefficients in the equation $Q_{n+1} = xQ_n^y$ (see discussion of parameters, below)
n = sequence of days during the computation period

The SRM modification for the personal computer was used for this study.

The snowcovered area parameter, S, has previously been provided by satellite imagery, snowline overflights, or aerial photography. In this project, snowcovered area was obtained from the GIS model output.

SRM's output includes a computed versus observed hydrograph for the snowmelt season, a goodness-of-fit measure (the Nash-Sutcliffe r^2), percent seasonal difference between computed and actual runoff, and mean runoff for computed and observed data. The program also supports the summary output with graphical representations of snow depletion curves and tables of basin variables. These outputs were used for overall evaluation of the success of the parameter estimation method.

The following six parameters, required in addition to the snow covered area values in SRM, and the methods used for their estimation or calculation, are discussed in part because of the sometimes intuitive judgment necessary to derive them successfully.

Runoff coefficients, the most problematic of the basin parameters, were calculated using each 15 day period's total runoff and precipitation, the latter including estimated contributions from snowmelt during the period. The GIS melt computations were used for this, averaged for the basin's zonal areas. SRM allows separation of runoff coefficients from snow and rain, which is especially difficult for an area such as the Independence River, with alternate inputs during the winter season of rain and snow, and the very rapid ripening processes of the snowpack. The coefficients for 1987 ranged from .40 to .78, with the higher values as expected during times of melt.

Temperature lapse rates of .27 degrees Fahrenheit (.1 degrees Celsius) for every 100 feet (31 meters) were used, which translates to .72 degrees F (.27 C) for each of the four elevation zones. The base temperature station (at Stillwater Reservoir - see Figure 1) is near the hypsometric mean of Zone 2 in the basin, so that temperatures were extrapolated both up and down from the observed value.

Critical temperatures were chosen on the basis of previous work in the watershed (Colquhoun, 1971) and from analysis of the GIS output. The amount of melt calculated by the GIS was compared to the water equivalent found at each available snow survey on the corresponding date, to serve as a check of the melt computations' reliability. The amount of melt is a function of the degree-day values, so that critical temperature (above which precipitation falls as rain, below as snow) selection could also be judged on the basis of the correspondence of melt amounts and the snow survey data.

Degree-day factors were calculated as functions of the snow density, derived from the snow survey water equivalents. The equation used by SRM for degree-day factors is

$$a = 1.1\frac{(\text{density of snow})}{(\text{density of water})}$$

As expected, degree-day factors increased toward the end of melt for the 1987 season. (It should be noted, however, that 1987 was a season with a single large melt event. This area may have several distinct snowpacks with several melt events during a single season. In these cases, snow densities (and therefore degree-day factors) and runoff coefficients cycle up and down several times during a single season. Further study will reveal if the model works as well for years in which this alternation occurs.)

Recession coefficients are calculated daily within SRM from the equation $Q_{n+1} = xQ_n^y$ (Martinec, Rango, Major, 1983), although SRM does allow one change to be input if necessary.

The coefficients were determined from the slope of a line drawn halfway between the 1:1 line and the lower envelope curve of a log plot of Q_n versus Q_{n+1}, as suggested for basins of this size by Martinec and Rango (1983).

Finally, the time lag value of 12 hours was taken from Colquhoun's (1971) previous work on snowmelt modeling in the Independence River basin, and verified through analysis of precipitation and runoff data for the watershed.

Other decisions in the process of model preparation included the treatment of additional precipitation during the study period, as mentioned earlier. While the snowpack was judged to be dry, or at least not fully "ripe", rain and snow amounts were added to the overall water equivalent at the start of the corresponding 15 day period. When the snowpack was at the point of melt (in 1987, this was determined to be by March 15), precipitation was considered available for immediate runoff, and not added to the water equivalent values remaining in the distributed model for each zone.

RESULTS

At the time of this paper, only one year's calibration of the SRM had been completed, that for 1987. Project objectives include at least four additional years of study, including the 1990 season for verification.

The snowmelt season of 1987 was one of constant snow cover until a week of high temperatures at the end of March, during which the majority of the snowpack was melted. The snowpack was fully ripe at the time of the melt event, having reached a density of .35 inches/inch (350 kg/m^3) at the beginning of the March 1-15 period. Precipitation (rainfall) inputs during and after the week of intense melt were judged to flow through the melting pack and enter as immediate runoff, and were thus not added to the daily water equivalent values.

SRM results for the 1987 run, as shown in Figure 2, were promising. As shown by the hydrographs, the volume and timing of the computed runoff both relate well to the observed flow.

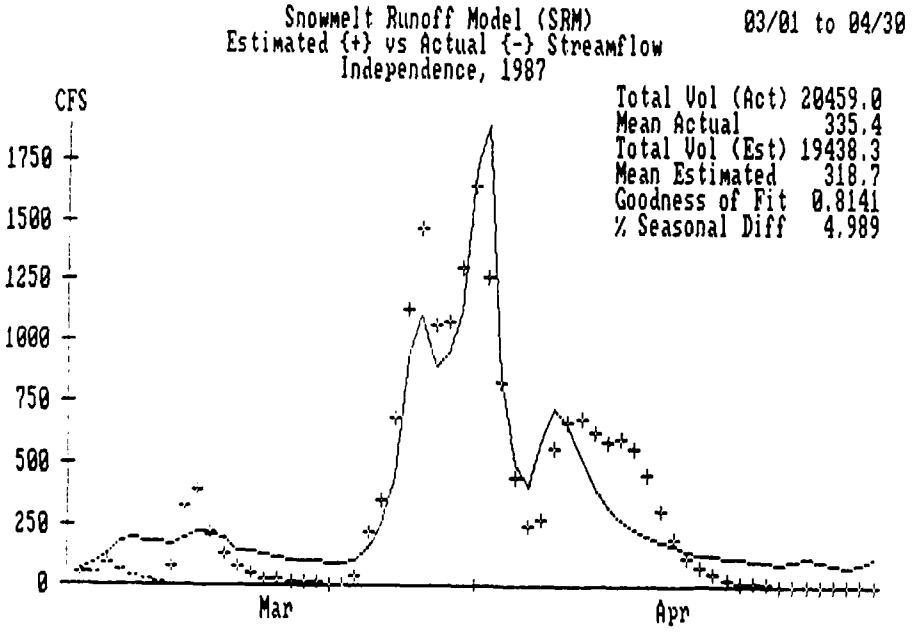

Figure 2: SRM output for 1987

Although differences in actual and estimated total volumes are quite small (with a percent seasonal difference of 4.989) and the hydrographs during the major melt event represent a good computed estimate, there are significant differences in base flow between the computed and actual hydrographs. Base flow was under-estimated and the smaller melt and/or precipitation events were over-estimated. In part this may be explained by the damping effect of the coarse sand deposit which underlies the main channel, on the basin response. This deep deposit's effects are also seen in rainfall hydrographs for the basin, which are much less flashy than those from comparable subbasins in the area.

The recession coefficient calculations may also be subject to additional refinement, although the major recession limb fit is obviously quite good.

GIS model results

The snow depletion computations derived from the irradiance index and degree-day data estimated a very short period of disappearance of snowcovered area, from a three day period for Zone 1, the lowest elevation zone, to a five day time span for the highest zone. However abrupt the snow depletion curves look, they do conform to the standard curve for this process and were sufficient for a successful test of the SRM for 1987. Figure 3 illustrates the depletion curves for the four elevation zones.

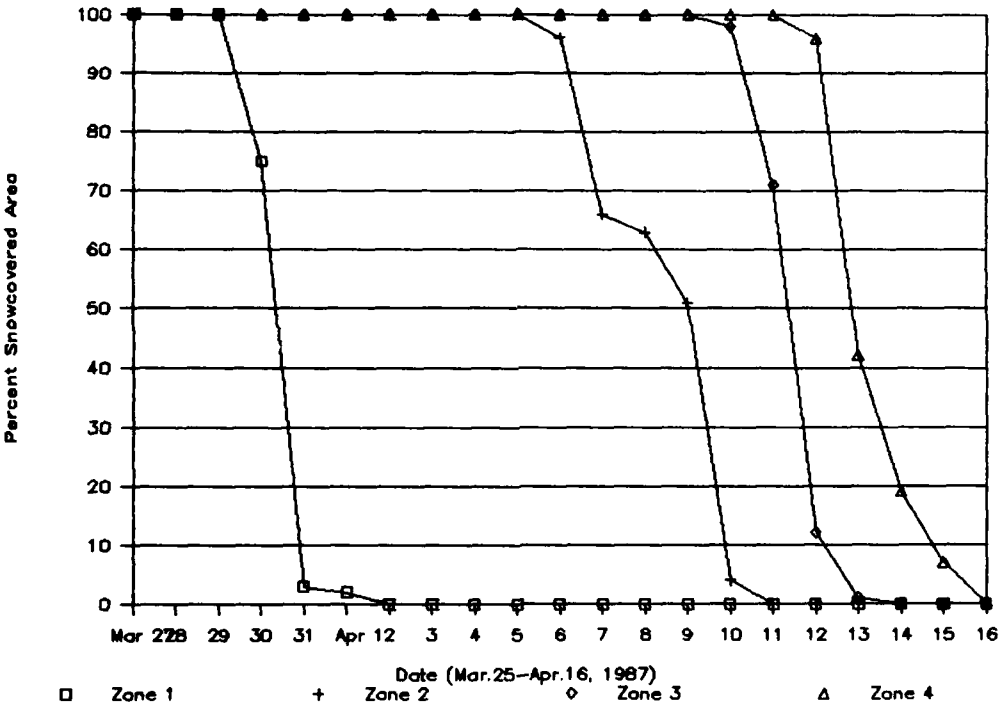

Figure 3: Snow depletion curves, 1987 season (Zone 1 is the lowest, Zone 4 the highest elevation zone)

EVALUATION

The successful results for 1987 are especially encouraging because of the various generalizations and rather subjective decisions made in analysis of SRM's basin variables and in the preparation of all basin parameters. The GIS model is quite primitive, with only one layer of attribute data, a spatial distribution of potential direct solar irradiance based upon averaged classes of aspect and slope facets in the watershed. With inclusion of other data layers of factors affecting snowmelt processes, especially that of forest cover in this project area, the index of irradiance values could be modified and refined to reflect more accurate distribution of snowmelt and thus snowcovered area.

Overall success of the model can only be judged after more years' calibration and verification. As mentioned already, the climate of the western Adirondack area and of northeastern uplands in general, is quite variable, with major thaws likely at any time during the winter months, and with rapid changes in snowpack conditions and depths throughout the season. It is possible that the SRM will be less adaptable to such climatic changes. GIS spatial modeling capabilities, however, should be especially applicable in these conditions, because of their ability to store and update many layers of data, and to provide rapid, repetitive analyses such as that of the melt computations outline in this project.

Ideally, the snowmelt runoff model itself would be built on a GIS platform, which would eliminate duplication of snowmelt computations as carried out in this project (one in the IDRISI melt computations, the other in the SRM flow equation), and allow distribution of climatic variables within the main model. This project's purpose, however, was to test the GIS snowcovered area estimates as substitutes for those obtained from satellite imagery or other remotely sensed data, for use in an existing snowmelt runoff model. The success of the distributed melt and snowcovered area computations from the simple index used in IDRISI encourages further and more complete analysis of geographic information systems as modeling tools in the spatial distribution of variables affecting snowmelt and runoff processes.

REFERENCES

Colquhoun, James R.; Predicting Snowmelt Streamflow from an Adirondack Watershed; unpublished M.S. thesis, State Univ. of N.Y. Coll. of Env. Sci. and Forestry, 1971. 99 pages

Dickinson, R.B.B. and Daugharty, D.A.; Effects of Forest Cover and Topography on Snow Cover in the Nashwaak Experimental Watershed Project; 2nd Conference on Hydrometeorology, American Meteorological Society, 1977, pages 245-250.

Eschner, A.R., Lillesand, T.M. and Meisner, D.E.; Satellite Remote Sensing of Snowcover in the Adirondack Mountains; NOAA Report; State University of New York College of Environmental Science and Forestry, 1977.

Kaufmann, M.R. and Wetherred, J.D.; Determination of Potential Direct Beam Solar Irradiance, USDA Rocky Mountain Forestry and Range Experimental Station Research Paper RM-242; U.S. Department of Agriculture, 1982. 23 pages

Lee, Richard; Potential Insolation as a Topoclimatic Characteristic of Drainage Basins; Hydrology, 1962. Pages 30-38.

Martinec, J., Rango, A., and Major, R.; The Snowmelt Runoff Model (SRM) User's Manual; NASA Reference Publication 1100; National Aeronautics and Space Administration, 1983. 74 pages.

Martinec, J.; Modelling the Snow Accumulation and Snowmelt Runoff; Deutscher Verband fur Wasserwirtschaft, Vol. 7, 1984, pages 59-76.

Martinec, J., and Rango, A.; Areal Distribution of Snow Water Equivalent Evaluated by Snow Cover Monitoring; Water Resources Research, Vol. 17, No. 5, October, 1981, pages 1480-1488.

Reifsnyder, W.E. and Lull, H.H.; Radiant Energy in Relation to Forests, USDA Technical Bulletin Number 1344; USDA Forest Service, 1965. 53 pages

Thompstone, R.M. and Pilon, P.; Square Grid Interpolation of Snow Cover for a Hydrometeorological Information System; Eastern Snow Conference, 1979.

US Army Corps of Engineers; Reconnaissance Report: Black River Basin, New York; US Army Corps of Engineers Buffalo District, October 1988, 131 pages.

Waller, R.M. and Ayer, G.R.; Water Resources of the Black River Basin, New York; New York State Department of Environmental Conservation Basin Planning Report BRB-1, 1975, 205 pages

Preliminary Investigations on Monitoring the Snow Water Equivalent Using Synthetic Aperture Radar

R. LECONTE
Canada Centre for Remote Sensing
1547 Merivale Road
Ottawa, Ontario K1A 0Y7, Canada

T. CARROLL
National Remote Sensing Hydrology Program
Office of Hydrology
National Weather Service, NOAA
6301 34th Avenue South
Minneapolis, Minnesota 554050, U.S.A.

P. TANG
Saint John River Forecast Centre
Department of the Environment
P.O. Box 6000
Fredericton, New Brunswick E3B 5H1, Canada

ABSTRACT

A research project was undertaken to evaluate the utility of airborne Synthetic Aperture Radar (SAR) data for the estimation of SWE over open areas. This cooperative effort involved the cooperation of the Canada Centre for Remote Sensing, the St. John River Forecast Centre, and the U.S. National Weather Service. In addition to the SAR acquisition, the study involved extensive ground measurements in the region of Woodstock and Perth-Andover, New Brunswick. Preliminary results suggest that SAR data may be suitable for the extraction of SWE values over open areas. Future effort will focus on a thorough quantitative analysis of the data, in which the effects of topography, surface roughness, vegetation, and the snowpack structure on the ability to extract SWE values will be evaluated.

INTRODUCTION

Snow is a major component of the hydrological cycle in temperate and boreal environments. As such, snow cover properties, such as the snow water equivalent (SWE) and the areal extent of the snowpack, have been identified as among the most important parameters for flood forecasting, hydroelectric reservoir management, and in water supply and demand management across most of North America. Unfortunately, traditional measurement techniques (snow courses) may not provide accurate and frequent estimates of SWE and snow areal extent over moderate to large areas. Improved water balance estimates could be achieved by increasing the number of snow courses, however, this would result in increasing costs and sampling time. Remote sensing offers new possibilities to snow hydrology because large areas can be quickly investigated at minimum costs. Unfortunately, the presence of clouds can severely compromise the efficiency and limit the potential usefulness of the "traditional" optical sensors (such as Landsat and SPOT) for snow cover monitoring. Microwave systems, on the other hand, are virtually weather independent, which gives them a significant advantage over optical systems for obtaining repeated coverage of a given area.

This paper will describe a cooperative project initiated by the Canada Centre for Remote Sensing (CCRS) in conjunction with the St. John River Forecast Centre (RFC) and the US National Weather Service (NWS), for the estimation of SWE in open areas using active microwave methods. Airborne Synthetic Aperture Radar (SAR) data were collected over a portion of the St. John River Basin during the 1989-1990 winter season. The airborne data collection program was supported by an extensive ground truth program (snow courses) and airborne gamma ray surveys of SWE.

MICROWAVES AND SNOW

Microwaves occupy the portion of the electromagnetic spectrum between 0.3 and 300 GHz (100 and 0.1 cm). However, frequencies employed in remote sensing typically fall within a much smaller window, 1 to 37 GHz (30 to 0.8 cm). Microwaves in this window travel almost unimpeded through the atmosphere, which confers to systems operating at those frequencies the ability to penetrate through clouds.

Snow is a three-component mixture consisting of air, ice particles, and liquid water. At temperatures below 0^0C, snow is said to be dry, since it contains no "free" liquid water. It will, however, contain small amounts of "liquid-like" water in thin films around, and bound to, ice crystals (Hobbs, 1974).

The air and ice that constitute dry snow have different electrical properties, which is reflected in the value of their dielectric constant. The microwave response properties of snow-covered terrain depend strongly, among other factors, on the dielectric properties of the snow volume. The combination of air (dielectric constant $\epsilon = 1$) and ice ($\epsilon = 3.2$) results in dry snow having a ϵ between 1.2 to 2.0 for snow densities ranging from 0.1 to 0.5 g/cm3 (Hallikainen and Ulaby, 1986). In wet snow, however, the high value of the dielectric constant of liquid water (typically around 80 at frequencies of 1 to 10 GHz) is such that, even with small amounts of free water in a snow pack, the resulting dielectric constant is substantially increased.

Two factors give dry snow a unique behaviour with respect to microwaves. First, microwave energy can penetrate the pack without being significantly absorbed (Matzler and Schanda, 1984). The dry snow is said to be "lossless". The second factor is that, because the microwaves can enter the snow volume, they can be subjected to scattering within the pack. It is the combination of these properties which confers to the microwaves the potential for remote sensing SWE.

Liquid water in the snow presents two complications for microwave remote sensing (Bernier, 1987). First, small amounts of liquid water in a snow pack turns the snow into a "lossy" medium. The wet snow will absorb most of the microwave energy, with little scattering occurring. Because the penetration depth of the pack (depth to which 63% of the microwave energy is absorbed) is reduced to the order of one wavelength with a 4-5% snow wetness (Matzler and Schanda, 1984), scattering is limited to a thin layer and retrieval of SWE becomes impractical. The second problem relates to the difficulty of measuring the snow liquid water content in the field (Colbeck, 1978), especially at shallow depths where complete penetration of the microwaves through the pack may occur.

The present study focuses on interactions of dry snow with microwaves in the 3.1 - 5.7 cm wavelengths (9.8 to 5.3 GHz).

ACTIVE MICROWAVE SYSTEMS FOR SWE ESTIMATION

Techniques for microwave remote sensing can be classified as either passive or active. Passive systems employ downward pointing radiometers which record natural upwelling microwave energy. Such radiometers have been aboard many satellites, and their potential for measuring SWE has been demonstrated by various researchers (Goodison, 1989; Rango et al., 1989; Chang et al., 1987). The ground resolution of these systems is on the order of 30-50 km.

Active systems, such as SAR, emit microwaves toward the ground and measure the reflected, or backscattered, signal. The SAR is an imaging system, in that it converts the backscattered energy into digital values that can be displayed as video image. It is also a side-looking system, meaning that the microwave beam is emitted at an angle off the nadir flight line. SAR can achieve a much finer resolution than passive systems, typically in the order of 10-100 meters. To date, the only satellite which carried a SAR onboard was SEASAT, which was launched in 1978 and decommissioned after only three months because of a major electrical failure. Consequently, research in the use of active sensors for SWE extraction has been limited to a few ground-based scatterometer experiments (Stiles and Ulaby, 1980; Matzler and Schanda, 1984) and airborne missions (Goodison et al., 1980; Bernier and Fortin, 1989; Leconte and Pultz, 1990). Although encouraging results have been obtained, no algorithms have been developed for extracting SWE from SAR data. With the advent in the 1990's of many

SAR platforms (ERS-1 in 1991, RADARSAT in 1994, EOS dedicated platform in 1998-99) there is a need for increased research in this area.

The amount of backscatter received by the SAR antenna is the sum of surface scattering at the snow-air interface, volume scattering within the snowpack, scattering at the snow/soil interface and volumetric scattering from the soil. Atmospheric scattering is usually very small and can be neglected. Figure 1 illustrates the concept.

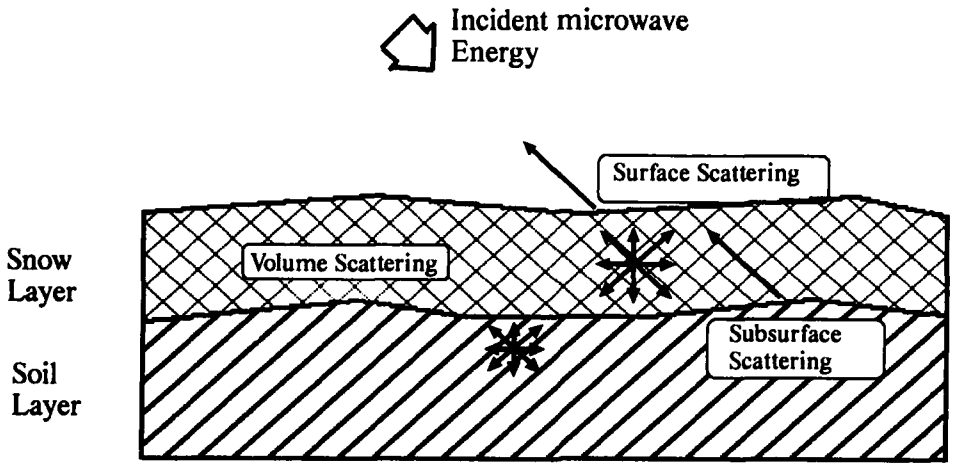

Figure 1: Scattering mechanisms in a snow covered surface

Volume scattering in dry snow is the result of dielectric discontinuities in the electric properties of ice crystal and air. The level of scattering is strongly influenced by scene and instrument parameters. Scene parameters include the structural properties of the pack (crystal size and shape, and stratigraphy), and the snow depth and density. Volumetric backscatter increases with an increase in snow quantity (Stiles and Ulaby, 1980). For a given wavelength, scattering increases with snow grain size and layering (Bernier, 1987). The most significant instrument parameter is probably the microwave wavelength. Typically, wavelengths shorter than snow crystal size (0.05 to 1 mm) are strongly scattered even by the thinnest snowpack, while wavelengths longer than 10 or 15 cm travel almost unaffected through most seasonal dry snowpacks (Bernier, 1987).

In addition to the snowpack characteristics, the soil surface roughness, soil moisture levels, and overlying vegetation are parameters whose influence on the total backscatter signal will be significant, especially at longer wavelengths. Schanda (1987) observed that at lower microwave frequencies (longer wavelengths) the measured backscatter values were strongly affected by reflections from the soil below the snow cover due to the large penetration depth in dry snow. Leconte and Pultz (1990) noted that, depending on the soil surface roughness, an increase in SWE could result in either an increase of the total backscatter signal (caused by an increased volumetric scattering), or a decrease of the total radar return (resulting from a reduced contribution from the soil surface caused by attenuation in the snowpack). This makes estimating SWE from SAR data a difficult task because of the problem in discriminating between volumetric scattering within the snowpack and surface scattering at the ground/snow boundary. The problem increases in complexity in a forested environment, as trees scatter most of the incident microwave energy, especially at shorter wavelengths, with little left energy reaching the snowpack. To date, research has been limited to open areas (Goodison et al., 1980; Bernier and Fortin, 1989; Leconte and Pultz, 1990).

Finally, when the snow is dry, the contribution from the air/snow surface is negligible because of the small dielectric discontinuity at the boundary, and can usually be neglected (Stiles and Ulaby, 1980).

SAINT JOHN RIVER BASIN STUDY

Study Site

The study site is located in the potato cultivation belt in western New Brunswick, north of Woodstock and south of Perth-Andover. The area extends 40 km E-W and 90 km N-S (Figure 2).

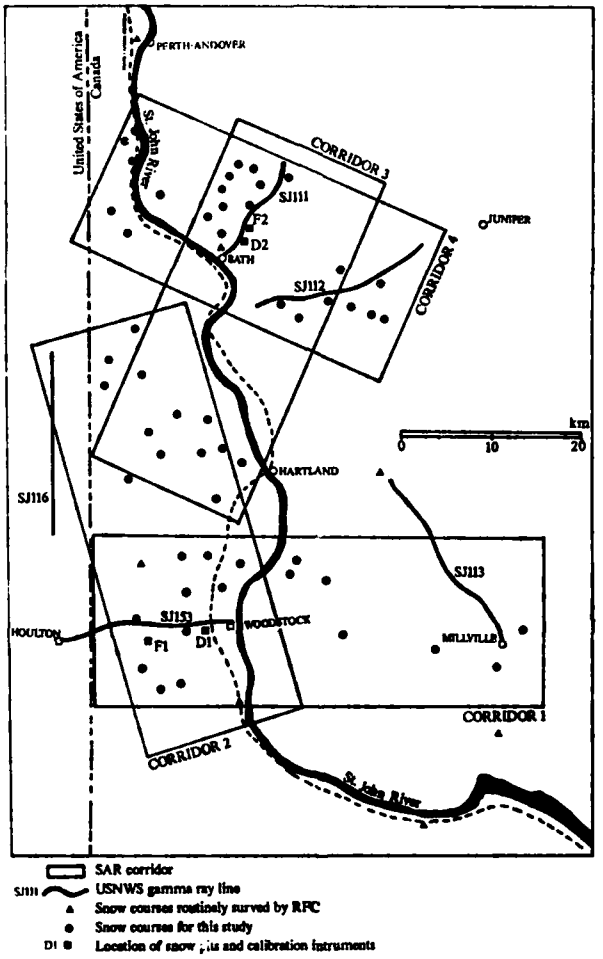

Figure 2: Study site

The St. John River runs through the study area in a N-S direction. The area west of the river is characterized by a rolling topography, where more than 30 percent of the surface area is agricultural land. Snow depth is relatively uniform over the region, with a small increase toward the north and west. Snow records indicate that SWE accumulation typically reaches 100 mm. The study area located east of the St. John River is characterized by rougher terrain, with elevations ranging from less than 100 meters at the river to more than 250 meters in the eastern most section. Accordingly, variations in SWE are more pronounced, with values typically between 100 and 175 mm. This area is mostly forested, with about 10-15 percent of land devoted to agriculture, mainly in the Bath area (see Figure 2). The St. John RFC routinely performs snow surveys at a few locations in or around the study area. Gamma ray surveys are also conducted once or twice a year by the NWS. The location of the snow survey courses and gamma ray flight lines is also shown in Figure 2.

SAR Experiments

The system used is the C/X SAR system installed in CCRS's Convair-580 aircraft. It is a digitally controlled, two-channel radar, operating simultaneously at C (5.7 cm, 5.3 GHz) and X band (3.2 cm, 9.6 GHz), transmitting microwave energy at either horizontal (H) or vertical (V) polarization and receiving both polarizations simultaneously. It was demonstrated that this system could discriminate targets with very low backscatter values, making it well adapted for monitoring SWE. Data can be acquired in three nominal imaging modes: "nadir", "narrow swath", and "wide swath". The characteristics of the imaging modes are described in Table 1. A more detailed description of the system can be found in Livingstone et al (1988) and will not be repeated here.

Table 1: Imaging modes of the C/X SAR system

Mode	Incidence angle (deg) from	to	Resolution (m) Range	Azimuth	Swath width (km)
Nadir	0	74	6	6	22
Narrow swath	45	76	6	6	18
Wide swath	45	85	20	10	63

Note: the specifications are for an optimum aircraft altitude of 6 km.

Two SAR flight missions took place during the 1989-1990 winter season. Ideally, the SAR flights were to occur so that temporal differences in SWE would be maximized. The target window for the first mission was from November 15 to December 15. The first SAR deployment occurred on December 13 and 14 1989, when the snow cover was relatively thin, although in some locations the SWE had already reached 70 to 80 mm. The second flight mission occurred on February 6 and 7 1990, one week following a storm that left approximately 45 cm of snow in the Fredericton area.

The corridors that were imaged cover a surface area of approximately 3000 sq. km (Figure 2). The study site is roughly subdivided into two sub-areas, the West site (west of the St. John River) and the East site. The West site is mostly covered by corridors 1 and 2 (see Figure 2), while corridors 3, 4, and a portion of corridor 1 cover the East site. The rationale for selecting two distinct sub-areas was based on the snow conditions usually encountered in those areas. Typically, the Woodstock site is characterized by relatively uniform snow depths and SWE, while a strong gradient in SWE is usually encountered at the East site due to variations in elevation.

On each mission, the four corridors were flown 2 to 4 times, covering various combinations of polarizations (HH, HV, VV) and incidence angle ranges (0-74 degrees for nadir mode; 45-76 degrees for narrow swath mode).

In order to extract quantitative information on geophysical parameters, such as SWE, SAR data need to be calibrated. This can be achieved by deploying, in the study area, point targets of known reflectance values (or "radar cross section" in the microwave jargon). The brightness of each pixel making a SAR image is then converted into a radar backscatter value (absolute calibration), or is adjusted to another SAR data set (relative calibration), with algorithms using radar cross section values and SAR system parameters as input data.

Point targets that were used for the SAR experiments are trihedral Corner Reflectors (CR) and Active Radar Calibrators (ARC). A trihedral CR consists of three metal plates assembled together to form orthogonal planes. The size and geometry of the reflector determines its radar cross section, which in turn is related to the brightness of the target on a radar image. A CR will appear as a single bright point on a SAR image. An ARC is an electronic device which receives the incident microwave signal, amplifies and modulates it, and returns a signal corresponding to a target of known cross section. A "recirculator" allows more than one bright point to appear on a radar image.

Snow Data Collection Campaign

Snow Surveys:

There were 52 open fields identified for the snow sampling exercise (Figure 2). In addition, 4 fields were selected for the deployment of the ARCs and CRs. Two sites were used for the December mission (D-1, D-2), and February mission (F-1, F-2) (Figure 2).

The selected fields covered surface areas ranging from 20 to 200 hectares, and the elevation varied from 100 to more than 300 meters. Some fields were sheltered by wood lots, while others were more exposed to wind. The intent was to select fields which would represent a wide range of SWE accumulation both spatially (from field to field) and temporally.

Coinciding with the mid-December flight, samples were taken at 50 sites for both snow depth and water equivalent. Depending on the variability of the measurements obtained, three to five snow samples were taken using a Mount Rose Federal snow sampler. The distance between the samples was approximately 30 meters.

On February 6 and 7, only 37 of 52 sites were sampled due to the shortage of personnel and unfavourable weather conditions. Estimates were made for the remaining 15 sites based on a partial survey carried out on March 2 along with local weather data. Results of the surveys are summarized in Table 2. Values of SWE were corrected to account for positive biases introduced by the sampler. A 10% overestimate in SWE was assumed (Goodison, 1978).

Table 2: Results of the snow surveys, December 89 and February 90

	West site (27 fields)		East site (25 fields)	
	Dec. 89	Feb. 90	Dec. 89	Feb. 90*
mean SWE (mm)	51	113	59	132
max SWE (mm)	107	176	87	190
min SWE (mm)	17	27	25	81
mean depth (cm)	31	44	32	51
max depth (cm)	49	76	45	83
min depth	13	18	18	28

* Values for 15 fields were estimated from a survey on March 2, 90.

The fields had also been visited before and after the snow season and the following information was collected:

- ground cover type (bare, vegetated);
- tillage practice (row direction, row spacing, peak-to-trough height);
- surface roughness (smooth, intermediate, rough, based on a visual interpretation of the surface).

The field characterization was supplemented by ground photographs. At least three shots were taken for each field: a vertical photograph showing fine scale details of the surface; an oblique photograph showing vegetation and tillage practice; and a photograph covering most of the field.

Airborne Gamma Radiation Snow Measurements:

The U.S. National Weather Service has developed and maintains the National Operational Hydrologic Remote Sensing Center based in Minneapolis, Minnesota. The Center is responsible for making airborne snow water equivalent measurements and satellite areal extent of snow cover measurements over the U.S. and southern Canada. The airborne and satellite snow cover data are provided in real-time and used operationally by various federal, state, provincial, and private agencies in the U.S. and Canada when issuing spring flood outlooks, water supply forecasts, and river and flood forecasts.

The technique used to make airborne snow water equivalent measurements uses the attenuation of natural terrestrial gamma radiation caused by the mass of the snow cover. Root mean square errors are typically less than 1.0 cm of snow water equivalent over agricultural environments and approximately 2.0 cm over forested areas. The technique requires the estimation of the background gamma radiation, which is a function of soil moisture and obtained by flying the area in absence of a snow cover. Details of this technique and the associated errors have been thoroughly discussed by Carroll and Carroll (1990, 1989A, 1989B) and by Glynn, et al. (1988) and will not be presented here.

Airborne data are routinely collected over the St. John River basin. Each flight line is typically 16 km long and 300 m wide covering an area of approximately 5 sq km. Consequently, each airborne snow water equivalent measurement is a mean areal measure integrated over the 5 sq km area of the flight line.

On February 7-12, 1990, an airborne gamma radiation snow survey was conducted over 49 previously established flight lines in the St. John River basin. One additional flight line (SJ153) was added to the operational network in support of this study. Consequently, no background radiation data for flight line SJ153 were available to directly calculate snow water equivalent using the appropriate background radiation measurements. Nonetheless, it is possible to estimate the background radiation for SJ153 from the mean of the background radiation data for three nearby flight lines and to infer a reasonable airborne snow water equivalent value for the line. The average background radiation, normalized to 25 percent soil moisture for lines SJ113, SJ116, and SJ117, were used to estimate the background radiation for SJ153.

Some estimate of mean soil moisture conditions in the upper 20 cm of soil is required to calculate snow water equivalent. Since no ground-based soil moisture data were available for this analysis, typical values ranging from 15-35 percent gravimetric soil moisture were used.

Table 3 presents the results of the February, 1990, survey for the five lines of specific interest to this study: SJ111, SJ112, SJ113, SJ116, and SJ153, and using gravimetric soil moisture estimates of 15, 25, and 35 percent. Overall, the airborne gamma SWE estimates were higher than the snow survey data. A possible explanation for this apparent discrepancy lies in the fact that only open fields were surveyed, as opposed to the 5 sq km coverages of the gamma ray lines, which included both forested and open sites. The closest fit was observed along the flight lines SJ111 and 112 with a 35% gravimetric soil moisture (respectively 133 and 151 mm as compared to average ground measurements of 130 and 153 mm), a mostly agricultural area.

Table 3: Results of the Gamma Ray survey, February 90

FLIGHT LINE	SOIL MOISTURE	SWE (cm)	FLIGHT LINE	SOIL MOISTURE	SWE (cm)
SJ111	15	16.2	SJ153	25	13.7
SJ112	15	18.1	SJ111	35	13.3
SJ153	15	15.2	SJ112	35	15.1
SJ111	25	14.7	SJ113	35	14.5
SJ112	25	16.5	SJ116	35	16.0
SJ113	25	16.0	SJ153	35	12.2
SJ116	25	17.5			

Snow Pit Measurements:

Coinciding with the SAR overflights, the snowpack was characterized from measurements obtained in snow pits. Jones (1983) recommended use of at least one snow pit for each SAR flight corridor. Due to limited resources, however, it was decided to minimize the number of snowpits by locating them at the intersections of flight corridors. These locations coincide with those of the calibration targets (Figure 2).

The variables and parameters measured in the snow pits were: snow depth, SWE, snow density using a Mount Rose snow sampling kit; vertical temperature profile using thermoresistors;

vertical density profile using a portable snow density kit; vertical dielectric profile using portable dielectric probes (Brunfeldt, 1987); crystal shape and size using a magnifying lens; and depth of layers in the snowpack.

The snowpack December 89 was observed to be homogeneous, that is there was no layering present. The density increased slightly with depth from approximately 0.15 to 0.20. SWE was found to be 64 mm and 38 mm at locations D-1 and D-2, respectively. Crystals had angular shapes and a diameter ranging from 0.5 to 1.5 mm. The snowpack was said to be dry during the SAR overpass. The measured temperature in the pack hence remained below 0^0C. Air temperature varied from -16 to -12^0C, and the first few centimeters of the ground were frozen.

During the February 1990 mission, the snowpack was more stratified, and the grains were more rounded and bonded (melt-freeze metamorphism) . The diameter of a typical cluster of grains averaged 2-3 mm. The SWE and snow density had increased significantly, with average values of 97 mm and 0.27 for site F-1, and 102 mm and 0.30 for site F-2. The temperature in the pack remained below 0^0C during the SAR flight, again preserving a dry pack. This was confirmed by dielectric measurements which never exceeded 2.05. The soil surface was frozen, and temperature measurements at the bottom of the snow pack were very near the freezing point (-1^0C at F-1, and -2^0C at F-2). This may suggest that, due to inherent variations in soil cover type, aspect, and SWE, the entire surface of some fields may have not been completely frozen. This was confirmed on a few occasions during the snow surveys.

Description of the Imagery

Although the primary objective of this study is to develop a methodology to extract quantitative information on the snowpack from SAR data, a qualitative analysis of the imagery is an essential first step. This type of analysis would provide insight on specific mechanisms and processes which should contribute to the radar backscatter as observed on the images. The quantitative analysis of the SAR data has only been recently initiated and no preliminary results are yet available. Due to space limitations, only the C-HH image of line 4 will be presented here.

December 89 Data:

The C-band HH nadir mode data of line 4 is shown in Figure 3. This image represents raw SAR data (no geometric or radiometric corrections) produced from the Real Time SAR Processor on board the aircraft. The look direction is south, meaning that the radar illumination is from north to south (top to bottom on the figure). The uneven illumination in the across track direction (perpendicular to the flight line) is the result of an unequal distribution of the microwave energy across the swath. Note the compression of the data in the top portion of the figure. This compression is an inherent characteristic of any imaging radar as radars are side looking instruments and are range measuring devices. This geometric distortion becomes more apparent at steeper incidence angles (typically from 0 to 30 degrees).

The C-HH imagery shows that the agricultural fields exhibit large variations in radar backscatter values. While some fields are characterized by a very low radar return, others display rather bright signatures. One possible explanation for these differences may be related to differences in SWE, however, examination of the SWE values does not support this assumption. For instance, some fields having similar SWE values clearly showed different radar returns. An alternative explanation relates to variations in ground cover type and/or roughness. Most of the fields surveyed were bare with varying levels of surface roughness while some had vegetation and other were pasture. It would appear, therefore, that the ground surface is an important contributor to the total radar backscatter. This hypothesis was further supported by field observations showing that the snowpack was dry at the time the SAR imagery was taken, thereby allowing transmission of the microwave energy through the pack.

Generally speaking, forests appear brighter than do agricultural fields. Volumetric scattering within the forest canopy is the major contributor to the total radar backscatter. The signature of agricultural fields is a combination of scattering within the snowpack, surface scattering from the soil surface, and multiple scattering at and between the soil/snow interface and the snowpack.

Figure 3: SAR C-HH line 4 image of Woodstock site: 13/12/89

The city of Woodstock can be clearly identified on the radar image. The particular geometry of houses and buildings (orthogonal planes) results in the generation of high backscatter values. Smooth streets act as specular reflectors of the microwave energy, hence their dark signature. In addition, the St. John River was not completely frozen, and large ice floes are visible on the imagery.

Field D-1, where an ARC and a corner reflector were deployed during the SAR overpasses, is shown in Figure 3. A total of 5 recirculation points were generated by the ARC, while the corner reflector is seen as a single point on the imagery. Figure 4 displays an enlarged portion of the C-HH imagery, showing field D-1 and surrounding fields. The CR and the ARC are now clearly visible.

February 90 data:

The C-band HH nadir mode image is shown in Figure 5. The horizontal "banding" in the imagery is caused by an unequal distribution of the microwave energy in the across track direction. The image is similar to that obtained in December 89, with forested areas appearing as bright targets, and agricultural fields appearing as darker tones. Although similar in appearance to December, the signature of these fields differ in two ways:

1) The appearance of thin bright linear features, especially in the mid to upper portion of the imagery;

2) A noticeable reduction in contrast between some of the fields.

Figure 4: ARC and CR at site D-1

Figure 5: SAR C-HH line 4 image of Woodstock site: 06/02/90

The presence of the bright linear features running across some of the fields does not lend itself to an obvious explanation. Examination of Figure 5 reveals that most of these fields are located in the upper portion of the imagery, i.e. at steep incidence angles. This suggests that these features may be incidence angle dependent. The configuration of the features may also suggest that they are related to drainage patterns within the snowpack or at the soil surface. The observed presence of an unfrozen soil surface in some of the fields reinforces the latter hypothesis. When saturated, the unfrozen soil may generate high backscatter values. However, these drainage patterns should then run along the main slope of the fields.

Further examination reveals that all of these features are oriented along an approximate north-south axis. Consequently, another possible mechanism would be related to snow drifting which results in an uneven snowpack surface. The presence of "waves" at the surface of the pack is not an uncommon occurrence. Westerly winds would generate waves oriented in a north-south direction. Following a rainfall episode, an ice layer forming at the top of the pack would preserve the ondulating pattern. The existence of such a layer, 3 to 5 cm thick, was confirmed by field measurements. Its occurrence may be responsible for the observed linear features. It should be noted that the fields which exhibit these linear features are located in areas which are very exposed to winds, whereas other fields located approximately at the same range from the radar, but which are more sheltered, do not exhibit these patterns (see Figure 5).

Assuming that the soil surface did not change between the two SAR missions, the differences in backscatter values should be related in some complex fashion to variations of the snow cover properties. The apparent reduction in contrast between agricultural fields may be the result of an increase in the SWE. Using a simple backscatter model developed by Ulaby et al. (1982), Leconte and Pultz (1990) have proposed that the total backscatter from a snow covered surface will increase with an increase in SWE for smooth fields, whereas a decrease in the total radar return should occur in rough fields. The model does not account for any multiple scattering effects which may occur between layers in a snowpack, and therefore should be used with caution in analyzing the February data. Nevertheless, observations from this simple model seem to support the hypothesis that increasing the SWE decrease the dynamic range of the observed radar signatures. Another explanation for this apparent reduced contrast may be related to the presence of liquid water in the pack. However, ground measurements indicated that the pack was dry, and that dielectric values did not differ from that of dry snow. There is a need to further investigate these hypotheses through a rigorous digital analysis of calibrated SAR data, in which topographic, surface roughness, and system related effects will be removed or minimized.

Analysis of the SAR data

It becomes obvious from the SAR imagery shown above that the extraction of SWE from SAR data is not a straightforward task, as the contribution to the total backscatter from the soil surface cannot be neglected and, in many situations (longer wavelengths, thin snow packs), it dominates the signal.

Two modelling approaches will be utilized for the quantitative analysis of the SAR data. The first approach, known as the "change detection technique", consists in relating temporal changes in radar returns to changes in snow coverage. Ulaby, et al. (1982) have indicated that this approach may be quite useful in estimating SWE over large areas. Roth, et al. (1985) also noted that improved capabilities for snow mapping are expected through multidate observations.

In addition to the change detection technique, which is entirely empirical, a semi-empirical approach, based on the "cloud model" developed by Ulaby, et al. (1982), will be tested. The model as the following form:

$$\sigma^{\circ}(\theta) = \gamma^{2}(\theta) * \frac{\sigma_{v} \cos\theta'}{2k_{e}} * \left(1 - \frac{1}{L^{2}(\theta')}\right) + \frac{\sigma_{s}^{\circ}(\theta')}{L^{2}(\theta')} \qquad (1)$$

where

$\gamma(\theta)$	=	power transmission coefficient of the snow-air boundary, dimensionless
θ	=	angle of incidence from nadir
σ_v	=	volume reflectivity of snow, 1/cm
k_e	=	volume extinction coefficient of snow, 1/cm
	=	k_a+k_s, the absorption and scattering coefficients, respectively
θ'	=	angle of refraction, related to θ by Snell's law
$\sigma_s^\circ(\theta')$	=	backscattering coefficient of the underlying ground medium
$L(\theta')$	=	loss factor of the snow layer
$L(\theta')$	=	$\exp(k_e\ d\ \sec\ \theta')$, where d is the snow depth in cm.

This approach ignores diffuse scattering (which accounts for multiple scatter in the snowpack) and multiple reflections between the air-snow and the snow-soil interfaces within which the snow layer is bounded.

Shi, et al. (1990) have proposed an interesting approach for SWE estimation based on equation (1), which employs ratios and differences of HH and VV polarization images. This approach, or a variation of it, will be tested in this study. Carver (1987) has also suggested an approach based on the cloud model, which employs a combination of three frequencies. However, because only C- and X-band data are available, this approach will not be considered.

An essential requirement to both the change detection technique and the cloud model approach to SWE estimation is for calibrated imagery. For example, the change detection approach requires the SAR data to be relatively calibrated, so that any change in reflectances caused by system instabilities be removed, leaving only changes resulting from variations in SWE. Calibration algorithms are under development at CCRS, and softwares will be available in a near future.

In addition to the calibration of the SAR data, other preprocessing tasks will be performed in preparation for the SWE analysis. These are:

- geometric corrections of the imagery (for example to remove the range compression characterizing nadir mode images);
- radiometric corrections (for example to remove the antenna pattern);
- filtering of the data to reduce the "speckle", a salt and pepper texture inherent to any SAR images;
- registration of the imagery to a common base map.

The proposed analyses will make full use of the capabilities of digital image analysis systems and will be carried out in a GIS environment. Field boundaries and the gamma ray coverages will be digitized and attributes, such as slope, aspect, snow depth, SWE, roughness, will be entered in a data base for optimal use by the GIS. Average radar backscatter values will be extracted for each field and gamma ray coverages and imported into the GIS data base, allowing to investigate any relationships between the radar signal and SWE.

CONCLUSION

The very preliminary results obtained so far suggest that SAR data may be suitable for the extraction of SWE values over open areas. However, several issues will need to be addressed. Among them:

- the effect of soil surface properties (roughness, vegetation) on SWE estimation from SAR data;
- the effect of topography on the ability to extract SWE from SAR data;
- the effect of snowpack stratification, grain size and shape, and other structural features on the backscatter properties of the snowpack;
- the possibilities and limitations of SAR for SWE estimation in forested environments.

It is evident here that a simple qualitative analysis of airborne SAR data will not be sufficient for extraction SWE, and that sophisticated image analysis techniques will be required.

In addition, the translation from airborne to satellite data will complicate the issue because of the coarser resolution of these systems. Nevertheless, satellites such as RADARSAT, will have certain advantages over airborne systems: less costly repetitive coverage; larger areas of coverage; smaller incidence angle variations across a swath; and since these systems will be electronically more stable, use of external calibration (using ARCs and CRs) may not be necessary.

The 1990's will bring forth the launch of several satellites carrying onboard SAR payloads. The all weather capability of these systems warrants an assessment of their suitability for the extraction of snow cover information for hydrological applications. This study is a step in that direction.

REFERENCES

Bernier, P.Y. (1987). "Microwave remote sensing of snowpack properties: potential and limitations". Nordic Hydrology, Vol. 18, pp. 1-20.

Bernier M., and J.P. Fortin (1989). "Suivi de la couverture de neige au moyen d'un radar a ouverture synthetique". Proceedings of the IGARSS'89 12th Canadian Symposium on Remote Sensing, Vol. 3, pp 1251-1255.

Brunfeldt, D. (1987). "Theory and design of a field portable dielectric measurement system". Proceedings of IGARSS'87 Symposium, Ann Arbor, 18-21 May 1987, pp 559-563.

Carroll, S.S. and Carroll, T.R. (1990). "Simulation of airborne snow water equivalent measurement errors in extreme environments". Nordic Hydrology (in press)

Carroll, S.S. and Carroll, T.R. (1989A). "Effect of uneven snow cover on airborne snow water equivalent estimates obtained by measuring terrestrial gamma radiation". Water Resources Research. 25 (7), pp 1505-1510.

Carroll, S.S. and Carroll, T.R. (1989B). "Effect of forest biomass on airborne snow water equivalent estimates obtained by measuring terrestrial gamma radiation". Remote Sensing of Environment. 27 (3), pp 313-319.

Carver, K. (1987). "Synthetic Aperture Radar". Earth Observing System Instrument Panel Report, Vol. IIf, NASA, 233 pages.

Chang, A.T.C., J.L. Foster, and D.K. Hall. (1987). "Nimbus-7 SMMR derived global snow cover parameters". Annals of Glaciology 9, 7 pages.

Colbeck, S. (1978). "The difficulties of measuring the water saturation and porosity of snow". Journal of Glaciology, Vol. 20, pp. 189-201.

Glynn, J.E., Carroll, T.R., Holman, P.B., and Grasty, R.L. (1988). "An airborne gamma ray snow survey of a forest covered area with deep snowpack". Remote Sensing of Environment. Vol. 26, No. 2, pp. 149-160.

Goodison, B.E. (1989). "Determination of areal snow water equivalent on the Canadian Prairies using passive microwave satellite data". Proceedings of IGARSS'89 12th Canadian Symposium on Remote Sensing, 10-14 July 1989, Vol. 3, pp 1243-1246.

Goodison, B.E., S.E. Waterman, E.J. Langham (1980). "Application of syntheric aperture radar data to snow cover monitoring". Proceedings of the 6th Canadian Remote Sensing Symposium, Halifax, N.S., May 21-23 1980, pp. 263-271.

Goodison, B.E. 1978. "Accuracy of snow samples for measuring shallow snow packs: an update". Proceedings 35th Annual Meeting Eastern Snow Conference, pp. 36-49.

Hallikainen, M., and F.T Ulaby (1986). "Dielectric and scattering behaviour of snow at microwave frequencies". Proceedings of IGARSS'86 Symposium, Zurich, 8-11 Sept 1986, pp. 87-91.

Hobbs, P.V. (1974). "Ice physics". Clarendon Press, Oxford, U.K. 837 pages.

Jones, E.B. (1983). "Snowpack ground truth manual". NASA contract NAS 5-26802, 42 pages.

Leconte, R. and T.J. Pultz (1990). "Utilisation of SAR dta in the monitoring of snowpacks and wetlands". Proceedings of the Workshop on Application of Remote Sensing in Hydrology, Saskatoon, Sask., February 13-14, 1990.

Livingstone, C.E. et al. (1988). "CCRS C/X airborne synthetic aperture radar: an R and D tool for the ERS-1 time frame. Proceedings of IEEE Nat. Radar Conf. Ann Arbor, Mi. April 20-21.

Matzler, C., and E. Schanda (1984). "Snow mapping with active microwave sensors". International Journal of Remote Sensing, Vol. 5, No. 2, pp. 409-422.

Rango, A., et al. (1990). "Average areal water equivalent of snow in a mountain basin using microwave and visible satellite data". IEEE Transactions on Geoscience and Remote Sensing, Vol. 27, No. 6, pp 740-745.

Rott, H., G. Domik, C. Matzler, H. Miller, K.G. Lenhart (1985). "Study on use and characteristics of SAR for land snow and ice applications". Final report, ESA contract No. 5441/83/D/IM(SC), 117 pages.

Schanda, E. (1987). "On the contribution of volume scattering to the microwave backscattered signal from wet snow and wet soil". International Journal of Remote Sensing, Vo. 8, No. 10, pp. 1489-1500.

Shi, J., J. Dozier, and R.E. Davis. (1990). "Simulation of snow-depth estimation from multi-frequency radar". Proceedings of the IGARSS'90, Washington, D.C., pp. 1129-1132.

Stiles, W.H., and F.T. Ulaby (1980). "Microwave remote snesing of snowpacks". NASA contractor report 3263, Contract NAS5-23777, 404 pages.

Ulaby, F.T., R.K. Moore, A.K. Fung (1982). "Microwave remote sensing - active and passive". Vol II, Addison-Wesley Publishing Company.

Operational Airborne and Satellite Snow Cover Products of the National Operational Hydrologic Remote Sensing Center

T.R. CARROLL

National Operational Hydrologic Remote Sensing Center
Office of Hydrology
National Weather Service, NOAA
6301 34th Avenue South
Minneapolis, Minnesota 55450, U.S.A.

ABSTRACT

The Office of Hydrology of the National Weather Service maintains a cooperative National Operational Hydrologic Remote Sensing Center, based in Minneapolis, to generate remotely sensed hydrology products. Terrestrial gamma radiation data sensed from low-flying aircraft provide information to infer snow water equivalent over a network of more than 1500 flight lines covering portions of 25 states and 7 Canadian provinces. Additionally, hydrologists use Advanced Very High Resolution Radiometer (AVHRR) data and Geostationary Operational Environmental Satellite (GOES) data to map digitally areal extent of snow cover over regions covering two-thirds of the U.S. and southern Canada where snow cover is a significant hydrologic variable. This paper reviews the techniques: (1) to make airborne snow water equivalent measurements using terrestrial gamma radiation data, (2) to make satellite areal extent of snow cover measurements, and (3) to reduce and to distribute, in near real-time, both alphanumeric and graphic products to end-users in the U.S. and Canada.

1 INTRODUCTION

The National Weather Service maintains a cooperative National Operational Hydrologic Remote Sensing Center, based in Minneapolis, to generate remotely sensed hydrology products. The National Weather Service, the U.S. Army Corps of Engineers and other Federal, state, and private agencies use the real-time, airborne snow water equivalent data and satellite areal extent of snow cover data operationally when issuing spring flood outlooks, water supply outlooks, river and flood forecasts, and reservoir inflow forecasts. Hydrologists in the Minneapolis office ingest and process the airborne and satellite data and distribute products electronically, in near real-time, to NWS and non-NWS end-users in both alphanumeric and graphic format.

2 AIRBORNE GAMMA RADIATION SNOW MEASUREMENT TECHNIQUE

The potassium, uranium, and thorium radioisotopes in the upper 20 cm of soil emit natural terrestrial gamma radiation. A detection system on-board an aircraft flying 150 m above the ground senses the terrestrial radiation. The water mass in the snow cover attenuates, or blocks, the terrestrial radiation signal. Consequently, the difference between airborne radiation measurements made over bare ground and snow covered ground provides sufficient information to calculate a mean areal snow water equivalent value with a root mean square error of less than one cm. Each flight line is typically 16 km long and 300 m wide covering an area of approximately 5 sq km. Consequently, each airborne snow water

equivalent measurement is a mean areal measure integrated over the 5 sq km area of the flight line. Figure 1 is a map of the 1990 airborne snow survey flight line network.

Carroll and Carroll (1989A, 1989B, 1990) have reported, in detail, on the techniques used to make airborne snow water equivalent measurements in a prairie, forest, and mountain snowpack environment. Fritzsche (1982) has reported on the physics and calibration of the airborne gamma radiation spectrometer developed under contract by EG&G, Inc. Fritzsche discusses the details of the system hardware and the radiation spectral data collection and analysis procedures that will not be discussed here.

Equation (1) gives the relationship used to make airborne snow water equivalent measurements:

$$SWE = \frac{1}{A}\left[\ln\frac{C_o}{C} - \ln\left(\frac{100 + 1.11\,M}{100 + 1.11\,M_o}\right)\right] g\ cm^2 \qquad (1)$$

where:

C and C_o = Uncollided terrestrial gamma count rates over snow and bare ground,

M and M_o = Percent soil moisture over snow and bare ground,

A = Radiation attenuation coefficient in water, cm^2/g

Compton tails associated with the peaks of higher energy, the cosmic radiation component, the aircraft and fuel, the pilots, and the detection system itself contribute extraneous radiation to the spectra. The raw radiation count rates for various photopeaks must be "stripped" of the extraneous radiation to give the pure, uncollided radiation count rates (Fritzsche, 1982). Air mass between the airborne sensors and the terrestrial radiation source also attenuates the radiation signal. Consequently, the detection system continuously records air temperature, air pressure, and radar altitude necessary to calculate and to compensate for the intervening air mass. Software strips the appropriate photopeaks of extraneous radiation and normalizes them to a standard air mass of 17 g/cm^2.

2.1 Airborne Measurement Error and Simulation

The principal sources of error in airborne snow water equivalent calculation using the relationship given in equation (1) are: (1) errors in the normalized count rates (C, C_o), (2) errors in the estimate of mean areal soil moisture over the flight line (M, M_o), and (3) errors in the radiation attenuation coefficient (A) derived from calibration data. Carroll and Carroll (1989B) simulated the principal sources of error for airborne measurements made over forested watersheds with as much as 60 cm of snow water equivalent. Airborne snow water equivalent measurements can be made in forest environments with 60 cm of water equivalent with an error of approximately 12 percent. The simulated results agree closely with the empirical errors derived from ground snow survey data collected in a forest environment with 48 cm of snow water equivalent (Carroll and Vose, 1984). In addition, the simulation technique can be used to assess the effect of the principal sources of error on airborne measurements made over agricultural environments with 2.0 to 15.0 cm of snow water equivalent. The error of the airborne snow measurement is, in part, a function of snow water equivalent and ranges from 4 to 10 percent. Again, the errors derived from the simulation agree closely with the errors derived using airborne and ground-based snow survey data collected over an agricultural environment (Carroll, et al., 1983).

3 SATELLITE AREAL EXTENT OF SNOW COVER MEASUREMENTS

In the operational satellite snow cover mapping program, AVHRR data are ingested, radiometrically calibrated, and geographically registered to one of 17 windows (Figure 2). Analysts use a digital image processing system to generate a snow/no-snow/cloud cover byte plane image classification from the satellite data. Hydrologists process the snow cover image classification using a geographic information system where digital elevation model (DEM) and digital, hydrologic basin boundary data sets reside. Six windows in the West, approximately 1000 km by 1000 km, contain DEM and basin boundary data sets. The geographic information system generates percent areal extent of snow cover statistics for each of approximately 5 elevation zones in each of approximately 400 major river basins in the western U.S. Ten additional windows contain basin boundary data sets to map snow cover for the Upper Midwest, the Great Lakes, New England, and southern Canada.

During the 1990 snow mapping season, the Center mapped 2,113 river basins in North America on multiple occasions using AVHRR and GOES satellite data (Figure 3). During the period January 31 through May 7, 1990, analysts mapped 65 windows (Figure 2) and generated 9,123 snow cover analyses using the NWS basin boundary data set (Figure 3).

Baglio and Holroyd (1989) recently completed research to evaluate different snow cover mapping techniques using GOES, AVHRR, and Landsat Thematic Mapper (TM) data over the San Juan Mountains in southwestern Colorado. They developed change detection and multispectral space classification techniques to evaluate snow cover mapping techniques using GOES and AVHRR data. The research developed procedures to screen cloud cover and to map snow cover under forest canopy using AVHRR data in the West. Landsat TM data sets provided a base with which to compare the GOES and AVHRR snow cover mapping techniques. Szeliga, et al. (1990) developed techniques to use digital elevation model (DEM) data to ensure temporal and spatial solar normalization for the multiple 1987 and 1988 satellite image data sets.

3.1 Refinements in Snow Cover Assessment

Holroyd and Carroll (1990) and Holroyd, et al. (1989) describe techniques and refinements used to map areal extent of snow cover using AVHRR data that will not be reviewed here. The Center has incorporated the refinements into the NWS operational snow mapping procedures. The major refinements include: (1) scaling of AVHRR data in bands 1, 2, and synthetic band 6, (2) terrain corrections, and (3) change detection.

Data scaling of bands 1 and 2 within the 0-255 byte data range was originally giving an albedo resolution of 0.5 percent. The comparatively low resolution represented only a 5-bit data range and did not take advantage of the full byte range available for electronic transmission or the 10-bit resolution of the spacecraft data stream. Consequently, we now rescale bands 1 and 2 to an albedo resolution of 0.25 percent.

The original data scaling of band 6 (i.e., band 3 minus band 4) within the 0-255 byte data range produced a saturation of band 3 and occasionally band 4 at radiative temperatures of 46 degrees Celsius or higher. To correct for the image saturation, the classification algorithm arbitrarily classifies all pixels that have a band 3 value greater than 245 (40 degrees Celsius or higher) as snow-free.

Classified images from the early morning NOAA-10 satellite accentuate the snow on the east-facing slopes and under represent snow on the west-facing slopes. Similarly, images from NOAA-11 in the early afternoon and NOAA-9 in the late afternoon have snow cover apparently enhanced on the sunlit slopes and diminished on the shaded slopes.

To correct the images made over rugged terrain, we use 30 arcsecond digital terrain data and: (1) resample to the 901 m pixel size and projection of the AVHRR imagery, (2) calculate the slope and aspect of the terrain, and (3) calculate the solar incidence angle, i, by equation (2).

$$\cos(i) = \cos(z)\cos(s) + \sin(z)\sin(s)\cos(A-a) \qquad (2)$$

where z is the solar zenith angle, s is the terrain slope angle, a is the terrain aspect angle, and A is the solar azimuth angle. The band 1 values divided by cos(i) give the brightness values appropriate to flat terrain and a vertical sun. These terrain corrections reduce the solar azimuth bias associated with the areal extent of snow cover. Of course, the corrections are not perfect because terrain variability introduces substantial variability of solar incidence angle within each pixel.

4 AIRBORNE AND SATELLITE SNOW COVER END-USER PRODUCTS

The NWS typically conducts airborne snow surveys from January through March each year using two aircraft simultaneously to support spring snowmelt flood outlooks and water supply forecasts. Maps and a User's Guide are available that give the current airborne flight line network, the details of the airborne snow water equivalent measurement technique, and the procedures to access electronically the snow water equivalent data in real-time.

Hydrologists distribute the alphanumeric and graphic airborne and satellite snow cover data over both the National Weather Service computer network and the commercial MCI Mail electronic mail network. Real-time messages transmit the airborne and satellite data 4 hours after the snow survey aircraft land anywhere in the country and 36 hours after the satellite overpass. The Center endeavors to map areal extent of snow cover for all 17 windows approximately once a week, the effect of cloud contamination notwithstanding. Figure 3 shows the NWS basins where snow cover was mapped in 1990. New basins in the West and southern Canada will provide greater coverage for satellite snow cover mapping in the future.

This paper describes, in some detail, the content and procedure to access the real-time, alphanumeric and graphics products available to U.S. and Canadian end-users. Each snow cover mapping season, we:

1. Map areal extent of snow cover in the U.S. using the National Weather Service basin boundary data sets. We no longer use the USGS hydrologic unit code basin boundaries as we have in the past,

2. Distribute real-time fax maps of the areal extent of snow cover with the basin boundaries, snow cover, and cloud cover for all the basins we map,

3. Provide real-time, electronic, IBM-PC compatible maps (in PCX format) of areal extent of snow cover, with basin boundaries (and color-coded by elevation zone in the West), for all the basins we map, and

4. Provide real-time raster images, in a lat/long geographic projection, of snow/no-snow/cloud cover for use in image processing or geographic information systems for all the basins we map.

Each snow season we distribute the alphanumeric products over AFOS (the NWS communications network) and MCI Mail as described in the current User's Guide (version 3.0; 1988 November 1).

4.1 Regions for Airborne and Satellite Snow Cover Data Collection

Figure 1 is a map of the 1990 Airborne Snow Survey Program national flight line network. The snow survey aircraft make airborne snow water equivalent measurements over selected basins, requested by NWS field offices, where snow water equivalent information is critical to spring flood outlooks, river and flood forecasts, or water supply forecasts.

Figure 2 is a map of the 17 windows for which we collect AVHRR and GOES satellite data to map areal extent of snow cover. Figure 3 is a map of the 2,113 NWS basin boundaries used in 1990 to calculate percent areal extent of snow cover. In the western U.S. (windows 1, 2, 3, 4, 12, and 17), we mapped areal extent of snow cover in 1990 for 494 total basins and for 298 basins by elevation zone. Each of the 298 basins contains 2 to 5 elevation zones. We have the capability to ingest the satellite data as far north as 55 degrees. We do not, however, have a complete basin boundary data set for southern Canada and no digital elevation data set for Canada. We plan to obtain the Canadian basin boundary data set for Alberta, Saskatchewan, Manitoba, southern Ontario, and Nova Scotia from the Environment Canada Water Resources Branch in Hull. Consequently, in 1991 we hope to map areal extent of snow cover south of 55 degrees north (windows 12-16) using Canadian basin boundaries.

4.2 Basin Boundary Maps and Database

Large-scale maps are available that show the NWS basins given in Figure 3. Two maps describe each window: one map contains the NWS basin boundaries, the associated SHEF ID for each basin, and state boundaries; the second map contains the NWS basin boundaries, flight line locations, and state boundaries. Additionally, the NWS basin boundary databases and the airborne flight line databases (that provide the salient characteristics including SHEF IDs, basin name, and elevation zones) are available in hardcopy, IBM-PC ASCII, and Lotus file formats.

4.3 Real-Time Snow Cover Products

4.3.1 Airborne Snow Water Equivalent by Line and Basin (MCI/AFOS-ASCII)

The real-time, alphanumeric, airborne snow water equivalent data, by flight line and basin, are available on AFOS and MCI Mail. AFOS product MSPRRMASP gives the airborne snow water equivalent data by flight line; AFOS product MSPRRMASB gives the mean areal airborne snow water equivalent data by basin. We post both AFOS products to MCI Mail (bulletin board NWS AIRBORNE SNOW). We calculate and distribute the mean areal airborne snow water equivalent estimates, by basin, for airborne data collected only in the Upper Midwest and in the East. The User's Guide gives the data format.

4.3.2 Satellite Areal Extent of Snow Cover by Basin/Zone (MCI/AFOS-ASCII)

Alphanumeric, percent areal extent of snow cover data, by basin (and by elevation zone in the western U.S.), are available in real-time on MCI Mail (bulletin board NWS SATELLITE SNOW) as described in the User's Guide. We added a number of basins and elevation zones in the West in 1990. As a result, the satellite snow cover messages tend to be long and to overwhelm AFOS. Some AFOS messages can exceed ten AFOS pages and consequently complicate AFOS data transmission and storage. To minimize this complication, we send out a one page AFOS message (MSPRRMASC) giving the mapping date and window number (Figure 2) each time we generate a snow cover map. In this way, it is possible for all NWS field offices and all non-NWS end-users to access the MCI Mail bulletin board (NWS SATELLITE SNOW) using a PC and the procedures given in Appendix 2 of the User's Guide and download the current satellite snow cover data.

4.3.3 Satellite Areal Extent of Snow Cover by Basin (FAX-Map)

We fax satellite areal extent of snow cover maps for each of the 17 windows (Figure 2), in real-time, upon request. The faxed maps include the areal extent of snow cover, cloud cover, and state and NWS basin boundaries. Elevation zone snow data are not included on the faxed maps. We send the faxed maps at night; consequently, to receive the faxed snow cover maps, you need to provide us with the telephone number of your fax machine that must be capable of receiving unattended fax messages.

4.3.4 Satellite Areal Extent of Snow Cover by Basin/Zone (MCI/PCX-Map)

In addition to the faxed snow cover maps, we distribute, in real-time using MCI Mail, maps of the satellite areal extent of snow cover, by basin, for each of the mapping windows upon request. The maps include state and NWS basin boundaries, snow cover, and cloud cover for all 17 windows. For the West windows (1, 2, 3, 4, and 17), the maps are also color-coded by elevation zone. The IBM-PC compatible images are in PCX format (by Z-Soft Corporation) that can be viewed and edited by a number of PC programs including PC Paintbrush and MS Paintbrush. Additionally, we provide the software necessary to display the PCX files in a time-series fashion on an IBM-PC VGA system with a screen resolution of 640 by 480. In this way it is possible for end-users to receive and display, in real-time, a time-series of satellite areal extent of snow cover maps for specific basins of interest during the snow season. The MCI Mail subject line for each PCX map file contains the window number and the date of the satellite image (e.g., W12-900314).

4.3.5 Satellite Areal Extent of Snow Cover by Window (Raster Map)

The PCX image files of areal extent of snow cover are not suitable for digital image processing. Consequently, we can provide a digital image of snow/no-snow/cloud cover in a geographic projection (i.e., longitude/latitude format) suitable for use in any geographic information system or digital image processing system upon request. The raster image does not have the basin boundaries imbedded in the image. The digital basin boundaries, however, are available upon request.

4.3.6 IBM-PC Demonstration Diskette

As an example of the PCX snow cover maps available over MCI Mail, an IBM-PC demonstration diskette is available upon request. The demonstration diskette contains snow cover images from the 1990 snow mapping season and a program that allows you to view a time-series of the snow cover maps on an IBM-PC compatible system with a VGA monitor and graphics board (resolution 640 by 480).

4.4 MCI Mail Electronic Mail System

MCI Mail is a commercial electronic bulletin board system. MCI Mail users typically set up their own MCI account with a specific user name. All MCI Mail subscribers (as well as subscribers from other commercial electronic bulletin board systems) can exchange electronic ASCII mail using any PC communications package. Additionally, it is possible for any MCI Mail user to set up a bulletin board system and post ASCII files to the bulletin board for other subscribers to download at their convenience.

We have created three bulletin boards to which we post ASCII files containing airborne snow water equivalent data, satellite snow cover data, and schedule and program information. Additionally, we have set up a general NWS MCI Mail account that will allow any end-user to access the bulletin boards and download the ASCII files described below, at no cost, using a PC and any standard communications package. Appendix 2 of the program User's Guide gives the instructions necessary to access the MCI Mail bulletin boards.

4.4.1 NWS/MCI Mail Bulletin Boards

We maintain three MCI Mail bulletin boards:

1. NWS AIRBORNE SNOW contains alphanumeric airborne snow water equivalent data. The subject line contains the states and dates for which data are collected (e.g., MNWIMI900215/18).

2. NWS SATELLITE SNOW contains alphanumeric satellite areal extent of snow cover data. The subject line contains the window number and the date of the satellite image (e.g., W12-900314) used to generate the data set.

3. NWS SNOW SCHEDULE contains general information including airborne and satellite data collection schedules (to the extent that our crystal ball will permit).

We purge data sets from each of the three bulletin boards two weeks after posting; old data sets can be reposted upon request.

4.4.2 Required End-User MCI Mail Account Number

And now the bad news. There ain't no way to post and retrieve a binary file (i.e., a PCX snow cover map file) to the MCI Mail bulletin board system. It is possible only to transfer a binary file directly to another MCI Mail account. Consequently, it is necessary for each user who wants to receive the real-time, color coded, satellite snow cover PCX map to subscribe to MCI Mail ($25 per year) and provide us with their MCI Mail user name.

And now for more bad news---binary files can be downloaded from MCI Mail accounts only by using Lotus Express or Norton Commander (version 3.0) commercial PC software. Unfortunately, standard PC communications packages do not have the capability to download binary files from MCI Mail---only ASCII files. If you intend to download the snow cover maps, you will need a copy of Lotus Express or Norton Commander (version 3.0) to download the binary PCX image/map files from your specific MCI Mailbox to your PC. The Norton Commander software is a DOS shell that will allow you to download MCI Mail binary and ASCII files, in background, and view the PCX map files among many other things. Norton Commander lists for $149 and is available for $89 from PC Connection at (800) 243-8088.

NOTE: It is not necessary for you to have your own MCI Mail account or Nort on Commander to download the ASCII files posted to the MCI Mail bulletin board system---only to receive the binary, PCX map files.

4.4.3 US and Canadian Access to MCI Mail

MCI Mail has recently changed all of their telephone access numbers in the U.S. Consequently, the MCI Mail telephone access numbers given in Appendix 2 of the User's Guide are obsolete. MCI Mail can be accessed from anywhere in the U.S. at 300 or 1200 baud by calling (800) 234-6245. User's can access the NWS/MCI Mail bulletin boards by: (1) using their own MCI Mail account and user name, or (2) using the NWS account, user name, and procedure described in Appendix 2 of the User's Guide. Canadian access to MCI Mail remains unchanged. We can provide instructions for those in Canada who want to access our MCI Mail account (user name NWSSNOW) as described in Appendix 2 of the User's Guide.

4.4.4 Setting Up an MCI Mail Account

You can set up your own MCI Mail account at a cost of $25 per year by calling MCI at (800) 444-6245 or (202) 833-8484. Once you set up an MCI Mail account to receive the PCX binary map files, give us your MCI Mail user name so we can routinely send you the PCX binary map files for your area of interest.

4.5 Airborne And Satellite Data Collection Schedule

We conduct airborne snow surveys at times and in regions of the country where snow water equivalent information is critical for use in spring flood outlooks, water supply outlooks, and river and flood forecasts. Snow cover conditions and the NWS field offices' requirements for airborne snow data dictate the airborne snow survey schedules during the snow season. We post the airborne data collection schedule to the MCI Mail bulletin board.

In 1991, we plan to begin satellite snow cover mapping on January 2. Our goal is to map snow cover for each window once a week; cloud cover, however, gets in the way. Consequently, if we are unable to map each window once a week, we endeavor to map each window as frequently as possible when cloud cover permits.

4.6 End-User Requests

Interested users can receive more information on any of the aforementioned snow cover products, maps, or data sets by contacting:

Mr. Milan Allen
Satellite Hydrology Program Manager
National Operational Hydrologic Remote Sensing Center
National Weather Service, NOAA
6301 - 34th Avenue South
Minneapolis, Minnesota 55450

Telephone: (612) 725-3232
FTS 725-3232
FAX 725-3338

If you have any questions, suggestions, or require any additional information, please give Milan a call.

5 SUMMARY

We are developing techniques to incorporate DEM data and forest canopy cover data into the snow cover classification procedures to better estimate snow cover in areas where the snow surface is obscured from view by: (1) cloud cover, or (2) dense forest canopy. Research is also continuing toward improvement of normalization procedures to include corrections for within image effects of terrain and for effects of atmospheric scattering and absorption. Additionally, we are working on techniques and procedures to generate, in near real-time, a raster (or grid-cell) snow water equivalent data set using: (1) ground-based point snow water equivalent data, (2) airborne line snow water equivalent data, (3) satellite areal extent of snow cover data, (4) digital elevation data, and (5) forest canopy cover data sets.

6 REFERENCES

Baglio, J.V. and Holroyd, E.W. (1989) Methods for operational snow cover area mapping using the Advanced Very High Resolution Radiometer - San Juan Mountain test study. Research technical report, USGS EROS Data Center, Sioux Falls, South Dakota, March, 1989, pp. 82.

Carroll, S.S. and Carroll, T.R. (1989A) Effect of uneven snow cover on airborne snow water equivalent estimates obtained by measuring terrestrial gamma radiation. Water Resources Research. 25 (7), 1505-1510.

Carroll, S.S. and Carroll, T.R. (1989B) Effect of forest biomass on airborne snow water equivalent estimates obtained by measuring terrestrial gamma radiation. Remote Sensing of Environment. 27 (3), 313-319.

Carroll, S.S. and Carroll, T.R. (1990) Simulation of airborne snow water equivalent measurement errors in extreme environments. Nordic Hydrology (in press)

Carroll, T.R. and Vose, G.D. (1984) Airborne snow water equivalent measurements over a forested environment using terrestrial gamma radiation. Proceedings of the Eastern Snow Conference, New Carrollton, Maryland, 6-8 June 1984. pp. 19.

Carroll, T.R., Glynn, J.E., and Goodison, B.E. (1983) A comparison of U.S. and Canadian airborne snow water equivalent measurements. Proceedings of the Western Snow Conference, Vancouver, Washington, 19-21 April 1983.

Fritzsche, A.E. (1982) The National Weather Service gamma snow system physics and calibration. Publication No. NWS-8201, EG&G, Inc.; Las Vegas, Nevada. pp. 37.

Holroyd, E.W. and Carroll, T.R. (1990) Further refinements in the remote sensing of snow-covered areas. Presented at the American Society of Photogrammetry and Remote Sensing annual meeting; Denver, CO; 1990 March.

Holroyd, E.W.,III, Verdin, J.P., and Carroll, T.R. (1989) Mapping snow cover with satellite imagery: comparison of results from three sensor systems. Proceedings of the 57th Western Snow Conference; Fort Collins, CO; April 18-20; pp. 10.

Szeliga, T.L., Allen, M.W., Baglio, J.V., and Carroll, T.R. (1990) Comparison of methods of solar normalization of AVHRR data and their effects on snow cover classification. Presented at the Second North American NOAA Polar Orbiter's User's Group Meeting; New Carrollton, Maryland; 1990 May 24-25.

Figure 1

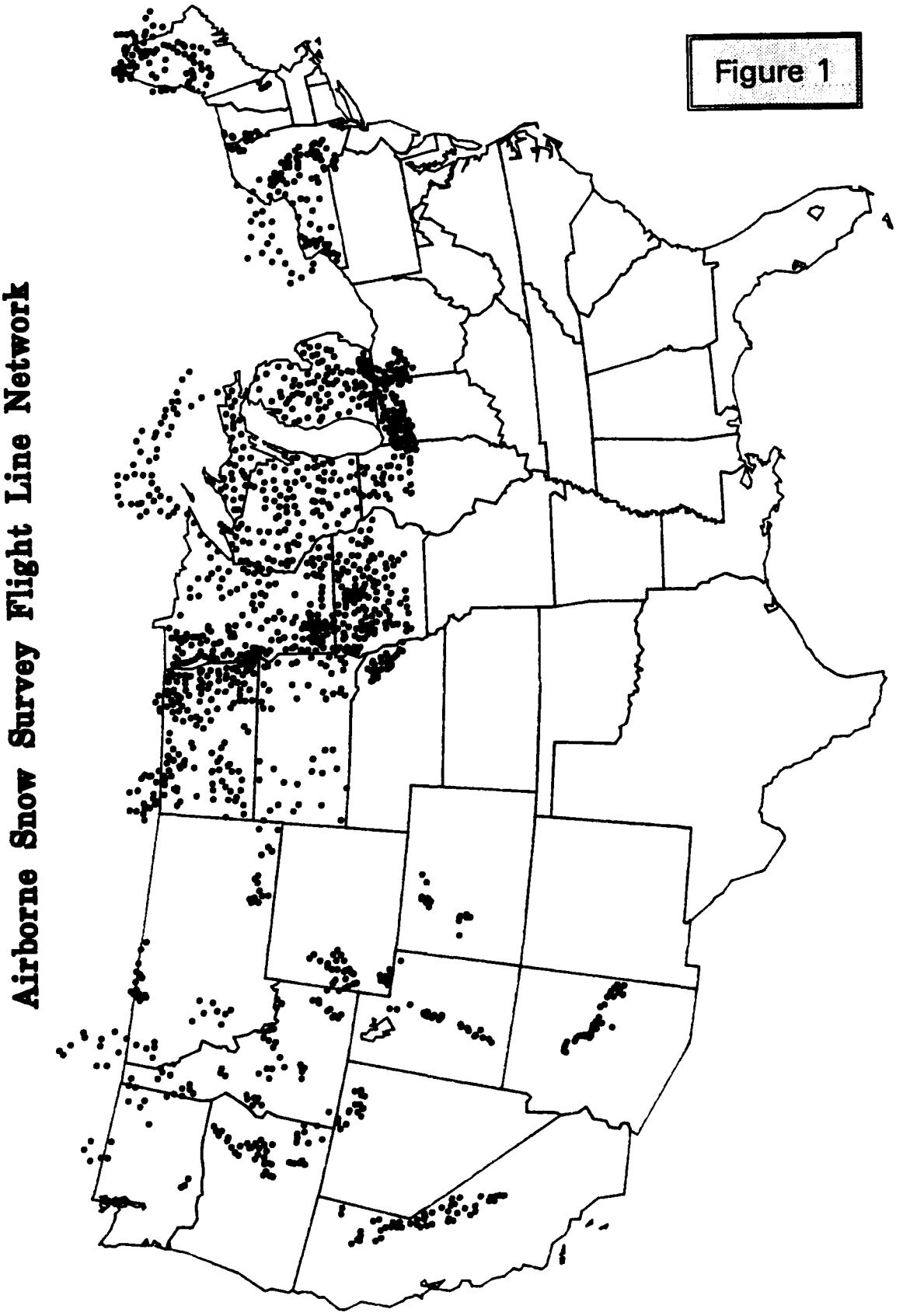

Airborne Snow Survey Flight Line Network

1990 Snow Mapping Windows

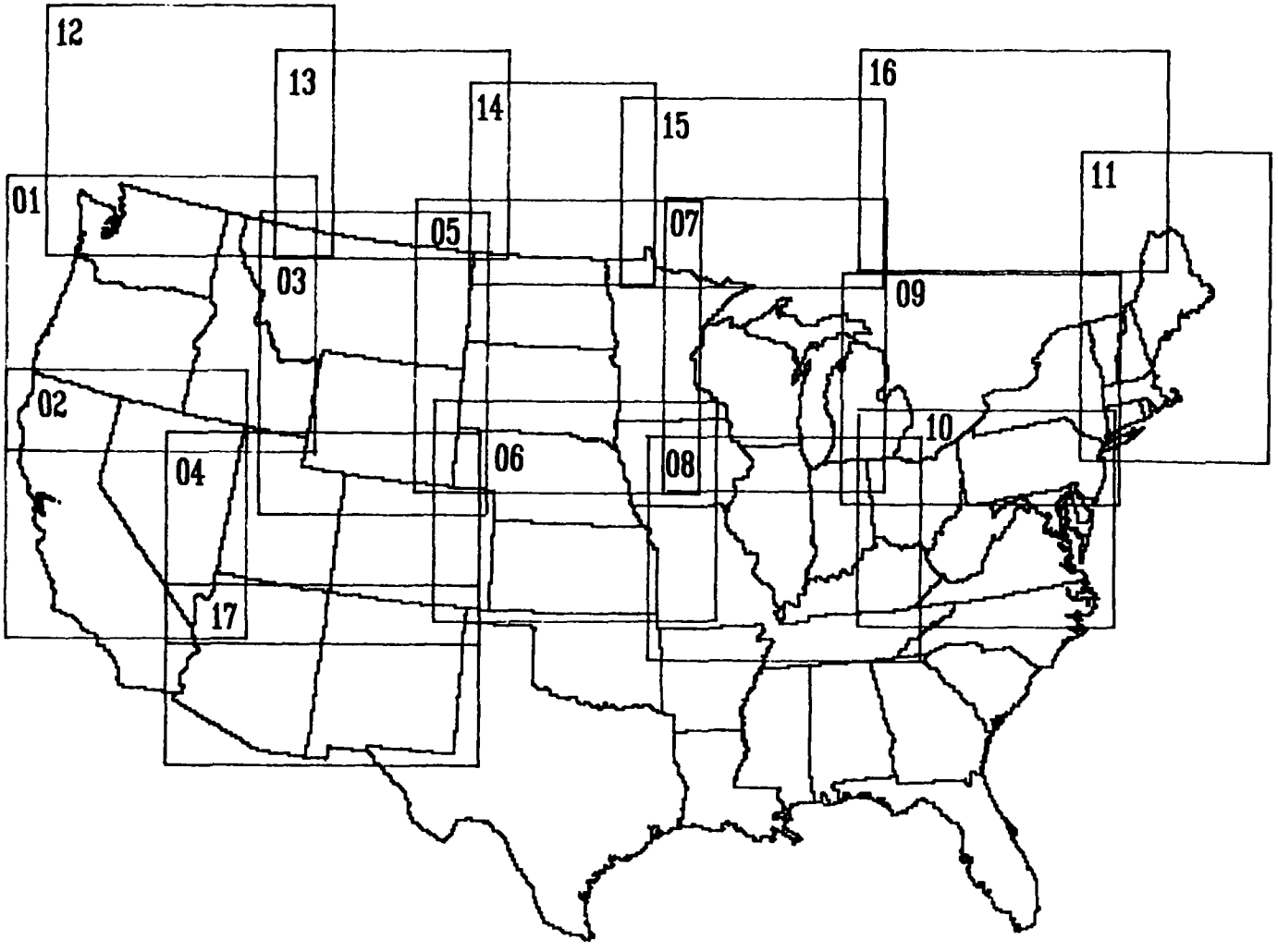

Figure 2

Figure 3

1990 Snow Mapping Basins

Recent Developments in Snow-Chemistry Research in the Western United States

R.E. DAVIS

U.S. Army Cold Regions Research and Engineering Laboratory
72 Lyme Road
Hanover, New Hampshire 03755-1290, U.S.A.

R.C. BALES

Department of Hydrology and Water Resources
University of Arizona
Tucson, Arizona 85221, U.S.A.

ABSTRACT

Three active areas of detailed research in snow and ice chemistry will be described with emphasis on the connection between processes at different scales: i) modeling chemical hydrographs from seasonal snowpacks in alpine watersheds, ii) studying processes affecting ion redistribution in, and elution from snow, and iii) investigating the interaction of trace gases in snow. First, in alpine watersheds where snowmelt runoff dominates basin hydrology, accurate hydrochemical modeling depends on developing adequate descriptions of snowmelt chemistry. Whole-watershed hydrochemical modeling using point descriptions of snowmelt chemistry, along with distributed estimates of snowmelt volume, is being pursued for the Emerald Lake (Sierra Nevada) and other alpine watersheds in the western U.S. Second, tracer studies at the Sierra Nevada Aquatic Research Laboratory are being used to develop point estimates of snowmelt volume versus chemistry for use in the distributed watershed models. Complimentary field studies are ongoing at the U.S. Forest Service's Glacier Lakes site in Wyoming, and the Mammoth Mountain (California) field site of the University of California, Santa Barbara. Third, recent studies by researchers at the University of Arizona and the U.S. Forest Service have used chromatographic methods to examine the interaction of reactive gases (SO_2, H_2O_2) with ice surface, continuing earlier investigations of gaseous deposition to snow.

CHEMICAL HYDROGRAPH FROM ALPINE SNOWPACKS

Whole-watershed studies at Emerald Lake (Sequoia National Park) of California's Sierra Nevada (Williams and Melack, 1989, 1990) and at the Glacier Lakes Experimental Ecosystem Site (GLEES) in the Snowy Range of Wyoming (Clow et al., 1988) have identified ionic pulses in the first fractions of streamflow during spring melt. Williams and Melack (1989) show that sampling the chemistry of all subbasins in a watershed is necessary to adequately characterize solute inputs to lake systems. Furthermore, they show a case in which spatial and temporal variations in the melt over the watershed do not change the magnitude of the solute pulse, rather, they extend the pulse duration. The importance of melt-freeze cycling is pointed out by Williams and Melack (1990), who showed that increased concentrations of solutes in meltwater can be associated with a series of melt-freeze cycles. Snowpack and lake monitoring is continuing at several sites in the Sierra Nevada under the California Air Resources Board monitoring program. At GLEES the ionic pulse was less distinct and soil contributions to lake-inflow chemistry appeared to be quite important (Clow et al., 1988). Studies by the University of Wyoming and the U.S. Forest Service are continuing at GLEES, which the Forest Service plans to use as a long-term ecological research site.

Figure 1 shows data from Williams and Melack (1990) for snowpack and meltwater concentrations of major ions over time, showing the initial high concentration factor of the initial melt. This figure also shows another large ionic pulse starting on April 23 after a series of melt-freeze cycles. While the ionic pulse starting on April 23 follows a series of preceding melt-freeze cycles, the cycles themselves may not be the direct cause. Instead it may be the lack of continued melt flow diluting the concentrations of species in solution. Figure 2 shows a time series of the movement of SO_2 and NO_3^- down through the pack at the same site. In this figure in high concentrations are seen near the base of the pack, where the ions will be

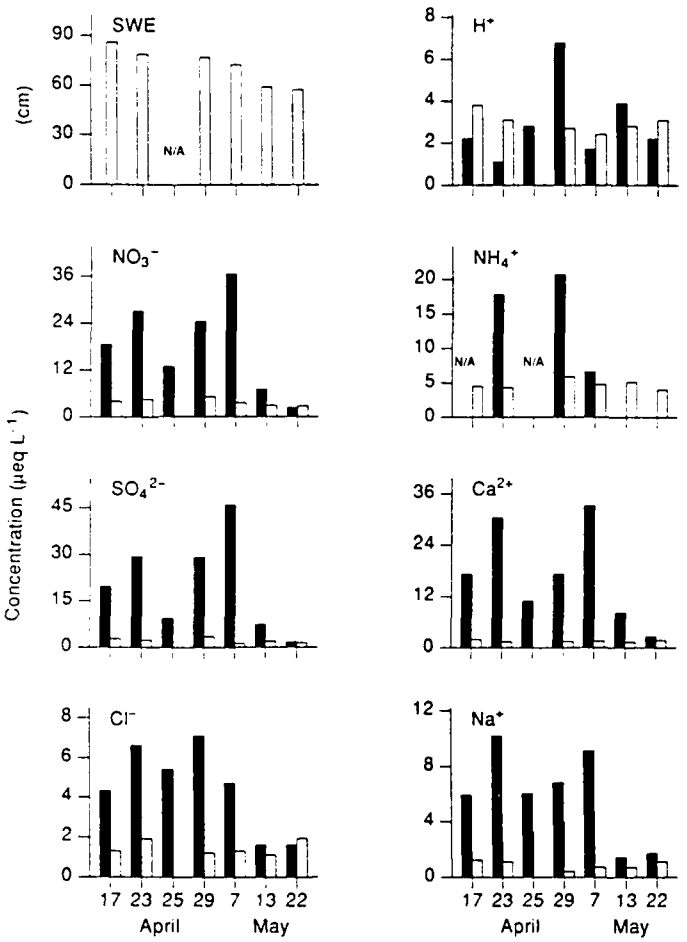

Figure 1. Snow water equivalent and the concentration of major ions in the snowpack (clear bars) and in the snowpack meltwater (black bars) at a sub-basin in the Emerald Lake watershed, California, in 1987. Solute concentrations in the initial melt fraction are higher than the bulk snowpack concentrations. Solutes increased in concentration around April 23, after a series of melt-freeze events, and the increase in concentration on April 29 is due to rainfall *(After Dozier and Melack, 1989)*.

removed at the onset of new melt flow. This condition was previously described in a laboratory setting by Colbeck (1980).

Whole-watershed hydrochemical modeling using point descriptions of snowmelt chemistry, along with distributed estimates of snowmelt volume, is being pursued for the Emerald-Lake and other alpine watersheds in the western U.S (Wolford et al., 1988; Sorooshian et al., 1989). Figure 3 shows a partial division of the Emerald Lake watershed into sub-basins, and the measured chemical and flow hydrographs for three lake inflows. Each inflow is an aggregation of runoff from multiple sub-basins. The chemical hydrograph at any scale, from a single point to the whole basin, can be empirically fit with this three-parameter exponential expression

$$\frac{C}{C_a} = \frac{d\,MF}{d\,VF} = \alpha b_1 e^{-b_1 VF} + (1-\alpha) b_2 e^{-b_2 VF} \qquad (1)$$

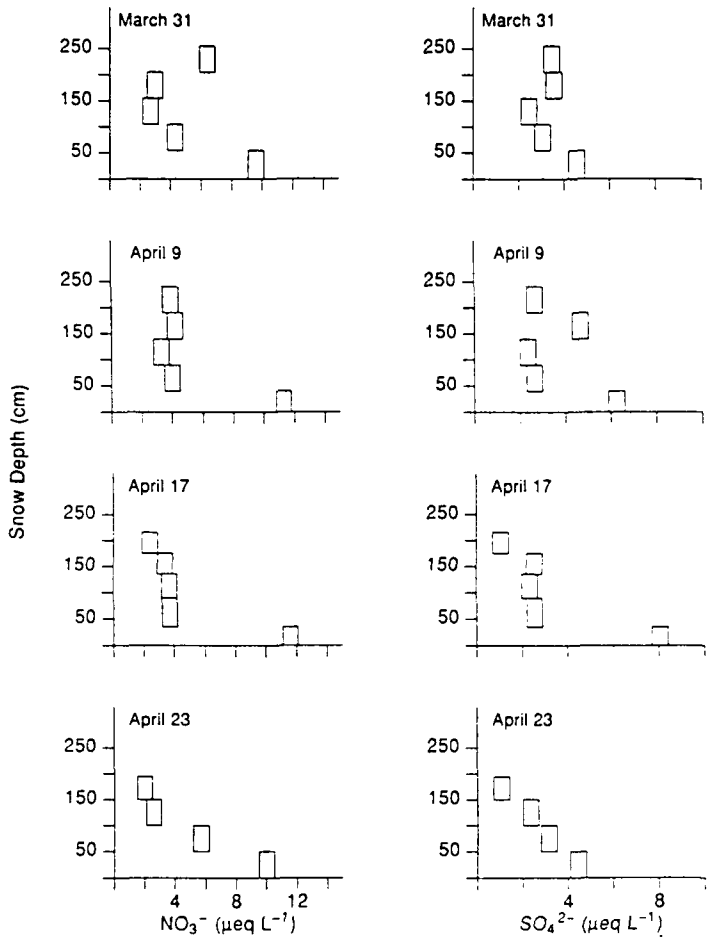

Figure 2. A time series of the concentrations of two major ions, NO_3^- and SO_2 at the same site in the Emerald Lake watershed in 1987. The concentrations near the top of the declining pack decrease over time while the concentrations near the bottom of the pack increase *(After Dozier and Melack, 1989).*

where

α	weighting parameter (0 – 1)
b_1 and b_2	empirical parameters
VF	volume fraction of melt
C_a	average initial in snowpack
C	concentration of meltwater draining from pack

Integrating the above equation, obtains the mass fraction MF eluted

$$MF = \alpha\left[1 - e^{-b_1 VF}\right] + (1 - \alpha)\left[1 - e^{-b_2 VF}\right] \quad (2)$$

When one aggregates snowmelt from several points that melt at different times, the aggregated chemical hydrograph should have a significantly lower peak than a point estimate (Figure 4). Note that the initial peak *observed* will depend on what volume fraction of snowmelt is sampled. Williams and Melack (1990) point out that the pulse was not much reduced when the flows from multiple sub-basins were measured,

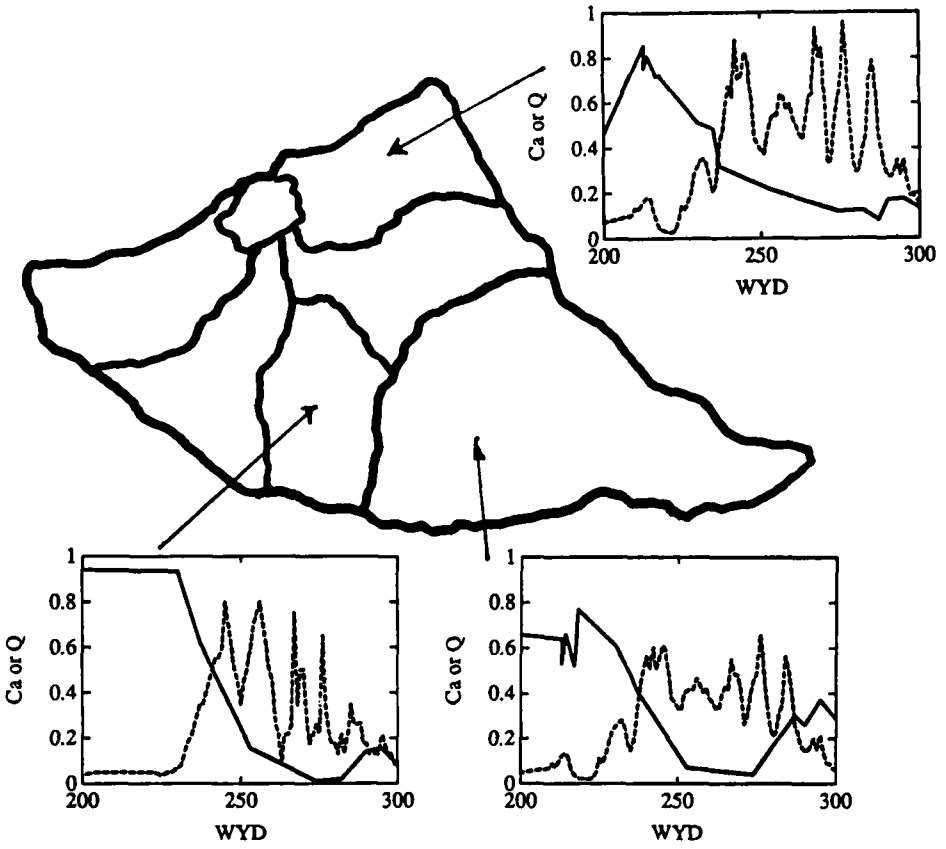

Figure 3. Chemical (dashed line) and melt (solid line) hydrographs for three inflows to Emerald Lake watershed, and an example of hydrologic subdivisions; for hydrochemical modeling, subdivisions are divided based on runoff, snow accumulation and melt, and soil-vegetation types.

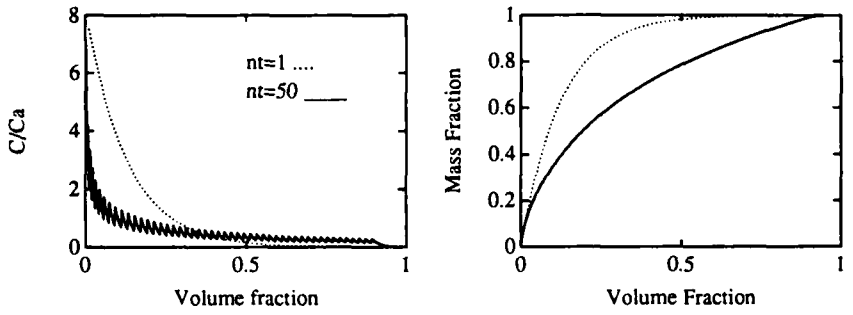

Figure 4. Example chemical hydrograph for one point and for 50 contributing points, each lagged in time for the previous one by 10 percent of the volume at that point. Axes are a) snowmelt concentration divided by the (initial) average in the pack as a function of fraction of the snowpack melted, and b) cumulative mass fraction released as a function of fraction melted.

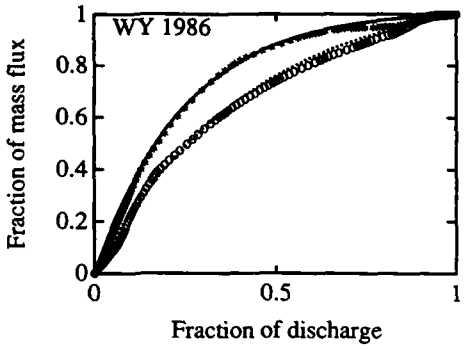

Figure 5. Chemical hydrographs for two Emerald Lake inflows, 1986 water year. Data are for NO_3^-, based on daily flow values and weekly chemistry sampling. These are basically integrals of the chemical hydrographs shown in Figure 3.

however, suggesting that the aggregation on Figure 4 should be over fewer points. Figure 5 shows the fraction of solute mass flux reaching the lake inflow as a function of the fraction of snowmelt discharge, pointing out the differences in melt patterns over the watershed.

Ongoing laboratory studies at the Sierra Nevada Aquatic Research Laboratory (SNARL), which is operated by the University of California, Santa Barbara (UCSB), field studies at the U.S. Forest Service's GLEES site, and field studies at Mammoth Mountain, California (UCSB) are aimed towards developing point estimates of ion concentrations in meltwater for use in the distributed watershed models. The point-based model being initially tested and extended is from Hibberd (1984), and the mass balance of the solutes is given by

$$\frac{\partial C_i}{\partial t^*} + (S + \beta)\left[\frac{\partial C_m}{\partial t^*} + u^* \frac{\partial C_m}{\partial z^*}\right] = (S + \beta) D^* \frac{\partial^2 C_m}{\partial z^{*2}} \tag{3}$$

where

C_i	mass concentration solute in immobile phase
C_m	mass concentration solute in mobile phase
S	effective saturation of the pore space
β	$= \frac{S_i}{1 - S_i}$
S_i	irreducible liquid water content
u^*	percolation velocity
D^*	dispersion coefficient
t	time
z	vertical distance coordinate

The flux u^* is obtained using Colbeck's (1978) theory. Two alternative chemical models may be used to relate C_i and C_m

$$\frac{\partial C_i}{\partial t} = K \frac{\partial C_m}{\partial t} \tag{4}$$

or

$$\frac{\partial C_i}{\partial t} = k_1 (C_m - C_i) \tag{5}$$

where K is a partion coefficient, and k_1 is a first order kinetic release coefficient. Work to develop mathematical descriptions of snowmelt chemistry at a point is in progress (Bales and Davis, manuscript in preparation), to go along with efforts at developing a distributed snowmelt model (Marks and Dozier, 1988).

In a laboratory study, Bales et al. (1989a) observed that the initial ionic distribution at both the mesoscale and microscale influence relative concentrations in solute released from the pack. Figure 6 shows the vertical profiles of SO_4^{2-} and Br^- measured at intermediate and late stages of melting; the SO_4^{2-} was applied to the top of the pack and the Br^- to the middle. Tracers applied at the top of the pack come out before those at depth, with 80 percent of the species at the top removed in first 20 percent of meltwater (Figure 7). For a mid-depth tracer, 70 percent of solute mass was removed in first 20 percent of meltwater.

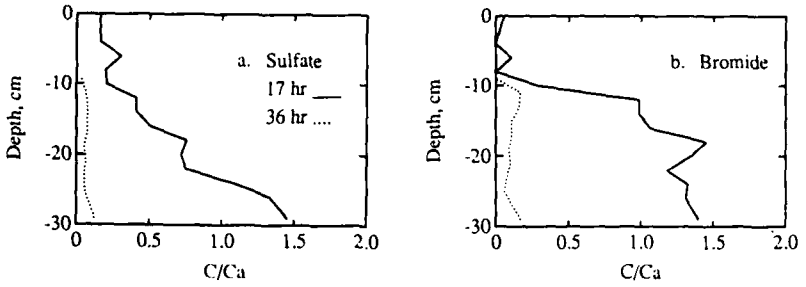

Figure 6. Solute profiles at two times during melting of a laboratory snowpack. Conditions: $1 \times 1 \times 0.4$ m snowpack; $\rho = 370$ kg m^{-3}; tracers applied, top: 1 L of 0.04 M NaBr and mid: 1 L of 0.05 M KCl, HNO_3 and Na_2SO_4; melt rate = 0.66 cm hr^{-1}; 57 percent of pack melted in 34 hr (Bales et al., 1989).

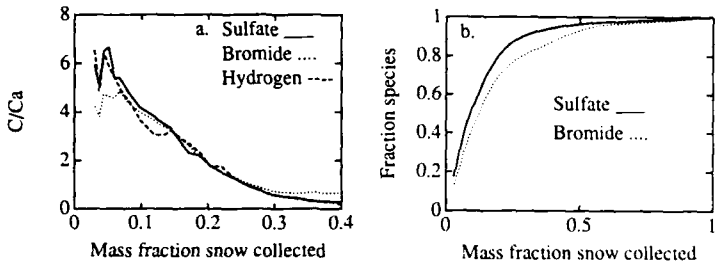

Figure 7. Solute release for same experiment as Figure 6: a) cumulative mass of ionic mass released as a function of fraction of snowpack melted in cold-room experiments, b) chemical hydrograph for release of SO_4^{2-}, H^+ and Br^- from a snowpack.

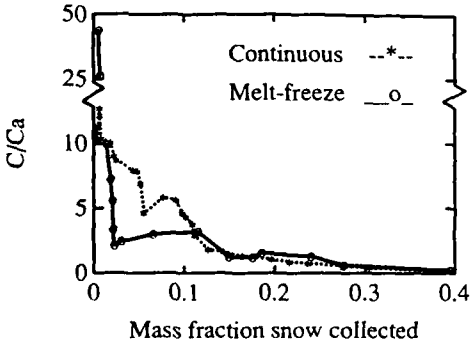

Figure 8. Chemical hydrograph from melting of laboratory snowpack; conditions similar to those of Figure 7, except that three melt-freeze cycles were imposed prior to final melting.

However, results also show that there is partial mixing and an important *immobile* region on snow grains; some of top tracer comes out late and some of mid-depth tracer comes out in the first meltwater (Bales et al., 1989a). There was no *preferential* elution of three different salt tracers applied at the top of the pack; all arrived together in meltwater (Figure 7). Figure 8 shows the effect of melt-freeze cycles compared with continuous melt; the melt freeze cycles result in an ionic pulse much larger in amplitude than the case of continuous melt. This shows that melt-freeze cycles can also cause a stronger ionic pulse from initially dry snowpacks, in this case it results from the concentration of solutes on less grain surface. The melt-freeze process causes grains to grow rapidly and solutes to be flushed from interstices, more readily leached.

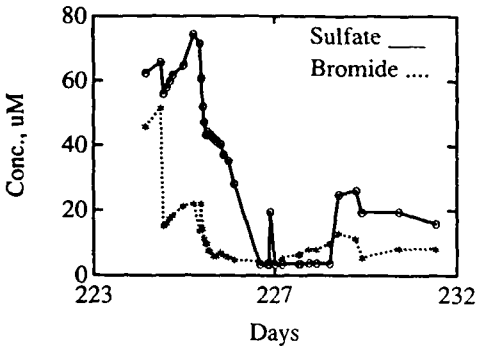

Figure 9. Meltwater concentrations for one lysimeter at the Glacier Lakes field site. Snowpack depth was ~2 m (Bales et al, 1990).

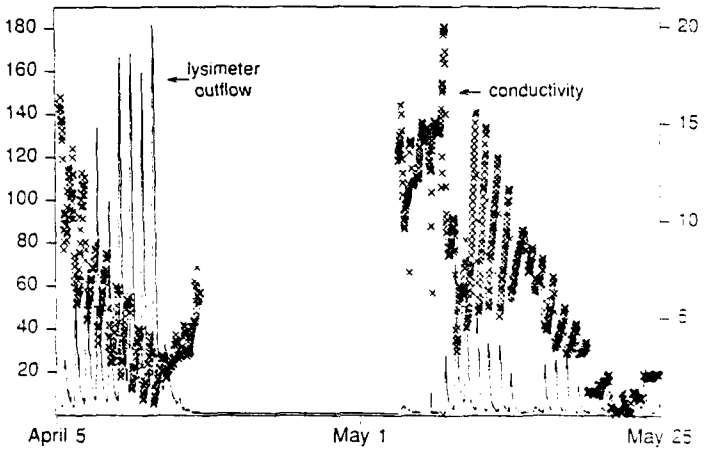

Figure 10. Measurements from lysimeters at the Mammoth Mountain snow study plot. Daily melt hydrographs are show for two melt episodes; the associated chemical hydrographs are shown with measurements of meltwater conductivity. In each case a pulse in concentration is seen at the onset of melt arrival at the base of the pack.

Figure 9 shows an ionic pulse of four to ten times the average snowpack concentration in snow lysimeters at GLEES, observed on the first day of melt, with both background ions and tracers showing a peak (Bales et al., 1990). Snow pits showed solute depletion from the base and possible additions to the top of the pack during melt. Figure 10 shows the results of tracer tests at Mammoth Mountain, California, in which the daily hydrographs are shown, averaged from a pair of lysimeters, along with the conductivity of the melt water. This shows a sharp peak at the start of the first melt episode, followed by a period of subfreezing surface conditions, then a higher peak when melt flow resumes to the base of the pack.

ION REDISTRIBUTION IN AND ELUTION FROM SNOW

Besides contributing data for developing point estimates of ion release from melting snowpacks, the studies at the Mammoth-Mountain and Glacier lakes field sites and at SNARL are investigating process-level questions concerning ion redistribution in snow. Detailed observations are being made of snow stratigraphy and chemistry in controlled field plots. For example, the 2-m snowpack at Glacier lakes showed rapid initial melt (2 cm dy^{-1}), but most of the tracer mass applied directly above the lysimeters was diverted away by ice lenses and preferential flow paths. In neither lysimeter or snow-pit data for 1988 was there a clear relation between stratigraphy and chemistry, however (Bales et al., 1990). Two further sets of measurements for 1989 and 1990 are being analyzed.

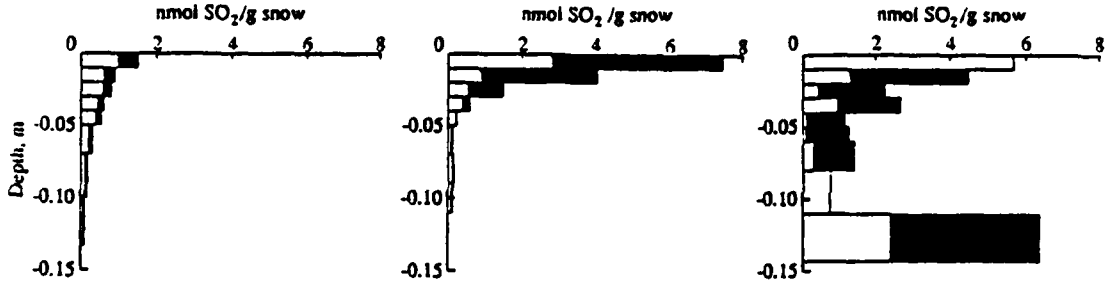

Figure 11. Depth profiles of HSO_3^- and SO_4^{2-} in snow. SO_2 gas in the air above the snow diffused down into the pack, and was taken up in the liquid water on the surface of the snow grains.

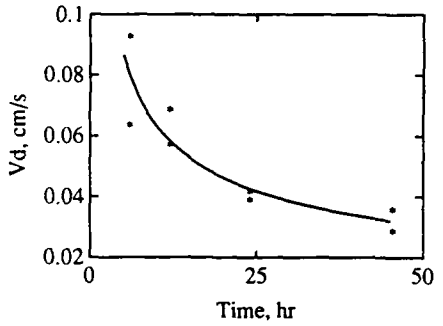

Figure 12. SO_2 deposition velocity to snow as a function of time. Experimental conditions: –0.5°C, SO_2 at ~25 ppbv (*After Conklin, 1988*).

INTERACTION OF TRACE GASES WITH SNOW

Recent studies have looked at the uptake of SO_2 and NO_x by snow and ice and the presence of trace species such as H_2O_2 in snowpacks.

There is both thermodynamic and indirect experimental evidence for a disordered interfacial region on ice at temperatures below 0°C. This surface *liquid-like* region is related to surface roughening, depends on facets, and is stable above ~20°C. One example of this phenomenon is the increased adsorption of SO_2 onto ice from -11 to -3°C observed in studies carried out at Desert Research Institute, Reno, NV (Sommerfeld and Lamb, 1986). Ongoing studies with ice spheres show that uptake of NO exhibits a similar temperature dependence *[R. Sommerfeld, unpublished data, U.S. Forest Service, Fort Collins, CO.]*

Experimental studies (Valdez et al., 1987) and mathematical modeling (Bales et al., 1987) of SO_2 deposition show that snow acts as a perfect, though diffuse, sink for reactive gases. The major factor determining the deposition velocity (flux to surface divided by atmospheric concentration) is the liquid-water content of the snow (Figure 11). Measured deposition velocities averaged 0.06 cm s^{-1}, with values of 0.02 cm s^{-1} for cold, dry, old snow; 0.05 cm s^{-1} for cold, dry, new snow (greater surface area); and 0.07 cm s^{-1} for wet, old snow. Ozone and SO_2 concentrations did not affect deposition velocity (Valdez et al., 1987). The diffusive transport and reaction model for SO_2 uptake compared well with experimental results, with liquid-water mass fraction being the main parameter. The model also predicted that deposition velocity should drop with time because the pH of the surface liquid layer drops as more SO_2 is taken up; SO_2 solubility decreases at lower pH because it is an acid (Bales et al., 1987). Later experiments provided validation to this predicted time dependence (Figure 12). Further studies in progress are aimed at a quantitative validation of how uptake depends on oxidant concentration *[M. H. Conklin, unpublished data, U. Arizona].*

Valdez et al. (1989) observed that SO_2 uptake onto growing ice surfaces at -15°C was in amounts equivalent to Henry's law equilibrium between the gas phase and deposited H_2O. This is consistent with uptake into a 10-100 nm liquid-like layer at the growing interface, with SO_2 release inhibited by diffusion in the layer. At equilibrium, SO_2 should be largely excluded from the ice.

Hydrogen peroxide is an important oxidant in some alpine and polar regions and has been found to be stable in snow and ice. Concentrations in snow pits and in fresh snow from the Sierra Nevada and Snowy Range are on the order of a few $\mu g L^{-1}$ and show decreases with depth (time), however *[M. H. Conklin, manuscript in preparation, U. Arizona].*

SUMMARY

Similar relationships between meltwater hydrographs and chemical hydrographs are seen at the watershed scale, a point scales, and in the laboratory. For the most part, chemical hydrographs peak during the rising limb of the meltwater hydrograph, which shows the importance of understanding snowpack processes early in the ablation season. To understand these relationships at the process level, we must first examine the microscale phenomena that are responsible for the distributions of solutes that control uptake and transport by liquid water. Next, we must identify water flow processes in snow that affect the removal of species from various parts of the snowcover. Finally we need to integrate the knowledge of these processes to account for a variety of flow paths at the watershed scale.

REFERENCES

Bales, R. C., R. E. Davis and D. A. Stanley, Ionic elution through shallow, homogeneous snow, *Water Resources Research,* 25, 1869-1877, 1989.

Bales, R. C., R. A. Sommerfeld and D. G. Kebler, Ionic tracer movement through a Wyoming snowpack, *Atmospheric Environment, (In press),* 1990.

Bales, R. C., M. P. Valdez and G. A. Dawson, Gaseous deposition to snow: II. Physical-chemical model for SO_2 deposition, *Journal of Geophysical Research,* 92, 9789-9799, 1987.

Clow, D. C., N. Swoboda-Colberg, J. I. Drever, and F. S. Sanders, Chemistry of snowmelt, soil water, and stream water at the West Glacier lake watershed, Wyoming, *EOS,* 69, 1198, 1988.

Conklin, M. H., Time dependence of SO_2 dry deposition to snow, *EOS,* 69, 1053, 1988.

Marks, D., and J. Dozier, Climate and energy exchange at the snow surface in the alpine region of the Sierra Nevada, *EOS,* 69, 1213, 1988.

Sommerfeld, R. A. and D. Lamb, Preliminary measurements of SO_2 adsorbed on ice, *Geophysical Research Letters,* 13, 349-351, 1986.

Sorooshian, S., R. C. Bales, V. K. Gupta, P. A. Noppe, and R. A. Wolford, Development of Watershed Models for Emerald Lake Watershed in Sequoia National Park and Other Lakes of the Sierra Nevada, *Draft final report for the California Air Resources Board on contract A732-035,* University of Arizona, Tucson AZ, 217 p., 1989.

Valdez, M. P., R. C. Bales, D. A. Stanley, and G. A. Dawson, Gaseous deposition to snow: I. Experimental study of SO_2 and *no*2 deposition, *Journal of Geophysical Research,* 92, 9799-9789, 1987.

Valdez, M. P., G. A. Dawson, and R. C. Bales, Sulphur dioxide incorporation into ice depositing from the vapor, *Journal of Geophysical Research,* 94, 1095-1103, 1989.

Williams, M. W., and J. M. Melack, Effects of spatial and temporal variation in snow melt on nitrate ion and sulphate ion pulses in melt waters within an alpine basin, *Annals of Glaciology,* 13, 285-288, 1989.

Williams, M. W., and J. M. Melack, Solute chemistry of snowmelt runoff in an alpine basin, Sierra Nevada, *Water Resources Research, (In press),* 1990.

Wolford, R. A., S. Sorooshian, R. C. Bales, and G. A. Dawson, A hydrochemical and water balance model for Emerald Lake watershed, Sierra Nevada, California, *EOS,* 69, 1199, 1988.

A Prototype Physically-Based Model for the Prediction of the Spatial Distribution of Snowcover

K.M. SAMBLES, A. HARRISON AND M.G. ANDERSON

Department of Geography
University of Bristol
University Road
Bristol BS8 1SS, United Kingdom

T. PANGBURN

U.S. Army Cold Regions Research and Engineering Laboratory
72 Lyme Road
Hanover, New Hampshire 03755-1290, U.S.A.

ABSTRACT

A prototype digital model, SNOMO, has been developed to predict the pattern of snowcover and snowdepth distribution over a small catchment during the melt season. The catchment is subdivided into homogeneous areas on the basis of elevation, slope angle, aspect and vegetation cover using a GIS driven algorithm. The energy-budget of the snowpack is calculated for each area. A simplified version of the snowpack internal structure and characteristics is used to alleviate data availability problems. The energy-budget terms are used to calculate the amount of melt, which is then subtracted from the existing snowpack depth in terms of centimetres of snow. The model has been tested on the W3 watershed (8.4km^2), part of the Sleepers River Research Watershed, Danville, Vermont. Point predictions are shown to accord well with observed values and spatial predictions of snow distributions for the complete catchment are presented.

INTRODUCTION

This paper presents a prototype distributed physically-based model, SNOMO (SNOw MOdel), that has been developed in response to the following criteria:

(1) A dichotomy exists at present between, as Ferguson & Morris (1987) state: "the sophistication of physics-based models available for predicting snowmelt at a point ... and the crudity but convenience of traditional models for snowmelt at the basin scale using valley-level air temperature as the main or sole predictor".

(2) There are currently no physically-based models that predict the pattern of snowcover and snowdepth distribution.

We realise that there are advantages (Roberge et.al., 1988) and disadvantages (Anderson, 1978) of using both index and physically-based models, but argue that to be of utility as a research tool a model would have to be a physically-based distributed model. A physically-based distributed model allows the simulation of varied environments and the modelling of the changes in the physical characteristics of the snowpack and the detailed snowcover and snowdepth distributions, these attributes are unobtainable with an index model.

The objectives of the proposed model are:

1 To simulate the pattern of snowcover and snowdepth distribution during the melt season.
2 To simulate the changes in the physical characteristics of the snowpack during the melt season.
3 To operate at an optimum complexity which ensures a balance between data availability, computational time and model methodology, but which utilizes fully physically-based equations wherever possible.
4 To simulate the volume of meltwater runoff.

The pattern of snowcover and snowdepth distribution is dependent upon the scale of the area which is being considered. This paper will consider the local scale, using Stepphun & Dyck's (1974) definition, that is 1000-5m^2. At this scale snowmelt patterns relate to local, within-field terrain variables (elevation, aspect and slope angle), vegetation distribution and vegetation variables (canopy density, tree species) and land use practices. These factors modify the snowpack energy-budget, resulting in differential snowpack conditions and depths. Additional factors such as snow drifting will also cause differential snowpack conditions and depths.

MODEL DESCRIPTION

2.2 Model structure

The basic structure of SNOMO is shown in figure 1. SNOMO operates on the basis of the subdivision of the catchment into computational areas (cells). The cells are homogeneous with respect to slope angle, aspect, elevation and vegetation cover. The snowdepth is calculated for each cell using the equations and logic structures described below. The results for each cell are then summarized for the whole catchment to obtain the pattern of snowcover and snowdepth distribution over the catchment.

SNOMO is based on the calculation of melt using the energy-budget equation:

$$\Delta Q_m = Q^* + Q_c + Q_e + Q_g + Q_p - \Delta Q_s \qquad (1)$$

where,

ΔQ_m latent heat storage change due to melting or freezing.
Q^* net radiation
Q_c sensible heat flux
Q_e latent heat flux
Q_g heat introduced to the pack from the ground
Q_p heat introduced to the pack by rain
ΔQ_s net heat storage term

(units: $MJm^{-2}day^{-1}$)

The components Q^*, Q_c and Q_e of equation (1) are calculated using a modified version of the Terrain Surface Temperature Model (TSTM), Balick et.al. (1981a & b). The TSTM is a finite difference physically-based energy-budget model originally used for the calculation of the surface temperature of a surface (soil, man-made or vegetated). The modifications made in SNOMO to the original TSTM are extensive and are primarily concerned with the reduction of the input requirements, the lengthening of the simulation time, the extraction of the output values for the components Q^*, Q_c and Q_e of equation (1) and the interfacing of the modified TSTM with the prototype model SNOMO. The modified TSTM calculates the snowpack surface temperature and this is also used in equation (1), as part of the calculation of ΔQ_s (equation 3). If required (for example, for validation purposes) the incoming and reflected long- and shortwave radiation and the snowpack temperatures at depth can be extracted from the modified TSTM, as these are calculated within the TSTM.

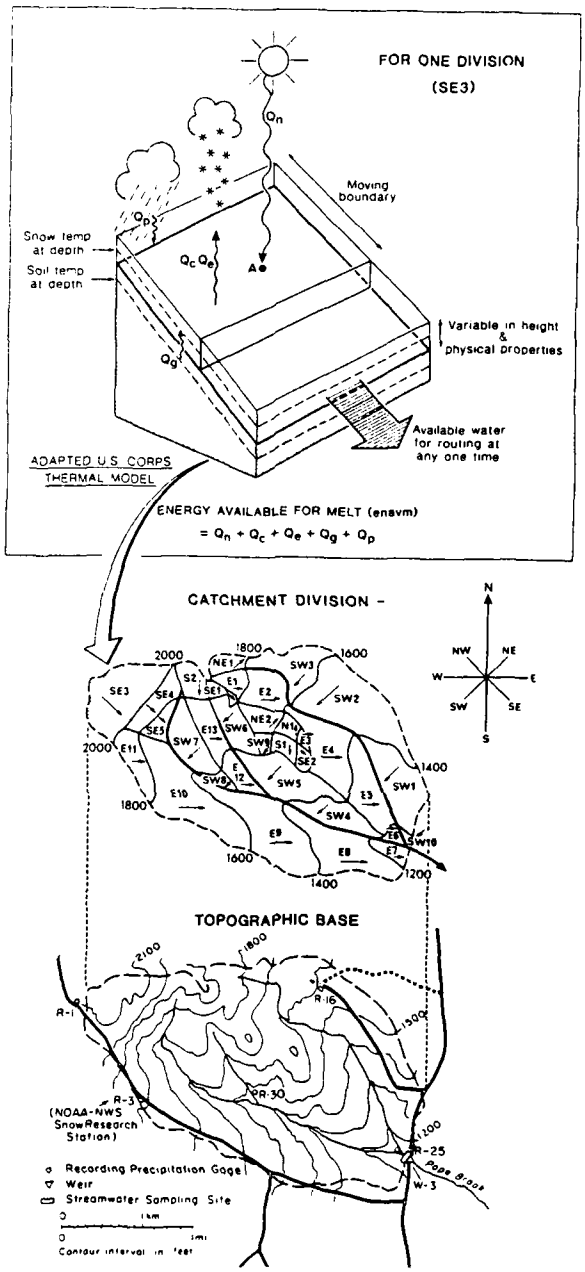

Figure 1. Basic structure of SNOMO.

The remaining components of equation (1) are calculated using physically-based equations taken from the literature. Q_p is calculated using equation (2), taken from Male & Granger (1978):

$$Q_p = \rho_w Cp_w (T_p - T_{sn}) P/1000 \quad (2)$$

where,

ρ_w density of water, kgm^{-3}

Cp_w specific heat of water, $kJkg^{-1} \cdot C^{-1}$

T_p temperature of rain, °C

T_{sn} temperature of snow, °C

P precipitation rate, $mmday^{-1}$.

ΔQ_s is calculated using equation (3), taken from Anderson (1976):

$$\Delta Q_s = (d\rho_{sn})^t \left[(Cp_i T_{sn})^{t+\Delta t} - (Cp_i T_{sn})^t\right] \quad (3)$$

where,

d depth of snowpack, m

ρ_{sn} density of snow, kgm^{-3}

Cp_i specific heat of ice, $MJkg^{-1} \cdot K^{-1}$

T_{sn} snow temperature, °K - calculated by TSTM

t time unit, one day

Q_g is set to zero. It is realised that in reality Q_g is usually greater than zero. However, various studies (Male & Gray, 1981 and Kuusisto, 1986) indicate that in most snow environments Q_g is a small or insignificant component of the snowpack energy-budget. Therefore to simplify the modelling conditions for the prototype model Q_g is set to zero.

The meltrate (in centimetres of snow or millimetres of water equivalent) is therefore expressed as:

$$\Delta r = \frac{\Delta Q_m}{L_f \rho_{sn}} .100 \quad (4)$$

where,

Δr melt rate, cm snow day^{-1}

L_f latent heat of fusion, $MJkg^{-1}$

SNOMO models the physical characteristics of the snowpack such as the albedo, thermal diffusivity and density by the operation of a simplistic snowpack layering routine. The snowpack is modelled as either 'old' snow, 'new' snow or as a layered combination of both. The maximum number of snow layers is two ('old' underlying 'new' snow). The 'old' and 'new' snow each have a characteristic density, albedo, emissivity, thermal conductivity and thermal diffusivity which is unvaried throughout the simulation. The values for these characteristics are obtained from the literature (Oke, 1987, Grey & Male, 1981 and Balick et.al., 1981a). A logic structure converts 'new' snow to 'old' snow and vice versa, depending upon the occurrence and timing of snowfall or melt and the relevant physical characteristics are utilized to calculate melt. Mean snowpack density is also calculated if the pack is two-layered. Compaction and reduction in pack height occurs with conversion of 'new' to 'old' snow. The modification of the snowpack energy-budget components by forest vegetation is modelled

by VEGIE, a submodel of the TSTM (Balick et.al., 1981b). Again, VEGIE has been modified to accommodate addition to SNOMO.

The equations and logic structure discussed above are the basic components of SNOMO. The input data required for SNOMO is shown in table 1. If a forest snowpack is being modelled then the vegetation input parameters shown in table 1 are also required. These can be obtained from the relevant literature (Geiger, 1965 and Deardorff, 1978), if the vegetation cover type is known. SNOMO has been designed to require a minimum of daily field measured data. The minimum daily measurements that are required are cloud cover, relative humidity, air temperature, precipitation and wind speed. A stochastic sensitivity analysis performed on the variables relative humidity, wind speed, air temperature and precipitation concluded that the model SNOMO was insensitive to these variables. SNOMO is designed, at present, to model the pattern of snowcover and snowdepth distribution over small catchments (<20km^2). SNOMO is designed to operate using daily meteorological input data that is taken from a site that is either within the catchment boundary or in close proximity to the boundary. The input variable air

Table 1. Operational data requirements

Instrument shelter height
Latitude

For each cell:
Air pressure
Air temperature (maximum and minimum) *
Cloud cover amount *
Cloud cover type
Elevation
Initial snowdepth
Julian day
Precipitation amount
Relative humidity *
Slope angle
Slope aspect
Snow density
Snow surface absorptivity
Snow surface emissivity
Snow heat conductivity
Snow thermal diffusivity
Wind speed *

For a vegetated cell, in addition:
Foliage cover fraction
Foliage emissivity
Foliage height
Foliage shortwave absorptivity
State of vegetation

* daily input data.

temperature is modified for elevation from its measurement site using a local lapse rate.

The subdivision of the watershed into computational units (cells) is facilitated by the use of a GIS. The subdivision of the catchment into homogeneous units (cells) was undertaken as follows:

(1) The topographic and vegetation cover maps and the catchment mask were digitized.

(2) A Digital Elevation Map (DEM) was created from the digitized topographic map, using the algorithm by Roberts (1980).

(3) Maps of slope angle and aspect were obtained from the DEM using algorithms from Garg & Harrison (1990).

(4) The slope, aspect and elevation were taken from the digitized topographic map and clustered to determine a set of spatially unique terrain classes. The clustering algorithm used was that available on the I^2S image processing system. The means and standard deviations of the values in each terrain class are available.

(5) The boundaries of the terrain classes were smoothed and isolated pixels, edge affects and misclassified areas were removed. The catchment mask was also superimposed. This resulted in set of terrain cells each with a dominant terrain class (slope angle, aspect and elevation).

(6) The vegetation map was superimposed upon the terrain cells and the vegetation within each cell assigned the dominant vegetation type.

The subdivision algorithm resulted in the subdivision of the catchment into cells. The location, area, mean slope angle, mean aspect and mean elevation of each cell is known. The primary advantages of the subdivision algorithm are that it is objective, repeatable and provides some indication of the variability within each cell.

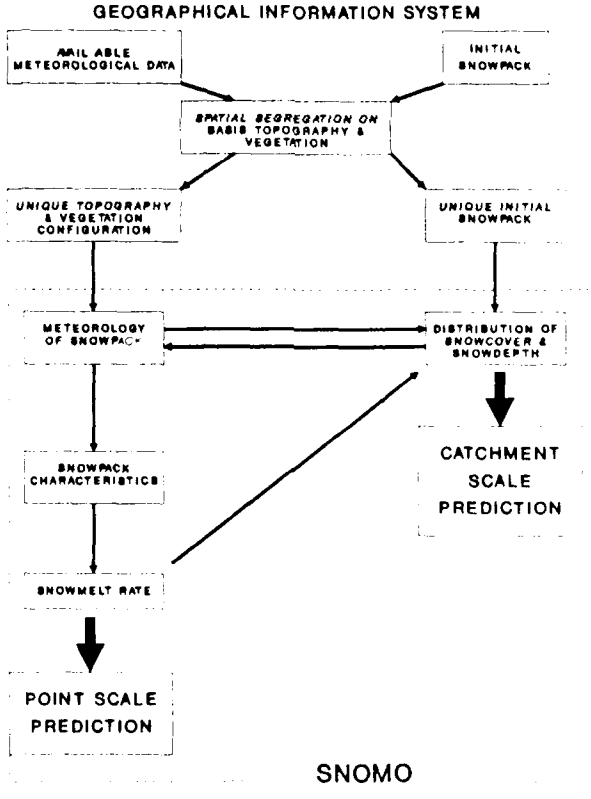

Figure 2. Relationship between SNOMO and the GIS.

The relationship between SNOMO and the GIS is shown in figure 2. The equations discussed above are solved for each cell and spatial output is obtained using the ARC-INFO data manipulation package. The primary output from the prototype model SNOMO is snowdepth and snowmelt volume (snowmelt volume = Δr x cell area). Additional outputs are snow temperatures and the snowpack energy-budget components of incoming and reflected short- and longwave radiation, Q_c, Q_e, Q_p and Q_g. These outputs are calculated for every cell. The results for every cell are plotted on the catchment division map for the simulated catchment to obtain the spatial distribution of these outputs. The spatial distribution of the snowdepth output indicates the snowcover distribution.

MODEL APPLICATION

Watershed selection

The W3 catchment, Sleepers River Research Watershed, Danville, Vermont, is considered to be representative of the landuse, cover, soil and topographic conditions that are found in the northern areas of the New England states and southern Quebec. A more detailed description of W3 is given in Anderson, et.al. (1977) and Pionke, et.al.(1978). The basin has an area of 8.4km^2 and varies in elevation from 346 to 695 metres above mean sea level. Vegetation cover is predominantly forest, coniferous, deciduous and mixed with some areas of open pasture. There is no arable land at W3. The main deciduous species are Birch (yellow - Betula allegheniensis, white - B. papyrifera and grey - B. populifolia), Beech (Fagus americana) and Maple (sugar - Acer saccharum and red - A. rubrum). The major coniferous species are Red Spruce (Picea rubra) and Balsam Fir (Abies balsamea). There has been and continues to be forestry activity in certain areas of W3, mainly in the coniferous areas which has resulted in large tracts of clear-cut.

Model predictions

The model was run for the 1988 melt season at W3. Figure 3 shows the predicted snowdepths against the observed snowdepths at the Townline meteorological station. Figure 3 shows that an acceptable level of correspondence is achieved for those days on which observations are available from the meteorological station. Figure 3 also shows

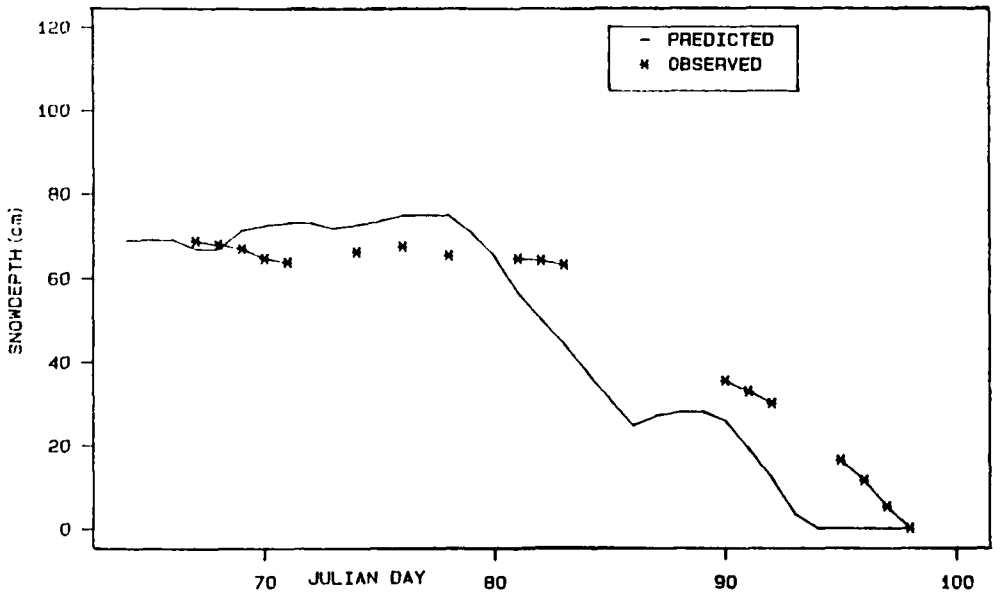

Figure 3. Predicted against observed snowdepths for the Townline meteorological station, W3 catchment, 1988.

that the model has a tendency to overpredict the snowmelt, that is to predict that the snow melts faster than in reality. This results in a four day discrepancy between observed and predicted total snow disappearance. This level of predictive accuracy is within acceptable limits due to the problems in obtaining a representative snowdepth. Snowcover is highly variable and a predictive discrepancy of about 10cm and 4 days is acceptable at present. The model is a prototype and further investigations as to its sensitivity to variables such as cloud cover and initial snowdepth will be conducted.

Table 2. *Comparison between the calculated and observed snowdepths (centimetres) for points over the W3 catchment.*

CELL 29 (Deciduous, 1832m elevation, 8.45°slope, 99°aspect)

Julian day	Calculated	Observed (1)	Observed (2)
83	72	65	73
90	61	46	49
97	23	15	13

CELL 30 (Deciduous, 1969m elevation, 9°slope, 143°aspect)

Julian day	Calculated	Observed (1)	Observed (2)
83	68	65	73
90	55	46	49
97	12	15	13

CELL 9 (Mixed, 1226m elevation, 4°slope, 77°aspect)

Julian day	Calculated	Observed
83	60	55
90	53	30
97	21	0

CELL 24 (Open, 1563m elevation, 6°slope, 79°aspect)

Julian day	Calculated	Observed (1)	Observed (2)	Observed (3)
83	46	47	49	58
90	28	24	21	26
97	0	0	0	0

Table 2 shows the calculated and observed results for selected cells within the W3 catchment and demonstrates the range of conditions that exist at W3. Again the simulations are acceptable. Table 2 illustrates the problem of validating a model such as SNOMO. The difficulties of obtaining a representative snowdepth, to use as a validation tool are apparent. The observed values in table 2 are snowcourse values, that is they are the mean value of 5 snowdepths measured at adjacent snowcourse sites. Some cells (cells 29, 30 and 24) possessed more than one snowcourse site within the cell. The variation of the measured snowdepth between these sites is as much as 9cm. The utility therefore of validating a model such as SNOMO, which predicts snowdepth, and expecting exact correspondence between the simulated and the measured snowdepths is questionable. Correspondence within a certain range of values and exhibition of a correct melt trend would be of more use and is the result that SNOMO achieves

Figure 4 shows the results of the spatial plotting of the cell results showing the first day of zero snowcover (melt day). Validation of this prediction and the spatial predictions is not really possible at present because of insufficient snowcover data

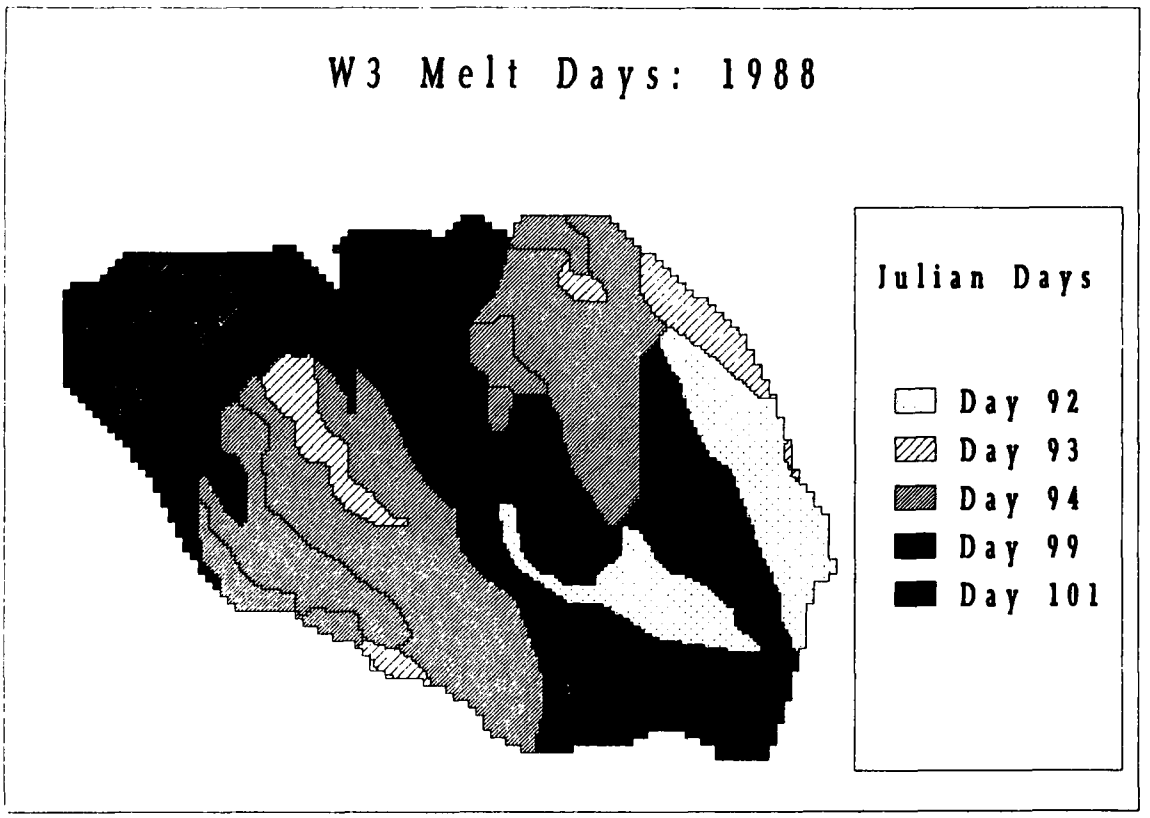

Figure 4. Melt day prediction for the W3 catchment, 1988.

over the entire catchment, only spatially restricted point observations (such as at Townline) are available.

The scope of the prediction that the SNOMO scheme offers clearly facilitates the establishment of field research designs in respect of snowdepth field measurement programmes. This is a major element of validation concern because of the resources and time demands in establishing field depths over large spatial areas on a daily basis. The argument would therefore be that initial prototype predictions could be undertaken using SNOMO to devise a field validation design against which subsequent runs of SNOMO would then be validated.

DISCUSSION

A GIS driven physically-based catchment scale distributed model has been developed and presented (equations 1-4). Initial results of this energy-budget scheme appear encouraging in terms of both point predictions and spatial resolution when applied to the catchment scale. Problems of validation of this snowcover prediction model appear to represent the next area of research. We have suggested that prototype runs on selected input data scenarios may be an appropriate approach to the problem of selecting field locations for snowdepth measurements during melt at the catchment scale. The primary utility of the prototype model SNOMO is in the calculation of spatial snowdepth and snowcover distribution. The variable initial snowpack extent is an important variable in many snowmelt forecasting models, for example, Rango & Martinec (1982) and Ferguson (1984). The calculations used in SNOMO are physically-based unlike, for example, the Leaf & Brink model (1973a & b) which calculates spatial melt using a mixture of temperature and semi-physically-based methods. The use of physically-based equations enables the additional output (if required), on a spatial basis, of the energy-budget values of incoming and reflected short- and longwave

radiation, Q_c, Q_e, Q_p and Q_g. The spatial and physical basis of the prototype model SNOMO enables the potential inclusion of SNOMO into a suite of models to predict the eco/hydro-system, for example in a forest ecosystem model. The subdivision of the catchment is conducted using an original computerized division method. This is advantageous when compared to current manual division methods, for example Leaf & Brink (1973a & b) and Stepphun & Dyck (1974). The SNOMO subdivision is objective, repeatable and gives an indication of the variability present in the resultant subdivision.

ACKNOWLEDGEMENTS

The work reported in this paper was funded in part by a contract to the University of Bristol, United Kingdom from the U.S. Corps of Engineers Cold Regions Research and Engineering Laboratory. Hugh Greenan and Bill Roberts at W3 aided field data acquisition.

REFERENCES

Anderson, E.A. (1976). A Point Energy and Mass Balance Model of a Snow Cover. NOAA Technical Report NWS 19, U.S. Dept. of Commerce, Silver Spring, MD, 150pp.

Anderson, E,A (1978). Streamflow simulation models for use on snow covered watersheds. Proc. Modelling of Snow Cover Runoff, S.C. Colbeck and M. Ray (eds), U.S. Army Cold Regions Research and Engineering Lab., Hanover, N.H., 26-28 September 1978, 336-350.

Anderson, E.A., Whipkey, R.Z., Greenan, H.J. & Machell, C.T. (1977). NOAA-ARS cooperative Snow Research Project--Watershed Hydro-climatology and Data for Water Years 1960-1974, U.S. Dept. of Commerce, Silver Spring, MD, 304pp.

Balick, L.K., Link, L.E., Scoggins, R.K. & Solomon, J.L. (1981a). Thermal Modelling of Terrain Surface Elements. Technical Report EL-81-2, prepared by the Environmental Laboratory, Waterways Experiment Station, in collaboration with Mississippi State University, for the U.S. Army Engineer Waterways Experiment Station, EC, Vicksberg, Miss.

Balick, L.K., Scoggins, R.K. & Link, L.E. (1981b) Inclusion of a simple vegetation layer in terrain temperature models for thermal infrared (IR) signature prediction. Miscellaneous Paper EL-81-4, U.S. Army Engineers Waterways Experiment Station, EC, Vicksberg, Miss., pp39.

Deardorff, J.W. (1978). Efficient prediction of ground surface temperature and moisture with inclusion of a layer of vegetation. J. Geophysical Res., 1889-1902.

Ferguson, R.I. (1984). Magnitude and modelling of snowmelt runoff in the Cairngorm mountains, Scotland. Hydrol Sci. J., 29, 1, 49-62.

Ferguson, R.I. & Morris, E.M. (1987). Snowmelt modelling in the Cairngorms, N.E. Scotland. Trans. Royal Soc. Edinburgh: Earth Sci., 78, 261-267.

Garg, P.K. & Harrison, A.R. (1990). Quantitative representation of land-surface morphology from digital elevation models. Proc. 4th Int. Symp. on Spatial Data Handling, Zurich, 1990, in press.

Geiger, R. (1965). The climate near the ground. Harvard Univ. Press, Cambridge, Mass., pp611.

Gray, D.M. & Male, D.H. (1981). Handbook of Snow. Pergamon Press, Oxford, 776pp.

Kuusisto, E. (1986). The energy balance of a melting snow cover in different environments. In: Modelling Snowmelt-Induced Processes (ed. E.M.Morris), IAHS Publ. No. 155 (Proc. Budapest Symp.), 37-45.

Leaf, C.F. & Brink, G.E. (1973a). Computer simulation of snowmelt within a Colorado Subalpine Watershed. USDA Forest Ser. Res. Paper RM-99, Rocky Mt. Forest and Range Exp. Stn., Fort Collins, Co., pp22.

Leaf, C.F. & Brink, G.E. (1973b). Hydrologic simulation model of Colorado subalpine forest. USDA. Forest Ser. Res. Paper RM-107, Rocky Mt. Forest and Range Exp. Stn., Fort Collins, pp23.

Male, D.H. & Granger, R.J. (1978). Energy mass fluxes at the snow surface in a Prairie environment. In: Proc. Modeling Snowcover Runoff, (eds. S.C.Colbeck & M.Ray), US. Army Cold Regions Research and Engineering Lab., Hanover, NH., 101-124.

Male, D.H. & Gray, D.M. (1981). Snowcover ablution and runoff. In: Handbook of snow, Gray, D.M. and D.H. Male (eds), Pergamon Press, Oxford, 360-436.

Oke, T.R. (1987). Boundary Layer Climates, 2nd Edition, Methuen & Co. Ltd. (London).

Pionke, H.B., Bahleda, K. & Chamberlain, B.J. (1978). Data directory, data and data collection site characteristics for the Sleepers River Watershed, N. Danville, Vermont. Northeast Watershed Research Centre, USDA-SEA-FR, 111 Research Building A, University Park, Pennsylvania 16802.

Rango, A. & Martinec, J. (1982). Snow accumulation derived from modified depletion curves of snow coverage. In: Hydrological aspects of Alpine and High Mountain areas, IAHS Publ. No. 138 (Proc. Exeter Symp.), 83-90.

Roberge, J., Stein, J. & Plamondon, A. (1988). Evaluation d'un modele de fonte nivale en foret Boreale (Evaluation of a snowmelt model in a boreal forest environment). J. Hydrol., 97, 161-179.

Roberts, P.A. (1980). Computer-based techniques for converting a contour map into an equispaced grid of points. Technical Report TR 80110, Royal Aircraft establishment, Farnborough, UK.

Stepphun, H. & Dyck, G.E. (1974). Estimating true basin snowcover. Proc. of Symp. on Advanced Concepts and Techniques in the Study of Snow and Ice Resources, Nat. Acad. Sci. Wash. D.C., 314-328.

Objective Guidance for 1- and 2-Day Mesoscale Forecasts of Lake-Effect Snow

W.A. BURROWS

Atmospheric Environment Service
Meteorological Services Research Branch
4905 Dufferin Street
Downsview, Ontario M3H 5T4, Canada

ABSTRACT

Lake-effect-snow-possible (LESP) days were identified for each of 29 climatological stations in the lee of Lake Huron and Georgian Bay for the November to April winters of 1984-1988 using output from 0-24 hour and 24-48 hour forecasts by the Canadian Meteorological Center (CMC) operational spectral Numerical Weather Prediction (NWP) model. Twenty-four hour observed snow amounts on LESP days were separated into 5 ordered categories. The distribution of snowfall on LESP days for the aggregate of the 29 stations is centered on category 3, but the distributions for individual stations are centered on categories 1 or 2. This suggests lake-effect snow occurrence and amounts are likely to be over-forecast by meteorologists for even relatively small public forecast areas.

A recent non-parametric classification procedure known as "Classification and Regression Trees (CART)" was used to classify the categorical snowfalls by predictor threshold values in decision trees. Predictors were designed from the physics of lake-effect snow formation and calculated from the NWP model output data on a 63 km interpolation grid. Predictors most frequently used by CART to create the decision trees involved low-level divergence (convergence) at nearly every station, followed by predictors related to air-water temperature difference. The method shows considerable promise for timely many-site production of objective operational mesoscale guidance for 1 and 2, day forecasts of 24-hour lake-effect snow accumulation.

1. INTRODUCTION

Lake-effect snowfall is one of the challenging and important mesoscale forecast problems around the Great Lakes. On occasion a great deal of snow falls in a 24 hour period over small areas, with wide variation in amounts over relatively small distances. It has been estimated that as much as one-half the annual snowfall around the shores of Lake Michigan is due to lake effects (Braham and Dungey, 1984). A similar or even greater fraction appears to be the case around Lake Huron and Georgian Bay as well (Figure 1).

Peace and Sykes (1966) concluded that "while the formation of lake-effect bands is caused by heating of the air by a warm lake, the location and movement of snow bands are controlled by winds aloft". Thus lake-effect snow, while it is a mesoscale phenomenon, is strongly controlled by characteristics of the synoptic scale environment in which it occurs. This has enabled meteorologists to predict the occurrence of lake-effect snow in

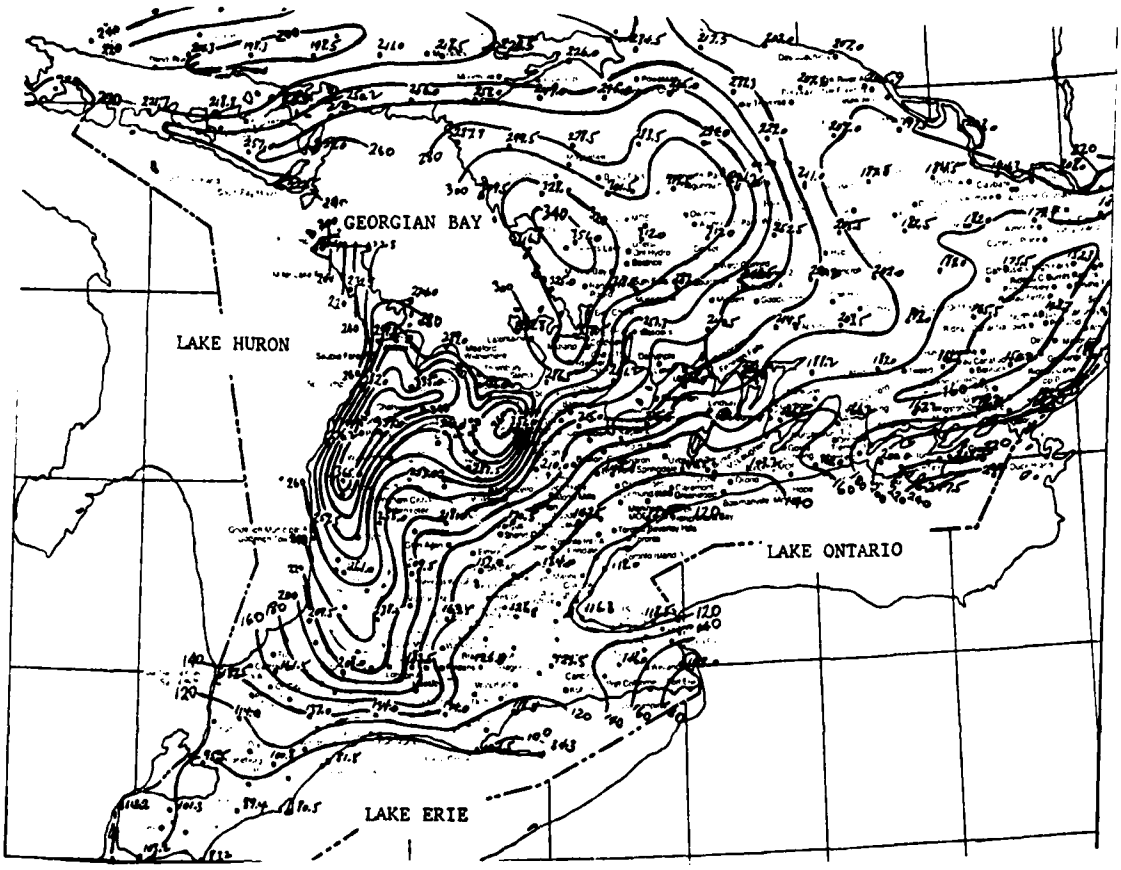

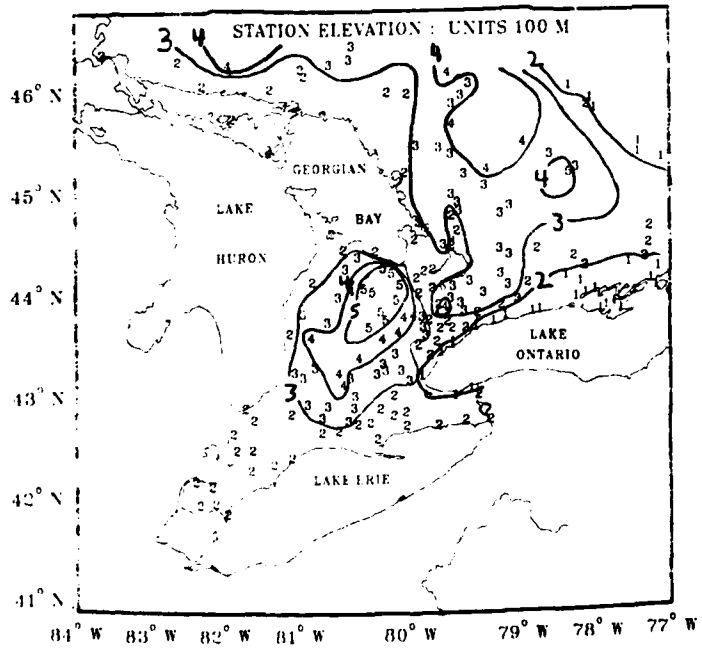

Figure 1: Top: mean annual snowfall (cm) for 1951-1980 for southern Ontario, from Crowe(1985), reproduced in Burrows (1990). Bottom: southern Ontario elevation in 100's of meters.

broad regions to the lee of large water bodies with good success by using output from operational NWP models. However, the mesoscale details of the snowfall, such as band movement and snow amounts at specific points are often not well forecast. There is little objective operational guidance available to forecasters for mesoscale lake-effect snow prediction, likely because the scale on which lake-effect snow occurs is well below the resolution of current operational NWP models. Present forecast procedures in operational weather offices generally rely on subjective manual or semi-computerized interpretation of model output fields using decision tree methods and accumulated office experience (e.g. Dockus, 1985; Niziol, 1987; Murphy, 1989). These methods, while useful for specific sites, are too time-consuming to be simultaneously applied in an operational forecast mode for a large number of sites covering broad, complicated areas. Research studies using mesoscale models have appeared in the literature (e.g. Hjelmfelt, 1990; Lavoie, 1972), but these have not to this author's knowledge, led to production of regular objective forecast guidance in the field. A method for generating objective forecast guidance for lake-effect snow using an operational NWP model was developed by Dewey (1979a,b), but was never implemented.

A growing number of public and private sector users are interested in timely, accurate many-site forecast guidance for snow amounts within public forecast regions. Aware of this, Burrows (1990) studied the feasibility of producing objective mesoscale forecast guidance for 24-hour lake-effect snow amounts for 1-Day and 2-Day projection times for climatological stations in the southern Georgian Bay region. "Perfect Prog (PP)" forecasts of 24-hour snow amount in 5 categories were produced using multiple discriminant analysis (MDA). Using the MDA probabilities as predictors, the forecasts were tuned with a statistical classification procedure known as Classification and Regression Trees (CART) developed recently by Brieman et al (1984). CART establishes rules by which categorical or continuous predictands can be classified in a decision tree by threshold values of user-specified predictors. It is non-parametric (makes no assumptions about the statistical distribution of the predictors), and will use both single predictors and linear combinations of predictors offered to it.

It was suggested in the above work that while the tuned PP statistical forecasts lacked the accuracy to be useful as guidance, there was considerable promise that better forecasts could be generated if the CART procedure were more fully employed and if a better predictor set were designed. The latter would be possible if NWP model output data were used for derivation of predictors instead of analyzed observed data (i.e. "Model Output Statistics (MOS) (Glahn and Lowry, 1972)" approach instead of PP approach). This indeed turned out to be the case, and the resulting method for producing mesoscale lake-effect snow forecast guidance will be implemented experimentally for use at the Ontario Weather Center. This paper describes the development of the forecast system.

2. PREDICTAND

Daily snowfall data for the winters of 1984-1988 (1 November to 30 April, except to 25 March 1987 and to 8 April 1988) were gathered for 29 climatological stations to the lee of Lake Huron and Georgian Bay shown in the left panel of Figure 2. (The right panel is the interpolation grid for NWP model data and is discussed in Section 3). A climatological day at these stations is defined as 8am today to 8am tomorrow. The total number of days without missing data during the study period ranged from a low of 600 to a high of 643, with about 633 days available at many stations. The data set was screened at each station to separate out "lake-effect snow possible" (LESP) days. These were defined as at least 12 hours in a 24 hour period when the CMC NWP model forecast a local off-water 850 mb wind fetch and either a lake-850 mb temperature difference of at least 13 degrees C (dry adiabatic), or 8 to < 13 degrees with upward vertical motion at 700 mb in the middle of Lake Huron (which is always free of ice). Water temperature was taken from time-mean charts published in Saulesleja (1986). Snow amount in cm at each station was divided into 5 categories: 1= 0-trace, 2= >trace-5, 3= >5-12.5, 4= >12.5-22.5, 5= >22.5.

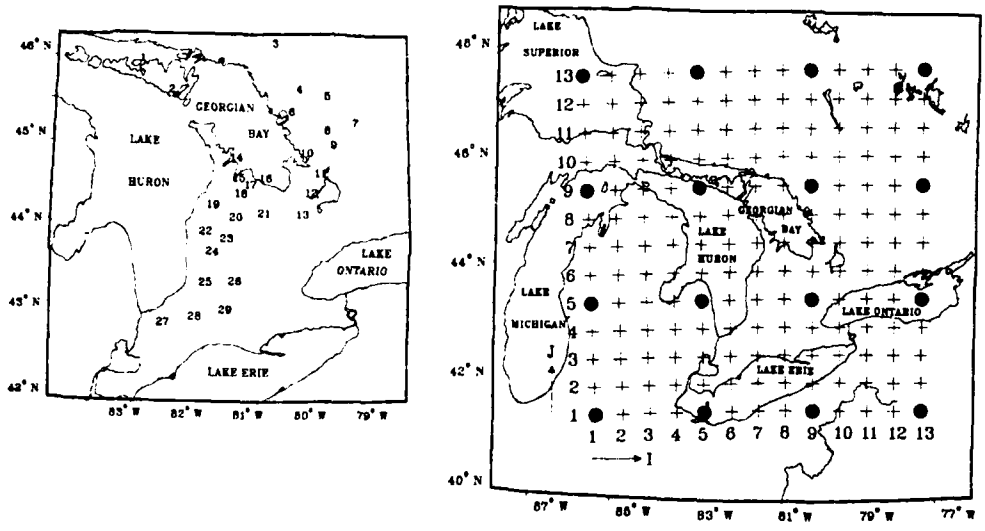

Figure 2: Left panel: Location of climatological stations included in this study. Right panel: NWP model output data grid points (solid circles), interpolation grid points for calculation of predictors (crosses).

The top left panel of Figure 3 shows the fraction of days at each station that qualified as LESP days when classified with Day 1 NWP forecast data (units days per thousand, e.g. 455 means .455). Results are what would be expected, considering the prevailing west to northwest winds over this region. The number of LESP days varies with the fetch direction at each station. The maximum fraction of LESP days occurs to the lee of central Lake Huron, with fewest occurrences at the northern and southern extremities of Lake Huron, and occurrences decreasing with distance inland. Table 1 shows the highest snow category that was observed at any of the 29 stations when a LESP day was observed at any one of them. Little difference is seen between the two projection times. This suggests the NWP model forecasts of the large scale flow in this region for 0-24 hours and 24-48 hours projection times tend to be consistent for LESP days. A normal distribution *centered on category 3* is seen for LESP days identified with both 00-24 hour (Day 1) and 24-48 hour (Day 2) NWP model forecast data.

Table 1: The highest snow category (Cat) observed when a LESP day was identified at any of the 29 stations, shown as a percent of total LESP days for each category. Results are for LESP days determined by Day 1 and Day 2 NWP model forecast data.

Cat	%Day 1	%Day 2
1	06.8	07.0
2	24.9	22.4
3	33.3	35.8
4	22.7	22.7
5	12.3	12.1

A different story emerges from the results for *individual* stations. The remaining panels in Figure 3 show the fraction of LESP days when snowfall occurred in categories 1-5 at each station. For the aggregate of stations it was seen in Table 1 that snow was observed by at least 1 of the 29 stations on about 93% of the LESP days. However, Figure 3 shows that on roughly 25-65% of the LESP days at *individual* stations no snow fell (CAT 1) or if snow did occur, snowfall was not more than 5 cm (category 2) on roughly another 30-50% of the LESP days (CAT 2). Thus the maximum number of snow occurrences on LESP days for

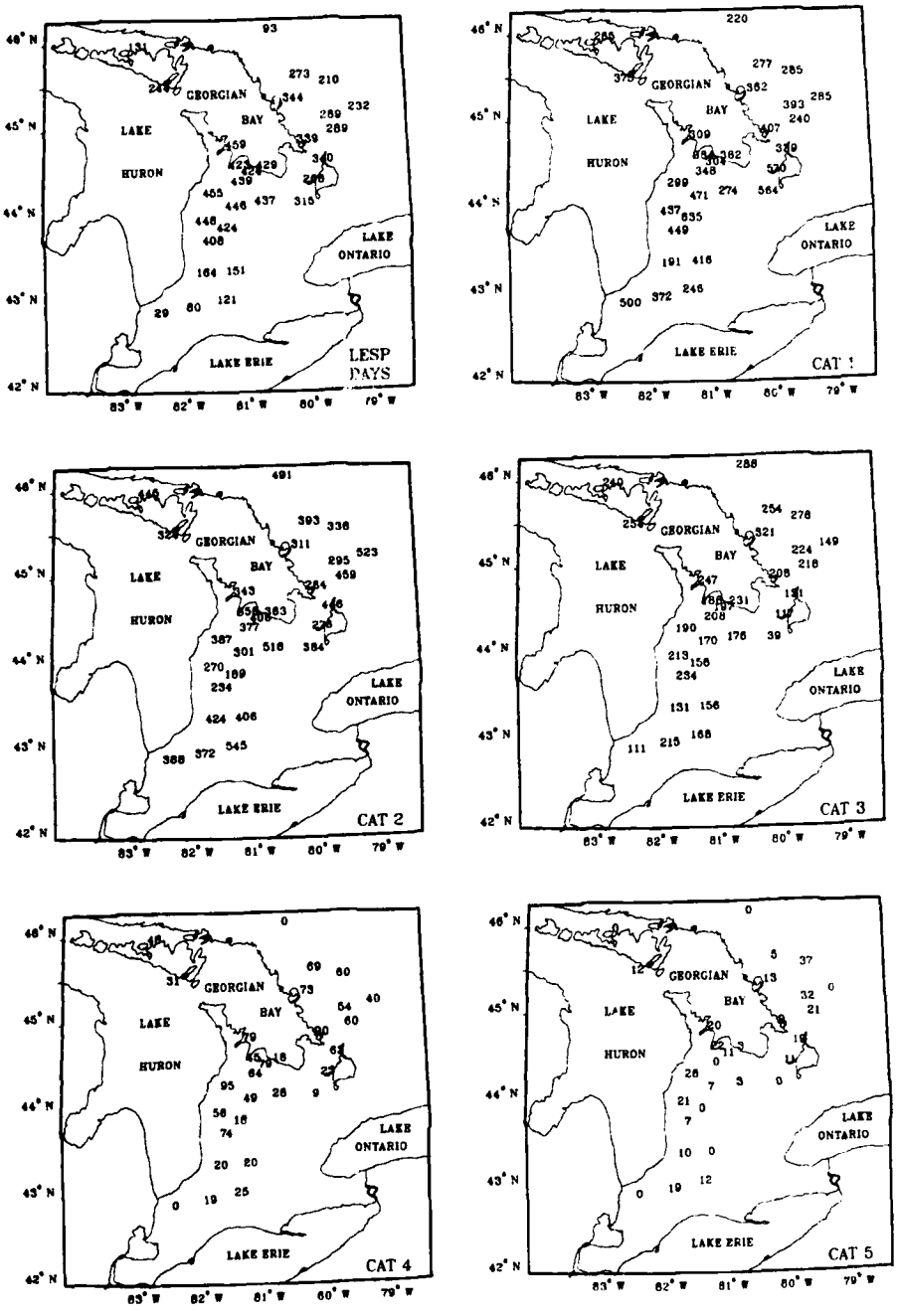

Figure 3: LESP DAYS: number of days that "lake effect snow possible" (LESP) days were identified with Day 1 (0-24 hr) NWP model forecast data; CAT 1, ..., CAT 5 number of LESP days when 24-hour observed snow amount was in category 1 (0 - trace), or category 2 (>trace-5cm), or category 3 (>5-12.5 cm), or category 4 (>12.5-22.5 cm), or category 5 (>22.5 cm). Units days per thousand days (e.g. 455 means .455).

individual stations is centered on *categories 1 or 2*, even in the heart of the "snowbelt" region to the lee of central Lake Huron and central Georgian Bay. (More than 90% of the snow occurrences on LESP days were in these two categories in the highly populated region to the lee of southern Georgian Bay). Heavy snowfalls on LESP days at individual stations are relatively rare: 0-10% for category 4 snowfalls and 0-4% for category 5 snowfalls. The most occurrences of category 5 snow on LESP days at any station was only 8 in the 4 years.

The above results imply that *over-forecasting* the amount and occurrence of snow in lake-effect storms for individual stations and small areas is likely to be a problem for even relatively small public forecast areas. This is because the maximum snowfall will occur over a small portion of a region, but a forecaster will tend to predict the maximum amount everywhere to be safe.

3. PREDICTORS

1200 UTC NWP model forecasts of wind, temperature, geopotential height, and vertical motion at 6-hour intervals from 0 to 48 hours projection time were interpolated with a bi-cubic spline algorithm to a mesoscale grid of about 63 km spacing over southern Ontario (shown in the right panel of Figure 2). The solid circles are locations of the NWP model data (about 254 km resolution), the crosses are interpolated points. Data on the 63 km interpolation grid can be thought of as representing the "between-grid-point" variation of data on a 254 km scale, thus shoreline-water differential frictional effects on boundary layer winds be poorly represented. We are therefore dealing with relations between mesoscale lake-effect snow formation and upper air controls on the much larger synoptic scale.

Predictors known or expected to be physically related to formation of lake-effect snow were designed and calculated on the 63 km grid. Comprehensive recent discussions of the meteorological parameters and features important in the process of lake-effect snow formation can be found in Dockus (1985), Niziol (1987), Murphy (1989), and Hjelmfelt (1990). A total of 129 separate potential predictors were designed to accommodate the 24-hour period of the predictand. These are derived from physical parameters shown in Tables 2 and 3. Lake water temperature and mean ice cover were estimated as space averages surrounding the grid points from time-mean charts for periods of variable length during the winter season in Saulesleja (1986). Low level divergence was calculated from interpolated east-west and north-south (u and v) wind components by calculating local small-scale derivatives at each interpolation grid point.

4. CART

CART was used to find predictand classification trees for each station using Day 1 and Day 2 NWP model forecasts of predictors. Trees were created with the basic 129 predictors for 28 of the 29 stations (station 27 had only 18 LESP days). For stations where only 1 or 2 cases of the rarest category occurred, those observations were classified at the next lowest category before CART was run. Since it is a recent development and is not widely known in meteorological circles, a brief description of CART and its use in this study follows. For greater detail the reader is asked to refer to Brieman et al (1984).

CART is given a data base consisting of predictand and predictor values which it uses to establish a decision tree that classifies the predictand. Computer output from the CART program for Day 1 at station 19 (Paisley, Ontario) is shown in Figure 4. The predictand was snow category (1-5) on LESP days. The "Tree Sequence" summary shows CART first found a tree that classified all the data perfectly (Tree 1 with 65 Terminal Regions), then began "pruning" "nodes" in the "weakest links" up from the bottom of the tree until 1 tree remained (Tree 12). Tree 12 would assign the "initial class assignment", which is the category which gives the lowest misclassification cost (.614) if all data were classified as a single category (2 here). This will be the most common category if unit

Table 2: Physical parameters important for lake-effect snow production. Operations "*av, mx, mn, ch*" mean respectively: average value, maximum value, minimum value, and change between end and beginning, in a 24-hour period. Operation N6 is the number of 6-hour times within a 24-hour period (0-5) that a specified condition applies. Location identifiers such as "65, 68, 88" denote points (I=6,J=5), (I=6,J=8), (I=8,J=8) in Figure 2, respectively. "loc" denotes station location.

1. lake - 850 mb temperature difference. (*av*, *mx*, *mn* at 68)
2. 500 mb temperature. (*mn* at 68).
3. ice cover. (percent).
4. lake - 850 mb temperature difference plotted against lake - 700 mb temperature difference [in Figure 5 of Niziol (1987), define an index: 0=outside graph, 1=conditional, 2=moderate, 3=extreme]. (*av*, *mx*, *mn*, *ch*, *N6* of index value at 68).
5. 1000 mb wind direction. (*av*, *ch* at 65, 68, 88).
6. 850 mb wind direction. (*av*, *ch* at 65, 68, 88).
7. 700 mb - 1000 mb wind direction difference. (*av*, *mx*, *mn*, *ch*, *N6* at 65, 68, 88).
8. 700 mb - 1000 mb wind direction difference in two ranges: 0-30 degrees, 30-60 degrees. (*N6* at 65, 68, 88)
9. 850 mb wind speed. (*av* at 65, 68, 88).
10. 1000 mb wind speed in 12 direction segments 360-30 degrees, 30-60 degrees, ..., 330-360 degrees. (*av* at loc).
11. simultaneous positive vorticity advection at 500 mb, 700 mb, 850 mb. (*N6* at 68).
12. 500 mb advection of absolute vorticity. (*av*, *mx* at 68).
13. 700 mb vertical velocity. (*av*, *mx*, *mn*, *ch* 65, 68, 88).
14. 700 mb temperature advection. (*av*, *mn* at 68).
15. 1000 mb divergence within lines and areas defined in Table 3. (*av*)
16. 1000 mb divergence within lines and areas defined in Table 3. (*N6* of min for all J=1-13 at each I within a specified line or area, summed over each I within that line or area)
17. [700 mb + 1000 mb] divergence within lines and areas defined in Table 3. (*av*).
18. 700 mb wind maximum for all J=1-13 in Figure 2 occurs within strips [I=2-4], [I=4-6], [I=6-8]. (*N6* in each strip).
19. 500 mb low center vicinity of James Bay. (yes or no).
20. 850 mb wind direction at 4,9 is between 280 degrees and 340 degrees and direction at 4,9 minus direction at 9,7 is at least 20 degrees. (*av*, *N6*).
21. times "fetch importance index" (1 to 3) defined arbitrarily in 4 local direction sectors for each station from 850 mb wind direction]. (*N6* of index values).

Table 3: I and J values in Figure 2 for horizontal and vertical space averages in divergence predictors (Pred) in Table 2. Div01 - 13 are averaged over ranges of I and J in Figure 2 (e.g. Div01 is calculated over the area I= 4 to 12, J=4 to 10, and Div06 along the line I=4 to 9, J=8); Div14 - 18 are calculated over diagonal lines (e.g. Div14 is calculated from the points I=4,J=9 to I=6,J=8).

Pred	I	J	Pred	I	J	Pred	I	J	Pred	I	J
Div01	4-12	4-10	Div06	4-9	8	Div11	9-12	4-6	Div14	4,9	6,8
Div02	5-7	4	Div07	4-9	9	Div12	9-12	7-9	Div15	5,8	6,6
Div03	5-7	5	Div08	4-11	10	Div13	4-5	9	Div16	5,6	6,5
Div04	4-7	6	Div09	7-9	3-5				Div17	7,9	8,8
Div05	4-9	7	Div10	7-9	6-8				Div18	7,8	8,7

misclassification costs are assigned. The final tree selected is Tree 5, the one which had the minimum "cross-validated cost" relative to Tree 12. If no tree structure were found with a cross-validated cost less than 1, then Tree 12 would have been selected.

TREE SEQUENCE

TREE	TERMINAL NODES	CROSS-VALIDATED RELATIVE COST			RESUBSTITUTION RELATIVE COST	COMPLEXITY PARAMETER
1	65	0.97	+/-	0.047	0.00	0.000E+00
2	35	0.91	+/-	0.048	0.17	0.353E-02
3	28	0.91	+/-	0.048	0.25	0.703E-02
4	19	0.90	+/-	0.048	0.37	0.8.0E-02
5*	13	0.89	+/-	0.048	0.47	0.105E-01
6	11	0.91	+/-	0.048	0.51	0.123E-01
7	8	0.95	+/-	0.048	0.58	0.140E-01
8	5	0.92	+/-	0.048	0.67	0.176E-01
9	4	0.92	+/-	0.048	0.71	0.281E-01
10	3	0.94	+/-	0.048	0.77	0.351E-01
11	2	0.96	+/-	0.047	0.86	0.562E-01
12	1	1.00	+/-	0.047	1.00	0.842E-01

INITIAL MISCLASSIFICATION COST = 0.614
INITIAL CLASS ASSIGNMENT = 2

CLASSIFICATION TREE DIAGRAM

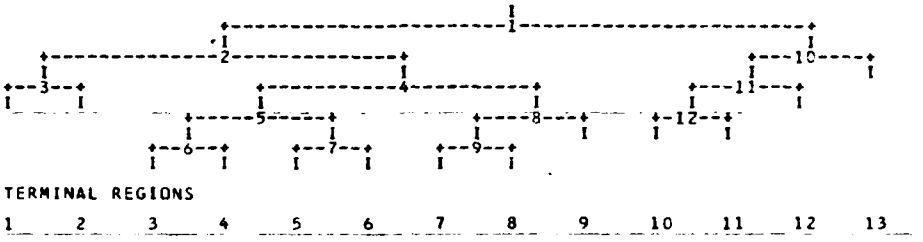

Figure 4: Tree sequence summary and classification tree diagram for Tree 5 found by CART for LESP days classified with Day 1 (0-24 hr) NWP model forecast data for Station 19 in Figure 2.

The cross-validated relative cost (.89 +/-.048 for Tree 5) can be thought of as a "skill score with respect to climatology" for each tree. A ten-fold cross-validation method was used here to evaluate the cost of each tree when searching for the optimally-pruned tree. This works by splitting the four-year "learning sample" into ten "cross-validation sub-samples", each containing 90% of the learning sample and about the same distribution of data in the categories. For every "complexity value" (a number inversely proportional to the number of nodes) reached by the main tree as it is pruned, CART takes each cross-validation sub-sample and grows "auxiliary trees" up to the complexity value reached by the main tree. It then evaluates the misclassification cost of each auxiliary tree by running down the tree the 10% of data not contained in its cross-validation sub-sample and storing the results in a "cross-validation classification matrix". *Cross-validation approximates a test of the main decision tree with an independent data set in a conservative manner* (misclassification costs are over-estimated because the full learning sample is not used to grow the auxiliary trees). It is recommended for small data sets or data sets that are sparse in some categories, such as categories 4 and 5 in this study. (For data sets with relatively large numbers of cases in each category, one can set aside a specified fraction of the data as an independent set on which to evaluate the misclassification cost of the main tree as it is grown).

Three tree construction rules for splitting the samples in the nodes were tested: "gini, twoing, and ordered twoing". The reader is referred to Brieman et al (1984) for a full explanation of these terms. "Ordered twoing", which treats the decision in each node

as a choice between two ordered classes when splitting cases to the left or to the right, seemed appropriate here since snow amount increases with category number.

Table 4 shows the decision rules CART found for segregating cases in the nodes, and the data populations in the Terminal Regions (final classification nodes), for the classification tree diagram in Figure 4. In Node 1, events with greater snow amounts overall are sent left into Node 2 while events with smaller overall snow amounts are sent right into Node 10. The test for sending data left or right in Node 1 is based on a linear combination of three predictors. The rules are physically realistic. A leftward split into Node 2 occurs for events where, relative to all the cases, the 700 mb-1000 mb wind direction change over southern Lake Huron between is 0 and 30 degrees for a relatively large portion of a 24-hour period, 24-hour average low level convergence over southern

Table 4: First part: Decision tree rules found by CART for splitting the nodes in the Day 1 learning sample for station 19 for the classification tree diagram shown in Figure 4. Classes assigned to cases going left or right are shown for each node, with final classification categories in Terminal Regions highlighted in bold. Predictors are coded to follow the explanation in Tables 2 and 3. For example: #8/0-30/*N6*/68 means predictor number 8, 0-30 degree range, operation *N6*, calculated at grid point 68; #15/02/*Av* means predictor number 15, Div02 in Table 3, operation *Av*. Units of some quantities are shown, divergence units are 10^{-6} s^{-1}, vorticity advection units are 10^{-11} s^{-2}. Second part: data populations in terminal regions in Figure 4.

Decision Rules:

Node 1: **L=2 R=1** : split left if (-.613*[#8/0-30/*N6*/68]
+.553*[#15/02/*Av*] -.563*[#1/*Mx*]) <= -12.0

Node 2: **L=2 R=3** : split left if (-.251*[#15/02/*Av*]
+ .585*[#1/*Mx*] -.222*[#10/270-300]
+ .738*[#11]) <= 14.8

Node 3: **L=2 R=3** : split left if [#7/*Mn*/68] <= 51.3 degrees

Node 4: **L=4 R=3** : split left if [#5/*Av*/68] <= 306 degrees

Node 5: **L=3 R=4** : split left if [#2] <= -40.7 degrees C

Node 6: **L=3 R=5** : split left if [#10/270-300] <= 2.15 ms^{-1}

Node 7: **L=4 R=3** : split left if [#10/270-300] <= 10.9 ms^{-1}

Node 8: **L=2 R=3** : split left if [#13/*Ch*/65] <= 3.05 mb hr^{-1}

Node 9: **L=2 R=3** : split left if [#14/*Av*/68] <= .05 degrees C hr^{-1}

Node 10: **L=1 R=2** : split left if [#1/*Av*] <= 20.1 degrees C

Node 11: **L=1 R=2** : split left if [#20/*Av*] <= 32.0 degrees

Node 12: **L=2 R=1** : split left if [#13/*Mn*/68] <= -8.15 mb hr^{-1}

Data Population In Terminal Regions:

Terminal		Category				
Region	Class	1	2	3	4	5
1	2	15	51	11	1	1
2	3	1	0	4	0	0
3	3	0	1	5	0	0
4	5	0	0	0	0	5
5	4	2	7	5	24	1
6	3	1	0	4	0	0
7	2	2	9	2	2	0
8	3	0	0	4	0	0
9	3	0	1	14	0	1
10	2	3	7	1	0	0
11	1	60	19	4	0	0
12	2	1	6	0	0	0
13	2	1	9	0	0	0

Lake Huron was relatively large, and a relatively large 24-hour maximum water-850 mb temperature difference occurred over northern Lake Huron. In Node 2, events with relatively greater low-level convergence, relatively large water-air temperature difference, relatively large local 1000 mb wind speed in the 270-300 degrees sector, and relatively greater positive vorticity advection over northern Lake Huron, are sent right into Node 4. Cases in the remaining nodes are sent to the left or right based on a test of a single variable. The category 4 and 5 snow cases fall into Terminal Region 4 or 5 based on tests of 500 mb temperature, and 1000 mb wind speed and direction.

The learning sample data populations in the terminal regions allow a *statement of confidence* to be made about the classification forecast assigned to the node, and allow for less specific forecasts to be made. For example in Table 4, if the predictor values cause a case to fall down the tree into Terminal Region 4, a forecast of category 5 snow is made with 100% confidence for station 19. However, if the predictor values cause a case to fall down the tree into Terminal Region 11 we can make a forecast of "no snow" with 72% confidence, or "no more than 5 cm of snow" with 95% confidence, or "snowfall will not exceed 12.5 cm" with 100% confidence.

Table 5 shows the learning sample and cross-validation matrices which resulted from segregating the data for station 19 by the rules given in Table 4. Differences in the total number of cases in each category between Days 1 and 2 occurred since the number of days which qualified as LESP days varied due to differences between the NWP model forecasts of the synoptic scale flow for 0-24 hours and 24-48 hours for the same day. The fit of the data in the learning sample by CART shown in Table 5 appears to be very good, although the cross-validation matrices are less impressive but still reasonable. The category with the maximum number of cases in each predicted category matches the correct observed category in all the matrices with only one exception. The high degree of matching was typical for every station for as many categories as CART would fit, and is a desirable attribute.

Table 5: Learning sample and cross-validation sample classification matrices for Day 1 and Day 2 forecasts for station 19 (Paisley, Ontario).

Day 1

		Learning					Cross-Validation				
Observed Class --------->		1	2	3	4	5	1	2	3	4	5
Pre-	1	60	19	4	0	0	47	36	9	0	0
-dic-	2	22	82	14	3	1	28	57	24	11	1
-ted	3	2	2	31	0	1	11	12	17	10	1
	4	2	7	5	24	1	0	5	4	6	3
Class	5	0	0	0	0	5	0	0	0	0	3

Day 2

		Learning					Cross Validation				
Observed Class --------->		1	2	3	4	5	1	2	3	4	5
Pre-	1	81	13	2	0	0	55	24	6	2	0
-dic-	2	11	90	12	5	0	34	56	18	10	1
-ted	3	4	5	39	11	5	6	20	21	9	2
	4	0	0	2	10	0	1	6	8	5	2
Class	5	0	0	0	0	3	0	2	2	0	3

In the majority of cases CART found trees that classified most or all of the observed categories at each station, to or within 1 standard deviation of the lowest cross-validated relative cost. However, CART could not find low-cost trees for some stations which had one very dominant snow category (usually category 1). For these cases a "second attempt", based on an idea described in Burrows(1990) for improving predictand-predictor

fits by MDA, was tried in an effort to take advantage of non-linear predictand-predictor relationships that might be present. Ten predictors were chosen from node paths that classified data up to the maximum observed category in trees whose cost was too high (more than one standard deviation above the minimum cost, and often with a large number of nodes). Squares, cubes, natural logarithms, and cross products of the 10 predictors were added to the basic predictor set, then CART was re-run with the enhanced set of 204 predictors. The limit of 10 predictors was arbitrarily imposed to limit the number of predictors in the enhanced set. The result was substantially lowered misclassification rates for several stations.

5. RESULTS

a. Classification Trees

A summary of the results for Day 1 and Day 2 classification trees appears in Table 6. CART found trees which classified all the observed snowfall categories at 14 of the 28 stations (50%) for Day 1 forecasts and 9 of the 28 stations (32%) for Day 2 forecasts. Trees that classified to within 1 category of the maximum observed category were found at 26 of the 28 stations (93%) for Day 1 forecasts and 25 of the 28 stations (89%) for Day 2 forecasts. About 84% of the trees for Day 1 and Day 2 had cross-validated relative costs less than or equal to 1 (i.e. skill as good or better than climatology). This was accomplished with trees having 5-15 nodes at most stations, which is reasonably few. The cross-validated misclassification costs averaged .50 for both Day 1 and Day 2 forecasts, while the misclassification costs for the learning trees were .20 for Day 1 forecasts and .23 for Day 2 forecasts. (The cross-validation misclassification costs may seem high, but we should recall that cross-validation will *over-estimate the true cost* of using the trees with independent data because the auxiliary trees were grown with only 90% of the data. The true costs if the trees were applied to independent data will be somewhere between the cross-validation sample and learning sample misclassification rates, and hopefully are not too far off the latter). As expected, the node-splitting rule that gave the lowest misclassification costs for most stations was "ordered twoing" (32 of 56 trees).

Table 6: For each station (Stn) in Figure 2: maximum category observed (Cats Obsv); maximum number of snow categories classified by CART trees, to within 1 standard deviation of minimum cross-validated relative cost (Cats Fcst); cross-validated relative cost (CV Cost); misclassification costs of auxiliary trees grown from cross-validation samples (CV Miscl Cost) and from the full learning sample (Lrn Miscl Cost).

Day 1 (0-24 hours)

Stn	Cats Obsv	Cats Fcst	CV Cost	CV Miscl Cost	Lrn Miscl Cost
1	4	4	1.00	.55	.17
2	5	5	.88	.55	.11
3	3	3	1.07	.54	.14
4	5	4	.82	.50	.20
5	5	5	.83	.55	.14
6	5	4	.76	.48	.25
7	4	4	1.01	.48	.10
8	5	5	.93	.56	.20
9	5	5	.93	.54	.18
10	5	4	.90	.53	.17
11	5	5	1.02	.56	.25
12	5	4	1.03	.44	.26
13	4	3	.94	.41	.19
14	5	4	.83	.53	.28
15	5	4	.85	.52	.24

Day 2 (24-48 hours)

Stn	Cats Obsv	Cats Fcst	CV Cost	CV Miscl Cost	Lrn Miscl Cost
1	4	4	.86	.46	.09
2	5	4	.83	.53	.25
3	3	3	1.07	.44	.08
4	5	4	.99	.63	.33
5	5	5	.92	.61	.22
6	5	4	.85	.54	.20
7	4	4	.99	.50	.14
8	5	5	.83	.49	.24
9	5	4	1.00	.54	.28
10	5	4	.93	.52	.33
11	5	5	1.02	.55	.21
12	5	4	.90	.39	.15
13	4	3	1.03	.43	.16
14	5	4	.88	.56	.28
15	5	3	.83	.49	.28

Table 6 (contd):

Stn	Day 1 (0-24 hours) Cats Obsv	Cats Fcst	CV Cost	CV Mscl Cost	Lrn Mscl Cost	Stn	Day 2 (24-48 hours) Cats Obsv	Cats Fcst	CV Cost	CV Mscl Cost	Lrn Mscl Cost
16	5	4	.86	.53	.20	16	5	4	.92	.54	.18
17	5	5	.90	.53	.26	17	5	4	.86	.52	.34
18	4	4	.82	.51	.15	18	4	4	.86	.53	.15
19	5	5	.89	.55	.29	19	5	5	.83	.52	.24
20	5	4	.88	.46	.19	20	5	4	.91	.51	.28
21	4	4	.85	.42	.17	21	4	4	1.10	.53	.13
22	5	5	.97	.55	.17	22	5	4	.98	.56	.34
23	4	4	1.11	.40	.12	23	4	3	.94	.33	.14
24	5	4	.84	.46	.34	24	5	4	.97	.52	.30
25	4	3	1.00	.48	.23	25	4	3	.98	.47	.34
26	4	3	.79	.46	.13	26	4	3	.93	.54	.22
27	-	-	-	-	-	27	-	-	-	-	-
28	5	3	.87	.55	.08	28	5	3	.84	.44	.17
29	5	3	.97	.45	.26	29	5	3	.83	.37	.28

CART gives an ad-hoc ranking of variable importance on a scale of 0-100 after the trees are constructed. *Predictors related to low-level divergence were ranked among the most important predictors more frequently than any other types of predictors at nearly every station.* The location of the line or area of this divergence was frequently upstream from each station, although low-level divergence (convergence) in the vicinity of Lake Ontario *downstream from* stations over southern and central Lake Huron was important as well. The importance of low-level convergence lines to the movement and location of lake-*effect cloud bands was noted by* Peace and Sykes (1966) and recently by Murphy (1989). The next most frequently picked set of predictors were those measuring the degree of air-water temperature difference, which is well known to be the primary mechanism for formation of lake-effect cloud bands.

b. Areal consistency

Figure 5 shows the observed snowfalls and residuals (observed category minus forecast category) for Day 1 and 2 classifications for a period of heavy lake-effect snowfall (5-6 January 1988). For the residuals a "0" is a perfect result, and a "*" denotes a station where the local 850 wind direction was not off-water for at least 2 of the four 6-hour intervals in a 24-hour period (i.e. non-LESP day). There is a preponderance of "0's" and "+/- 1's" for all the residuals for both Day 1 and Day 2 classifications. Of course, no system is perfect so there are a few 2's and 3's (but no 4's). Overall, the CART classifications for individual LESP days preserved the areal patterns of snowfall rather well in both Day 1 and Day 2 forecasts, even though the classification trees were found separately for each station. There were many other examples which verified this.

6. CONCLUSIONS

The need for detailed forecast guidance and careful assessment of the particulars of the synoptic situation on LESP days is clear. Analysis of the occurrence of snow for a four-year period at 29 stations in the lee of Lake Huron and Georgian Bay on "lake-effect snow possible (LESP)" days suggests that snow occurrence and amounts for individual stations and small areas are likely to be over - forecast in public forecasts, even in the heart of the "snowbelt".

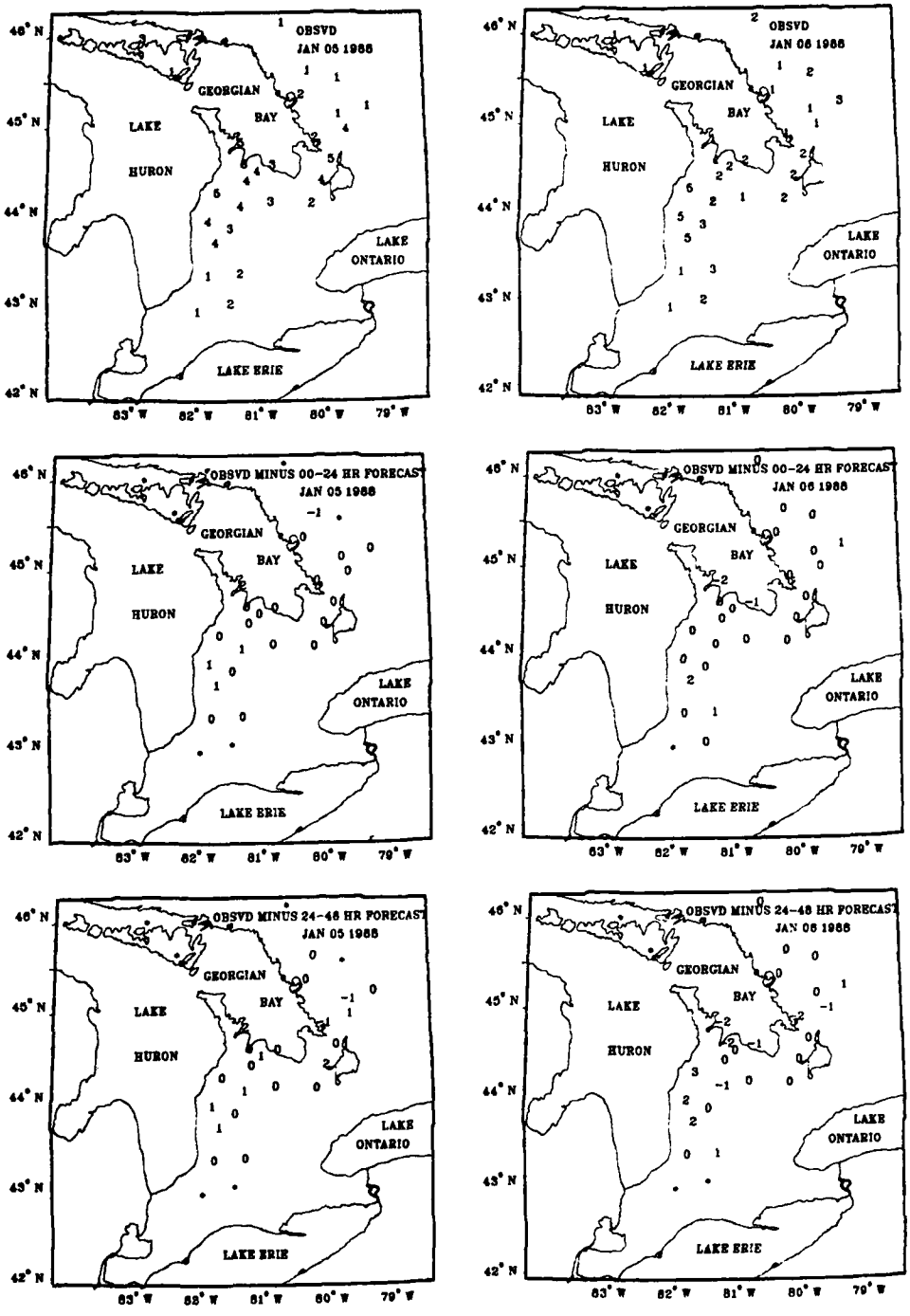

Figure 5: For 5-6 January 1988: Observed snow categories and difference between forecast and observed snow categories for Day 1 (00-24 hr) and Day 2 (24-48 hr) forecasts.

The classification-tree results show the CART-based MOS method outlined here has considerable promise for timely many-site production of useful, areally consistent objective operational mesoscale guidance for 1 and 2 day forecasts of 24-hour lake-effect snow amount. The trees had good skill for both 0-24 hour and 24-48 hour periods in classifying the category of snow occurrence at individual stations, given that a LESP day was expected. The node-splitting decision rules found by CART were in most cases easy to interpret physically and are a useful tool for insight into physical processes important in the formation and prediction of lake effect snow. Once obtained, the trees could be run on a local computer system to make forecasts if the required NWP data were communicated from a central mainframe computer. The trees are easy to use and could be portable to other NWP models by tuning predictor values from model output generated during a period of a few months when two model versions overlap.

An explanation of the CART method and its use here is given in Section 3. A parallel approach to an idea described in Burrows (1990) for including certain non-linear functions of important predictors into the predictor selection process was tried and resulted in significant reductions of misclassification rates for several stations.

Low-level divergence (convergence) induced by events in the upper air, usually located upstream and along lines or zones over the water, is the primary parameter controlling snow amount on days when lake-effect snow is possible.

ACKNOWLEDGEMENTS.

Comments on the manuscript by Dr. S. Venkatesh, Dr. M. Khandekar, and by anonymous reviewers with the Eastern Snow Conference are much appreciated.

REFERENCES

Braham, R.R., and Dungey, M.J., 1984: Quantitative estimates of the effect of Lake Michigan on snowfall. *J. Climate Appl. Meteor.* **23**: 939-949.

Breiman, L., Freidman, J.H., Olshen,R.A. and Stone, C.J., 1984: *Classification and Regression Trees*. Wadsworth & Brooks/Cole, Monterrey, 358pp.

Burrows, W.R., 1990: Tuned perfect prognosis forecasts of mesoscale snowfall for southern Ontario. *J. Geophys. Res.* **95**, No. D3: 2127-2141.

Crowe, R.B., 1985: Effect of carbon dioxide warming scenarios on total winter snowfall and length of winter snow season in southern Ontario, *Rep. 85-19*, p. 18, Can. Clim. Cent., Atmos Environ. Serv., Downsview, Ont., 1985.

Dewey, K.F., 1979a: Lake Erie induced mesosystems-an operational forecast model, *Mon. Wea. Rev.* **107**: 421-425.

----, 1979b: An objective forecast method developed for Lake Ontario induced snowfall systems. *J. Appl. Meteor.* **18**: 787-793.

Dockus, D.A., 1985: Lake-effect snow forecasting in the computer age. *Natl. Wea. Dig.* **10**: 5-19.

Glahn, H.R., and Lowry, D.A. 1972: The use of model output statistics (MOS) in objective weather forecasting. *J. Appl. Meteor.* **11**: 1203-1211.

Hjelmfelt, M.A., 1990: Numerical study of the influence of environmental conditions on lake-effect snowstorms over Lake Michigan. *Mon. Wea. Rev.* **118**: 138-150.

Lavoie, R.L., 1972: A mesoscale numerical model of lake-effect storms. *J. Atmos. Sci.* **29**: 1025-1040.

Murphy, B.P., 1989: Forecasting lake effect snow. Ontario Region Technical Note No. 89-7, Atmospheric Environment Service, Downsview, Ontario, Canada.

Niziol, T.A., 1987: Operational forecasting of lake effect snowfall in western and central New York. *Wea. and Forecasting* **2**: 310-321.

Peace, R.L., and Sykes, R.B., 1966: Mesoscale study of a lake effect snow storm. *Mon. Wea. Rev.* **94**: 495-507.

Saulesleja, A., 1986: *Great Lakes Climatological Atlas*. Environment Canada, Ottawa, 145pp. [Available through Canadian Government Publishing Center.]

Impacts of Heavy Snowfall During December 1989 in the Lake Erie Snowbelt

T.W. SCHMIDLIN

Department of Geography and Water Resources Research Institute
Kent State University
Kent, Ohio 44242, U.S.A.

ABSTRACT

December 1989 was the coldest December on record in the Lake Erie snowbelt. Snowfall totaled 100 to 200 cm, twice the average December snowfall. The snow had minimal impacts on schools districts. Over half (54%) of the districts had no closures due to snow but costs for snow removal increased for schools. Ski centers reported a 50% to 100% increase in revenues over December 1988 and the best December skiing in many years. Lake ports had higher operating costs and loss of shipments. Costs for snow and ice control on Interstate 90 in the snowbelt increased at least $1326/km over December 1988, but traffic flow was maintained. Person-hours spent on snow and ice control on I-90 increased 59%. An average of 111,000 kg/km (200 tons/mile) of salt and grit was spread on Interstate 90, an increase of 50,000 kg/km (89 tons/mile) over December 1988. Colleges, airports, and viticulture had only minor disruptions due to the snow.

INTRODUCTION

December 1989 was the coldest December of the century in the Great Lakes region (Climate Analysis Center, 1990). Unusually cold winter temperatures generally bring excessive snowfall to the snowbelts of the Great Lakes (Eichenlaub, 1970, Schmidlin, 1989). This pattern held in December 1989 as the persistent flow of arctic air across the lakes brought frequent lake-effect snowfall to the snowbelts. Numerous societal impacts of snowfall have been documented by others, but previous research focused on urban areas (Rooney, 1967; de Freitas, 1975). The goal of this research was to sample and describe the impacts of the heavy snow of December 1989 on human activities in the Lake Erie snowbelt.

THE REGIONAL SETTING

The Lake Erie snowbelt lies southeast of the lake from the eastern suburbs of Cleveland to the southern suburbs of Buffalo and extends about 80 km inland (Eichenlaub, 1970). Its boundaries are not firmly defined, but may be reasonably defined as that area with a mean annual snowfall of 200 cm (80 inches) or more (Figure 1). Lake effect snow occurs outside the snowbelt but mean snowfall is roughly doubled by the influence of the lake within the boundaries indicated (Eichenlaub, 1970; Changnon and Jones, 1972; Schmidlin, 1989). Average annual snowfall within the Lake Erie snowbelt is greatest, about 500 cm (200 in) on the highest ridges of western New York. Elevations within the snowbelt range from 175 m at the lake shore to 670 m on the highest ridges.

Contribution #9 of the Water Resources Research Institute

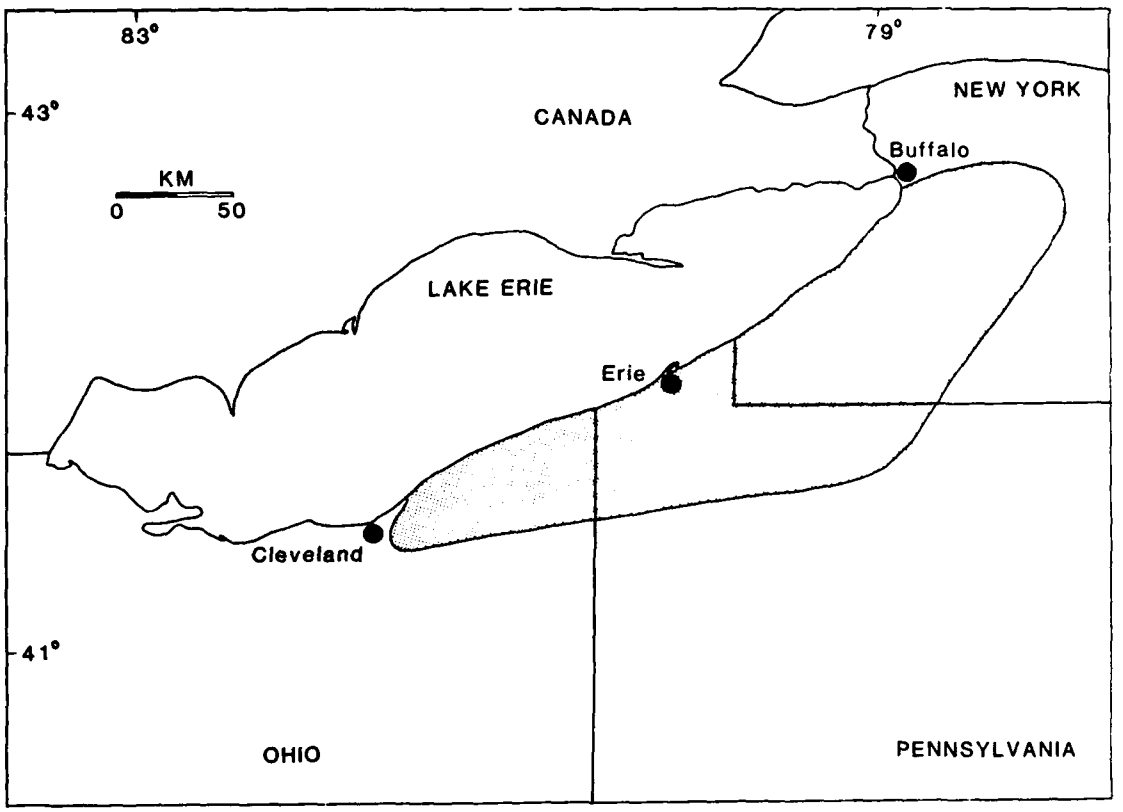

Figure 1. The Lake Erie snowbelt.

Population in the snowbelt is approximately 1.8 million. The major population centers are Erie, Pennsylvania (1987 metropolitan population 282,000), and portions of the Cleveland and Buffalo metropolitan areas. The flat land within 10 km of the lake shore forms a major agricultural, industrial, and transportation corridor with Interstate 90, U.S. Route 20, and rail lines parallel to the lake. Elsewhere, the landscape in the snowbelt is rolling to hilly with a patchwork of farms, forests, and numerous small communities. Drainage is primarily through small streams into Lake Erie but includes the upper portion of the Allegheny River which flows south into the Ohio River.

THE WEATHER OF DECEMBER 1989

Temperatures were below average nearly every day of the month and significant thawing did not occur until the last day of December (data are from NOAA/Climatological Data, by state). Overall, the average temperature for December 1989 in the Lake Erie snowbelt was about -9C (15.5F), which was 7C (13F) below the 1951-80 mean. Extreme minimum temperatures were in the -15C to -18C (5 to 0F) range along the lake shore but were colder than -25C inland from the lake (Figure 2). Minimum temperatures of -30C (-22F) in the Ohio portion of the snowbelt on December 24 were among the coldest December temperatures ever recorded in those regions.

Total snowfall for December 1989 was about twice the 1984-88 average. In general, the core of the snowbelt received 130-200 cm (50-80 in) of snowfall (Figure 3). The greatest total at an official station was 212 cm (83.5 in) at Sinclairville, New York. The National Weather Service at Erie, Pennsylvania, measured 170 cm (66.9 in) which was the greatest recorded for any month in over 100 years of record-keeping there. As is usual in lake-effect snowstorms, the snowfall pattern on individual days was very complex with snow squalls giving

30-40 cm in narrow bands 5-10 km wide. An example of this occurred on December 20 as an intense narrow band of snow developed over Erie County, Pennsylvania. This event gave 49 cm (19.2 in) of snow to Erie in 24 hours, including 30.5 cm (12 in) in 3 hours.

Measurable snow fell on 20 to 25 days during December 1989 in the snowbelt. The greatest amounts fell during the first and third weeks of the month. During the period December 15-22, snow totals ranged as high as 100 cm (40 in) at Sinclairville, New York, 78 cm (31 in) at Colden, New York, and 71 cm (28 in) at Chardon, Ohio. Depths reached 50-75 cm (20-30 in) across much of the region by Christmas. The depth of 99 cm (39 in) at Erie on December 21 exceeded the previous record depth of 76 cm measured in January 1985. Lake-effect snow is generally of low density. The 30.5 cm of snowfall measured at Erie in three hours on December 20 melted to only 0.66 cm of water to give a density of 0.022 g/cm3 and a snow/water depth ratio of 46:1. Snow/water ratios of 20:1 to 35:1 were common in daily snowfall. The 99 cm (39 in) deep snowpack at Erie on December 21 contained only 5 cm of water.

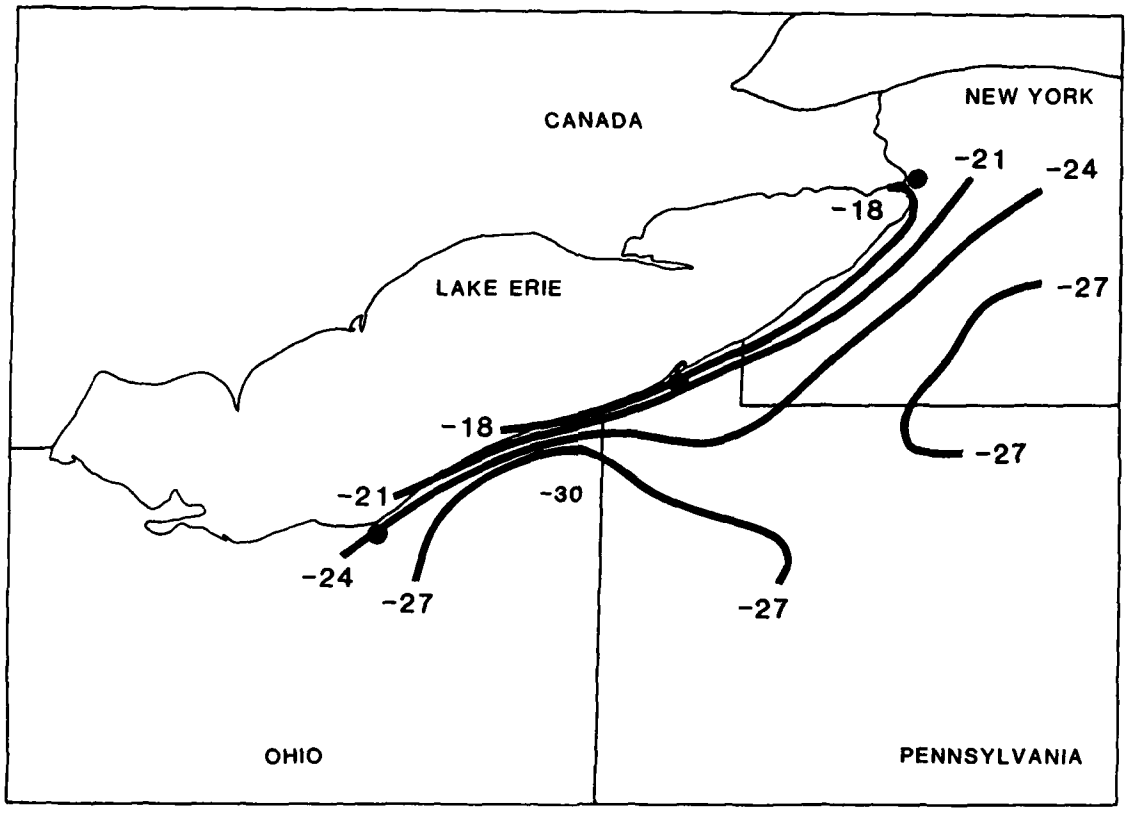

Figure 2. Minimum temperature (C) during December 1989.

IMPACTS ON THE REGION

Research on the impacts of heavy snow was completed primarily through surveys of affected segments of the society. Summaries are given below from surveys of school districts, colleges, ski centers, agriculture, lake ports, airports, highway departments, and retail outlets of winter goods. Other segments of society, such as health care, highway safety, general retail sales, and others, were undoubtedly affected but were not surveyed here.

School Districts

Surveys were sent to 52 school district superintendents in the Lake Erie snowbelt of Ohio, Pennsylvania, and New York. Replies were received from 39 (75%) districts. The last scheduled day of classes before Christmas break was December 20, 21, or 22 for 87% of the districts. Snowfall during December 1-22, 1989, accounted for about 90% of the monthly total in the snowbelt.

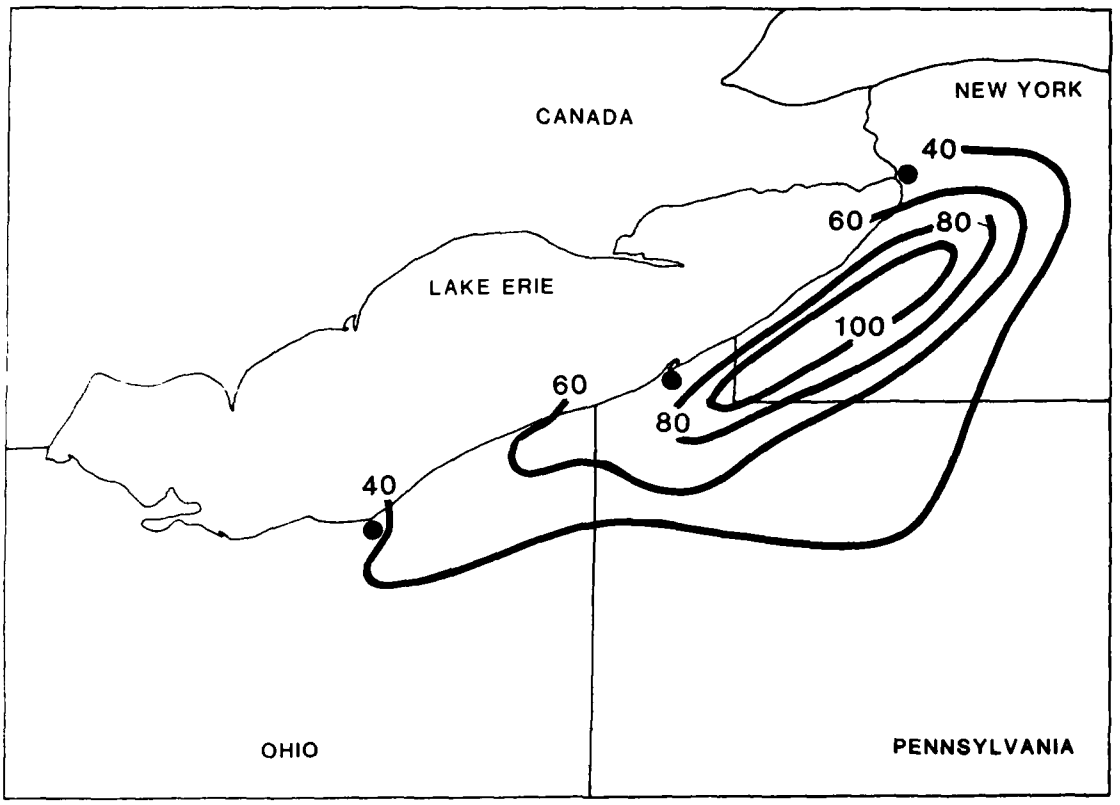

Figure 3a. Average December snowfall (cm) for 1984-88.

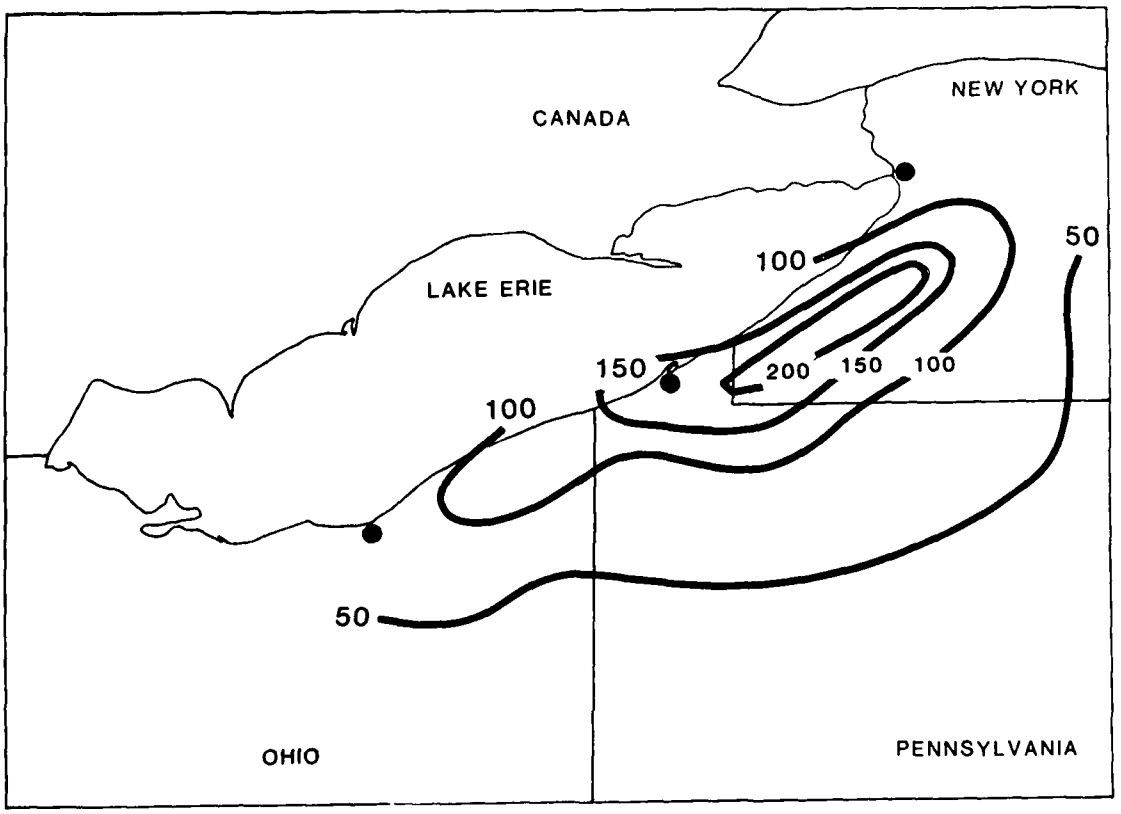

Figure 3b. Snowfall (cm) during December 1989.

Impacts of the unusually intense snow and cold on schools were minor. More than half of the districts (54%) reported no weather closures of schools during December 1989. Schools were closed for one day in 41% of the districts and for two days in 5% of the districts. More school districts reported closures in December 1989 than during December 1988 (46% vs. 10%) but most of the 1989 closures were for only one day and this represented only a minor disruption.

Snow removal operations proceeding normally in 59% of the districts. Of the districts reporting that unusual measures were taken for snow removal, most reported that extra equipment was required to remove the snow. Others reported that more overtime was paid to employees involved in snow removal and more sand and salt were used on parking lots and sidewalks. Several (18%) districts brought in heavy equipment, such as bulldozers and front-end loaders, to move snow when piles of snow prevented further plowing. Some of these services were provided by outside contractors.

The final question of the survey asked of any other impacts of the weather during December 1989 in the school district. Thirty-six percent indicated there were no other weather impacts in the district. However, 33% mentioned higher fuel costs to heat buildings and 23% noted the additional expenses for snow removal. Among the other impacts mentioned by school superintendents were:

a) the need to remove ice dams from eaves above building entrances.
b) cancellation of after-school sporting events
c) rescheduled Christmas concert
d) lower attendance due to snow and illnesses
e) weather-related distractions from school work were more numerous than usual
f) fewer absences in grades K-3, students were more focused on their studies.

One superintendent noted that school disruptions were minimal because most of the snow fell on weekends. Two other districts explained that their schools were prepared for heavy, frequent snow, since they are in the snowbelt. Another noted that the winter weather of December 1989 and other recent winters was not as bad as in the late 70's.

Colleges

There are no major universities within the Lake Erie snowbelt, as the snowbelt is defined here to exclude the cities of Cleveland and Buffalo. Three state universities or colleges with a total enrollment of 16,850 were surveyed - the State University of New York College at Fredonia (5400 students), Edinboro University of Pennsylvania (7500), and the Ashtabula Branch of Kent State University, Ohio (950). The last day of classes before the winter break was December 15 or 16 at all three.

There were no weather closures at these colleges except at the Ashtabula Branch of Kent State University where the campus was closed by snow on the last day of final exams. All students with exams on that day were given "incomplete" grades for those courses and the final exams were rescheduled. Other impacts at the campuses were minor and involved increased time and expenses for maintenance staff to remove snow and an increase in fuel used for heating buildings.

Ski Centers

Seven ski centers were surveyed - two in Ohio and five in the New York portions of the snowbelt. Not surprisingly, this segment of the economy profited from the cold, snowy weather. The seven ski centers averaged 29 days of skiing in December 1989, up from 21 days in December 1988, and four of the seven were open every day of the month. An increase in business over December 1988 was reported at all ski centers. One center reported that ticket sales exceeded any December in their 27 years of operation and revenues were up 110% over last year. In general, ticket sales and revenues were up 50% to 100% over 1988. The ski centers attributed the large increase in business to the weather and good snow conditions, rather than expansions or the general economy. Some reported the finest December skiing in years with excellent snowmaking conditions. One center noted that the weather of December 1989 allowed a deep base of snow to form which helped them survive the subsequent warm January. Several centers reported that bitterly cold weather and road closures hurt business on a few days.

Agriculture

Winter is a dormant period for agriculture in the Lake Erie snowbelt. However, grapes are grown on 15,000 ha (39,000 acres) of lake shore land in the snowbelt and this perennial vine is susceptible to winter cold damage. County extension agents indicated that winter damage was minimal. Snow cover is beneficial to the grapevine as an insulative cover from extreme winter cold. Minimum temperatures in the grape-growing areas were only -15C to -20C (5F to -4F), well above the critical winter temperature of -25C. Persistently cold temperatures during December allowed the vines to "harden" against the month's coldest temperatures on December 24.

Negative impacts of heavy snow reported from agricultural interests included a reduction in time available for winter pruning of grapevines and an increase in time spent on snow removal on farms. Three barns collapsed from the snow load in Erie County, Pennsylvania. Deep snow cover reduced freeze-up of rural pipes in the extreme cold temperatures.

Lake Ports

The combination of cold and snow affected operations at the Lake Erie ports. Ice covered western Lake Erie by mid-December and covered virtually the entire lake by December 25 (R.A. Assel, NOAA/GLERL, personal communication). This was about two weeks earlier than usual and obstructed shipping on Lake Erie and between Lake Erie and the upper lakes. Shipping schedules were uncertain so planning for port crews and facilities was difficult. At the Port of Conneaut, Ohio, the combination of cold and snow increased operating costs by 240%, increased mechanical failures by 310%, and caused 33% employee absenteeism. Ice-bonding agents, used to prevent freeze-up of port conveyor systems, were used extensively and conveyors were kept running continuously after mid-month to prevent freeze-up and start-up delays. The result was a 55% reduction in production levels. Approximately 500,000 gross tons of iron ore destined for the port of Ashtabula, Ohio, were not delivered during December due to ice conditions on Lake Erie.

Airports

Surveys were sent to seven airports and replies came from three. The largest, Erie International Airport where December 1989 snowfall totaled 170 cm, had 3258 take-offs and landings during Dedember 1989 with 25,611 commerical passengers. Monthly statistics on snow and ice removal costs are not kept by the Erie International Airport, but were reported to have been above average. The Erie Airport was closed occasionally by snow during December but for no longer than six hours. The number of take-offs and landings at Erie was down 7% compared to December 1988 but commercial passenger traffic was up 6%. The other airports surveyed were small county facilities. The Geauga County Airport (OH) reported one day with a closed runway due to poor braking conditions in snow and twice as much plowing as usual for December. Activities at the Corry-Lawrence Airport (PA) proceeded as usual for December and were not adversely affected by the weather.

Highway Maintenance

Frequent snowfall can have major impacts on highway travel and costs for snow removal. Costs of snow and ice control include labor, equipment, and materials applied (Cohen, 1981). Detailed summaries of impacts of December 1989 snowfall on maintenance of Interstate 90 were obtained from the offices of the Ohio Department of Transportation (ODOT) in Lake and Ashtabula Counties and from the Westfield Section of the New York State Thruway Authority in Chautaugua County. The ODOT offices are responsible for the maintenance of 90 km of Interstate 90, which runs along the Lake Erie shore in the snowbelt. The Westfield Section of the Thruway Authority maintains 45 km of Interstate 90 along the lake shore.

Interstate 90 was kept open in Lake, Ashtabula, and Chautaugua Counties throughout December. The count of 321,630 vehicles that crossed the Pennsylvania-New York border on I-90 during December 1989 was only 3.5% fewer than during December 1988. The cost of this effort was greater amounts of material spread on the highway, overtime paid to road maintenance crews, and more truck use for snow and ice removal (Table 1). The average of 111,000 kg/km (200 tons/mile) of salt ad grit spread on I-90 in the snow belt during December was 50,000 kg/km (89 tons/mile) greater than during December 1988. Using estimates of direct costs for wages and materials, the highway departments spent an

additional $1326/km on snow and ice control on I-90 in Lake, Ashtabula, and Chautauqua Counties during December 1989 compared to 1988. If this figure is extrapolated over the entire 280 km of I-90 in the snowbelt, an additional expense of $371,000 was incurred for snow and ice control on this highway during December 1989. This estimate is likely to be low because only direct costs were considered. Costs for increased equipment time on loaders in the maintenance yards and for repair of increased weathering of potholes and joint cracking were not considered in this analysis.

Retail Sales of Winter Goods

The least successful of the efforts to sample impacts of the December 1989 snowfall was a survey of retail outlets that specialize in winter goods. Of 34 surveys mailed to retail outlets dealing in ski equipment, hardware, snow removal, and snowmobile sales or repair, only 15% returned the survey. Thus, these results represent a very small sample of a large industry.

Replies came from three sporting goods stores and two hardware stores. An increase in sales of winter goods was reported from all respondents. The sporting goods stores reported a 15% to 65% increase in sales. A sporting goods store in a small town attributed their increase in sales to the fact that local residents were inhibited by snowy roads and did not drive to larger cities to make purchases. A hardware store reported a 20% increase in sales of snow-related equipment but decreased sales overall due to the frequent snowfall. Among items that sold well in hardware stores were snow shovels, snow blowers, sidewalk salt, and gutter heat tape (to prevent ice dams). One sporting goods store reportedly made extra efforts to remain open even in the worst weather because their skiing customers expected that service from a dealer of winter sporting goods.

CONCLUSIONS

This research sampled segments of society in the Lake Erie snowbelt that may have been affected by the unusually cold and snowy weather of December 1989. Snowfall totaled 100 to 200 cm, about twice the December average. School districts maintained nearly normal operations through the month although extra expenses were incurred for snow removal and heat and some after-school events were cancelled. Colleges and universities similarly maintained nearly normal operations. Downhill ski centers experienced the best December skiing conditions in many years and sales were 50% to 100% greater than the previous year. Skiing was available nearly every day during December 1989. Agricultural impacts were minimal due to the dormant nature of winter agriculture in the region and the protective properties of snow cover in vineyards. Ports on Lake Erie lost revenues and had increased equipment costs due to the frequent snow, severe cold, and early ice on Lake Erie. Interstate 90 had no closures but hours spent on snow and ice control increased 59% and the amount of salt and abrasives spread on the road increased 82% over December 1988.

Negative impacts of excessive snowfall in the lake Erie snowbelt were most evident in transportation industries. These impacts took the form of increased costs to prevent disruptions. Positive impacts were most evident in the skiing industry. From this study, it appears that many aspects of society, including schools and agriculture, had minimal impacts from the heavy snowfalls. Using Rooney's (1967) hierarchy of snow disruptions, many activities in Lake Erie snowbelt displayed third order (inconvenience) disruptions from the snowfall of December 1989. Previous research has shown that societies in the traditionally snowy climates, where significant snow is experienced each year, cope relatively well with snowstorms (Rooney, 1967, 1969). Snowfall with a low water content, as is typical of lake effect snow, is easier to cope with than heavy, dense snowfall (Rooney, 1967). The study of snow impacts on society presented here agrees with those earlier conclusions. Costs for coping with the greater snowfall of December 1989 in the Lake Erie snowbelt increased over recent years, but serious disruptions were minimal.

ACKNOWLEDGMENTS

Keith Eggleston, Northeast Regional Climate Center, Cornell University, supplied climatic data for New York and Pennsylvania. Steve McLaughlin provided snowfall data from the western New York snow spotters network. Costs of the survey were supported by the Department

of Geography at Kent State University. Appreciation is extended to the persons who took the time to return information on impacts to their facility. Cynthia Sitko assisted with this project as undergraduate research at Kent. Travel to the 47th Eastern Snow Conference was supported by the College of Arts and Sciences at Kent State University.

REFERENCES CITED

Changnon, Jr., S.A. and D.M.A. Jones. 1972. Review of the influences of the Great Lakes on weather. Water Resources Research 8:360-371.

Climate Analysis Center. 1990. Weekly Climate Bulletin. No. 90/02, January 13, 1990, National Weather Service/NOAA, Washington, DC.

Cohen, S.J. 1981. User oriented climatic information for planning a snow removal budget. Journal of Applied Meteorology 20:1420-1427.

de Freitas, C.R. 1975. Estimation of disruptive impact of snowfalls in urban areas. Journal of Applied Meteorology 14:1166-1173.

Eichenlaub, V.L. 1970. Lake effect snowfall to the lee of the Great Lakes: Its role in Michigan. Bulletin of the American Meteorological Society 51:403-412.

Rooney, Jr., J.F. 1967. The urban snow hazard in the United States. The Geographical Review 57:539-559.

Rooney, J. 1969. The economic and social implications of snow and ice. In Water, Earth, and Man, R.J. Chorley, ed., Methuen and Company, Ltd., London, p. 389-401.

Schmidlin, T.W. 1989. Climatic summary of snowfall and snow depth in the Ohio snowbelt at Chardon. The Ohio Journal of Science 89:101-108.

Table 1. Comparison of snow and ice control operations on I-90 in Lake and Ashtabula Counties, Ohio, and Chautauqua County, New York, during December 1988 and 1989. Numbers are combined for all three counties unless specified.

	December		
	1988	1989	Increase
Days working snow and ice control			
Lake County	17	26	53%
Ashtabula County	19	28	47%
Chautauqua County	10	22	120%
Regular person hours expended	2882	4738	64%
Overtime person hours expended	2822	4314	53%
Truck kilometers	95,918	149,944	56%
Materials			
Salt (kg)	5,278,622	8,493,842	61%
Ice grits (kg)	2,996,927	6,532,602	118%

Note: Ice grits are a mix of gravel, limestone, cinders, and other abrasives that are mixed with salt to provide traction. The use of ice grits is increasing due to environmental concerns over use of highway salt, abandonment of the "bare-pavement" policy on I-90 in Ohio, and the lower cost of ice grits compared to salt.

A Comparison of Great Lakes Winter Severity and Ice Cover Winter 1990 vs. the Historical Record

R.A. ASSEL AND D.C. NORTON

U.S. Department of Commerce
National Oceanic and Atmospheric Administration
Great Lakes Environmental Research Laboratory
2205 Commonwealth Boulevard
Ann Arbor, Michigan 48105-1593, U.S.A.

ABSTRACT

The large temperature anomaly reversal from December 1989 to January 1990 is described along with its associated impact on early winter snowfall and ice formation. Winter temperature severity is evaluated in terms of magnitude and date of occurrence of the annual maximal freezing degree-day accumulations at several locations on the perimeter of the Great Lakes. Winter severity from the turn of the century to the early 1980s is compared with the 1990 winter severity. The extent and date of occurrence of maximal ice cover for the 1990 winter is placed in a historical perspective by comparing it with the annual maximal ice covers of the preceding three decades.

INTRODUCTION

The winter of 1989-90 in the Great Lakes was notable because of severe temperatures in December followed by unusually mild temperatures in January and February. In this paper we present a descriptive analysis of this winter, early winter monthly air temperature and snowfall, results of a preliminary analysis of winter severity, and an analysis of the annual maximal ice cover on the Great Lakes. These contemporary values are compared with both short-term (28 year) and long-term (86 year and 93 year) variations to place the winter of 1990 in a historical perspective.

WINTER 1990 HIGHLIGHTS

December 1989 and January 1990 Air Temperature Anomalies

Winter 1990 (December to February) ranked as the 20th warmest and the 27th driest over the contiguous United States since 1895; it also had the coldest December and the warmest January of this century (Weekly Weather and Crop Bulletin 1990, vol.77,no.10). In this study, regional average temperature was defined using the stations given in Figure 1. Preliminary analysis of these temperatures shows that during winter 1990 the Great Lakes region experienced the largest reversal in regional December to January departure from monthly normal temperature over 92 previous winter seasons (Figure 2a). Regional December 1989 temperature (-10.5°C) was the lowest (Figure 2b) in the past 93 years, and January temperature (-2.0°C) was the third highest (Figure 2c) during the past 93 years.

Figure 1. Location map of snowfall stations and air temperature stations listed in Table 1 and Table 2

Ice Cover and the Great Lakes - St. Lawrence Seaway Navigation Season

The severe December temperature brought above-normal ice cover to the Great Lakes and severe ice conditions on the St. Lawrence Seaway (Climate Perspectives 1989, vol.11, no.'s 49, 51, 52a). The navigation lift locks at Sault Ste. Marie, Michigan closed on December 28 and the St. Lambert Lock on the St. Lawrence Seaway closed on December 22, 1989. Mild January and February temperatures resulted in below-normal ice covers on the southern portion of the Great Lakes. The St. Lawrence Seaway opened March 28, and ice cover was virtually gone from the southern portion of the Great Lakes by the end of March.

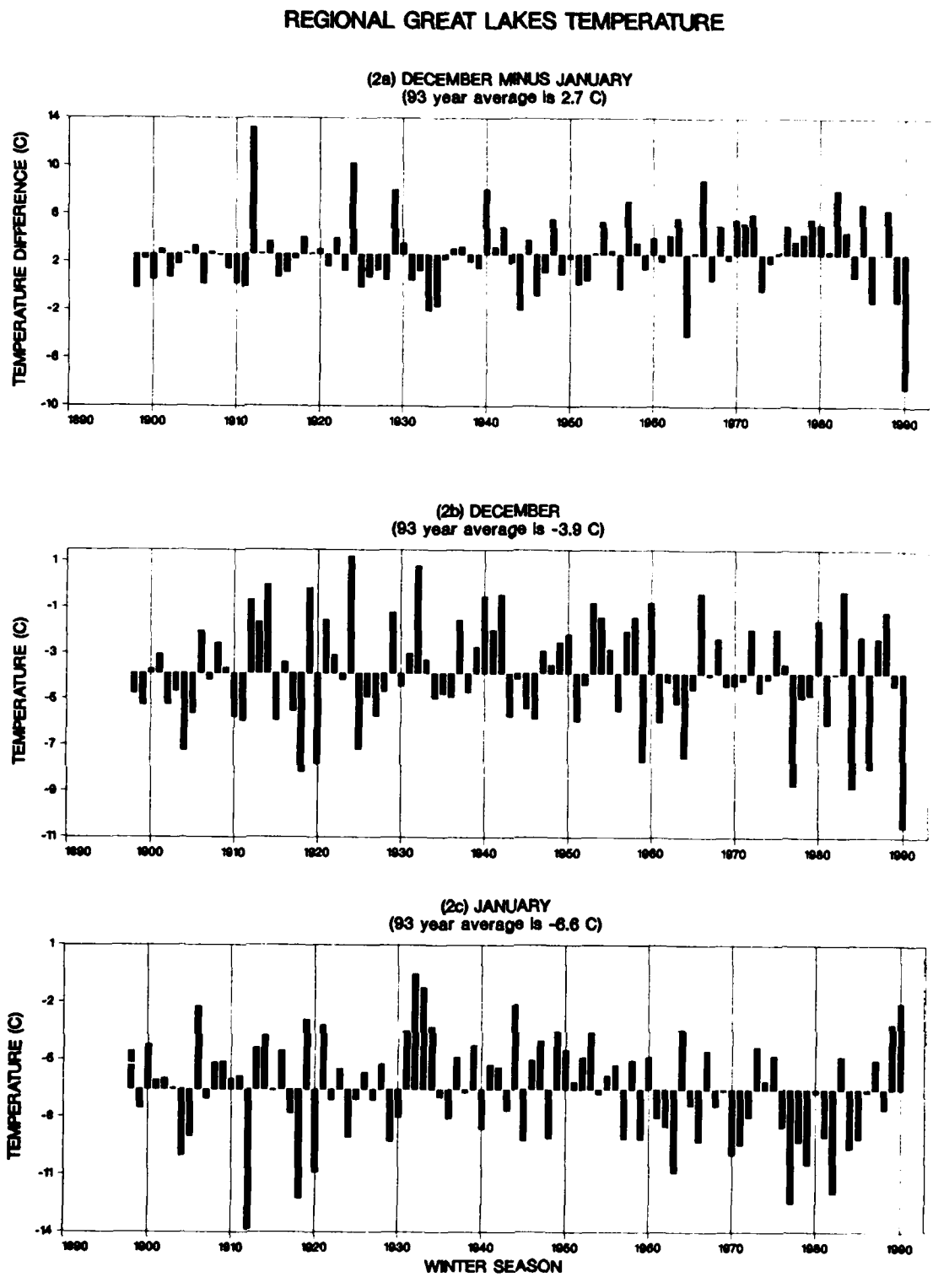

Figure 2. Regional Great Lakes temperature (°C) for the winter seasons 1898 to 1990 (a) December minus January difference, (b) December, and (c) January. Temperatures are plotted as bar graphs above or below the 93 year average.

Precipitation, Temperature, Lake Levels, and Flooding

The below average December 1989 air temperature also brought above average snowfall to the Great Lakes, particularly in the lake-effect regions along the south and east shores of Lakes Superior, Michigan, Erie, and Ontario (Table 1, Figures 3a - 3b). December 1983 regional temperature (-8.8°C) was the second lowest December temperature in the 93 year record, (Figure 2b) and lake-effect snowfall accumulations were also much above-normal (Figure 3c). Average January 1990 temperatures were above freezing in the southern portion of the Great Lakes, bringing rain and below average snowfall with large anomalies in the lake-effect snowfall regions in the Great Lakes (Figures 4a - 4b, Table 1). January 1989 regional temperature (-3.3°C) was second only to January 1990 in above-normal temperatures over the past 40 years. With the exception of Lake Superior where temperatures were 1.5°C to 2.5°C lower in January 1989 compared to January 1990, the January 1989 snowfall pattern over the Great Lakes south of Lake Superior was quite similar to January 1990 (Figure 4c). The large difference in the average rank of lake-effect stations (Table 1) from December 1989 to January 1990 is a measure of the influence of air temperature on snowfall in the shore zone of the Great Lakes. Note this influence is greatly attenuated by land along windward shores as evidenced by the much smaller difference between average rank of December and January snowfall. The mild January 1990 temperatures continued into February, resulting in periods of above freezing temperatures, rain, and snowfall across the southern Great Lakes Basin. Lake Erie had over 200 percent of normal precipitation in February (Weekly Weather and Crop Bulletin 1990, vol.77, no. 9). Notable storms occurred on February 3-4, 15-16, and 22-23. These storms brought freezing rain and snow causing hazardous traveling conditions and loss of electric power in some communities in the southern portion of the Great Lakes Basin (Climate Perspectives 1990, vol.12). The mild February temperatures also resulted in rising and above-normal lake levels for Lake Erie. Lake Erie levels normally decline in February to its minimal annual value (Figure 5). Temperatures were above-average for the third straight month in March, and precipitation was below-normal east of Lake Michigan (Weekly Weather and Crop Bulletin, 1990, vol.77, no. 14). Temperature anomalies of +15°F to +24°F (+8.3°C to +15.3°C) (Weekly Weather and Crop Bulletin, 1990 vol.77, no.11) occurred the week of March 11-17 resulting in rapid snow melt, rapid run-off, and flooding in some rivers and creeks (Climate Perspectives, 1990 vol.12, no.11) marking the end to one of the most atypical winters in decades.

Table 1. 1990 Monthly Snowfall Rank* For The 30 Winters from 1961 to 1990

Lake-Effect Shore	Dec. 89	Jan. 90	Windward Shore	Dec. 89	Jan. 90
Houghton, MI.	2	27	Duluth, MN.	18	27
Marquette, MI.	3	19	Thunder Bay, Ont.	16	10
Sault Ste. Marie, MI.	16	17	Green Bay, WI.	10	14
Traverse City, MI.	2	15	Milwuakee, WI.	21	8
Muskegon, MI.	2	30	Chigago, IL.	21	27
Cleveland, OH.	4	18	Alpena, MI.	3	8
Erie, PA.	1	23	Detroit, MI.	12	26
Buffalo, N.Y.	5	23	Toledo, OH.	21	28
Rochester, N.Y.	6	23	Toronto, Ont.	13	25
Oswego, N.Y.	1	23			
Average	4	22		16	19

* Rank 1 is the greatest monthly snowfall of the 30 winters, rank 30 is the least.

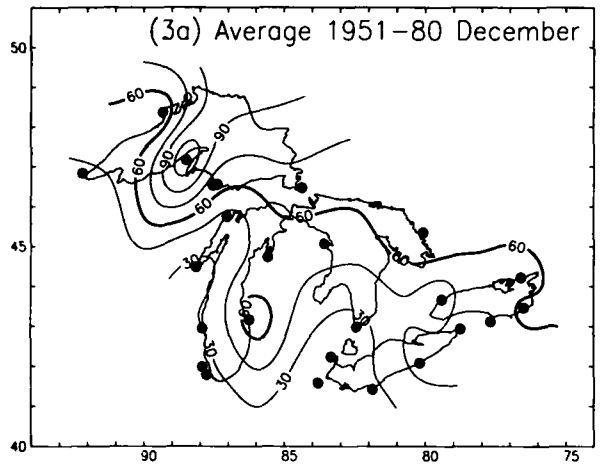

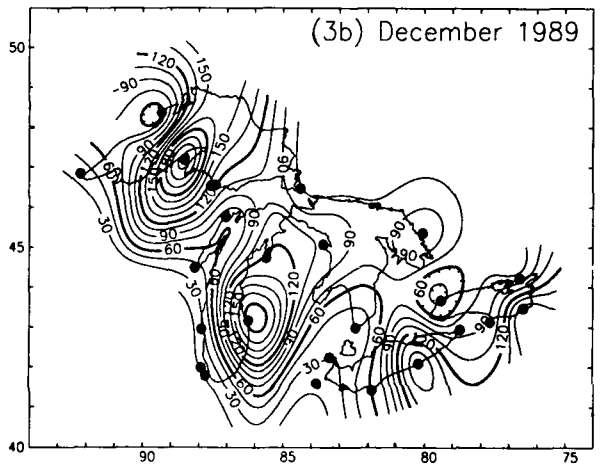

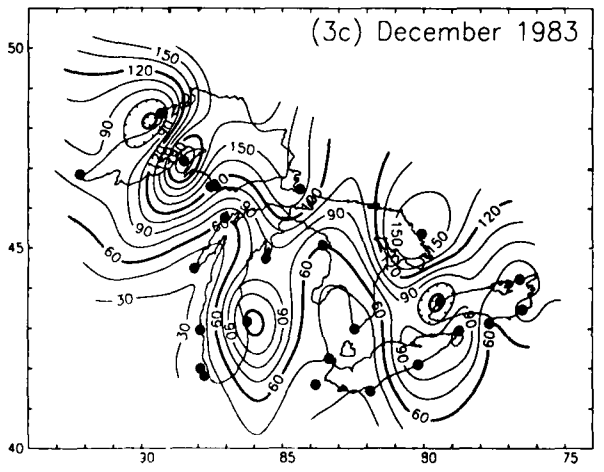

Figure 3. December snowfall (cm)
(a) 1951-80 Average, (b) December 1989,
(c) December 1983, contour interval
is 15 cm.

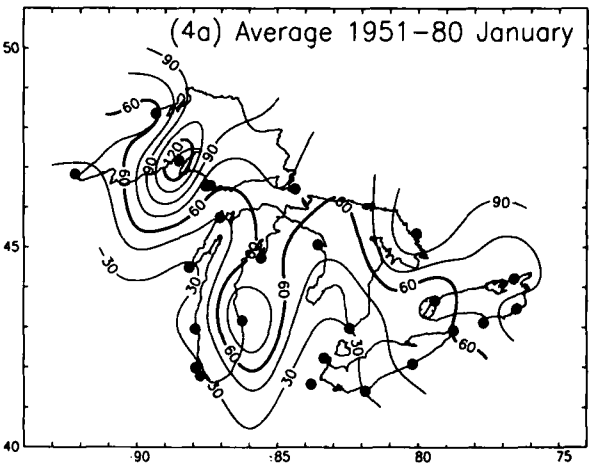

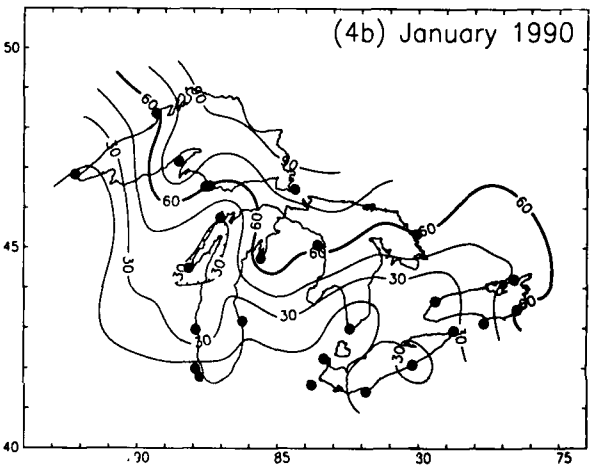

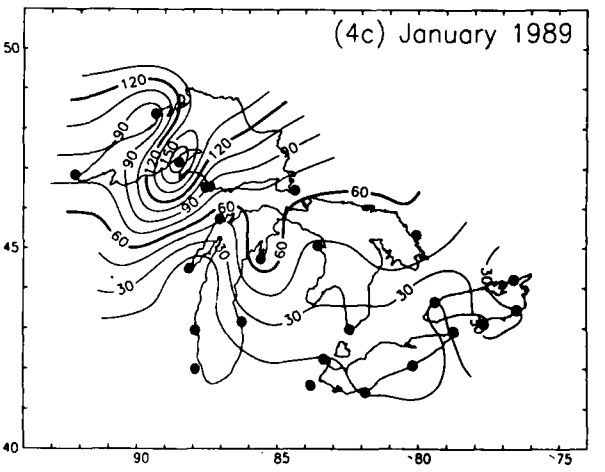

Figure 4. January snowfall (cm)
(a) 1951-80 Average, (b) January 1990
(c) January 1989, contour interval
is 15 cm.

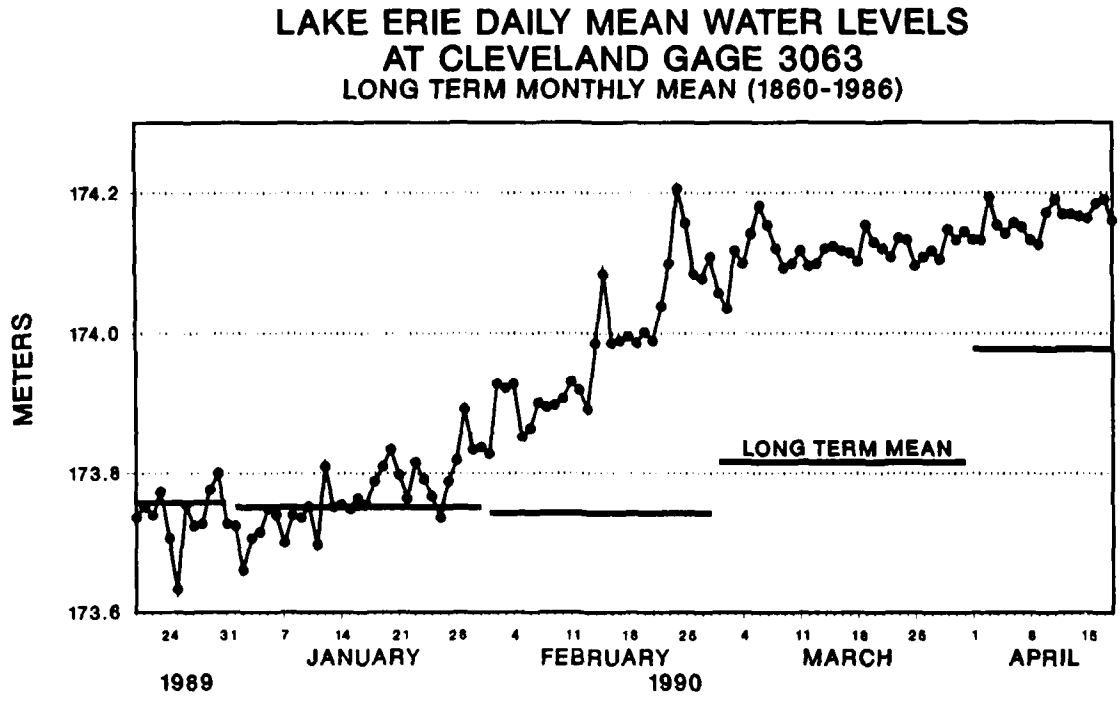

Figure 5. Lake Erie January to April 1990 daily mean water levels at Cleveland, Ohio and the long term monthly mean.

WINTER SEVERITY

Departure of the daily mean air temperature from 0°C is used to calculate freezing degree-days (FDD). If the daily mean air temperature is 3°C, then -3 FDD accumulate for that date; and if the daily mean air temperature is -3°C, then +3 FDD accumulate for that date. Assel (1980) calculated a running sum of daily accumulated FDD over a winter season starting in October and continuing to the end of April. If the running sum became negative it was reset to zero and a new running sum was started the next day. The running FDD sum usually reaches its maximum value (MFDD) in late winter or early spring and then declines as daily air temperatures rise above 0°C. The MFDD value is used as a measure of winter severity. Assel (1980) calculated MFDDs for 80 winters at 25 stations on the perimeter of the Great Lakes and used the MFDD to classify winter severity as normal, above-normal, or below-normal at each station for each of the 80 winters. If the MFDD was between the upper and lower 20 percent of the cumulative frequency distribution (cfd) of the 80 annual MFDD values, winter severity was normal. Winters with MFDD in the upper 20 percent of the cfd were classified as above-normal severity, and winters with MFDD in the lowest 20 percent of the cfd were classified as below-normal severity

In this study we calculated the MFDDs for 17 of Assel's (1983) original 25 Great Lakes stations for winter 1990 and ranked these MFDDs relative to a 86-winter base period (Table 2). Winter severity for 1990 is classified as normal at all but two Great Lakes stations. Milwaukee and Muskegon in the southern half of Lake Michigan had below-normal winter severity.

Table 2. Summary of MFDD - 86 winter average and 1990

Station	1990 MFDD	1990 RANK	86 WINTER AVE MFDD	DATE OF MFDD 1990	DATE OF MFDD 86 AVE
Lake Superior					
*Duluth, MN.	1214	52	1270	Apr 12	Apr 1
Thunder Bay, Ont.	1533	30	1429	Apr 1	Apr 5
Marquette, MI.	969	25	844	Apr 12	Mar 30
*Sault Ste. Marie, MI.	968	49	1013	Apr 7	Apr 2
Lake Michigan					
Green Bay, WI.	687	56	794	Mar 8	Mar 21
Escanaba, MI.	816	39	814	Mar 28	Mar 29
*Milwaukee, WI.	346	74	507	Mar 7	Mar 11
Chicago, IL.	258	54	351	Jan 1	Feb 28
Muskegon, MI.	257	70	378	Mar 8	Mar 12
Lake Huron					
*Alpena, MI.	688	37	675	Mar 8	Mar 26
Lakes Erie & St. Clair					
Detroit, MI.	246	64	328	Mar 7	Mar 7
Cleveland, OH.	227	46	254	Dec 28	Feb 24
*Toledo, OH.	263	49	320	Dec 30	Mar 1
*Buffalo, N.Y.	308	59	365	Mar 8	Mar 11
Lake Ontario					
Toronto, Ont.	511	21	403	Mar 11	Mar 12
*Rochester, N.Y.	331	49	370	Mar 10	Mar 11
Kingston, Ont.	718	33	677	Mar 9	Mar 21

rank = relative to 86 winters between 1897/98 - 1982/83
rank 1 = coldest rank 86 = warmest
winter severity classification:
rank 1 - 17 = above-normal severity
rank 18 - 69 = normal severity
rank 70 - 86 = below-normal severity
* Seasonal progression of daily FDD accumulations at these stations are portrayed in Figure 7. The daily FDDs given in Figure 7 are the average of Sault Ste. Marie and Duluth for Lake Superior and the average of Toledo and Buffalo for Lake Erie.

Winter 1990 was anomalous in terms of the seasonal progression of FDD accumulation because of the severe temperatures in December 1989 followed by the mild temperatures in January and February. These temperature anomalies produced much above-normal FDD accumulations in December and much below-normal FDD accumulations in January and February. Lake Erie and the southern portions of Lakes Michigan, Huron, and Ontario were virtually at their MFDD value by the end of December 1989, and FDD accumulations were in excess of 50 percent of their 1990 MFDD values at most other stations by the end of December 1989 (Figure 6). FDD accumulations actually decreased in January and part of February in the southern Great Lakes region due to above freezing air temperatures. A cold spell near the end of February and in early March resulted in the 1990 MFDD occurring near their long-term dates at most stations (Table 2). However, the much above-normal January and February temperatures at Chicago on the southern end of Lake Michigan and at Cleveland and Toledo along the southern shore of Lake Erie resulted in their MFDDs occurring in late December and early January, some two months earlier than the long-term average date.

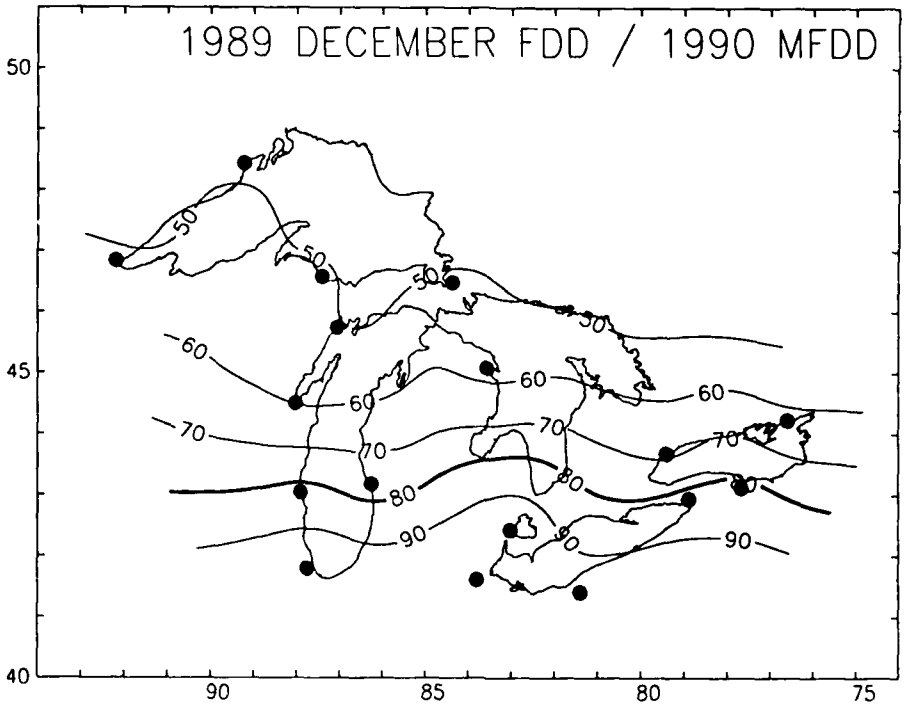

Figure 6. December 31, 1989 FDD accumulations expressed as a percentage of 1990 MFDD.

MAXIMAL ICE COVER CLIMATOLOGY - WINTERS 1963 TO 1990

Regular aerial ice reconnaissance observations of Great Lakes ice cover started in the early 1960s. The distribution of ice concentration and extent over the Great Lakes were recorded on lake outline base maps called ice charts. Source data for ice charts also included satellite imagery and side looking airborne radar imagery starting in the late 1960s and early 1970s respectively. The 28-winter average of the annual maximal ice cover and its variation are based on analysis of these historic ice charts. Annual maximal ice covers for the Great Lake were obtained from DeWitt et al., (1980) for winters 1963-1979 and from Assel (1986, 1987, 1989) for winters 1986, 1987, and 1980-82 respectively. Annual maximal ice cover was estimated for winters 1984, 1985, 1988, 1989, and 1990 using an electronic digitizer to measure ice concentrations from historic ice charts produced by the National Oceanic and Atmospheric Administration of the United States Department of Commerce and by the Ice Branch of Atmospheric Environment Service, Canada.

Winter 1990 Maximal Ice Cover

The seasonal progression of ice formation starts in the shallow bays and along the lake perimeter in December and January and progresses toward the deeper midlake areas in February and March. The maximal ice cover extent usually occurs in the last half of February or in early March (Assel et al., 1983). Winter 1990 maximal ice cover was within one standard deviation of the 28-winter average for all five Great Lakes (Table 3). Ice cover on Lakes Superior, Huron and Ontario was a little greater than the 28-winter average. Ice cover on Lakes Erie and Michigan was less than the average. This is in good agreement with winter severity which was milder on southern Lake Michigan and Lake Erie relative to its long-term average.

Table 3. Maximal Ice Cover on the Great Lakes

Lake	Percent Ice Sd.	Avg.	1990	Date of Maximal Sd.	Avg.	1990
Superior	25	69	75	14	Mar 1	Mar 5
Michigan	23	37	23	15	Feb 21	Dec 29, Jan 17-22, Mar 5-9
Huron	20	64	70	16	Feb 27	Mar 7
Erie	14	90	83	14	Feb 12	Dec 25, Jan 3, Mar 7-9
Ontario	19	25	26	13	Feb 23	Jan 17-22, Feb 4-7, Feb 26-Mar 9

Percent ice is the percentage of the total surface area of the lake covered with ice. Avg. is the 1963-1990 average of the maximal ice cover and Sd is the standard deviation of that average.

Date of 1990 Maximal Ice Cover

Maximal ice cover on Lakes Superior and Huron for 1990 occurred near the end of the first week in March, which is near the 28-winter average date. Lakes Erie, Michigan and Ontario were near their maximal ice cover several times during the winter (Table 3 and Figure 7), so it is difficult to say with certainty on which of these dates the actual date of maximal ice cover occurred. Lake Erie was near its maximal ice cover the last week in December, in early January, and near the end of the first week in March. Lake Michigan was near its maximal ice cover the end of December, in mid January and in early March. Lake Ontario was near its maximal ice cover during the third week of January, during the first week of February and from the end of February to March 9. These ice cover trends correspond to the 1990 anomalies in FDD accumulations. FDD accumulations were much above-average in early winter when they were near their MFDD value at the end of December for the southern Great Lakes. In January and part of February FDD accumulations on portions of the southern Great Lakes actually decreased (Figure 7), as did the ice covers on Lake Erie (starting in early January) and ice cover on Lakes Ontario and Michigan (in late January and again the second week of February). More seasonable temperatures from the last half of February to the first week of March brought both FDD and ice cover extent on the Great Lakes close to their seasonal maximal values.

Maximal Ice Cover - FDD Correlations

Previous studies have shown that ice formation and maximal ice cover on the Great Lakes is correlated with FDD (Richards 1963, Snider 1974, Rogers 1976). In this study a simple regression model was constructed where annual maximal ice cover was equal to MFDD times a coefficient. The model was calibrated using MFDD and maximal ice cover data for each of the Great Lakes over the 28-winters 1963 - 1990 (Table 4). The Lake Erie ice cover model was not as good as climatology, that is using the 28 winter average as a predictor of maximal ice cover, because of the low annual variation in maximal ice cover for that lake. The MFDD ice cover models showed modest improvement over climatology for the other four Great Lakes.

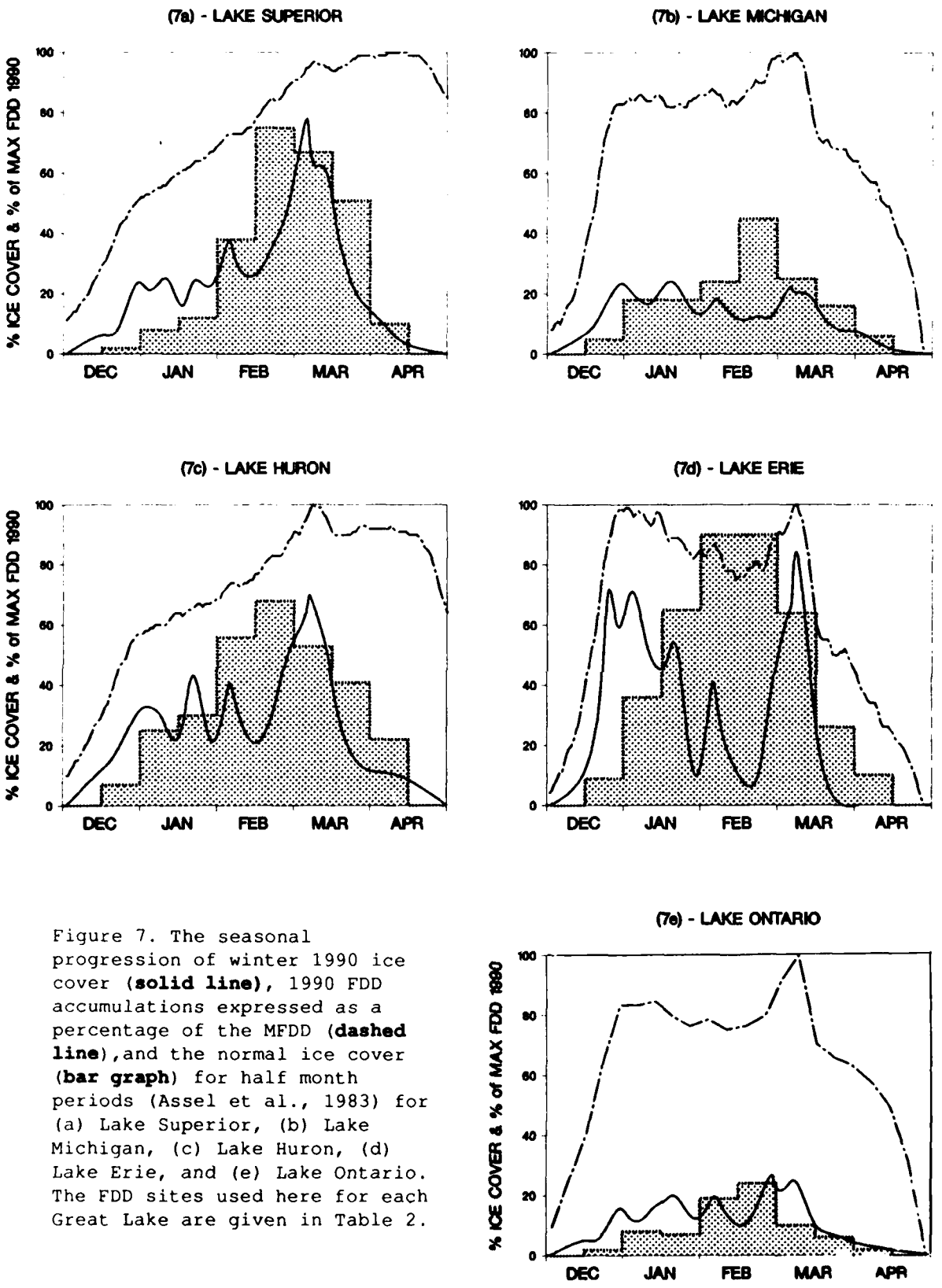

Figure 7. The seasonal progression of winter 1990 ice cover **(solid line)**, 1990 FDD accumulations expressed as a percentage of the MFDD **(dashed line)**, and the normal ice cover **(bar graph)** for half month periods (Assel et al., 1983) for (a) Lake Superior, (b) Lake Michigan, (c) Lake Huron, (d) Lake Erie, and (e) Lake Ontario. The FDD sites used here for each Great Lake are given in Table 2.

SUMMARY AND CONCLUSIONS

The 1990 winter was remarkable because of the large temperature anomaly reversal from December to January which was the largest reversal of its kind in the 93 year record. This large reversal in air temperatures and the above freezing average January temperatures in the southern portion of the Great Lakes Basin was reflected in much above-normal snowfall in December, much below-normal snowfall in January, and a virtual lack of lake-effect snowfall in January in the southern portion of the Great Lakes Basin. Mild temperatures continued into February, and several rain and freezing rain events occurred in the southern portion of the Great Lakes Basin. Record precipitation fell on the Lake Erie drainage Basin, reversing the normal seasonal decline of lake levels on that lake during February. December ice cover was much above-normal on the Great Lakes and the St. Lawrence Seaway. Lakes Erie, Michigan, and Ontario were near their seasonal maximal ice cover several times during the winter making it difficult to identify a single date of maximal ice cover. February ice cover on Lakes Erie, Michigan, and Ontario declined from their early season values at a time when they are usually increasing in extent. Lakes Huron and Superior reached their maximal extent near the end of the first week of March. Record breaking high temperatures near mid March brought rapid melting of snow cover, some flooding in the southern half of the Great Lakes and an end to one of the most unusual winter seasons in the past 30 years.

Table 4. MFDD ice cover model*

Lake	R^2	RMSE	Sd	C1
Superior	.93	19	25	.06024664
Michigan	.88	15	23	.06986341
Huron	.94	15	20	.08809692
Erie	.90	29	14	.20900114
Ontario	.76	16	19	.06993296

* ice cover = C1 x MFDD
R^2 = (correlation coefficient)^2
RMSE = root mean square error
Sd = standard deviation of observed ice cover

ACKNOWLEDGEMENT

Raymond Kelley of our staff digitized the ice cover charts for 1990 and provided the analysis of the water level data for Lake Erie. The National Weather Service provided advance copy of some of the snowfall, FDD, and air temperature data used in this report. The Navy/NOAA Joint Ice Center in Suitland, Maryland and the Ice Branch of the Atmospheric Environment Service in Ottawa, Canada provided the historic ice charts used in this analysis. This is GLERL Contribution number 707.

REFERENCES

Assel, R.A., 1980. Maximum freezing degree-days as a winter severity index for the Great Lakes, 1897-1977. Mon. Wea. Rev. 108(9)1440-1445.

Assel, R.A., 1983. Great Lakes degree-day and winter severity index update: 1897-1983. NOAA Data Report ERL GLERL-29. Great Lakes Environmental Research Laboratory, Ann Arbor, Michigan. 48105.

Assel, R.A., 1986. The winter of 1985-86. International Association for Great Lakes Research, Lakes Letter 17(2).

Assel, R.A., 1987. The winter of 1986-87. International Association for Great Lakes Research, Lakes Letter 18(2).

Assel, R.A., 1989. Impact of global warming on Great Lakes ice cycles, In: The Potential Effects of Global Climate Change on the United States, J.B. Smith and D.A. Tirpak, (Eds.), U.S. Environmental Protection Agency, EPA-230-05-89-051, Washington, D.C.

Assel, R.A., Quinn, F.H., Bolsenga, S., and Leshkevich, G.A., 1983. NOAA Great Lakes Ice Atlas. National Technical Information Service, Springfield, Virginia.

Climate Perspectives 1989. Canadian Climate Center, Atmospheric Environment Service, 4905 Dufferin St. Downsview, Ontario, Canada M3H 5T4.

Climate Perspectives 1990. Canadian Climate Center, Atmospheric Environment Service, 4905 Dufferin St. Downsview, Ontario, Canada M3H 5T4.

DeWitt, B.H., Kahlbaum, D.F., Baker, D.G., Wartha, J.H., Keyes, F.A., Boyce, D., Quinn, F.H., Assel, R.A., Baker-Blocker, A., Kurdziel, K.M., 1980. Summary of Great Lakes weather and ice conditions, winter 1978-79. NOAA Technical Memorandum ERL GLERL-31. National Technical Information Service, Springfield, Virginia

Richards, T.L., 1963. Meteorological factors affecting ice cover on the Great Lakes. Proceedings, Sixth Conf. on Great Lakes Res., Ann Arbor, Mich., Univ. of Michigan, Great Lakes Research Division, 204-215.

Rogers, J.C., 1976. Long-range forecasting of maximum ice extent of the Great Lakes. NOAA Technical Memorandum ERL GLERL-7. National Technical Information Service, Springfield, Virginia.

Snider, C.R., 1974. Great Lakes ice forecasting. NOAA Technical Memorandum NWS OSD 1, Ocean Services Division, Silver Springs, Maryland.

Weekly Weather and Crop Bulletin, 1990. NOAA/USDA Joint Agricultural Weather Facility, Room 5844 USDA South Building, Washington, D.C. 20250.

Use of Aeration to Prevent Ice Buildup at Gaging Station Controls

C.R. WAGNER

U.S. Geological Survey
Office of Surface Water
Stennis Space Center, Mississippi 39529, U.S.A.

ABSTRACT

The buildup of surface ice at gaging station controls distorts the stage-discharge relation and causes large uncertainties in the accuracy of stream-flow data. An effective means of reducing or eliminating ice cover at gaging station control structures would improve the reliability of winter discharge data.

The technique of bubbling air in the water beneath boats, docks, and locks to prevent ice buildup has been used successfully for many years. The U.S. Geological Survey implemented a pilot project to evaluate the effectiveness of this technique to maintain an ice-free environment at gaging station controls during the 1988-89 and 1989-90 winter seasons. Four sites having varying climatic conditions, control types, and stream widths were selected. Systems at two sites operated continuously and allowed only a minimal buildup of ice. At the other two sites, mechanical or operational problems resulted in several system failures. Experience gained during the first year improved second-year operation. Preliminary results indicate that this technique offers an effective way to prevent ice buildup at gaging station control structures.

Introduction

Many stream-gaging stations include a low-head concrete or sheet piling weir that serves as a control structure to create a stable stage-discharge relation. When ice forms on these man-made controls or on natural channel controls, the normal stage-discharge relation is disrupted, causing uncertainties in computation of actual flow. For many years it has been common practice to periodically remove ice buildup manually with ice chisels or similar tools. Once the ice is removed and flow conditions stabilize, the normal stage-discharge relation describes actual flow until new ice formation again disrupts normal relations. Manual ice removal may be required several times a week during winter periods. This process is inefficient and costly. A method that would prevent ice formation would be the best solution to this problem. Heaters enclosed above small artificial controls have been used with some success, but energy costs are high and many operational problems occur.

The technique of bubbling air into water beneath boats and docks to prevent ice formation has been used successfully for several decades. More recently the technique has been routinely used to prevent ice buildup at navigation locks.

The U.S. Geological Survey implemented a pilot project to evaluate the effectiveness of this system to maintain an ice-free environment at gaging-station controls during the 1988-89 and 1989-90 winter seasons. Four sites, three in New York and one in North Dakota, were selected for study.

Site Selection

The sites were selected to represent a variety of channel and control configurations as well as a range of climatic conditions. Electric power had to be available to operate the air pump.

FALL CREEK NEAR ITHACA, NY (STA. NO. 04234000)

This site is a long-term gaging station with a drainage area of 126 mi^2 (326 km^2) and winter flows in the range of 50 to 100 ft^3/s (1.4 to 2.8 m^3/s). The streambed is ledgerock with depths of 1 to 3 ft (0.3 to 1.0 m) for the reach several miles above the gage. The channel typically is completely ice covered. The creek receives little direct sunlight during the winter months. The gage shelter is on the left bank about 50 ft (15 m) upstream from the control, which is a concrete broad-crested weir 90 ft (27 m) long with a 1 ft (0.3 m) deep, 20 ft (6.1 m) long rectangular notch near the right end. The control is located at the head of a falls, where winter temperatures and the spray of water as it bounces over the ledgerock of the falls combine to gradually form an ice tunnel below the control. This formation normally builds until it finally meets the ice cover of the pool, causing siphonic action.

LITTLE TONAWANDA CREEK AT LINDEN, NY (STA. NO. 04216500)

This site is a long-term gaging station with a drainage area of 22.1 mi^2 (57.3 km^2) and winter flows in the range of 15 to 50 ft^3/s (0.4 to 1.4 m^3/s). The streambed is stable clay above the concrete control structure. The creek flows westerly and receives little direct sunlight during the winter months. The gage shelter is on the right bank about 10 ft (3 m) upstream from the bridge and control. The control is a partially reinforced concrete weir with a catenary-shaped crest and is located at the upstream side of the bridge. The downstream side of the control has about a 2 ft (0.6 m) vertical drop into a short sluiceway under the bridge then flows to a pool downstream. During the winter months the gage pool freezes over completely as does the pool downstream. Ice builds inward gradually until an ice tunnel is formed over the control, causing siphonic action.

MANOR KILL AT WEST CONESVILLE NEAR GILBOA, NY (STA. NO. 01350080)

This site is a relatively new gaging station with a drainage area of 32.4 mi^2 (45.9 km^2) and a winter flow in the range of 20 ft^3/s (0.6 m^3/s). The channel is shale-ledgerock and the stream flows in a westerly direction. The gage is located on the right bank about 20 ft (6 m) above a ledgerock control. The control is at the downstream end of a large natural pool with a smooth bedrock bottom. The control itself is about 15 ft (4.6 m) wide with 11 ft (3.4 m) of it forming a natural V-type notch 1 ft (0.3 m) deep at center.

HEART RIVER ABOVE LAKE TSCHIDA NEAR JUDSON, ND (STA. NO. 063445780)

This site is a new manometer-type gaging station with a sheet piling artificial control. The drainage area is 1,700 mi^2 (4400 km^2) and winter flows are in the range of 5 ft^3/s (0.4 m^3/s). The sheet piling control is about 30 ft (9 m) wide and forms a pool about 2 ft (0.6 m) deep. The distance from the lowest point of the piling to the downstream channel is about 1.5 ft (0.5 m). Since this is a new station, little was known about the freeze-up pattern, except that complete channel ice cover could be expected.

Equipment

An aeration system consists of an electrically driven air pump, mounted in the gage house, and a diffuser system to distribute the air and create bubbles on the streambed behind a control (Figure 1). The concept is that the bubbles will cause relatively warmer water from the streambed to rise to the surface. The warmer water and bubble-caused disturbance of the water surface will inhibit ice cover formation. Theoretically, the deeper the pool, the more warm water will be available and the more effective the system will be.

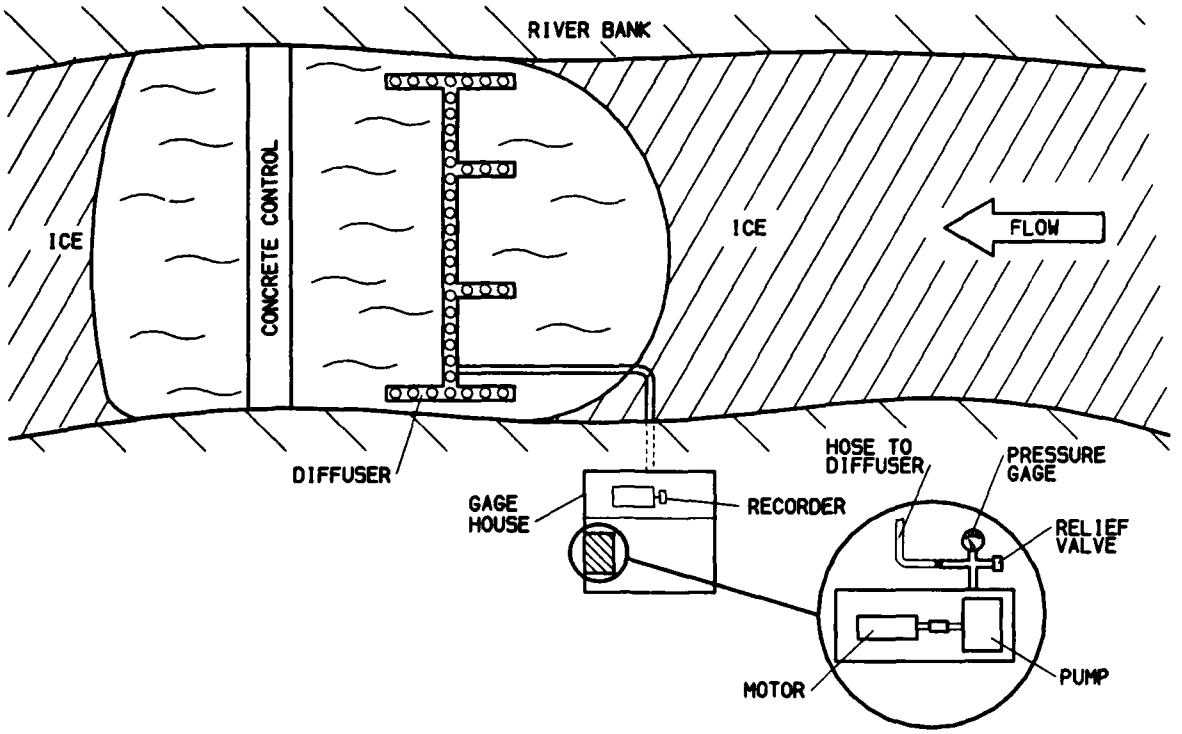

Figure 1.--Aeration System Diagram

The preferred air pump is a low pressure, high volume type with as few moving parts as possible to minimize wear during continuous operation. The pump selected was the AQUATHAW Model 500 Air Injection Pump[1] developed and sold by Hydro Aeration, Inc., of Cleveland, Ohio. This pump is powered by a 110 volt, 1/2 horsepower (370 W) electric meter. The pump, motor and controls are packaged in a weatherproof aluminum box. Diffusers were fabricated on site to fit individual channel configurations. The New York systems used 1 inch (25.4 mm) galvanized pipe with approximately thirty-five 1/16 inch (1.5 mm) holes spaced 1/2 ft (0.15 m) apart. The North Dakota system used copper pipe for the diffuser. The Fall Creek system had a single pipe installed perpendicular to the stream. The other systems had "fingers" at 90 degrees to the main pipe to distribute more air to the edges of the streams. The diffusers were held on the streambed by wedging them under large rocks or were held down with concrete-block weights. A variety of pipes and hoses were used to connect the pumps located in the gage houses to the instream diffuser. Inexpensive garden hose worked as well as anything else. Previous applications of this technology involved installations in still water, where bubbles move straight up. In the Survey's applications in moving water, a downstream velocity component requires that the diffuser systems are located upstream of the desired open-water area. Initial design of diffuser configuration and placement were engineering estimates.

Mr. Larry Frish, President of Hydro Aeration, Inc., has designed and installed many successful systems in marinas throughout the Great Lakes area. He took a very active interest in this project and provided a great deal of personal support, including several trips to New York to participate in the installation of the first site and several follow-up trips at no cost to the Survey.

[1]Use of brand names in this report is for identification purposes only and does not constitute endorsement by the U.S. Geological Survey.

Results

The four systems were carefully monitored and evaluated for performance of the system and effectiveness in preventing ice buildup. Two systems, those at Little Tonawanda Creek and Manor Kill, operated continuously through both winter periods and allowed only minimal buildup of ice. Reconfiguration of diffuser design might eliminate all ice buildup at these sites.

The Fall Creek and Heart River systems encountered several operational failures that caused the systems to shut down and thus allowed ice formation at times throughout the evaluation period. Once the air supply was cut off the systems froze and were difficult to reactivate. In one case the system wasn't activated early enough and was partially frozen, causing a pressure buildup that shut off the motor because of a thermal overload. The North Dakota site had a low-voltage power supply, which also caused thermal protection shutdown before a voltage-tolerant motor was installed. Pressure gages and pressure relief valves were determined to be essential in all future installations. Modifications to diffuser configuration and relocation in relation to the weir structure may be necessary to find the right combination at any specific site. The diffuser system at the Fall Creek site was washed away each year during spring breakup and high water. At the Heart River site, a bearing in the pump failed in the second winter.

Conclusions

The result of this pilot project indicates that this technique offers an effective and economical way to improve the accuracy of winter discharge data at many gaging stations. These systems will work best on small streams in areas of moderate winter temperatures. Stream width, velocity, and depth of water are critical factors, although these limits have not been quantitatively defined.

The Geological Survey has improved its knowledge of system design through experience with a variety of field conditions and can now design a system with a high probability of operational success. Future studies will be conducted to define operating limits of this technique.

Restigouche River Ice Project

S. BELTAOS

Rivers Branch
National Water Research Branch
Burlington, Ontario, Canada

B.C. BURRELL

Environmental Planning and Sciences Branch
New Brunswick Department of the Environment
Fredericton, New Brunswick, Canada

ABSTRACT

The Restigouche River, forming a portion of the boundary between the provinces of New Brunswick and Quebec, is a moderately steep river approximately 150 m wide. Hydrologic and climatic conditions often produce mechanical breakup events, typically in April as a result of rain and snowmelt, and this has resulted in severe ice jamming. In 1988, the National Water Research Institute and the New Brunswick Department of the Environment initiated a joint study of the ice breakup and jamming processes.

In this paper, an overview of ice jamming along the Restigouche River is presented based upon past records, physical evidence, and hydroclimatic considerations. Open water and ice season observations and measurements along a study reach of the Restigouche River from Wyer's Brook to Flatlands are described. Breakup and subsequent ice jamming observations during three winter seasons are reviewed, and the results of analysis applied to this data are briefly discussed.

INTRODUCTION

The Restigouche River Ice Project is a four year project that commenced during the 1987-1988 winter season. The primary objective is to gather information on the ice regime which could be used by researchers in understanding river ice processes, and/or in developing comprehensive river ice models or ice breakup models. The secondary objective is to document ice thicknesses, ice jamming and flooding within the Restigouche River Basin, thus increasing the amount of information currently available for future flood damage reduction efforts.

The Restigouche River was chosen primarily because of its winter ice regime. Breakup usually occurs during the spring as a result of an increase in flows due to a combination of rainfall and snowmelt. Mid-winter breakups are rare. Heavy ice runs and ice jamming are frequent occurrences along the Restigouche River and its tributaries. The size and slope of the river were also important considerations in its selection.

The Restigouche River Ice Project is a joint project of the National Water Research Institute (NWRI) of Environment Canada and the New Brunswick Department of the Environment (DOE), with assistance provided by the Water Survey of Canada (WSC).

Following descriptions of the basin and study reach, an overview of ice jamming along the Restigouche River is presented based upon documentation of past events, physical evidence, and hydrometric station chart analyses. The open water and ice season observations and measurements being carried out along a study reach of the Restigouche River from Wyer's Brook to Flatlands are briefly described. Investigations to date are then discussed and tentative conclusions drawn.

BASIN DESCRIPTION

The Restigouche River Basin (D.A. (drainage area) = 12,608 km^2) lies partly in New Brunswick and partly in the Province of Quebec (Figure 1). It is bordered on the south by the Miramichi and Saint John River basins, on the north by the St. Lawrence River basin, and on the east by tributaries to Chaleur Bay. The largest tributaries are the Kedgwick River (D.A. = 1585 km^2), Patapedia River (D.A. = 919 km^2), Matapedia River (D.A. = 2270 km^2), and the Upsalquitch River (D.A. = 3650 km^2).

Almost all of the Restigouche River drainage basin has exposed bedrock on the surface or is covered by less than about a metre of glacial till overburden. Gravel deposits are found in most of the major beds and valley floors within the region. (Montreal Engineering Company, Limited 1969).

The Restigouche River basin is nearly completely forested and forest harvesting is a major industry. The most populated portion of the Restigouche River basin is along the estuary from Tide Head to Dalhousie, and along the Matapedia River from Amqui to Matapedia. The remainder of the basin is sparsely inhabited.

The Restigouche River basin has a harsh winter climate with numerous storms and outbreaks of artic air. The normal monthly averages of mean daily temperature are below freezing for most of the basin during the months of November through March inclusive. January is normally the coldest month with mean daily temperature averaging around -13.5 °C. The range of temperatures for January is approximately - 45 °C to + 15 °C. The monthly averages of mean daily temperatures for February, March, and April are approximately -12, -6, and 1 °C respectively (Atmospheric Environment Service, 1984). Mean total annual snowfall ranges from 300 cm to 400 cm; with the average water content of the snowpack on March 31 ranging from 180 mm in the study area to 260 mm in the headwaters of Kedgwick River to the northwest and 240 mm in the headwaters of the Upsalquitch River to the southeast.

The Water Survey of Canada (WSC) operates and maintains three hydrometric stations in the New Brunswick portion of the Restigouche River basin. The furthest downstream of the stations is Restigouche River near Rafting Ground Brook (station no.: 01BJ007) with a drainage area of 7700 km^2. It is strategically located near the centre of the study area and thus is of prime importance to the entire project. At the start of the project, climatic instrumentation was established at this site. A gauging station also exists on the Upsalquitch River near Upsalquitch (station no. 01BE001) and on the Restigouche River above the Kedgwick River (station no. 01BC001).

The Ministere de l'environnement du Quebec operates two hydrometric stations on the Matapedia River : Matapedia (Rivière) Pres de Amqui (station no: 01BD008) and Matapedia (Rivière) en amont de la Riviere Assemetquagan (station no.: 01BD002).

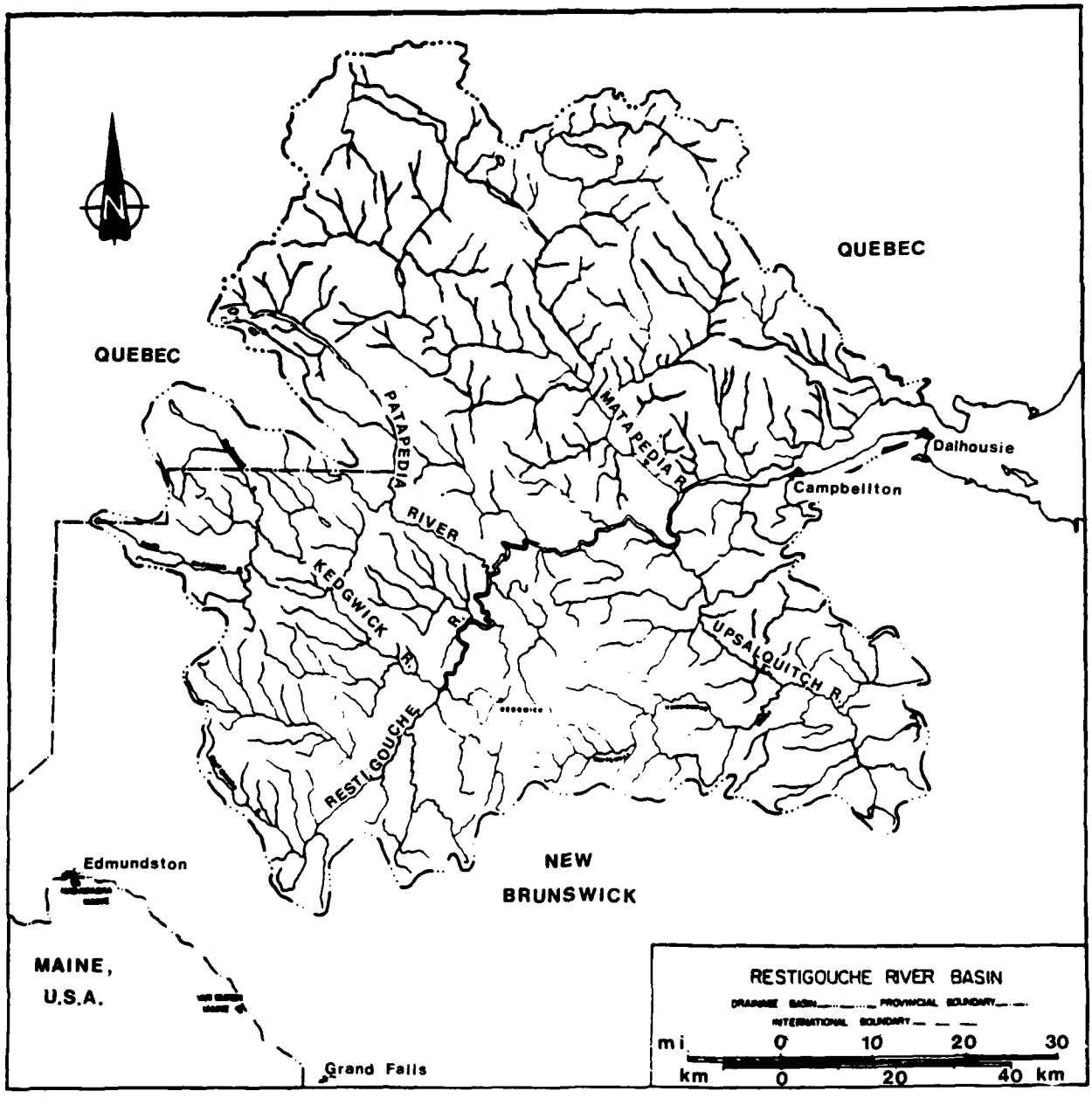

Figure 1 The Restigouche River Basin

THE STUDY REACH

The Study Area is the Restigouche River from Wyer's Brook to Tide Head, plus the lower reaches of two major tributaries, the Upsalquitch and Matapedia Rivers (Figure 2). Excellent ground access to the rivers is provided by riverside roads located on both or at least one of the banks. Auxiliary observations further up the Restigouche are carried out using fixed-wing aircraft.

Physical Description

The study reach from Wyer's Brook downstream to Matapedia is stable and mainly entrenched in bedrock. River widths average approximately 150 m. There is little opportunity for overbank storage for ice or water except for a short reach near Runnymede, Quebec.

Stream alluvial deposits exist along the Restigouche from Matapedia to Tide Head, and there are many islands in the river (which belong to New Brunswick). The river slope lessens from 0.8 m per km to approximately 0.4 m per km as the river winds its way pass these islands in small channels (Gidas 1979). The Restigouche River is tidal for approximately 40 km from Tide Head downstream to where it empties into the Bay of Chaleur (at Dalhousie).

Open-Water Hydraulics

From water surface elevation measurements and cross sectional profiles obtained during the ice-free period, the hydraulics of the river (near Rafting Ground) during open water periods were defined. The average slope in the reach has been determined as 0.82 m/km. The hydraulic resistance parameters for the river bed, n_b (Manning Coefficient) and K_b (equivalent sand-roughness height) decrease with increasing stage and only attain constant values when a stage of 2.50 m is exceeded. This trend is a common one in natural streams (Beltaos, 1987) and indicates that effects other than conventional boundary roughness and friction, are present. Such effects arise from the irregular planform and bottom geometry of natural streams. It is noted that the long-term mean discharge is 165 m^3/s for this site which translates to a gauge height of only 1.28 m. Most of the time, therefore, the flow takes place under conditions of varying apparent roughness (New Brunswick Department of the Environment and Environment Canada, 1990).

DOCUMENTATION OF PAST ICE JAMMING AND FLOODING

A brief review of some flood events are contained in reports by Kindervater (1985), Leger (1986), and in the notes of river observers. Past issues of local weekly newspapers (e.g. *The Campbellton Tribune*) were also reviewed for additional information on flood events during the past century. It can be ascertained from available documentation that at least 39 flood events have occurred within the Study Area during the past 100 years. Ice jamming was a contributing factor to 25 of these events. Ice jamming is thus a frequent occurrence with breakup ice jams creating the greatest flooding potential. Some of the more severe events have been along the Matapedia River, a tributary in the Province of Quebec, but there has been ice-related flooding at Wyer's Brook, Flatlands, and Tide Head in the New Brunswick portion of the basin; all within the study area. The 1974 event caused extreme flooding and resulted in recommendations for remedial measures to protect the community of Matapedia (Gidas, 1981).

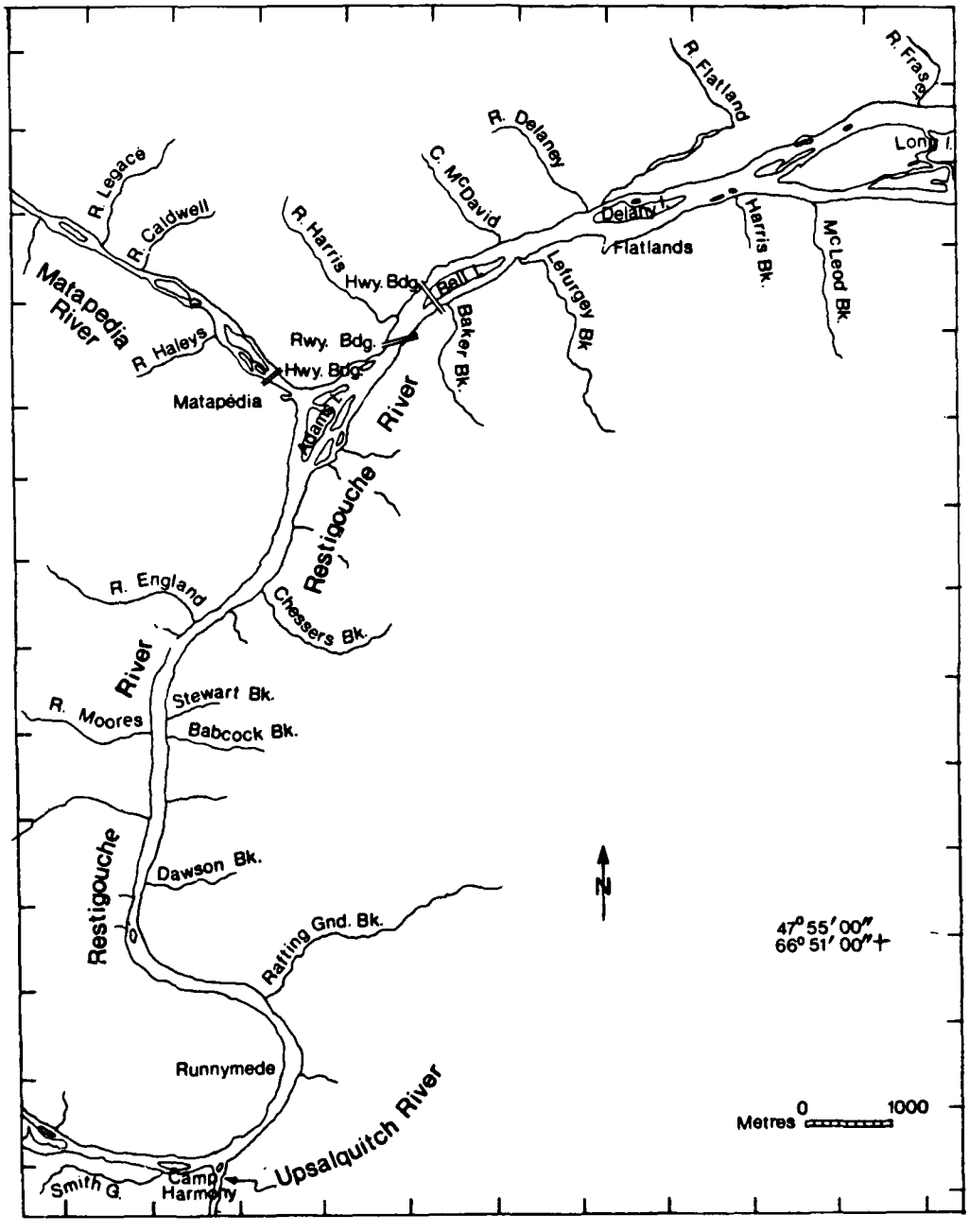

Figure 2 The Study Reach

HISTORIC FLOOD LEVEL PROFILE

An historic flood profile (Figure 3) for the Restigouche River from the Upsalquitch River confluence to Matapedia was determined based on a survey of the elevations of ice scars and known historic flood levels.

Over 100 scars were surveyed during a one week period along the Restigouche River from its confluence with the Upsalquitch River to Matapedia. The elevations of the top, centre and bottom of ice scars were recorded and their orientation to the river, width, height above ground level, apparent age, and distance along the river were noted. Most surveyed ice scars were along the true right (New Brunswick) bank, but some ice scars were surveyed along the left bank where accessibility on the Quebec side was better. If there had been additional time for this survey, then ice scars could have been surveyed along both banks for the entire river reach and ice scars dated by taking core samples.

Historic flood information from which elevations could be determined was limited and were based upon personal recollections or photographs. The photographs were primarily for Matapedia where no ice scars were surveyed.

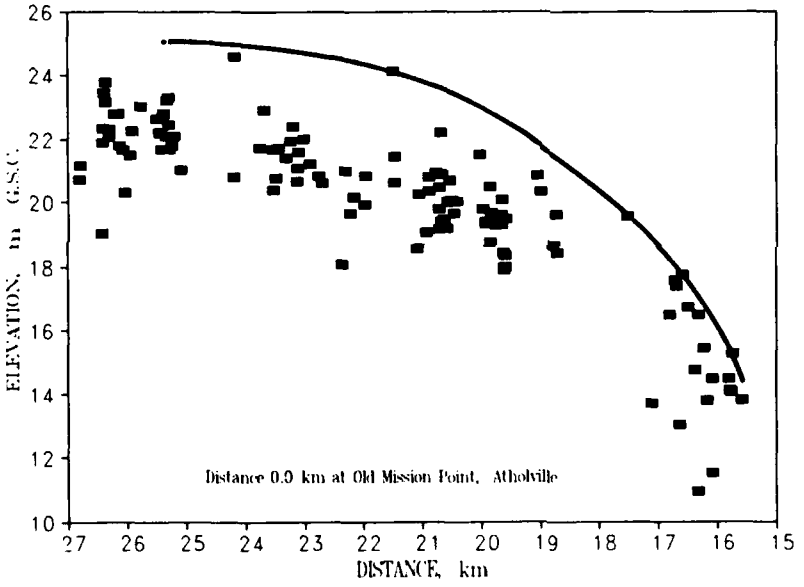

Figure 3 Historic Flood Profile

ANALYSIS OF ICE REGIME USING HYDROMETRIC STATION RECORDS

As background to the study, the Rafting Ground Brook gauge records (1968 to 1987), provided by the Water Survey of Canada (WSC) have been analyzed with regard to the processes occurring during the ice season.

Ice Regime

Typically, a stable ice cover forms in December, consisting of a slush accumulation 1 to 3 m thick. The initial ice cover is usually a thick accumulation of frazil slush (freeze-up jam). Solid ice grows downward into

the slush layer during the winter while the slush layer is being thermally eroded by the water flow under it. The solid ice thickness increases during the winter months, reaching a maximum of 50-80 cm at the end of March which is typically the time of the last winter measurement of discharge.

Figure 4 shows the growth of the solid ice cover as a function of the number of days (since freeze-up). The more conventional plot of solid ice cover thickness versus accumulated freezing degree-days also showed a relationship, but with more scatter than that of Figure 4. This graph can be used to estimate "end-of-winter" ice thicknesses just before thermal deterioration begins at which time the ice thickness should be a maximum.

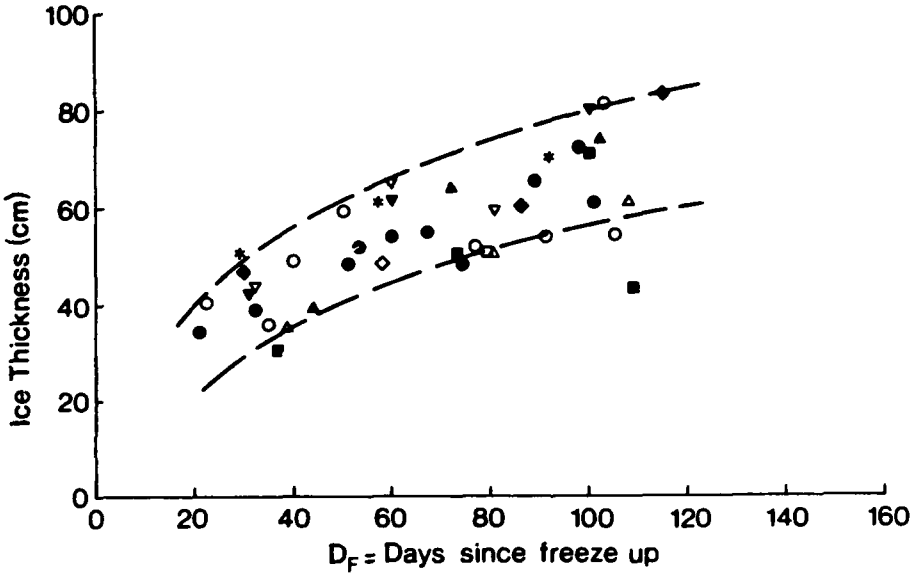

Figure 4 Solid Ice Cover Growth

The amount of slush present under the solid ice appears to remain unchanged during January but begins to melt away in February and even more so in March. Slush could be a significant factor in the breakup process. The slush, by absorbing the heat transferred from the flowing water under it, "shields" the solid ice cover and allows it to remain competent until the time of breakup. There should be very little slush left under the solid ice cover by the second half of April, the usual time of breakup.

Water level begins to rise toward the end of March, in response to a gradual rise in air temperatures and solar radiation fluxes which promotes melting. A rise in the river stage typically occurs in early April. If, at this time, no more runoff occurs, the ice cover will likely disintegrate in place. This is the thermal breakup, an event of no flooding potential that occurs in one out of three years. If, on the other hand, significant rainfall occurs at this time, a "mechanical" breakup takes place. This type of event occurs once in 4-5 years, and leads to major ice jams, thus having the greatest flooding potential. About one-half of the 18 events examined were

of a type intermediate between the thermal and mechanical breakup; they are triggered by moderate rain or by an ice run from the Upsalquitch River, a major tributary entering the Restigouche a few kilometres above the gauge site.

Breakup Prediction

Past work (Shulyakovskii, 1963; Beltaos, 1984) has empirically indicated that the local water level is often a good index of breakup initiation, defined as the time when the intact ice cover at a given site is first set in motion. The difference between the gauge height when breakup starts (H_B), and the gauge height representing the establishment of a stable ice cover during the preceding freeze up (H_F) is equal to the thickness of solid ice cover at the time of breakup initiation times a dimensionless coefficient. A more practical relationship can be deduced from a physically-based model (Beltaos, 1990):

$$X_B = KB(h_i)_o - (H_B - H_F) \qquad [1]$$

where X_B = function of thermal deterioration of the ice cover;
K_B = a coefficient;
$(h_i)_o$ = observed ice thickness near end of winter season prior to thermal deterioration; and
(H_B-H_F) = the difference in breakup and freeze-up water levels.

The right hand side of Eq. 1 can be evaluated using available data, by first determining H_F and H_B for each season which requires careful examination and interpretation of the gauge recorder chart. Next, the coefficient K_B is determined by consideration of the ratio $(H_B - H_F)/(h_i)_o$ for those breakup events deemed to approach a "premature" condition, i.e. minimal thermal decay of the ice cover ($S_T \approx 0$). For the present case, the data have indicated a value of 2.5 for K_B which is comparable to what has been found on several other rivers (Beltaos, 1990).

The left hand side of Eq. 1 describes such processes as ice melt and ice strength loss due to penetrating solar radiation (e.g. see Prowse *et al*, 1988). Such effects are not quantifiable at present but degree-days of thaw accumulated to the time of breakup initiation, $(S_T)_B$, seems to provide a satisfactory index. Figure 5 indicates a relationship between X_B and $(S_T)_B$. Thermal events are excluded as they represent disintegration of the ice cover rather than genuine breakup. A datum of -5°C has been used for temperature as suggested by Bilello (1980). However, there is considerable scatter which could be partly attributed to uncertainties in determining H_F and H_B as well as in selecting appropriate values for $(h_i)_o$. Because the breakup is usually preceded by a period of nearly constant stage, the scatter could limit its use in forecasting breakup as small errors in predicting H_B could result in large errors in predicting the timing of breakup. In such instances, it would be helpful to look at additional indicators of breakup, such as rainfall or arrival of an ice run from the Upsalquitch River. "Signs" of thermal breakup, as discussed earlier, should also be taken into account.

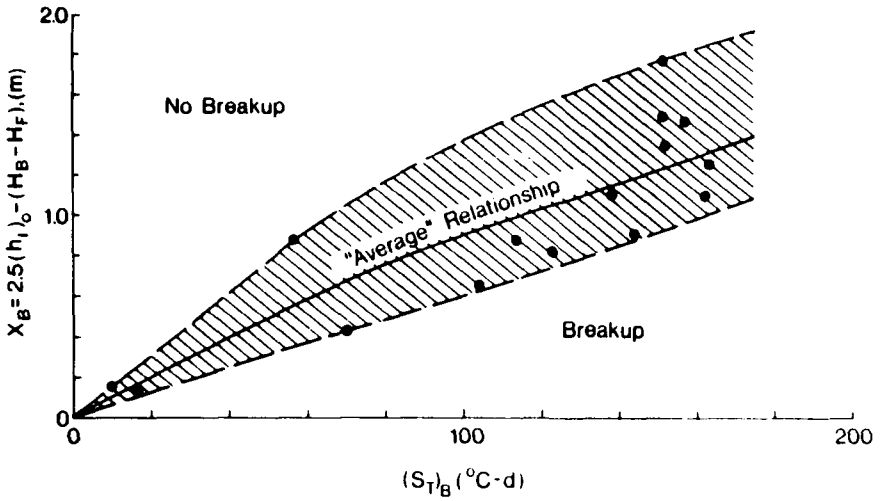

Figure 5 Breakup Forecasting Relationship

Ice Jam Levels

Factors affecting the occurence and severity of major ice jams include runoff, weather (particularly rainfall), ice thickness, the amount of accumulated slush, and snow cover conditions. Runoff, best represented by flow discharge, has a major influence on breakup flooding potential.

An upper envelope to peak breakup water levels can be calculated using the theory of "equilibrium, wide-channel" jams, as outlined by Beltaos (1983). The resulting stage-discharge curve is plotted in Figure 6 along with observed peak breakup (and peak freeze-up) levels. The data points closest to the ice-jam curve may be considered to have been caused by equilibrium jams near the gauge site while those points further removed (but still well above the "sheet-ice" curve) were probably caused by non-equilibrium jams or jams that formed far downstream of the gauge site. Those points close to the "sheet-ice" curve most likely reflect conditions of thermal breakup characterized by negligible, if any, jamming. The "sheet-ice" curve was generated by assuming sheet-ice cover of thickness 0.55 m and Manning roughness coefficient of 0.02; values deemed representative of breakup conditions. Freeze-up peaks also fall between the sheet-ice and ice-jam curves but occupy the low discharge range due to the generally low flow prevailing at the time of freeze up. The theory of "equilibrium, wide-channel" jams is seen to provide a good upper envelope to the data points, but this is all it can accomplish in this case where nothing is known about the location, extent and duration of the various ice jams that may have been responsible for the observed peaks.

The theoretically calculated jam thickness, t, is also shown in Figure 6 beside corresponding points on the ice-jam curve. There are no measurement data on the thickness of breakup jams but measured slush deposits are comparable to predicted deposits. The deviation of the data points in Figure 6 from the ice-jam curve is likely related to the mechanical competence of the ice cover. Examination of antecedent data revealed a trend for the deviation to decrease with increasing ice thickness (being of the factors defining ice competence) but there was considerable scatter. Attempts to reduce this scatter by introducing additional parameters, such as degree-days of thaw and thickness of the frazil slush deposit, were not successful.

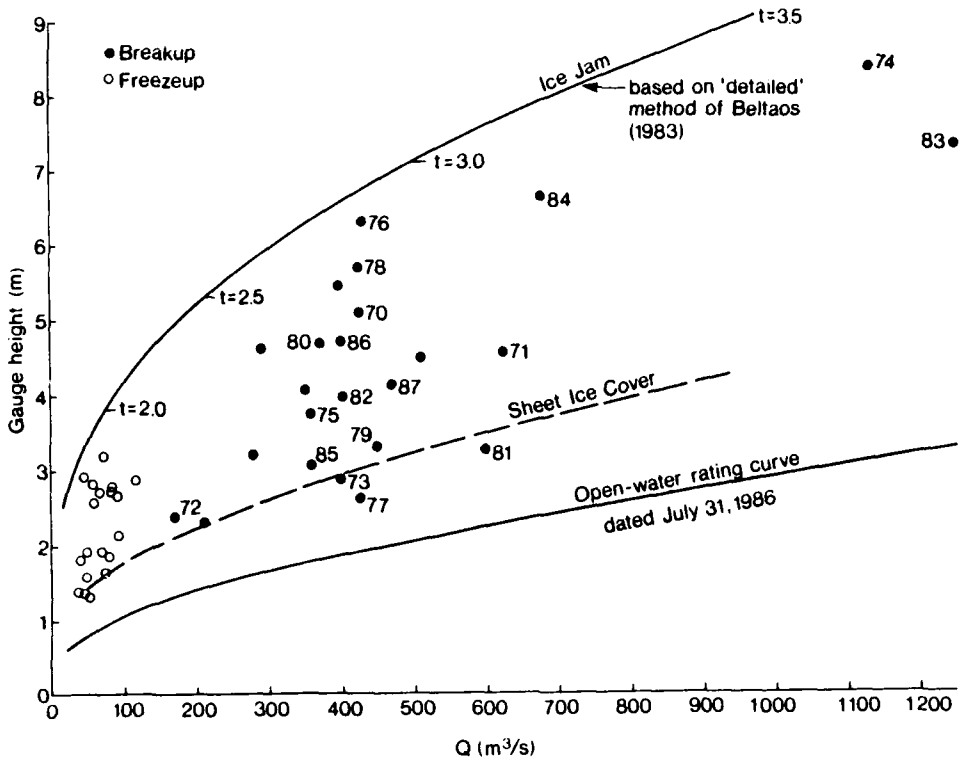

Figure 6 Effect on Discharge on Peak Breakup Water Levels

FIELD PROGRAM

The field program for a river ice investigation requires careful planning including consideration of information requirements and safety. Recent publications on river ice discuss data collection in more detail (IAHR 1986; Prowse, 1985).

Several tasks are undertaken during periods when the river is free of ice. These include the installation of temporary bench marks, the surveying of cross-sectional and longitudinal channel profiles, investigations of bed material, and levelling of ice scars and historic flood levels. These tasks are essential to the investigation and cannot be adequately and safely performed during the winter season.

During the winter period, ice thickness measurements at the hydrometric site are obtained when the WSC staff performed their winter discharge measurements. Additional ice thickness measurements are obtained by project staff at other sites. Particular attention was paid during the last winter to the thickness of slush under the solid ice cover.

As breakup approaches and until it ends, visual observations of the ice cover are carried out with increasing frequency. The size and position of major cracks, the raising of the ice cover from the shore open leads, and the presence meltwater are noted.

Particular attention is paid to ice jams which form after breakup is initiated. The head (upstream limit) and toe (downstream limit) of ice jams, and whether the jam completely or partially blocks the entire width of the channel, is determined. The surface conditions along the jam is described, and when possible, the reason why the downstream movement of ice becomes halted is identified. This could be an obstruction to ice passage (eg. an island), a competent downstream ice sheet, or bridging of ice floes across the channel.

The water level throughout the length of an ice jam and particularly near the toe, is valuable information. A series of water level points can be surveyed while the ice jam was still in place or less accurately later from photographs of the water surface near the river bank.

Following release of an ice jam, shear wall heights are measured to get an indication of ice jam thickness. Stranded ice floes provide an indication of breakup ice thickness and degree of thermal deterioration that has taken place since the end of winter.

OBSERVED BREAKUP EVENTS

April 3-11, 1988

The 1988 breakup event was the "mechanical" type notable for a long and persistent jam that formed in the study reach. It was triggered on April 4 by an ice run in the Upsalquitch.

Early on the morning of April 5, the road to Wyer's Brook was underwater as the Restigouche River from Camp Harmony to Rafting Ground Brook was jammed with ice which ran from the Upsalquitch River during the night. A shorter jam was present on the Upsalquitch River, held in place by the broken ice in the Restigouche River. By mid-afternoon, the jam in the Restigouche River extended from Wyer's Brook to Runnymede. At approximately 1650 hours, the ice pushed downstream.

For a few kilometres downstream of the moving rubble, the ice sheet was also in motion though its speed declined in the downstream direction. The movement of the ice sheet produced large pressure ridges.

By 1715 hours, all ice movement had ceased. The toe of the new jam (line separating ice rubble from the ice sheet - not always well defined) was below Grog Island at a location upstream of Babcock Brook. Ice and water went over the Restigouche River Road and the road to the Quebec community of Runnymede was also covered with ice and water. Sheet ice with pressure ridges existed for 1.5 km downstream. The ridging of the ice cover immediately downstream of the ice jam was most noticeable. Further downstream, the ice cover remained intact. During the night a lead developed at the toe and gradually expanded until it brought about the release of the jam approximately 3 days later.

At approximately 0730 hours on April 7, ice started to move at Wyer's Brook and some of it was going under the broken ice cover. The jam thus became two jams: one at Wyer's Brook and one downstream of Grog Island.

At 0945 hours on April 9, the downstream jam released followed by the upstream jam at 1430. The passage of broken ice was uneventful.

Shear wall heights of 3 m to 6 m were measured after the jam released, the larger values occurring where the toe had been. Together with water level profiles obtained while the jam was in place (Figure 7) and cross-sectional surveys, the jam configuration near the toe was re-constructed, as illustrated in Figure 8. Noteworthy is the extensive grounding of the jam at this location, a feature that has some interesting implications with regard to flow through the voids of the jam and the associated prediction of the local jam profile (Beltaos and Burrell, 1990).

April 10-21, 1989

The 1989 breakup represents an event intermediate between a mechanical breakup and a mature thermal decay breakup.

Ice on the Upsalquitch River had started to lift and run in places by the morning of April 10. Along the Restigouche River, there were areas where ice had started to break up including at the mouth of the Upsalquitch River where the river was clear of ice approximately 365 m downstream. There was an ice jam containing ice that had run from the Upsalquitch River downstream to Runnymede Lodge near the mouth of Rafting Ground Brook held by an intact downstream ice sheet.

The Upsalquitch River was free of ice on April 15. By late afternoon on the 15th, the toe (downstream end) of an ice jam on the Restigouche River was approximately 1.0 km downstream of Rafting Ground Brook where the ice had stopped against portions of a solid ice cover.

By the morning of April 18, the ice jam had moved downstream into the reach near the confluence of Chessers Brook and was 1.7 km long. A water surface profile near the toe of the ice jam was surveyed. The jam subsequently released and re-formed a couple of times on its way seaward. Significant thermal effects were manifested in the short lengths of the 1989 jams, indicating considerable melting.

April 1990 Breakup

The 1990 breakup event was a "mature" thermal breakup with only minor ice accumulations forming.

By mid-March, leads had already appeared in the ice covers of both the Restigouche and the Upsalquitch Rivers. By April 17, the latter river was completely open while the Restigouche had large open sections and leads downstream of the confluence. Reconnaissance flights over the Restigouche on April 19 and 20 reveal that the ice cover upstream remained largely intact for approximately 50 km, owing to very low runoff. The same was true of the Matapedia River. In both cases, the ice cover was still grounded near the banks and over shallows which illustrated the significance of the freeze-up level in the initiation of breakup.

The upstream ice in the Restigouche ran on April 22, causing a minor jam in the right channel of Long Island. The jam remained in place long enough to permit a water level survey near the toe. Shear wall heights, measured on April 23, were between 0.5 and 1.8 m with the larger value occurring near the toe. Following intermittent jamming and releasing on April 22 and 23, the Matapedia River finally ran into the Restigouche at 2100, April 23.

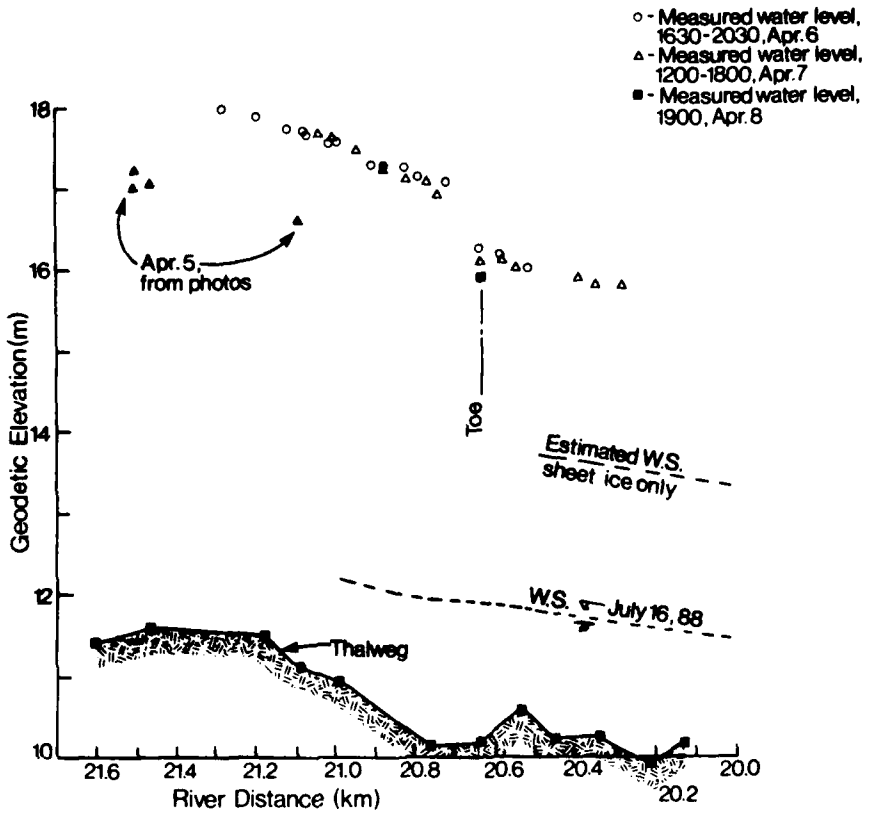

Figure 7 1988 Ice Jam Water Surface Profiles

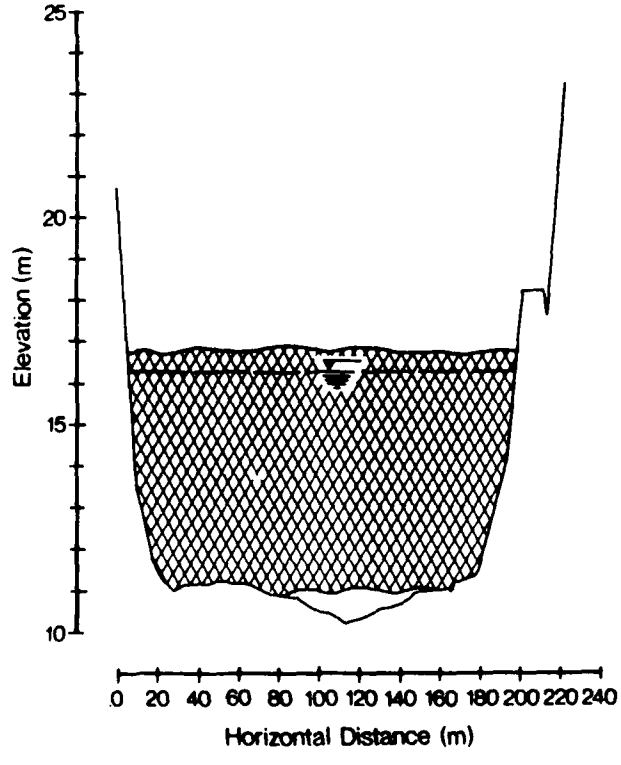

Figure 8 Cross Section of 1988 Ice Jam near Toe

Discussion

From the three years of observed data, it appears that the Upsalquitch is the first major tributary to lose its cover which causes the Restigouche downstream of the confluence to "open-up", either mechanically or thermally (or both). The ice in the upstream reaches of the Restigouche may or may not run at this time. The longer the delay, the lower are the chances of major jamming and flooding in the study reach. The Matapedia River seems to keep its ice cover much longer than the Upsalquitch and when it "runs" there seems to be plenty of open water downstream to receive the ice without major accumulations. Given the well-known variability of breakup events from year to year, these results should be considered tentative and subject to verification or modification based on additional observations in the future.

Grounding of ice jams is possible near the toe, a condition that is only beginning to be documented. More data of this kind are needed in order to fully understand and quantify toe conditions and, thence, learn more about the formation and release of ice jams.

SUMMARY AND CONCLUSIONS

A study of ice breakup and jamming processes in the Restigouche River, New Brunswick, has been described. Now in its third year, it consists of historical flood data collection and evaluation of flood levels; assessment of the ice regime using past hydrometric records; and field observations and measurements of ice breakup and jamming events, along with supplementary surveys (eg. ice thicknesses, cross-sections, river slopes, bed material).

Climatic conditions are such that only one breakup occurs each year. The channel width and slope are partly responsible for severe ice jams during "mechanical" events which are triggered by significant rainfall and occur once in 4-5 years. Using hydrometric records, approximate breakup forecasting methods have been developed.

In situ observations during 1988-1990 indicate that the Upsalquitch River, a major tributary, loses its ice cover first, causing the Restigouche to open-up downstream of the confluence. The movement and arrival of ice from upstream can aggravate the ice-jamming situation if it follows shortly after, as happened in 1988. Measurements indicate that severe grounding of ice jams can occur near the toe, a condition that has often been mentioned but not quantitatively documented before.

ACKNOWLEDGEMENTS

The authors thank the technical and support staff of NWRI and NBDOE for their contributions to this project. Special thanks are given to W. Moody, Senior Technologist with NWRI, who conducted the hydraulic surveys following breakup. Gratitude is also expressed for the specialized weather forecasts and climatological information provided by D. Comeau and W. Waite of NBDOE.

Dr. Dale Bray, Professor of Civil Engineering at the University of New Brunswick, is thanked for his comments on channel morphology and bed material.

REFERENCES

Atmospheric Environment Service. 1984. Climatic Normals. 1951 - 1980.

Beltaos, S. 1990. "Fracture and Breakup of River Ice Cover", Canadian Journal of Civil Engineering. Vol. 17, No. 2. April 1990. Pages 173-183.

Beltaos, S. 1987. Closure to Beltaos (1983). Journal of Hydraulic Engineering, ASCE, V. 113 (2), pp. 246-255.

Beltaos, S. 1984. "Study of River Ice Breakup Using Hydrometric Station Records". Proceedings Workshop on Hydraulics of River Ice, Fredericton, N.B., pp. 41-59.

Beltaos, S. 1983. "River Ice Jams, Theory, Case Studies and Applications". Journal of Hydraulic Engineering, ASCE, V. 109, (10), pages 1338-1359.

Beltaos, S. and Burrell, B. 1990. "Case Study of a Grounded Jam; Restigouche River, N.B." Proceedings Northern Hydrology Symposium (In preparation). July 10-12, 1990. Saskatoon, Saskatchewan.

Bilello, M.A. 1980. Maximum Thickness and Subsequent Decay of Lake, River and Fast Sea Ice in Canada and Alaska. U.S. Army Corps of Engineers, CRREL Report No. 80-6, Hanover, New Hampshire, U.S.A. 165 pages.

Gidas, Nicolas K. 1981. "Recherche sur les Meilleures Contre Les Inondations de la Matapedia Causees par les Embacles". Proceedings International Symposium on Ice. Vol. 1. International Association for Hydraulic Research. Quebec, Canada. Pages 266-275.

Gidas, Nicolas K. 1979. Analyse des diverses solutions possibles au probl eme d'inondation de Matapedia. Etude No. 0116-2, Direction Generale des Eaux, Ministere des Richesses Naturelles, Quebec.

IAHR. 1986. River and Lake Ice Engineering. George D. Ashton, Editor. Water Resource Publications, Littleton, Colorado, U.S.A.

Leger, R.D. 1986. A Report on Ice Jams on the Restigouche River Basin. A report prepared under the Employment Action Program. New Brunswick Department of the Environment.

New Brunswick Department of the Environment and Environment Canada. 1990. Restigouche River Ice Project Background Report. (In preparation).

Kindervater, A.D. 1985. Flooding Events in New Brunswick An Historical Perspective. Inland Waters Directorate - Atlantic Region, Environment Canada. Dartmouth, Nova Scotia.

Montreal Engineering Company, Limited. 1969. Maritime Province Water Resource Study Volume Three New Brunswick. Book 1. Produced for the Atlantic Development Board. January 1969.

Prowse, T.D., Demuth, M.N. and Onclin, C.R. 1988. "Using the Borehole Jack to Determine Charges in River Ice Strength". Proceedings 5th. Workshop on Hydraulics of River Ice/Ice Jams. 21-24, June 1988. Winnipeg, Manitoba. Page 283-302.

Prowse, T.D. 1985. Guidelines for River Ice Data Collection Program. Prepared for the NRCC Working Group on River Ice Jams. National Hydrology Research Institute, Environment Canada, Ottawa. 33 pages plus figures.

Shulyakovskii, L.G. 1963. Manual of Forecasting Ice Formation for Rivers and Inland Lakes. Israel Program for Scientific Translations, Jerusalem, 1966.

The Lake Ontario Winter Storms (LOWS) Project

T. NIZIOL[1], R.F. REINKLING[2], R.A. KROPFLI[2], G. BYRD[3], R. BALLENTINE[4], A. STAMM[4], R. PENC[5], R. CAIAZZA[6], AND C. BEDFORD[7]

[1]National Weather Service Forecast Office, Buffalo, New York 14425, U.S.A.
[2]National Oceanic and Atmospheric Administration, Wave Propagation Laboratory Boulder, Colorado 80303, U.S.A.
[3]State University of New York, Brockport, New York 14420, U.S.A.
[4]State University of New York, Oswego, New York 13126, U.S.A.
[5]Pennsylvania State University, University Park, Pennsylvania 16802, U.S.A.
[6]Niagara Mohawk Power Corporation, Environmental Affairs Department, Syracuse, New York 13202, U.S.A.
[7]Galson Technical Services, Inc., East Syracuse, New York 13057, U.S.A.

ABSTRACT

In January and February 1990, the Lake Ontario Winter Storms project applied advanced remote-sensing techniques to lake effect snow storms to determine if that technology could be used to provide more accurate forecasts and nowcasts of the location and intensity of snow bands. This paper describes the project and plans for analyzing results.

The sampling program included remote sensing, radiosondes, and traditional observer networks. Three experimental sites were equipped with advanced remote-sensing equipment including: Doppler radar, radiometer, 915-MHz wind profiler, two 405-MHz wind profilers, ceilometer, and Radio Acoustic Sounding System (RASS). Atmospheric soundings were taken at mobile and fixed sites. Surface conditions were monitored using an observer network, microbarographs and precipitation gauges.

Despite an unusually inactive lake-effect snow period, the project team plans to evaluate the performance of the remote-sensing technology, analyze several case studies, and model the lake-effect process.

1. INTRODUCTION

The field phase of the Lake Ontario Winter Storms Project (LOWS) was conducted in the Lake Ontario basin between 5 January and 1 March 1990 to study lake-effect storms. An overview of the project is presented in this paper.

Lake-effect snowstorms were the primary focus of LOWS. Lake-effect snowstorms bring localized but extremely heavy snowfalls and whiteouts to areas near the Great Lakes. In the eastern basin of Lake Ontario the storms cannot be observed with good resolution using current, standard meteorological sensors and observations because of their small vertical and horizontal extent.

Lake-effect snow research has been conducted in the eastern basin of Lake Ontario in the past with monitoring networks with more resolution than the standard network (McVeil and Peace, 1966). Previous work has indicated that mesoscale features such as the shape of the shoreline, topogrpahy, and convergence contribute to the location, orientation, and movement of lake-effect snowbands (Peace and Sykes, 1966).

Accordingly, Niagara Mohawk Power Corporation (NMPC) prompted and provided primary support for this study. The general goal was to determine if advanced remote sensors could be used to find an effective way to deal with the impacts of lake-effect snowstorms in NMPC service territory.

The objectives of LOWS are threefold:

(1) Technology transfer -- demonstrate the utility of a meso-beta array of specialized remote sensors for monitoring and predicting lake-effect snowstorms;

(2) Improve mesoscale prediction through better physical description and understanding of factors driving lake-effect storm evolution;

(3) Determine the utility of the remote sensors for monitoring and predicting the nature and evolution of subsynoptic features of synoptic-scale storms producing freezing rain.

In order to meet these objectives, a consortium of 13 organizations was formed (Table 1). Project elements included an array of six specialized remote sensors, and a full contingent of project-specific and standard meteorological observing systems, as well as the support of a unified operations center, forecasters, and numerical modeling.

2. CHARACTERISTICS OF LAKE-EFFECT SNOW EVENTS

Lake Ontario is particularly conducive to severe lake-effect storms because it remains unfrozen in winter and its east-west orientation gives prevailing winds a long fetch over the longest axis of the lake. Lake-effect snow is caused when flow across the lake is de-stabilized by the flux of moisture and heat from the relatively warm lake into cold, typically arctic, air. Lake-effect snow is localized, 5-20 km wide, and shallow, 2-4 km. When combined with orographic lifting the snowfall rate is enhanced significantly.

Features of lake-effect snow make it important for the region and interesting for meteorologists. Intense snowfall rates are the most important feature, snowbursts that deposit 70cm in 48-hr are not uncommon (Figure 1). A well-developed snow band develops its own self-perpetuating circulation with convergence flow into the band and significant variations of wind speed and direction across the band. However, even in well-developed bands there are fluctuations as the band moves or oscillates in response to small features. Lake-effect snow forms either in single or multiple bands. In typical arctic

Table 1. LOWS Participants and Their Contributions

Participants	Contributions
Atmospheric Env. Ser.	C-band Doppler Radar, Nowcaster, and Supplemental Radiosondes
Galson Technical Ser.	Surface Observer, Microbarograph, and Weighing Precipitation Gauge Networks, Forecast Committee, and Nowcasters
Kaman Sciences, Inc.	Administrative Management
National Weather Ser.	Lead Forecaster, Supplemental Radiosondes and Nowcasters
NYS Dept. Env. Cons.	Forecast Committee and Nowcasters
Niagara Mohawk Power	Forecast Committee and Nowcasters
NOAA Wave Prop. Lab.	Operations Director, X-Band Doppler Radar, 915 MHz Profiler, and Radiometer
Penn. State University	Nowcaster, RASS, and 404 MHz Profiler
Pulaski Academy	Surface Observations
SUNY at Brockport	Mobile Radiosondes and Forecast Committee
SUNY Env. Sci. & For.	Snow Surveys
SUNY at Oswego	Observation Center, Mobile Radiosondes, Forecast Committee, and Nowcasters
Systems Technology, Inc.	404 MHz Profiler

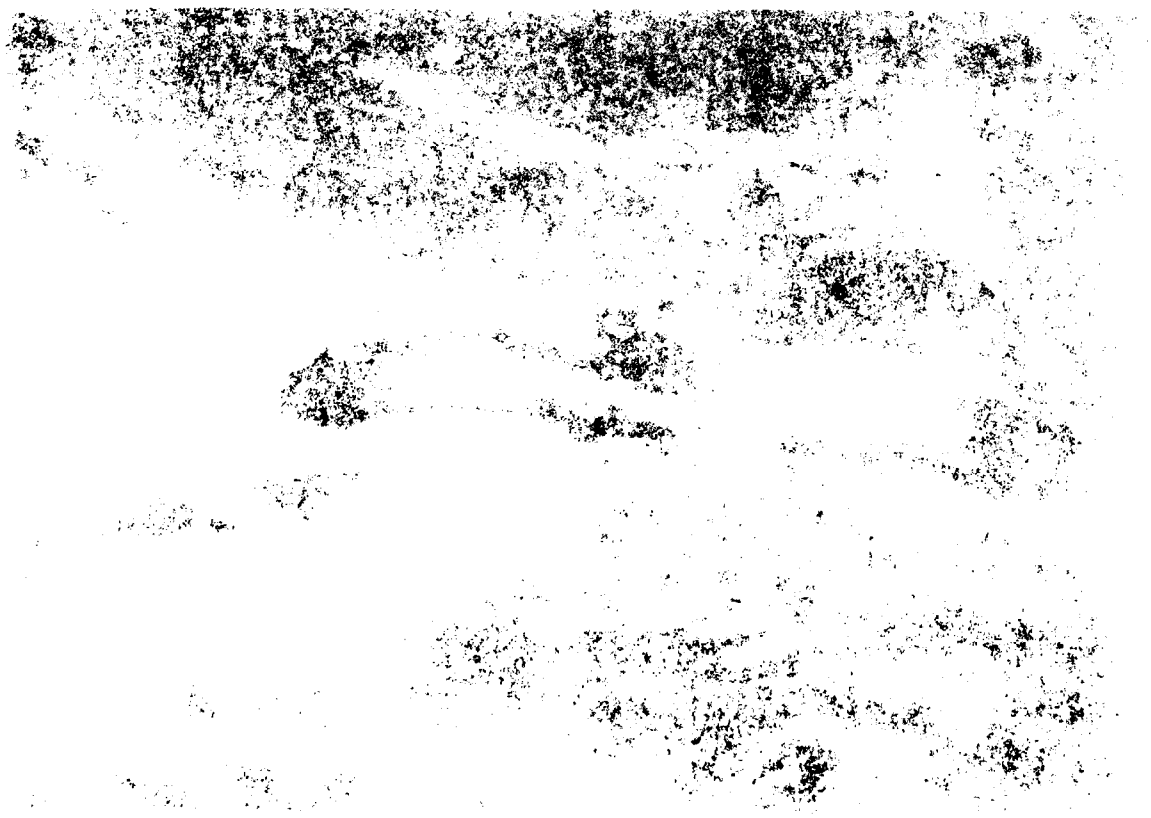

air episodes a well-defined capping inversion forms. The height of this inversion can limit development.

In order to understand lake-effect snow the following aspects must be considered: timing of onset and dissipation, type of banding, movement, intensity and loaction of bands. The primary forecast variables are described by Niziol (1987). These include cyclonic vorticity advection and low-level flow, the boundary layer structure and evolution of the capping inversion, steering level wind direction and speed, and directional shear between the surface and 700mb.

3. LOWS OPERATIONS AND MEASUREMENTS

The primary focus of the LOWS research effort was the eastern end of Lake Ontario (Figure 2). As described in Reinking et al. (1990) an experimental array of remote sensors, conventional observations, and mobile field teams was organized to collect data during intensive sampling periods (Figure 3).

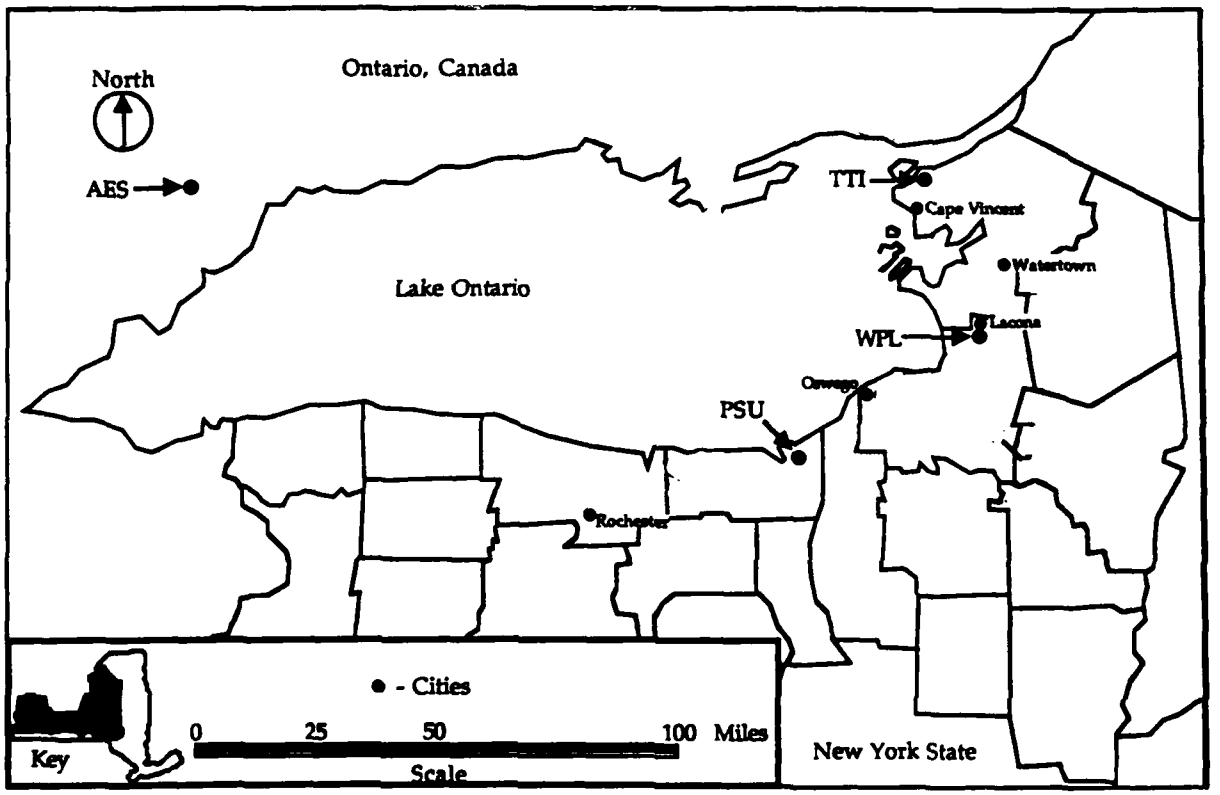

Figure 2 Lake Ontario Winter Storms Remote Sensing Installations

NOAA/WPL provided continuous measurements from three sensors near Lacona, New York (WPL, Fig. 2). Storm morphology, precipitation intensity, wind field information in the cloud system, and the height of the melting level, if any, within a 100 km radius were provided by an X-band (3.2 cm) dual-polarization, Doppler radar. Winds in the boundary layer and aloft were measured using a developmental 915 MHz wind profiling radar. A three-channel, passive, scanning microwave radiometer measured vapor and cloud liquid water integrated along the scan path.

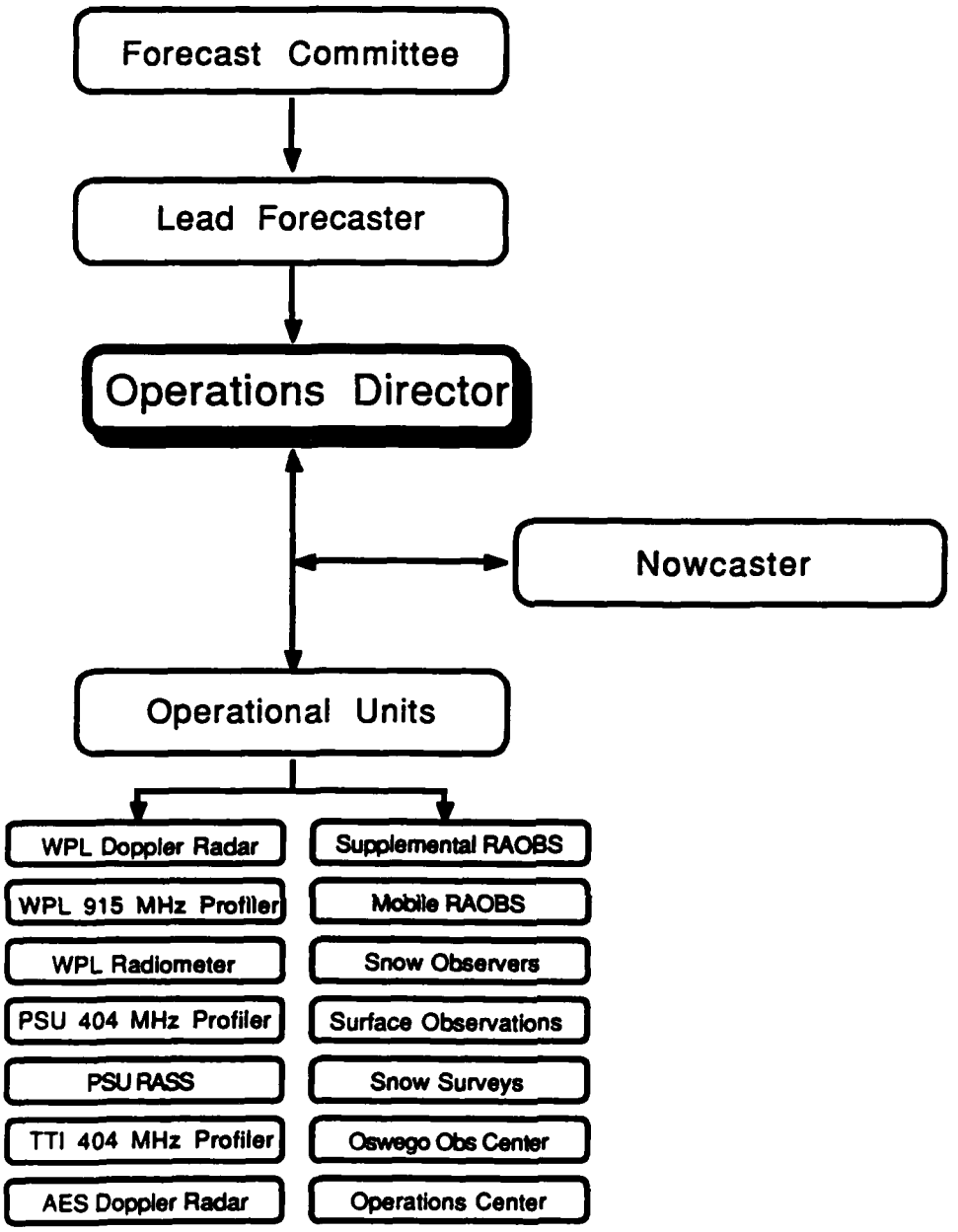

Figure 3. Lake Ontario Winter Storms Organization Chart

The remote-sensing array was completed with real-time measurements at three other sites. Wind and virtual temperature profiles were measured on the southeast shore with a 404 MHz profiler and a Radio Acoustic Sounding System (RASS) provided by Pennsylvania State University (PSU, Fig. 2). Winds were also sampled on the northeast shore from a 404 MHZ profiler provided by Tycho Technology, Inc.(TTI, Fig. 2). Upwind, at King City, Ontario, 40 km northwest of Toronto, the Atmospheric Environment Service provided 5 cm Doppler radar surveillance (AES, Fig. 2).

```
139
FPUS3 KBUF 111528
STATE FORECAST DISCUSSION
NATIONAL WEATHER SERVICE BUFFALO, NY
1018 AM EST THU JAN 11 1990

COLD FNT MVG ACRSS STATE THIS AFTN WITH MUCH COLDER AIR. SWIS SHOWS
SOME BREAKS COULD WORK INTO WESTERN ZNS AFT 18Z WITH DRY SLOT. TEMPS
LOOK GOOD. LOWERED WNDS A BIT THIS AFTN EAST ZNS SINCE SHLD REMAIN SOUTH
MUCH OF DAY AND FRNT NOT EXPECTED TO PASS SYR TIL EVE. VERY COLD AIR
BEHIND FRNT AND LINED UP WELL SO LAKE EFFECT SQUALLS SHLD DEVELOP LATE
TNGT AND FRI..SEE FOLLOWING DISCUSSION. WNDS LOOK CLOSE FOR HIGH WIND
WARNG THIS EVE AT LEAST ZNS 1/21 BUT WILL WAIT FOR LOOK AT NGM.

LAKE ONTARIO SNOW OUTLOOK
SYNOPSIS...RIDGE OVR AREA MOVG QUICKLY EAST...AS STRGLY DIFLUENT UPPER
FLOW TAKES OVR DURING DAY. VERY DEEP LOW PRES SYS MVS RAPIDLY ACRS ONT
SWEEPING COLD FNT ACRS WNY THIS AFTN. VERY TIGHT PRS GRAD WITH HI WNDS
DRG AND AFT CFP. STRG 22 VORT MAX CNTR CROSSES EAST END OF LK ONT TOO
WITH WELL ALIGNED WNDS AT ALL LVLS. DEEP CYCLONIC FLOW WITH ARCTIC AIR
POURING IN OVR REGION SHUD BE NR PERFECT SET UP FOR XNTD PERIOD LES.


NOW THRU THURSDAY 7PM...NO GO. AIR STILL TO WRM TODAY BEFORE CFP.
THURSDAY 7PM TO FRI 1PM...GO FOR SINGLE BAND EAST OF LK ONT. POSSIBLE
                          MEGA BAND WITH HVY SNWFL AND STRNG WNDS.
FRI 1PM TO FRI 7PM...GO. INDICATIONS FLOW BCMG MORE NW WITH TIME
                     SHIFTING TO MULTIPLE BANDS FROM ROC EAST TO
                     OSWEGO AND SYR...WELL INLAND DUE TO RATHER
                     STRONG WNDS.

TAN/JJP
```

Figure 4. Example Lake Ontario Snow Outlook, 3Z 11 Jan 1990.

Additional measurements were made during intensive sampling periods. Mobile teams from the State University of New York (SUNY) Colleges at Brockport and Oswego released rawinsondes at 3-6 h intervals from strategic points along the south and east shores of the lake. Deployment strategy focussed on a) evolution of the boundary layer during potential and realized lake-effect storms, b) comparison of environments within and adjacent to bands, and d) comparison of measurements with the remote sensors. All of the mesoscale sounding measurements were supported by standard and special NWS and AES (Atmospheric Environment Service) rawinsondes released at 6 h intervals from Flint and Sioux St. Marie in Michigan, Egbert in Ontario, and Buffalo. Weighing precipitation gages provided precipitation rates at selected locations; these were complemented by hourly observations from a volunteer network. Other supporting measurements are indicated in Table 1.

The experiment was organized to intensively sample lake-effect snow storms when they were forecast or observed. Ultimate decisions for operation were made by the Operations Director (OD) supported by the Forecast Committee and Nowcasters (Figure 3). During intensive sampling periods, each research group followed their experimental protocol and continued to operate until the OD ordered sampling to stop. Additionally, the OD issued guidance during the intensive sampling periods to the mobile sampling and remote sensing crews.

Primary forecast support for the project was provided in the Lake Snow Outlook produced by BUF (Figure 4). This product predicted the probability of lake-effect snow over the ensuing 48-hr period four times a day. It was appended to the New York State Forecast Discussion and distributed through normal channels. Each afternoon a member of the Forecast Committee (other meteorologists participating in the project) would call BUF after reviewing comments from the whole committee on an electronic bulletin board. Forecast ideas would be discussed and a forecast consensus developed. Then BUF would brief the OD so that plans for the next 48-hrs could be developed.

During intensive sampling periods operations were directed from the NMPC/Syracuse Operations Center. The Operations Center received all remote sensing measurements in real-time, had access to weather forecast charts, and conventional observations.

The Nowcasters were all volunteer meteorologists. However, the experience levels varied widely. Consequently, each Nowcaster has his own preferred data products to approach the problem. For example, Brian Murphy, Ontario Weather Centre introduced the project team to the AES winter severe weather forecast product FOCN03. This model lists 6-hourly forecasts of freezing level, 850 mb temperature, model winds from 3 levels in the RFE model, and 700 mb and 850 mb winds for specific cities (Murphy, 1989).

4. SUMMARY OF EVENTS

Some 5-7 major lake-effect snowstorms and 10-15 events with whiteout conditions are expected between late November and mid-March in a normal winter in the Lake Ontario region (R. Sykes, SUNY; informal manuscript). In 1989-1990, some lake-effect activity, including one very severe event, occurred in December. However, lake-effect activity was well below climatology while rain events were above normal during the January-February project period. A list of project case studies is given in Table 2.

Table 2. Case Studies from LOWS - 1990

	Event Type	Dates
*	Heavy Lake-effect Snow, Single Bands	11-12 January.
*	Light Lake-effect Snow, Frontal Boundary Band and Post-frontal Multiple Bands.	25 February
*	Light Lake-effect Snow, Multiple Bands	28 February.
*	Sub-marginal Lake-effect Events	19, 23, 27 January, 10, 17, 19-20 Feb.
*	Freezing Rain	15 February.

5. EXAMPLES OF OBSERVED STORM FEATURES

5.1 Lake Effect Single Bands.

Case of 11-12 January 1990. A series of major single bands produced 30-80 cm of snow in an east-west zone some 50 km wide extending inland over the WPL/Lacona site (Fig. 2) and the rising terrain of the Tug Hill Plateau to the east, and 10-30 cm over adjacent areas. Post-analysis is anticipated to reveal important precursors in the evolution of the water vapor field from the radiometer, the PBL temperature structure from the mobile sondes, and the wind field from the profilers and sondes. WPL radar monitoring revealed that the storm bands that successively developed were only 10-20 km wide and some 80 km long. The Cape Vincent wind profiler showed that bands formed in post-frontal arctic air after 6-7 h of sustained west winds with minimal directional shear (Figure 5).

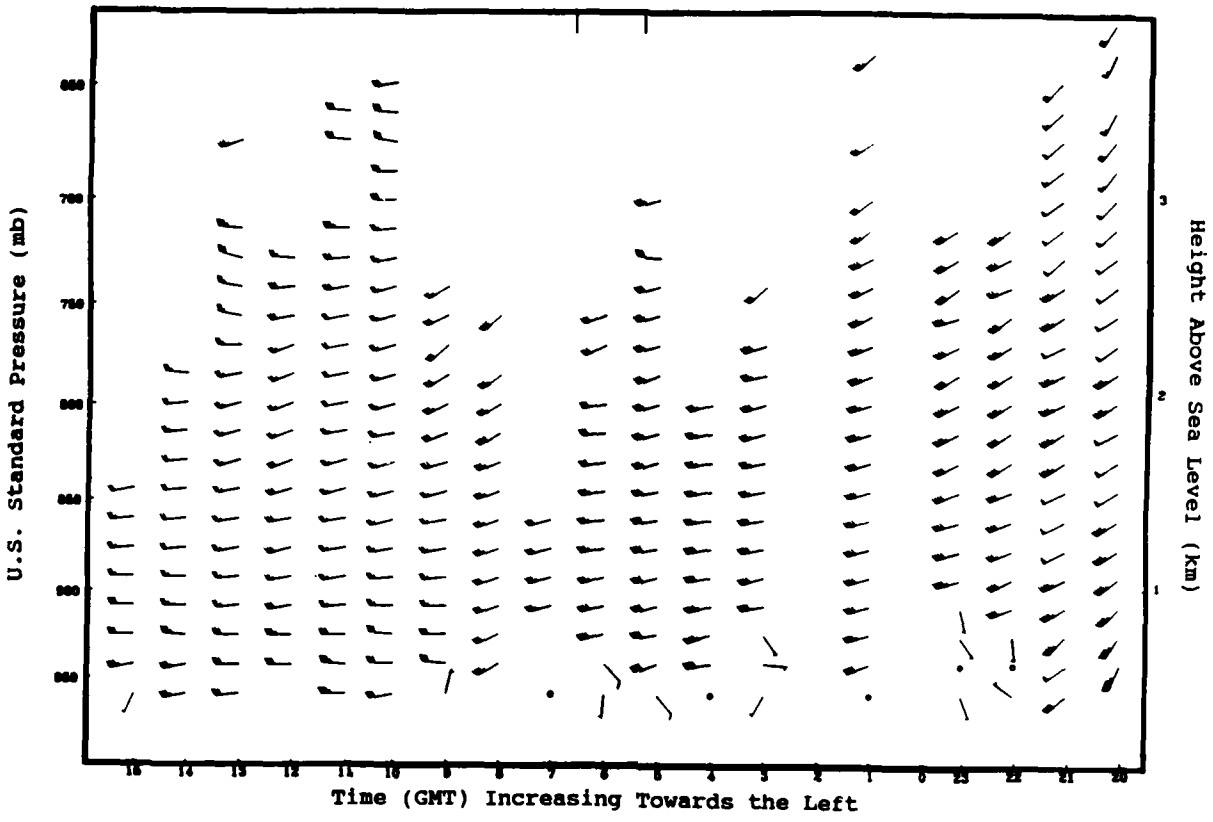

Figure 5. Wind Profiles for Cape Vincent, NY: Jan 11, 20Z through Jan 12, 15Z showing conditions from passage of arctic front (between 21 and 22Z, Jan 11) and development of single band at Lacona (14Z Jan 12).

An initial major band of 3-4 km depth developed over the center of the lake, rotated southward through the southeast shore with a pivot point near Lacona, and dissipated as it continued to rotate inland to Syracuse. This was replaced with a second band which repeated the cycle, apparently in association with temporary veering of the winds in the cloud layer, as observed with the wind profilers. Winds returned to westerly, and small, new, convective cells over the lake organized into a narrower, more convective and snake-like band that maintained an east-west orientation and advected through Lacona for a sustained 9-10 h period.

Intermittent whiteouts occurred during this storm. Within the successive bands, cloud liquid water measurements from the scanning radiometer revealed a steady supply of condensate advecting over Lacona and toward the higher terrain to the east (Fig. 6), and the radar revealed significant orographic enhancement of the resulting precipitation (Fig. 7). Dissipation then occurred as directional wind shear was introduced in the cloud layer and the capping inversion descended from about 3.5 to 2 km above the lake. A more complete outline of the evolution of this storm is presented by Reinking et al. (1990), and analyses of the lake-effect forecasts in relation to the actual event is are underway.

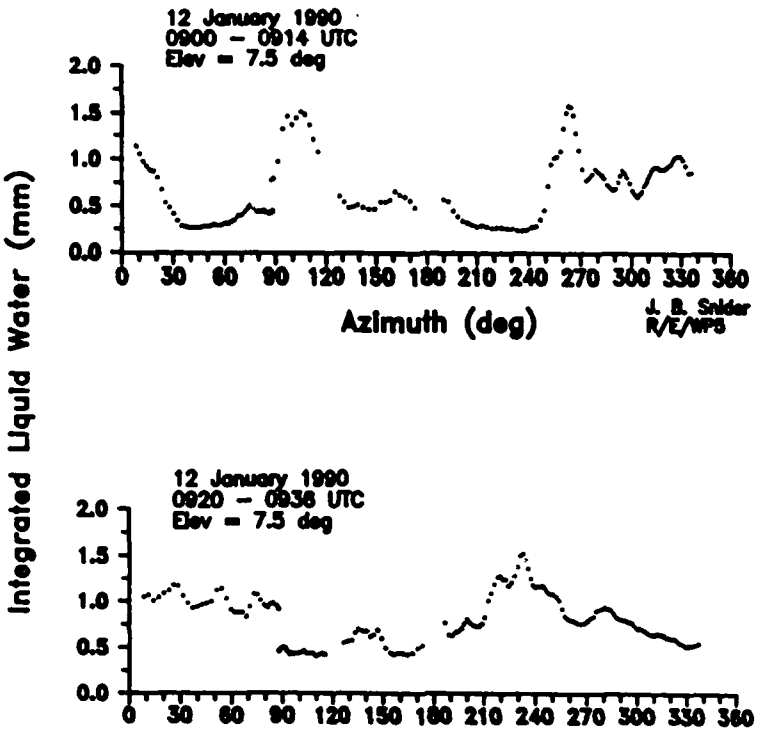

Figure 6. Sequential 360 deg. scans of cloud liquid water showing peaks in the major, single band upwind and downwind of microwave radiometer, and rotation of bands between scans.

5.2 Multiple Bands and Submarginal Lake-effect Events.

General observations suggest that diagonal fetchs across Lake Ontario result in several bands that form and are sustained simultaneously. Such multiple, parallel bands tend to be less intense than the single bands, probably because the shorter fetches allow less time for destabilization and development of a deep mixing layer and the accompanying, responsive confluence and land-lake circulations. Multiple bands tend to be organized as wind-parallel, or possible wind-shear parallel, cloud streets. Directional shear in the mixing layer may also contribute to such multiple rather than single banding, or at least to transitions from single to multiple banding.

For 28 February, radar reflectivities as strong as 25 dBZ depict two bands as they were sustained in northwesterly, cross-lake flow (Fig. 8). These bands were about 30 and 70 km long. Rawinsondes revealed little directional shear but considerable increase in wind speed with altitude in the mixing layer which was capped by a low (1.8 km) inversion. The bands produced light snowfall (2-5 cm) in zones about 20 km wide as they extended inland southeast of the 240 deg radial from the radar. The radial velocity field from the radar clearly defines convergence of low-level air into the stronger band and indicates lifting at the core of the band where radial velocities go to zero. The dynamics of these bands are being studied to reveal temperature, wind and water vapor precursors in relation to the snowfall produced.

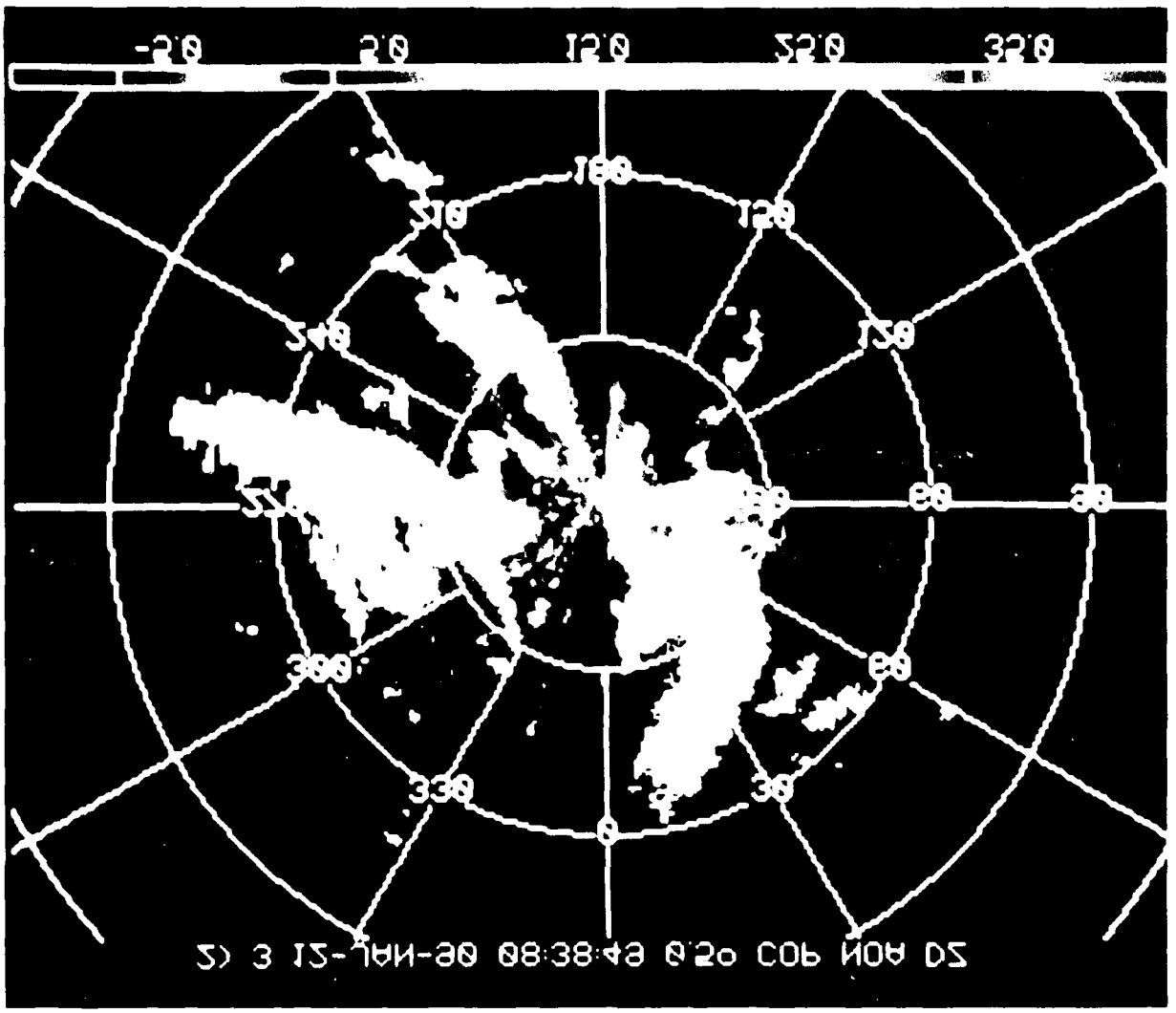

Figure 7. Reflectivity from the WPL/Lacona radar depicting bands that rotated southeastward to impact inland cities south and east of the 240 deg. radial. The band at 210 deg. was dying while that at 260 deg. was intensifying. Orographic broadening of the storm swath and enhancement of precipitation in the area extending to 30 to 40 km east of the radar are also evident.

Several cases with forecasts for a very marginal possiblility of lake-effect snow were monitored; these did not produce significant lake-effect clouds, but the data are useful in analysis and modeling efforts to define and quantify the factors that restrain development. In most of these cases, long over-lake fetches with strong winds developed, but lake-air temperature differences appeared to be too small and the capping inversions too low to allow destabilization and cloud development.

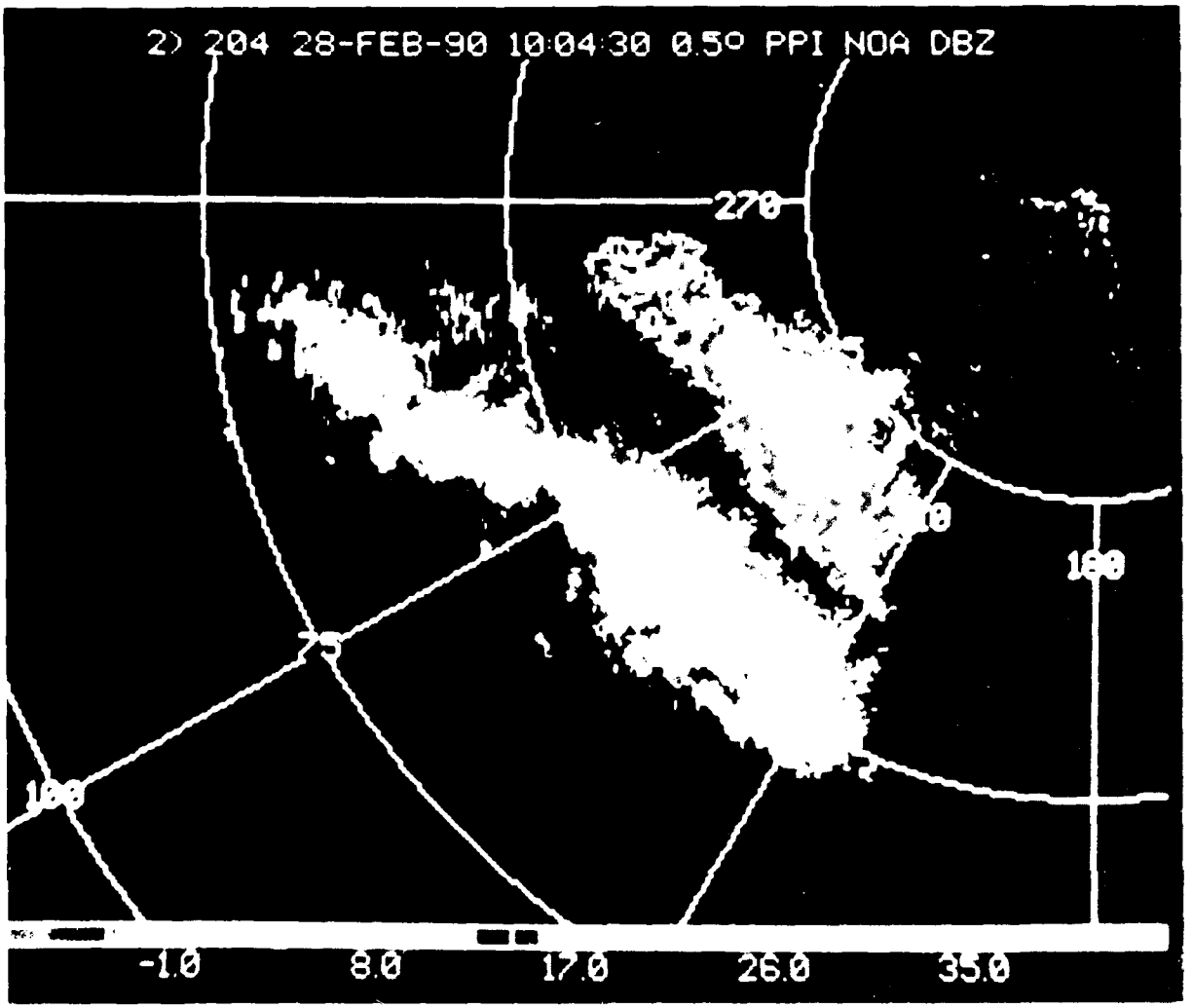

Figure 8. Radar reflectivity depicting parallel bands in northwesterly flow.

6. NUMERICAL MODELING

The SUNY Oswego Mesoscale Model will be used in LOWS analyses to simulate the development of lake-effect snowbands. In initial experiments, the model will predict wind, potential temperature, and specific humidity at 10 layers on a 45 x 31 unit horizontal grid with a 10-km mesh covering the Lake Ontario area. Flat terrain will initially be assumed. A 12-h simulation of the 11-12 January storm will be initialized using LOWS rawinsondes, profiler winds and Doppler radar data. This first test will determine if the model can produce snowbands of the same size, orientation and location as those observed. Model wind, temperature and humidity profiles and model precipitation will be compared with LOWS observations. Subsequent sets of experiments will a) test the model's sensitivity to changes in lake temperature, surface fluxes, latent heat releases, and initial conditions to learn more about the relative importance of the physical factors influencing the development of snowbands; b) include the effects of synoptic-scale forcing by using time-dependent lateral and upper boundary conditions to test the weakening or strengthening of observed snowbands; and c) include realistic terrain to test the model's ability to enhance precipitation over the Tug Hill plateau east of the lake.

In addition, the PSU/NCAR mesoscale model (MM4) is being applied. The structure and physics of this model are described by Anthes and Warner (1978). MM4 is hydrostatic and employs a terrain-following sigma coordinate system with 15 vertical levels. Provisions are included for variable terrain and high resolution boundary layer physics. A nested grid version of the model with 90 km and 30 km grid spacing was run in real time to examine model performance in the forecast mode for several of the LOWS cases. Also, case study analyses and sensitivity tests will be conducted with MM4 to study the physics and dynamics of the lake effect snow bands on detailed scale using a 2 km grid. Additional model development will incorporate the non-hydrostatic effects of latent heat releases on band development and morphology.

7. DISCUSSION

In post-analysis, there will be a careful examination of the technology transfer in terms of what succeeded what must be done differently or refined and what steps are needed to go to the operational mode, (e.g., remote sensor performance and practicality, remote sensing mesoscale coverage, and forecaster use of real-time integrated data products). First examinations of the data, while revealing some surmountable challenges like low profiler signals in cold clear air, demonstrate that a mesonet like that of LOWS would significantly improve locale-specific nowcasting of lake-effect snow. Steps to improving lake-effect storm forecasts along with the real-time monitoring will come from comparisons of the LOWS forecasts and observations and from examination of the data for precursors and physical factors that determined location of formation, movement, area of impact, intensity of whiteouts, and quantities of precipitation. The observations will be interfaced with the numerical modeling components in this effort.

The LOWS data set is available to the scientific community.

ACKNOWLEDGEMENTS

Primary support for LOWS came from Niagara Mohawk Power Corporation's Research and Development Department. The NOAA Wave Propagation Laboratory; National Weather Service Eastern Region; Atmospheric Environment Service; Pennsylvania State University; State University of New York Colleges at Brockport, Oswego, and Environmental Sciences and Forestry at Syracuse; Galson Technical Services; and New York State Department of Environmental Conservation all cost-shared the project to make this research possible. The SUNY mobile sondes and numerical modeling are supported by the National Science Foundation Grant ATM 89-14546. Additional support was provided by the Great Lakes Research Consortium. B. Orr, B. Martner, R. Zamora, J. Snider and P. Neiman of NOAA/WPL all made contributions to this manuscript. The staff of the Buffalo NWSFO and volunteers of the surface meteorological and snow measurement network provided essential support.

REFERENCES

Anthes, R.A. and T.T. Warner, 1978: Development of hydrologic models suitable for air pollution and other mesometeorological studies. Mon. Wea. Rev.,106: 1045-1078.

Hjelmfelt, M., and R.R. Braham, Jr., 1983: Numerical simulation of the airflow over Lake Michigan for a major lake-effect snow event. Mon. Wea. Rev., 111: 205-219.

McVehil, G.E., and R. L. Peace, Jr.,1966: Project Lake Effect. A study of lake snowstorms. Final Report Contract CWB-11231, Cornell Aeronautical Laboratory, Inc., 52pp. [Available from Calspan Corp. Buffalo, NY].

Murphy, B.P., 1989: Forecasting lake-effect snow in Ontario. Ontario Region Technical Note, Atmospheric Environment Service, Toronto.

Niziol, T.A., 1987: Operational forecasting of lake effect snowfall in western and central New York. Weather and Forecasting, 1: 311-321.

Peace, R.L. and R. B. Sykes, Jr., 1966: Mesoscale study of a lake effect snowstorm. Mon. Wea. Rev., 94, 495-507.

Reinking, R.F., R.A. Kropfli, B.E. Martner, and R. Caiazza, 1990: Initial findings from the Lake Ontario Winter Storms (LOWS) experiment. Preprints, 4th Conf. Mesoscale Processes, June 25-29, 1990, Boulder, Colorado. Amer. Meteorol. Soc., Boston (in press).

Regional Snowfall Intensity and the Great Lakes Anomaly

C.C. RYERSON AND R.E. BATES

U.S. Army Cold Regions Research and Engineering Laboratory
72 Lyme Road
Hanover, New Hampshire 03755-1290, U.S.A.

ABSTRACT

Snowfall intensity widely varies spatially and temporally within individual storms and within regions. However, regional snowfall intensity has not been mapped or characterized systematically as a climatic phenomenon. Snowfall intensity was compiled and mapped over the continental United States from four years of National Weather Service 6-hour synoptic reports to show general patterns. Intensities are generally greatest in both eastern and western mountain areas and along the East Coast, and are generally lowest in the northern Plains and Great Lakes. The low Great Lakes intensities were unexpected because of the frequent lake-effect storms along their southeast shores. Methodological and meteorological reasons for this pattern are discussed, and methods of resolving whether the Great Lakes patterns are true are suggested.

INTRODUCTION

Snowfall intensity widely varies spatially and temporally within individual storms and within regions. Intense snowfall seriously impacts activities relying upon transmission of electromagnetic radiation through the atmosphere. Heavy intensity snowfall reduces visibility and causes transportation system delays and accidents. If snows are wet and fall rates are heavy, they can reduce transmission efficiency of communications systems. Heavy snowfall rates also reduce the effectiveness of millimeter-wave, infrared and visible target acquisition systems used by the military. Strategic planners, weapons system developers, and battlefield commanders require mapped information on the spatial and temporal potential for encountering intense snowfall. Such maps are also useful for locating facilities such as airports and highways that rely upon visibility for their operation.

Estimates of snowfall intensity made by National Weather Service observers are based on visibility and spot radar estimates (Wasserman and Monte, 1972; Boucher and Wieler, 1985). Snowfall intensity, therefore, is not measured directly in a strict systematic manner because visibility is treated as an analogue of snowfall intensity. Perhaps because of this lack of systematic measurement and the subjectivity of visual estimates, snowfall intensity has not been mapped for large regions. Previous snowfall climatologies include only maps of mean annual snowfall, persistence of snowfall, depth of snow on the ground and snow density (Bates and King, 1966; Foster and Davy, 1988; Bilello, 1967, 1984; Ryerson and Bates, 1989).

Snowfall intensity can be measured with automatic weighing precipitation gauges, which record the water equivalent of snowfall continuously to an accuracy of 0.1 mm. Weighing gauges are "operational" instruments and the data are archived by National Weather Service offices into snowfall amounts in discrete time periods. Various research instruments such as weather radars, Airborne-Snow Concentration Measurement Equipment (ASCME) (Lacombe, 1983; Stallabrass, 1985) and optical snow gauges (Koh, 1987) can also be used to obtain snowfall intensities. However, these instruments are currently research tools only and have not heretofore provided data of sufficient temporal and geographic breadth for mapping. Some of these research instruments could be made operational and might be useful substitutes for discontinued snow surveys and for describing spatial and temporal snowfall rate patterns.

Snowfall intensity can be calculated from archived measurements of snowfall depth at regular intervals. Records of snowfall amounts sufficient for generalized regional snowfall intensity mapping are available from the National Climate Data Center, the Canadian Atmospheric Environment Service, the World Meteorological Organization, and other national and military weather services.

The purpose of this paper is to present maps of generalized continental United States snowfall intensities from archived 6-hour synoptic period snowfall depth data. In addition, one apparent snowfall intensity anomaly, the Great Lakes lake-effect area, will be discussed. Regional snowfall intensity is characterized with regard to topographic patterns and the characteristics of lake-effect storms.

BACKGROUND

Bates and King (1986) have compared storm snowfall intensity measured by four methods: hourly snowfall depth, hourly snowfall water equivalent, airborne snowmass concentration as measured with an ASCME (Lacombe, 1983), and intensity as measured by the National Weather Service using visibility. All measurements were integrated over one-hour time periods. Measurements by the four methods were made during the SNOW experiments at Camp Ethan Allen, Vermont, and Camp Grayling, Michigan.

TABLE 1. Snowfall Intensity Rate System (from Bates and King, 1986).

	Accumulation Rate		Suspended Snow	
Snowfall intensity	Snowfall (mm/hr)	Water equivalent (mm/hr)	Airborne snow concentration (g/m^3)	Visibility by eye (km)
Light (s-)	< 10	< 1	< 0.3	> 1
Moderate (s)	10–20	1–2	0.3-0.7	0.5 and < 1
Heavy (+)	> 20	> 2	> 0.7	< 0.5

Intensities were categorized into equivalent classes of light, moderate, and heavy snowfall (Table 1). Frequencies were then determined from synoptic analysis for each intensity class. In general, the National Weather Service visibility method suggested more frequent heavy intensity snows than did the other methods. This may be because fog or cloud droplet riming, which frequently accompanies heavy snowfall and reduced visibilities, gives the impression that the snowfall is heavy when it may be moderate or light. Any natural or man-made obscurant combined with snowfall will also cause the visibility method to give the impression of greater than true snowfall rates. Use of the visibility method can, therefore, give the false impression of greater snowfall intensities than actually exist. Bates and King (1986) and Bates (1983) recommend mapping snowfall intensity from snowfall water equivalent or snowfall depth measurements.

SNOWFALL INTENSITY MAPPING

Data for mapping snowfall intensity were summarized from TD-3290 *Summary Observation* records from the National Climate Data Center in Asheville, North Carolina. The *Summary Observations* contain 6-hour synoptic period records for maximum and minimum air temperature, precipitation (rainfall and snowfall water equivalent), total snowfall catch over the 6-hour period, and depth of snow on the ground. Total 6-hour snowfall catch data were obtained from the tapes for 286 first-order weather stations in the United States (including Alaska). Data were available on tape (when acquired in the summer of 1988) for only four years, 1984 through 1987. Because of the large volume of data, snowfall data only for the months of November through April were acquired for mapping.

Maps were drafted using snowfall data from 161 of the 286 National Weather Service stations. Some stations did not have complete four-year records, some stations recorded no snow, and some stations were outside the continental United States. Because of these problems, snowfall intensity was not mapped for areas south of 35° north latitude. Synoptic periods recording less than 1 mm of snowfall were not counted as snowfall periods.

Mapping snowfall intensity from the 6-hour records of snowfall catch presents problems of time resolution. Storms significantly shorter than 6 hours in length will have computed intensities that are significantly lower than those of longer storms. For example, a 1-hour-long storm that accumulates 7.6 cm of snow would have the same computed intensity as a 5-hour storm depositing the same amount of snow. All storms less than 6 hours in length will have downwardly biased intensities. Time resolution could be improved with hourly reports of precipitation type, but they could not be incorporated into this report.

MAP ANALYSIS

Snowfall Intensity

Several distinct patterns are apparent on the mean annual snowfall intensity map (Fig. 1). Highest intensity snowfalls occur in the Sierra Nevada, the northern Cascades, the southern Appalachians, and coastal New England, as expected, because of their orographic and/or coastal locations. Northern Maine experiences high intensities because of its northern coastal location along the prevailing winter storm track, and because intense low pressure systems frequently stall in this area, producing prolonged storms advecting abundant moisture from the Atlantic Ocean. The slight mid-Mississippi Valley rise also may be due to the prevailing winter storm track, especially where cyclogenesis is frequent. In addition, this southern location is near the freeze/thaw transition zone much of the winter, encouraging high absolute humidities that produce high intensity snowfalls with the upper air support provided by the Polar Front.

Low intensity snows are found in the northern Plains and Great Lakes region. Low intensities in the northern Plains could be expected because of the dry, polar continental air masses that dominate the winter. However, the Great Lakes region, especially areas to the south and east of the lakes, are noted for intense lake-effect storms. The short 4-year record undoubtedly does not represent long-term trends well, especially for extreme events. However, the lake-effect storms, because they are often short in length (Eichenlaub, 1979), may be mapped as

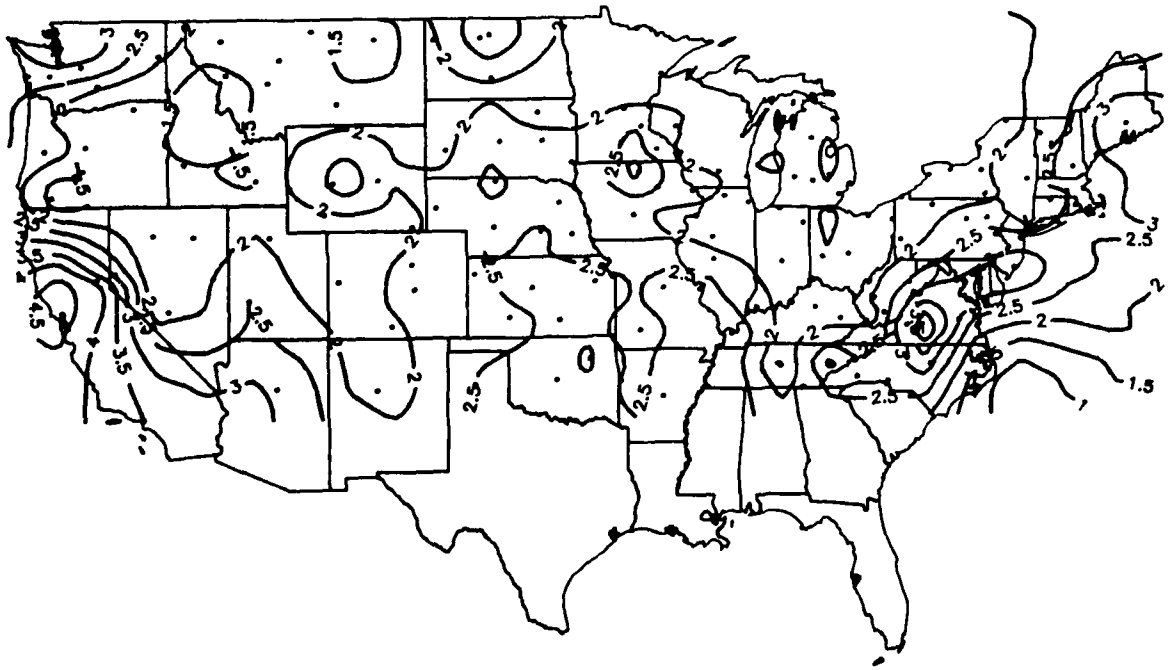

FIGURE 1. Generalized patterns of mean annual snowfall intensity (cm/6 hr, 1984–1987).

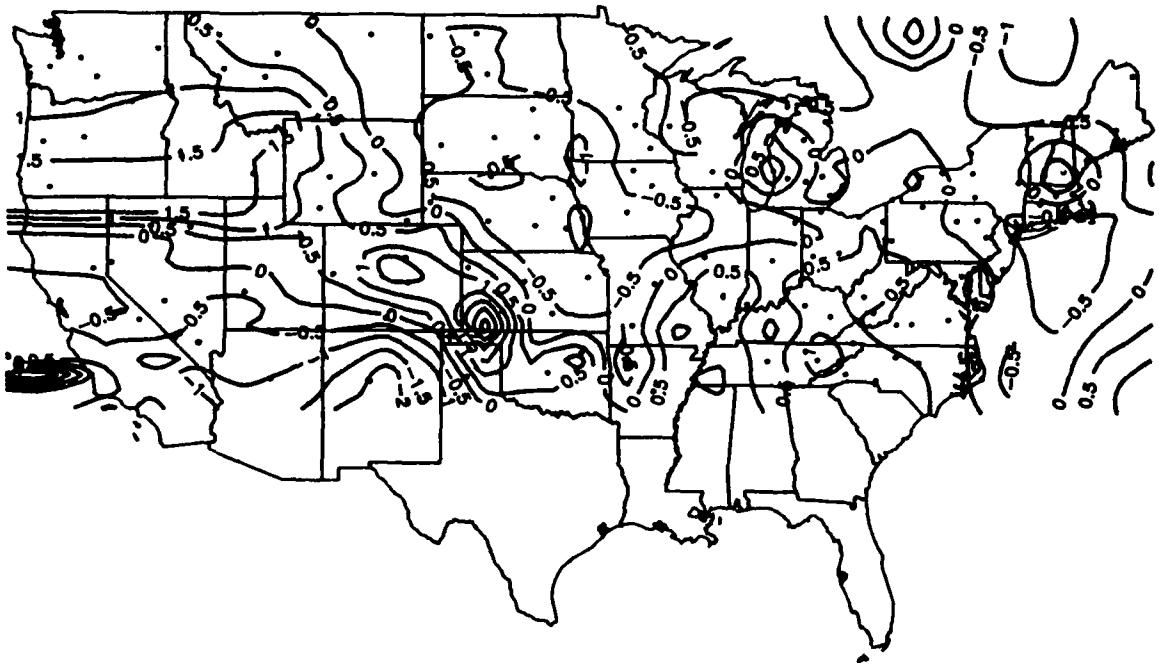

FIGURE 2. Standard deviations of mean annual snowfall intensity (cm/6 hr, 1984–1987). + Above mean, – Below mean.

too low in intensity because of their short duration. The general pattern suggests that light snowfall intensities are found in the most continental areas, with intensities generally increasing near the West Coast, in the southern tier states, and in New England.

The generally low intensity snowfalls in the Great Lakes snowbelts are noteworthy. To determine how anomalous the lake-effect intensities are with regard to intensities elsewhere, standard deviations were mapped (Fig. 2). Standard deviations are near zero in the eastern Great Lakes, indicating that intensities are near the continental mean, and are neither extremely high or low. The only significant deviation from zero in the Great Lakes area is on the eastern shore of Lake Michigan. The 0.5 standard deviation indicates that intensities are slightly higher than the national mean in this small lake-effect area near Muskegon.

Lake effect storms are very seasonal, with most occurring before the Great Lakes freeze over (Eichenlaub, 1979). Fewer lake-effect storms occur after January, especially to the lee of shallow Lake Erie, which freezes earlier and more completely than the other lakes. Maps were produced of snowfall intensity in early winter (November through January) and late winter (February through April) to determine how intensity varied with time.

Snowfall intensity in the Great Lakes region changes little from early to late winter, with mean intensities remaining near 2 cm per 6 hours for the entire year (Fig. 3 and 4). This is true although the length of storms may change seasonally. The predominant types of storms producing snow in lake-effect areas change from short-duration, localized convection phenomena in early winter to large, mid-latitude wave cyclones later in the winter. Residuals of snowstorm intensity between early and late winter indicate that there is little change in Great Lakes region snowfall intensity throughout the winter (Fig. 5).

Standard deviations indicate that early and late winter snowfall intensities in the lake-effect areas are near the national mean or slightly below during both seasons (Fig. 5 and 6). Standard deviations vary from zero to –1.0. However, early winter standard deviations show that intensities are not as depressed in two specific known lake-effect areas: from Gary, Indiana, to Traverse City, Michigan, and from Erie, Pennsylvania, to Watertown, New York (Eichenlaub, 1979). Standard deviations are between only zero and –0.5 in these areas, rather than between –0.5 and –1.0 in the remainder of the Great Lakes. These standard deviations, though low compared to those of the entire nation, suggest that lake-effect areas do have enhanced localized intensities, though overall intensities are somewhat depressed.

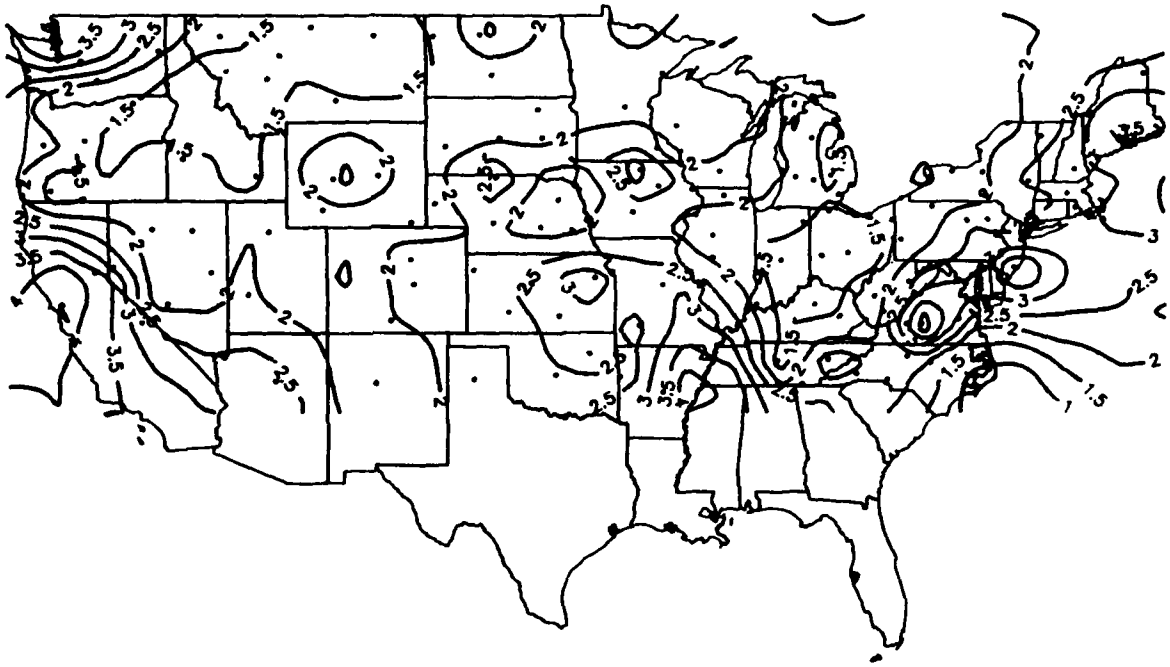

FIGURE 3. Generalized patterns of early winter snowfall intensity (cm/6 hr, 1984–1987).

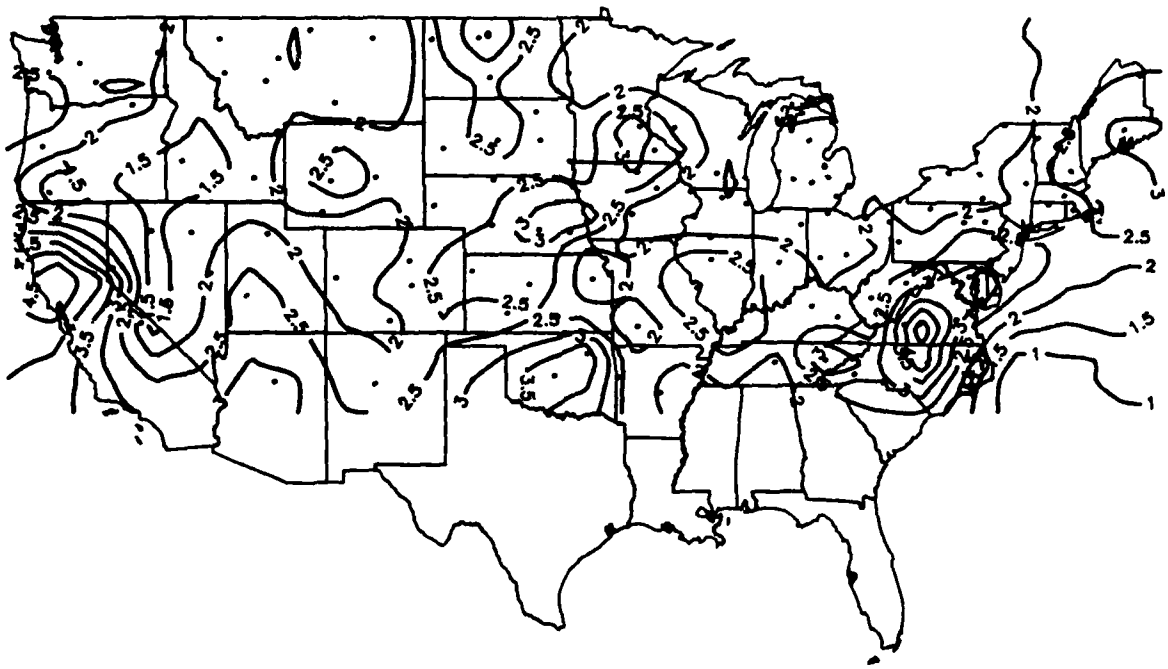

FIGURE 4. Generalized patterns of late winter snowfall intensity (cm/6 hr, 1984–1987).

Late winter, on the other hand, shows slightly depressed standard deviations and thus intensities in lake-effect areas compared to the remainder of the Great Lakes area (Fig. 7). This may be due to greater lake ice cover at this time.

Snowstorm Length

Lake-effect storms are noteworthy for being short, intense squalls with low visibility (Eichenlaub, 1979). Storm length, the mean number of consecutive 6-hour synoptic periods receiving snow at a station, were

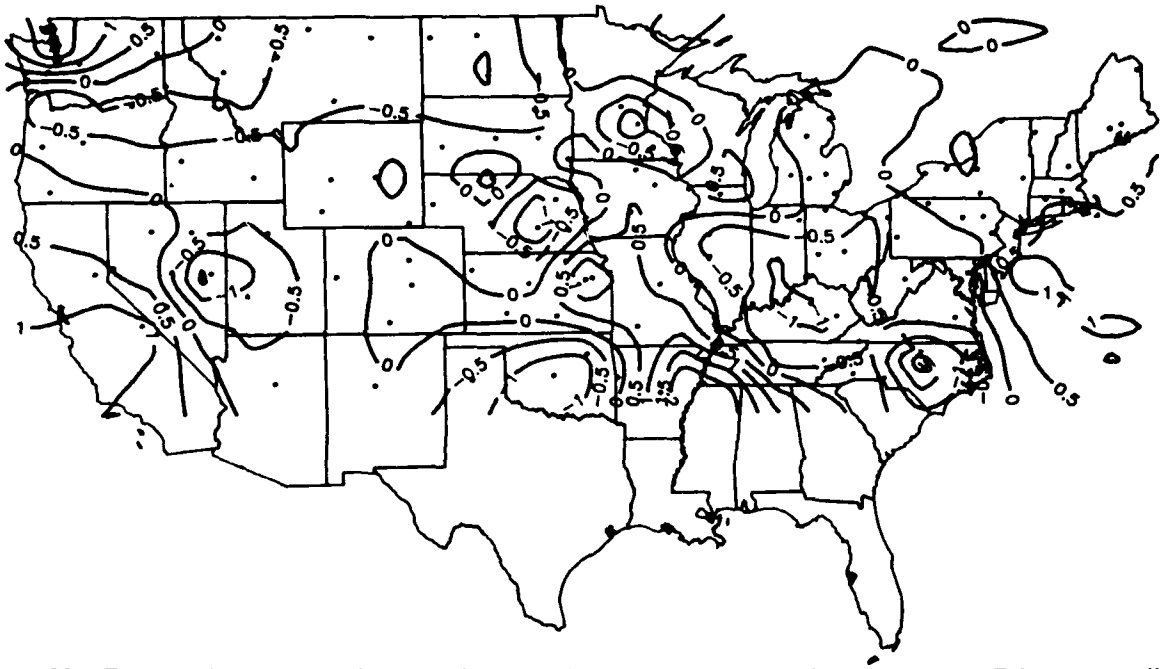

FIGURE 5. Residuals of snowfall intensity (cm/6 hr), early (November–January) to late (February–April) winter (1984–1987). + Early winter larger, – Late winter larger.

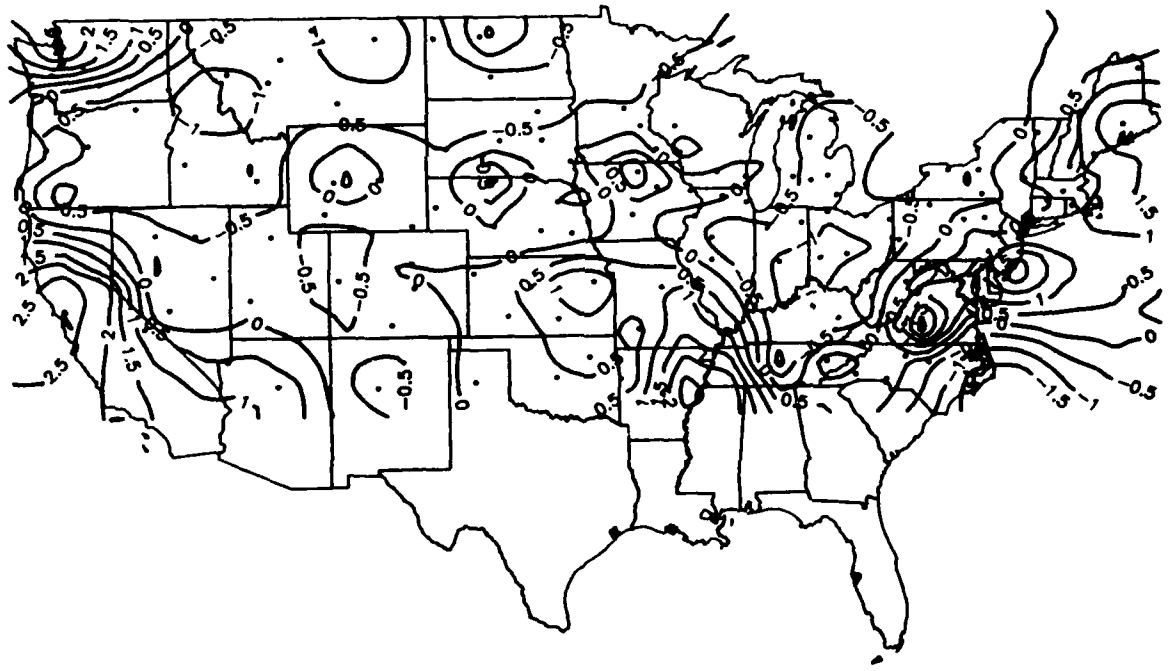

FIGURE 6. Generalized patterns of early winter snowfall intensity standard deviation (cm/6 hr, 1984–1987). + Above mean, – Below mean.

mapped to determine how long snow periods last regionally. In general, the Great Lakes snowbelt areas should record shorter storms, especially early in the winter, if most snowfall is lake-effect in origin. Areas dominated by large-scale cyclonic systems should record longer snowfall periods or more consecutive 6-hour synoptic periods with snow.

Typically, the Great Lakes experience the longest snowstorms of any part of the conterminous United States except for northern Wyoming and southern Montana, which are similar (Fig. 8 and 9). The Great Lakes lake-ef-

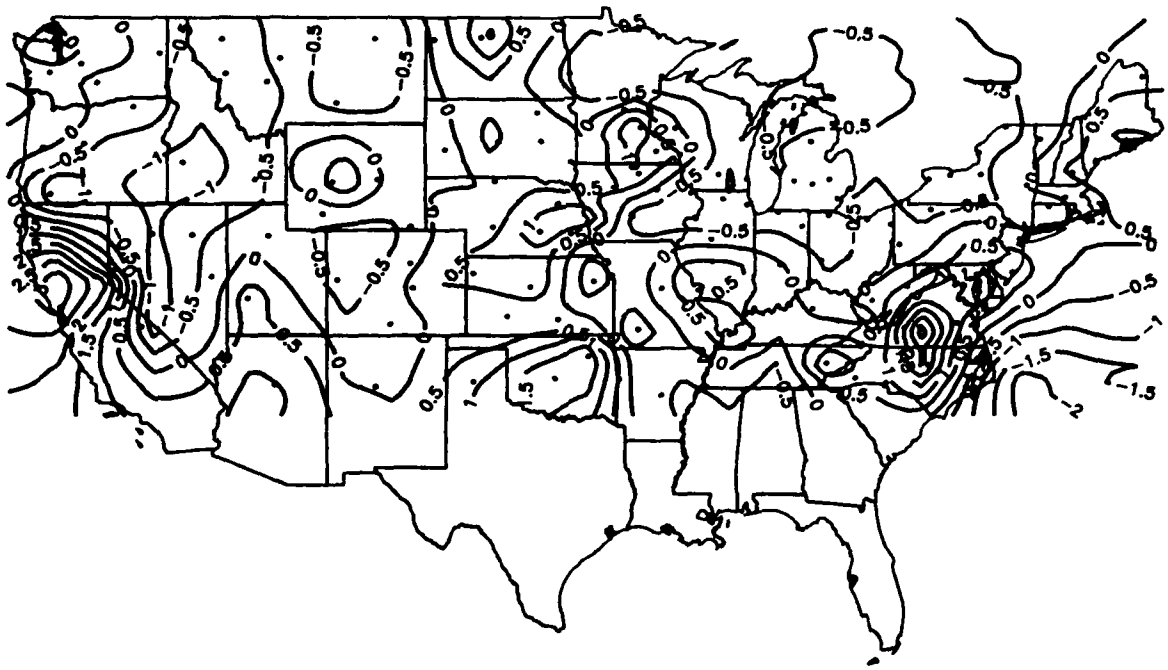

FIGURE 7. Generalized patterns of late winter snowfall intensity standard deviation (cm/6 hr, 1984–1987). + Above mean, – Below mean.

fect areas experience storms averaging about 2.5 synoptic periods in length. As with standard deviations of early winter intensities, storms are longest in specific known lake-effect areas from Gary, Indiana, to Traverse City, Michigan, and from Cleveland, Ohio, to Watertown, New York.

There are several possible reasons for the longer mapped storm periods in the lake-effect areas. Since individual lake-effect storms are generally fairly short, several storms occurring in unison due to persistent winds over a long lake fetch could give the appearance of long storms. The long snow periods, however, are more likely a result of the unique synoptic conditions. Wave cyclones traversing the Great Lakes, with their attendant warm and cold fronts, frequently bring significant snows to the area. However, once the cold fronts pass, cold, dry air from following high pressure enters from the west or northwest. With a long fetch over the warm lakes, the cold continental air heats, humidifies, and becomes unstable, creating snow squalls on the lee sides of the lakes. Since these lake-effect snows usually follow the cyclonic snowfall, there is usually little or no break in the snowfall as mechanisms pass from cyclonic to local convective in nature. These combined mechanisms could easily produce snowfalls 12–15 hours in length. When squalls are very active, there may be less than 12 hours separating cyclonic and lake-effect snow systems (Hill, 1971).

Late winter storm lengths are usually similar to those of the early winter in the Great Lakes (Fig. 9 and 10). However, lake-effect areas are no longer enhanced in length except in the Rochester, Syracuse, and Watertown, New York, area. This localized late-winter length enhancement is probably because Lake Ontario is deep and does not completely freeze over, producing lake-effect storms the entire winter (Eichenlaub, 1971).

Snowfall Days

The largest number of days with synoptic periods of snowfall amounts greater than 1 mm do occur in the Great Lakes (Fig. 11). Averaging 40 to 70 days annually, the number of snow days in the Great Lakes snowbelt areas conform more to expected patterns than do the snowfall intensity maps. The high number of snowfall days in the Great Lakes is due to the many short duration lake-effect snowstorms in the region in addition to the wave cyclones traversing the region. Days with snow are high in the Adirondacks, but begin to decrease in the Appalachians. Numbers of snow days are also not as great in the Rockies, the Sierra Nevadas, and the Cascades

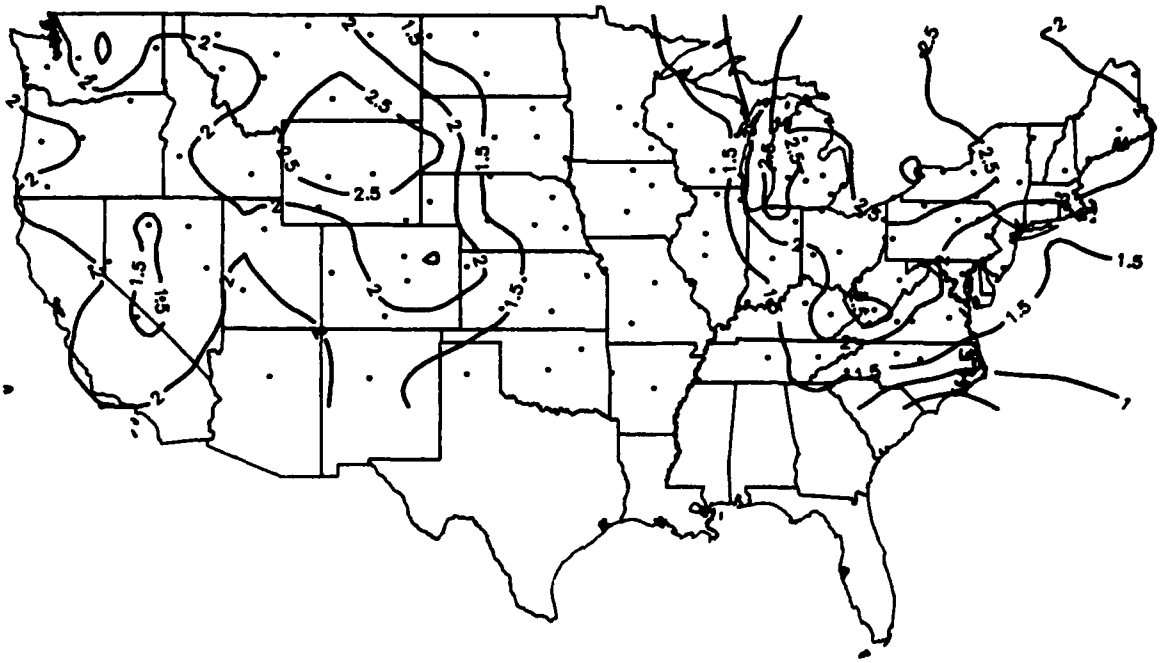

FIGURE 8. Early winter storm length in synoptic periods (1984–1987).

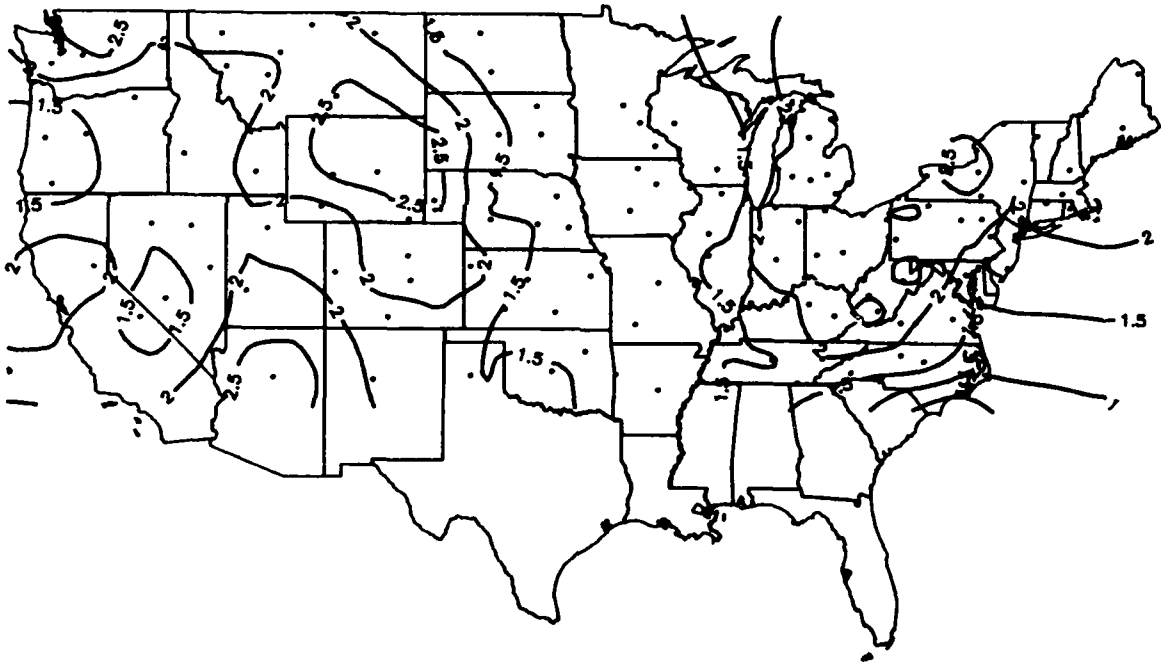

FIGURE 9. Late winter storm length in synoptic periods (1984–1987).

as in the Great Lakes. The western mountains experience fewer days with snow because the storms are cyclonic in origin and do not result from frequent, short-lived, shallow convection systems as do the systems along the Great Lakes. The effects of dry continental air to the north, and warm air to the south, contribute to depressed values in the Great Plains and lower Mississippi Valley.

DISCUSSION

The maps, despite the short period of record, indicate that mountainous regions tend to exhibit higher snowfall intensities, as expected. The Great Plains, dominated by dry, continental polar air for most of the winter,

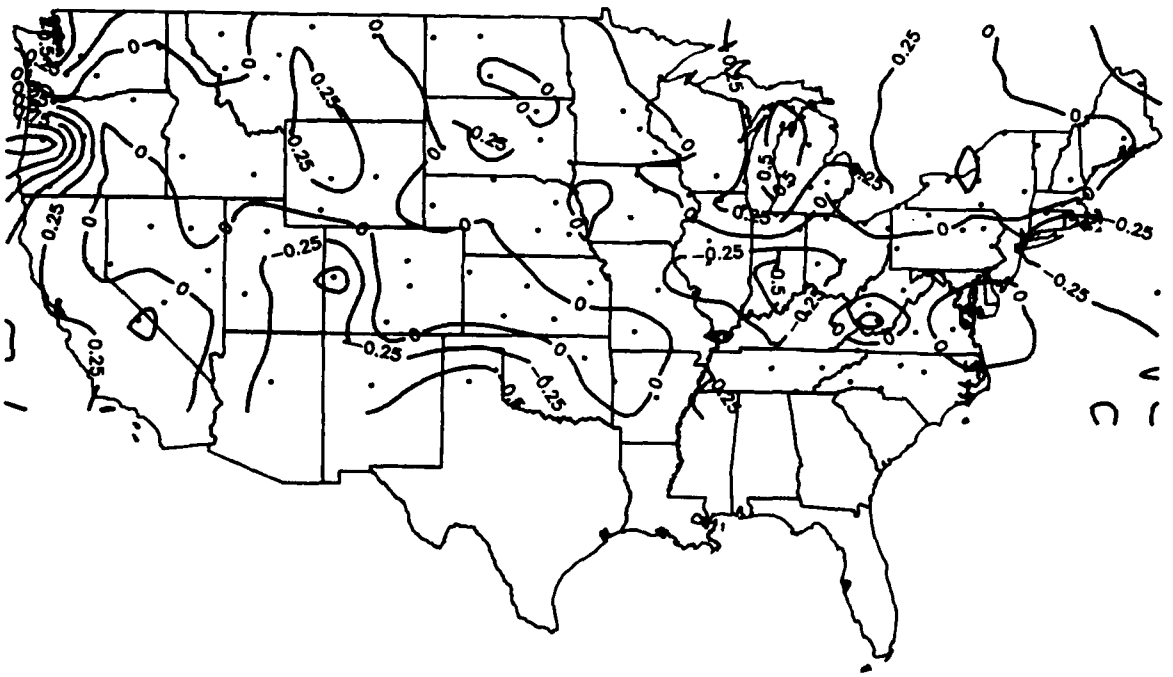

FIGURE 10. Residuals of snowstorm length, early (November–January) to late (February–April) winter (1984–1987). + Early winter longer, – Late winter longer.

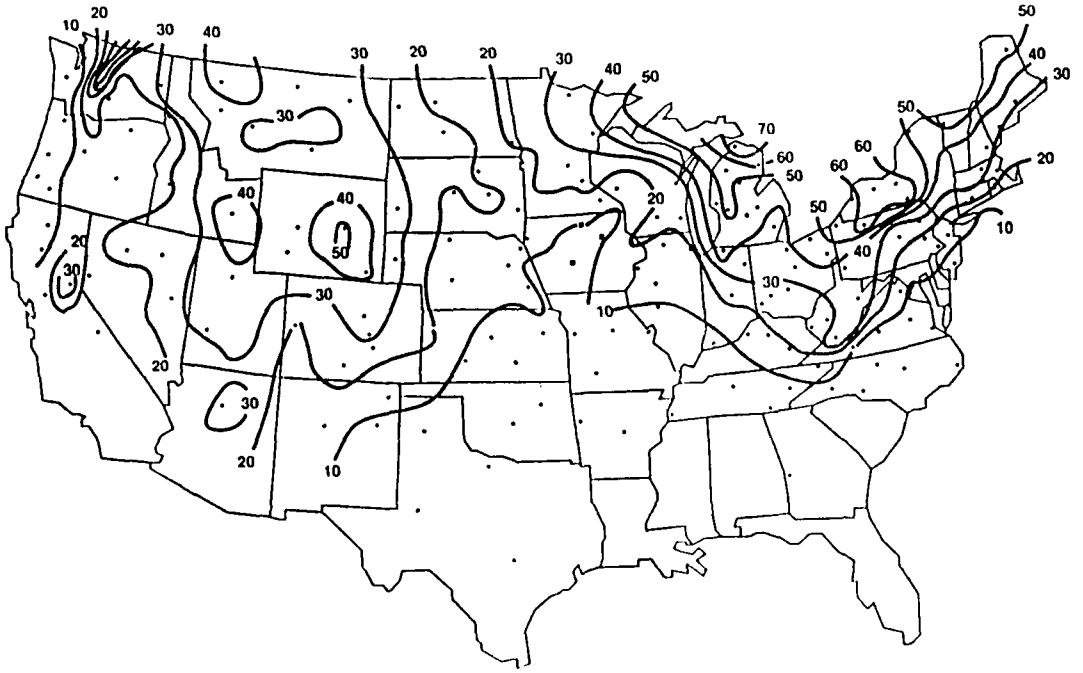

FIGURE 11. Mean annual days with snowfall for 6-hr period with more than 1 mm of snow (1984–1987).

have generally lower snowfall intensities. Coastal regions, and some southern areas, show somewhat higher intensities because of the warmer conditions and higher moisture contents that accompany snowfall in these regions. The primary inconsistency appears to be the Great Lakes snowbelt areas, which show relatively low mean intensities, despite the apparent high snowfall intensities experienced within these short, violent squalls. There are several possible reasons why the lake-effect areas appear to have low snowfall intensities.

The water equivalent of fresh snow in lake-effect storms varies widely. Snow water equivalents range from 6:1 to about 50:1, with 18:1 about average. The low density and thus greater snow depth for a given water con-

tent make lake-effect storms appear intense to the eye. When mapped for snow deposited in a given period of time, lake-effect storms are no more intense, and actually less intense, than storms elsewhere in the continental United States that produce denser snowpacks (Weinbeck, 1983; Eichenlaub, 1979; Hill, 1971). This may be due, in part, to the lower fall velocities of crystals producing low-density snows. The lowest fall velocities increase suspended snow volume and the apparent visual snowfall intensity.

Other mechanisms may also cause the lake-effect storms to appear more intense than snow deposited per synoptic period may indicate. Lake-effect storms are strong convective systems with occasional thunder, lightning, and snowdrifting. Strong surface winds produce blowing snow and reduced visibility, giving the appearance of heavier snowfall than is actually occurring. In addition, warm moist air rising from the lake surface produces convection fog in the colder, overlying air, often the precursor to lake-effect storms (Eichenlaub, 1979). Some of this fog could mix with falling snow, further reducing visibility.

A methodological reason for the low snowfall intensities mapped in the Great Lakes region may be the transient nature of lake-effect snows. Lake-effect snowstorms result largely from local instability over warm, humid waters of the unfrozen lakes (Eichenlaub, 1979). The storms are short because they have little or no upper air support and are not organized. As a result, they deposit most of their snow in a short period, and the intensity appears low when averaged over 6 hours. Mapping snowfall intensity from shorter observation time periods may cause the snowbelt areas to appear more significant. However, the length of snowfall periods, as indicated in Figures 8–10, argues somewhat against snowstorm length as a confounding problem. Nevertheless, only additional and more frequent monitoring could determine the intensity of frequent short bursts of snowfall that occur in lake-effect storms.

CONCLUSIONS

The maps presented raise questions about actual versus perceived snowfall intensity, data suitable for mapping snowstorm intensity, and the synoptic conditions producing high intensity storms. Lake-effect storms appear very intense. Whiteouts are common, and drifting snow coupled with large accumulated snow depths provide the impression of very intense storms. However, the total 6-hour snowfall catch of these storms, as indicated by the maps, suggests that these storms are not very intense.

Six-hour synoptic period summaries may not be adequate for mapping snowstorm intensity. Summary periods significantly longer than the event will always result in intensities being computed as smaller than actually occur. Significant and systematic seasonal and geographic variations in snowstorm length produce a confounding situation, because snowfall intensity is no longer a conservative value. It can vary with snowfall amount and with the length of the snowfall event when the summary period is longer than the event. The latter is likely true for the lake-effect areas of the Great Lakes. Mapping snowfall intensity based upon 1-hour summaries might show somewhat different patterns.

The patterns illustrated in the maps, if accurate, raise questions about mechanisms producing snowfall. They provide opportunities to identify regional mechanisms. Understanding of mechanisms allows extrapolation to areas of the globe where snowfall intensity measurements may not be available, but snowfall-producing mechanisms are similar.

The maps presented in this paper can be improved. We will combine hourly precipitation, temperature, and present weather observations to compute a surrogate hourly water equivalent of snow at each weather station. This will enable snowfall intensity to be mapped with greater temporal resolution. The 6-hour data maps provided a first estimate of patterns using actual snowfall data, but the maps may have masked regions experiencing high intensity, short-lived snowstorms, such as the Great Lakes lake-effect areas.

Though Great Lakes lake-effect storms have been studied extensively, much remains to be learned about their intensity, longevity, crystal type, visibility, and surface wind characteristics. The maps presented in this paper were intended to raise questions about the reasons for changes in snowfall intensity geographically, especially in the Great Lakes area.

SELECTED REFERENCES

Bates, R. and G. King, 1986: Intensity of Snowfall at Snow Experiments. In *Proceedings of the Sixth Annual EOSAEL/TWL Conference*, Atmospheric Science Laboratory (ASL) White Sands, New Mexico.

Bates, R., 1983: The Northeast Snowstorm of 15–16 December 1981. In *Proceedings of Snow Symposium II.* U.S. Army Cold Regions Research and Engineering Laboratory, 72 Lyme Road, Hanover, N.H., Special Report 83-4.

Bilello, M., 1967: Relationship Between Climate and Regional Variations. In *Snow Cover Density in North America.* U.S. Army Cold Regions Research and Engineering Laboratory, 72 Lyme Road, Hanover, N.H., Research Report 267.

Bilello, M., 1984: *Regional and Seasonal Variations in Snow Cover Density in the U.S.S.R.* U.S. Army Cold Regions Research and Engineering Laboratory, 72 Lyme Road, Hanover, N.H., CRREL Report 84-22.

Boucher, R., and J. Wieler, 1985: Radar Determination of Snowfall Rate and Accumulation. *Journal of Climate and Applied Meteorology*, Vol. 24, pp. 68–73.

Eichenlaub, V., 1979: *Weather and Climate of the Great Lakes Region.* University of Notre Dame Press, Notre Dame, Indiana.

Foster, D.J., and R.D. Davy, 1988: *Global Snow Depth Climatology.* USAF Environmental Technical Applications Center ETAC/TN, Scott AFB.

Hill, J., 1971: *Snow Squalls in the Lee of Lake Erie and Lake Ontario.* NOAA Technical Memorandum NWS ER-43, 21 pp.

Koh, G., 1989: Optical Technique for Characterizing Precipitation. In *Proceedings of Snow Symposium VII.* U.S. Army Cold Regions Research and Engineering Laboratory, 72 Lyme Road, Hanover, N.H., Special Report 89-7.

Lacombe, J., 1983: Technique for Measuring Mass Concentration of Falling Snow. In *Proceedings of SPIE.* The International Society of Optical Engineering, Vol. 414.

Ryerson, C, and R. Bates, 1989: Regional CONUS Snowfall Intensity and Inferred Global Patterns. In *Proceedings of the Tenth Annual EOSAEL/TWL Conference*, Atmospheric Science Laboratory (ASL) White Sands, New Mexico, pp. 335–345.

Stallabrass, J. 1985: Measurements of the Concentration of Falling Snow. *National Research Council of Canada Technical Memorandum 140*, pp. 389–410.

Wasserman, S., and D. Monte, 1972: A Relationship Between Snow Accumulation and Snow Intensity as Determined from Visibility. *Journal of Applied Meteorology*, Vol. 11, pp. 385–388.

Weinbeck, R., 1983: Time Variability of Lake Ontario Winter Precipitation Patterns. In *Proceedings, Eastern Snow Conference*, Vol. 28, Toronto, Ontario, pp. 195–197.

Annual Balance of North Cascade, Washington Glaciers Predicted From Climatic Records

M.S. PELTO

Department of Environmental Science
Nichols College
Dudley, Massachusetts 01570, U.S.A.

ABSTRACT

North Cascade glaciers supply 25% of the regions total summer water supply. The magnitude and timing of glacier runoff is determined by mass balance. From 1984-1989 the North Cascade Glacier Climate Project has monitored the annual balance of 10 North Cascade glaciers, using an efficient reconnaissance technique emphasizing probing, crevasse stratigraphy and ablation stakes. These 10 glaciers have a wide range of geographic characteristics (orientation, altitude, etc.), and provide a geographically representative group.

Three climatic variables are used to obtain a best fit equation of mass balance calculation mean ablation season temperature (AST), winter precipitation (WP), and ablation season length (ASL). Comparison of measured and calculated annual balance yields annual balance (bn) results with a correlation coefficient of 0.98, and a standard error of ±0.08 m/a of water equivalent. The degree of demonstrates that the overall annual balance of North Cascade glaciers can be accurately determined from local weather records. It must be cautioned that the mass balance of a specific glacier cannot be reliably calculated using the above equation. The mean annual balance of North Cascade glaciers from 1984 through 1989 is measured to be -0.20 m/a, and calculated to be -0.22 m/a.

INTRODUCTION

North Cascade glaciers supply 25% of the regions total summer water supply, hence, it is impossible to intelligently manage the regions water resources without understanding changes in glacier runoff. Glacier runoff from alpine glaciers is determined by the mass balance during the past several years (Bazhev, 1986). Thus, it is crucial to water resources management that glacier mass balance be determined in a timely fashion. Direct measurement is the standard method, however measurements are typically limited to an individual glacier, because of the financial costs and time required to complete measurements using traditional methods. Traditional methods emphasize determination of both winter and summer balances, requiring two field seasons (Ostrem and Stanley, 1969). Traditional methods often rely on runoff records

to determine ablation, and time consuming snowpit digging to ascertain snowpack depth. In this study emphasis is placed on more expeditious measurement techniques, such as probing, crevasse stratigraphy, and ablation stakes. The only practical way to monitor the annual balance of a large number of glaciers is utilization of time efficient methods or an army of assistants. A question that arises is, can mass balance be determined in a more timely fashion using climate records. This would provide cheaper and more timely data.

One of the primary objectives of the North Cascade Glacier Climate Project is to develop an accurate model for calculating the mass balance of North Cascade glaciers based on climate data. Two different approaches have been explored. The first, relating mass balance to daily classification of atmospheric circulation, using the techniques of Yarnal (1984). The second method utilizes climate data from eight weather stations in the North Cascades.

MEASUREMENT OF MASS BALANCE

The goal of the NCGCP mass balance study is determination of annual balance with reasonable accuracy on a number of glaciers rather than strict accuracy on a few glaciers. In this study, the annual balance is determined using direct field measurements late in the ablation season. Thus, only annual balance is measured, winter and summer balances are not determined.

In the fixed date method mass balance measurements are made on the same date each year, close to the end of the ablation season. Some ablation will probably occur after this date, but this ablation is measured as mass loss for the next hydrologic year. Thus, errors do not result from completing measurements prior to the end of the ablation season.

In the accumulation zone, annual accumulation layer thickness is determined using crevasse stratigraphy, and probing. The average density of measurements utilized in this study is 280 points/km^2, while the average density of measurements used in assessing the mass balance in the accumulation zone of Norwegian and other United States glaciers is 33 points/km^2 (Meier et al., 1971; Pytte, 1969). A comparison of the density of measurements used by the NCGCP, the U.S. Geological Survey (USGS), and Norges Vassdrags-Og Elektristetsvesen (NVE) are shown in Table 1.

The mean accumulation layer density observed in over 100 snowpits on ten different North Cascade glaciers from 1984 through 1987 is 0.58 g/cm^3, with a standard deviation of 0.01 g/cm^3. This narrow range indicates that late in the ablation season the density of snowpack on North Cascade glaciers is uniform, and need not be measured to determine mass balance. The lack of variation in snowpack density has also been noted on the South Cascade Glacier (Meier and Tangborn, 1965) and on the Blue Glacier in the Olympic Range of Washington (Armstrong, 1989). The uniformity of the density in the North Cascades results in part because ice lenses do not occur late in the summer.

Accumulation measurements are made using probing and crevasse stratigraphy; because both methods are quick and accurate. These two methods allow an unusually high density of measurements to be completed. At least 25% of the accumulation area on each glacier is a zone of overlap where both probing and

Table 1. The number of measurement sites used in mass balance studies by the United States Geological Survey (U) (Meier et al., 1971), Norges Vassdrags-Elektrissen (N) (Pytte, 1969), and by the North Cascade Glacier Climate Project (P).

Glacier	Ablation area		Accumulation area		Source
	Sites	Density pts./km^2	Sites	Density pts./km^2	
Gulkana	20	3	68	6	U
South Cascade	20	17	81	50	U
Wolverine	15	1	105	6	U
Alfotbreen	5	4	126	35	N
Austre Memurubre	8	3	316	52	N
Grasubreen	9	8	125	50	N
Hellstugubreen	13	7	216	144	N
Nigardsbreen	10	4	237	5	N
Vestre Memurubre	6	4	88	10	N
Columbia	3	10	165	250	P
Daniels	4	12	115	280	P
Eldorado	3	9	240	220	P
Foss	3	15	110	240	P
Lewis	2	30	31	310	P
Lower Curtis	3	10	185	280	P
Lynch	3	10	125	250	P
Rainbow	3	6	200	180	P
Spider	2	30	30	450	P
Yawning	2	20	40	260	P

crevasse stratigraphy are used to ensure unreliable data is not used. The standard deviation obtained in replicate measurements is smallest for crevasse stratigraphy, ±0.02 m and is ±0.03 m for probing.

The accumulation layer thickness is measured at each point to the nearest 0.01 m. Crevasse stratigraphy measurements are conducted only in vertically walled crevasses with distinguishable dirt bands. Crevasses lacking vertical walls yield inaccurate depth measurements. In the North Cascades the ablation surface of the previous year is always marked by a 2-5 cm thick band of dirty firn or glacier ice. The depth to the top of this dirty band is measured at several spots on each crevasse wall within a space of several meters. The average thickness is the accumulation layer thickness at that point. Crevasses have been avoided previously because of obvious dangers and the false density readings that can occur due to the snowpack having a free air face. Density readings from crevasse walls are not used and crevasses are approached on skis, which are not removed during measurement.

Since North Cascade glaciers rarely have ice lenses, probing is also an accurate method for measuring accumulation layer thickness. The probe is driven through the snowpack until the previous year's ablation surface is reached. This surface of glacier ice or hard dirty firn cannot be penetrated. The probing instrument is a 2.5 m long, 1/2 inch thick copper tube which is driven through the snowpack using a two pound weight. Probing transects are used in regions with few crevasses and are used to check the accuracy of

crevasse stratigraphic measurements. Probing transects are started from bare glacier ice and continued across the glacier to a snow depth of 2.5 m. At depths greater than 2.5 m, it becomes difficult to accurately distinguish the previous ablation surface. In the North Cascades, snowpack in excess of 2.5 m at the conclusion of the ablation season is rare. Where snowpack depth does exceed 2.5 m, glacier flow is typically extending, resulting in numerous open crevasses.

To ensure that mass balance measurements are consistent from year to year, measurements are made at a fixed network of points. The network is fixed spatially with respect to the surrounding bedrock walls.

Annual balance measurements are reported in meters of water equivalent, the product of the accumulation layer thickness and density of the snow pack (0.58 g/cm^3). Internal accumulation and superimposed ice are insignificant components in the mass balance of North Cascade glaciers (Meier and Tangborn, 1965). Errors in depth measurement are +0.05 m and the standard deviation in density is ± 0.01 g/cm^3. The resulting error in annual assessment for the accumulation zone is ± 0.08 m. All errors in this study are for one standard deviation of the three observed data values for each measurement site. The density of measurements in the accumulation zone is considerably greater than is typical for glacier mass balance surveys (Table 1), which results in smaller errors.

Ablation triangles are used to determine annual ablation down glacier of the snowline. An ablation triangle consists of three 3.3 m long fiberglass poles driven or drilled into the glacier at 3 m spacing forming an equilateral triangle. Three to four triangles are emplaced on each glacier. Longer stakes are too cumbersome to transport and emplace. Ablation measurements are made at nine points along the edge of the triangle at the conclusion of the ablation season.

Ablation triangles are placed in a sequence on areas of the glacier that first lose their snow cover to areas where snow cover persists for a significant portion of the ablation season. Each ablation triangle is then representative of ablation for other portions of the glacier that lose snowpack simultaneously. In the fixed-date method of mass balance measurement, the ablation season is assumed to end at the same time each year, this date marks the end of the hydrologic year for that glacier. Mass balance measurements are completed on the same dates each year. In some years, such as in 1987, the ablation season extends beyond the fixed date. Ablation occurring after this date will be measured as part of the mass balance of the next hydrologic year. Snow ablation occurring after mass balance measurement is completed and before the accumulation season begins is monitored by placing a single ablation triangle in the accumulation zone after measurements have been completed. This ablation triangle is checked the next year to determine the amount of snow ablation that occurred during the previous fall.

The stakes are drilled into the ice at the end of the ablation season and after the initial late July-early August measurement. Redrilling of the stakes is necessary to prevent melting out. Drill hole settling averages less than 0.05 m/a. The error in annual ablation measurements is ± 0.18 to 0.22 m, due to ice density variations, low sampling density, and stake settling.

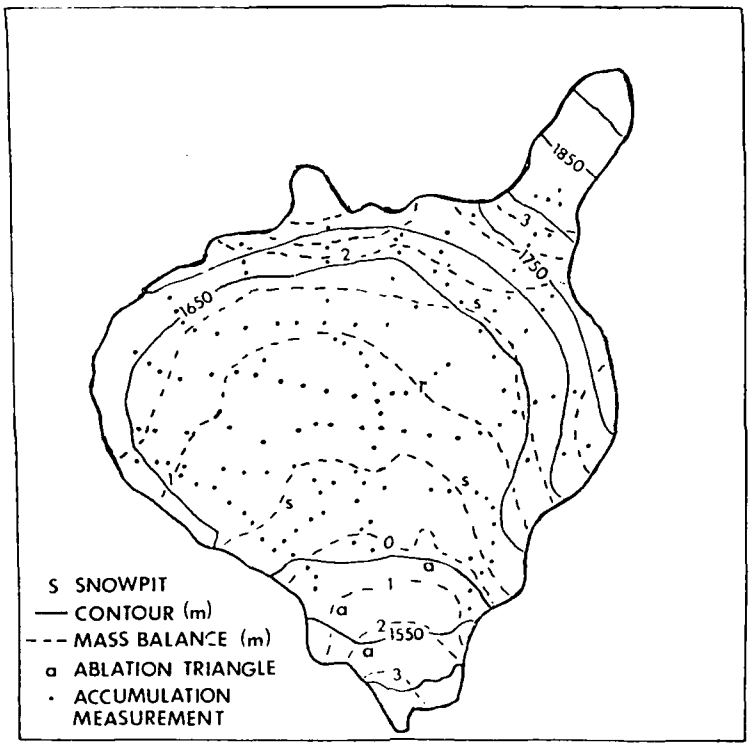

Figure 1. Mass balance map of the Lower Curtis Glacier in 1986. Mass balance is contoured in meters of water equivalent.

Because each measurement is the mean of nine measurements in a 25 m^3 area, the error of individual measurements is small. There are three to four measurement sites on each glacier. The sampling density is low at 10-30 points/km^2, but is comparable to the density used by the USGS and NVE noted in Table 1 (Meier et al., 1971; Pytte, 1969). On South Cascade Glacier a measurement density of 3 or 4 points/km^2 was used between 1973 and 1982 with a reported error of ±0.12 m (Krimmel, 1989). On Blue Glacier a density of 4 point/km^2 has been used (Armstrong, 1989). Measurement error in the ablation zone is larger than for other studies, despite a higher density of measurements, because the total number of measurements is small.

A mass balance map is then compiled for each glacier (Fig. 1). The mass balance for the entire glacier is calculated by summation of the product of glacier area within each 0.10 m mass balance contour, and the net balance in that interval. The error in mass balance calculation for North Cascade glaciers is ±0.12 to 0.15 m, except during years of extreme ablation when the error is higher. Errors increase as the ablation area increases and the accumulation zone, where better accuracy is possible, shrinks. The annual balance of 10 North Cascade glaciers is shown in Table 2.

Table 2. The annual balance of ten North Cascade glaciers, from direct measurements, in meters of water equivalent. See Figure 2 for glacier locations.

Glacier	Area km^2	1984	1985	1986	1987	1988	1989
Columbia	0.9	+0.21	-0.31	-0.20	-0.63	+0,14	-0.09
Daniels	0.5	+0.11	-0.51	-0.36	-0.87	-0.15	-0.37
Eldorado	1.4	+0.25	-0.14	-0.02	-0.45	+0.19	-0.06
Foss	0.7	+0.51	-0.69	+0.12	-0.38	+0.23	+0.09
Lewis	0.1	+0.67	-1.16	-0.34	-0.48	-0.31	-0.60
Lower Curtis	0.9	+0.39	-0.16	-0.22	-0.56	-0.06	-0.29
Lynch	0.8	+0.33	-0.22	-0.07	-0.30	+0.17	+0.03
Rainbow	1.5	+0.58	+0.04	+0.20	-0.26	+0.43	-0.24
Spider	0.1	+1.12	-0.63	+0.30	-1.15	+0.73	-0.15
Yawning	0.2	+0.09	-0.23	-0.14	-0.47	-0.06	-0.19

MASS BALANCE CALCULATION

The 8 North Cascade weather stations are at elevations 700-1800 m lower than the mean elevation of the glaciers (Fig. 2). Stevens Pass is the highest station at 1245 m, 700 meters below the mean elevation of North Cascade glaciers. The other seven stations are Stampede Pass 1210 m, Stehekin 388 m, Concrete 46 m, Holden 970 m, Diablo Dam 272 m, Upper Baker Dam 210 m, Ross Dam 379 m. It has previously been demonstrated that the four climatic variables controlling glacier mass balance are winter precipitation (November-April), ablation season temperature (May-September), summer cloud cover (June-August) and freezing levels during May and October precipitation events (Tangborn, 1980: Pelto, 1988). The two prime variables being winter precipitation and ablation season temperature, these two variables account for 81% of the variation in annual balance on the 11 glaciers where mass balance has been measured (Tangborn , 1980; Pelto, 1989). In southern British Columbia and in Washington winter precipitation is the dominant factor.

The importance of freezing level, is that snows falls above the freezing line, which may intersect the glaciers during October and May. From November through April North Cascade glaciers are above the freezing line except on rare occasions. May and October precipitation that falls when the temperature is below 5°C at Stevens Pass will fall as snow on North Cascade glaciers, and is included as winter precipitation. Thus, freezing levels are accounted for but not as a separate variable.

At present no cloud cover observations are being made in the North Cascades. Tangborn (1980) demonstrated that the correlation coefficient for summer cloud cover and summer temperature is approximately 0.90 in the North Cascade region. Thus, major errors will not result from not considering summer cloud cover separately from ablation season temperature.

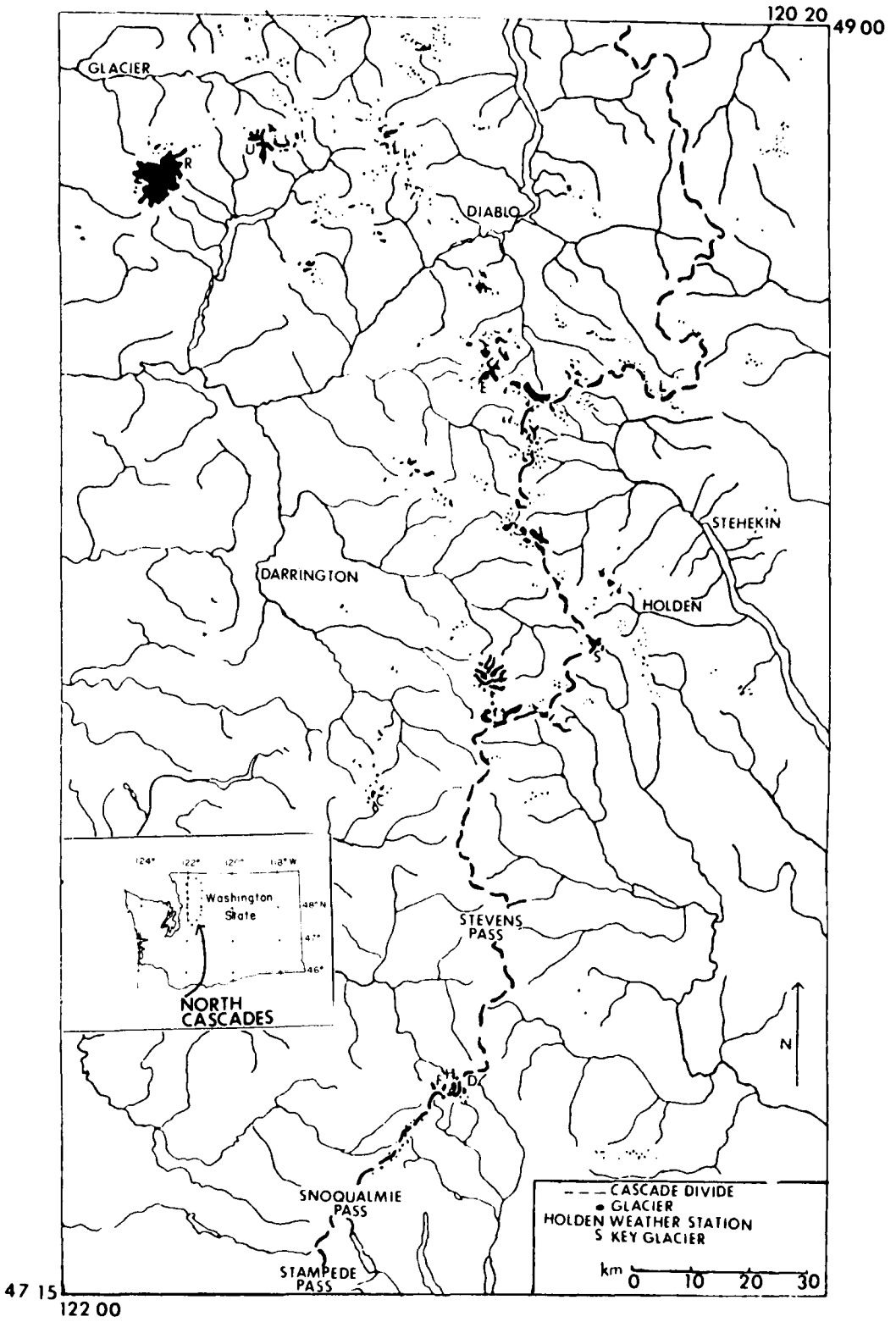

Figure 2. Location of glaciers and weather stations in the North Cascades.

Table 3. Climatic conditions in the North Cascades 1984-1988 compared to the long term mean. The data is the mean for eight North Cascade stations. This data is used in equation 1 and 2. Accumulation season precipitation is all precipitation occurring between October 1 and May 31 when the temperature at Stampede Pass is below 5°C. Ablation season temperature is the mean temperature from May 1 to September 30. Ablation season length is the period in days from the first occurrence of three consecutive days with mean temperature above 7°C at Stampede Pass to the last occurrence.

Year	Accumulation season precipitation (m)	Ablation season temperature (°C)	Ablation season length (days)
1984	1.95	12.7	136
1985	1.34	13.8	146
1986	1.54	13.4	156
1987	1.58	14.2	184
1988	1.69	13.5	151
1989	1.76	13.2	176
Mean	1.62	13.5	155
Mean 1920-1980	1.87	12.8	144

Multiple linear regression produced a best fit equation using ablation season temperature and winter precipitation data shown in Table 3. Input data are the mean temperature and mean precipitation for the eight stations. The climate input data are entered without units, as there is no clear method to change temperature into m.

$$bn = WP - [(AST-5)(21.5)] \quad (1)$$

Annual balance (bn) is in cm of water equivalent, Winter precipitation (WP) is entered in cm, and ablation season temperature (AST) is entered in degrees Celsius. Equation 1 is reasonably accurate when compared to the directly measured mass balance having a standard deviation of ±0.18 m/a, but in 1987 it is apparent the equation failed to yield a reasonable result (Table 4). The reason was the unusually early start of the ablation season in mid-April. An ablation season length variable is needed to account for the fact that the ablation season may begin before May 1 or extend beyond October 1. The resulting increase in ablation due to an extended ablation season cannot be addressed by using a mean temperature for the entire ablation period because the temperatures during the early and latter part of the ablation season are lower than the mean, and would reduce the mean AST. Ablation season length (ASL) is the interval between the first two consecutive days when the mean temperature at Stevens Pass exceeds 7°C and the last such occurrence. This temperature marks the boundary below which negligible ablation occurs on North Cascade glaciers. The multiple linear regression best fit equation utilizing ablation season length, winter precipitation and ablation season temperature proved more accurate and reliable than equation 1 (Table 4).

Table 4. Measured annual balance of ten North Cascade glaciers, and calculated annual balance of North Cascade glaciers using Equations 1 and 2.

Year	Mass balance measured(10)	Mass balance predicted	
		Eq. 2	Eq. 1
1984	+0.45	+0.48	+0.30
1985	-0.54	-0.46	-0.56
1986	-0.19	-0.29	-0.27
1987	-0.72	-0.79	-0.39
1988	-0.02	-0.11	-0.13
1989	-0.18	-0.10	0.00

$$bn = WP - [(AST-5)(21)(ASL/150)] \quad (2)$$

The standard deviation for predicted versus measured annual balance is ±0.09 m/a. The derived relationship is based on six years of record. This is a short time span and undoubtedly minor adjustments will result with a longer record. A six year period of record would be insufficient to determine an accurate relationship between a single dependent and independent variable. However, predicting the mass balance, from three independent variables with a six year period of record yields an equation that is significant and accurate.

Equations 1 and 2 cannot be applied with any accuracy to a single glacier. Table 2 indicated that considerable fluctuations occur between glaciers for a given year. Calculating the correlation coefficient for winter precipitation and ablation season temperature and annual balance indicates considerable variation as well. The reason for the variation in climate sensitivity and hence annual balance is the difference in geographic and topographic characteristics of the glacier.

Why is a simple equation based on three climatic variables sufficient to accurately predict mass balance in the North Cascades? Applying the same methods to large Alaskan glaciers has proved inaccurate. It is likely that the small size of North Cascade glaciers is the key. Because of their small size the entire area of a North Cascade glacier experiences the same regional and local weather systems. True the microclimate varies across the surface of North Cascade glaciers, but these fluctuations are due to topographic setting which is constant from year to year. On larger Alaskan glaciers different portions of the glacier will experience significantly different weather conditions.

The second method tested to predict glacier mass balance uses synoptic scale 500 millibar atmospheric circulation data to predict glacier mass balance using techniques developed by Yarnal (1984). This method utilized the NOAA Daily Weather Map series, classifying each day as one of 18 potential

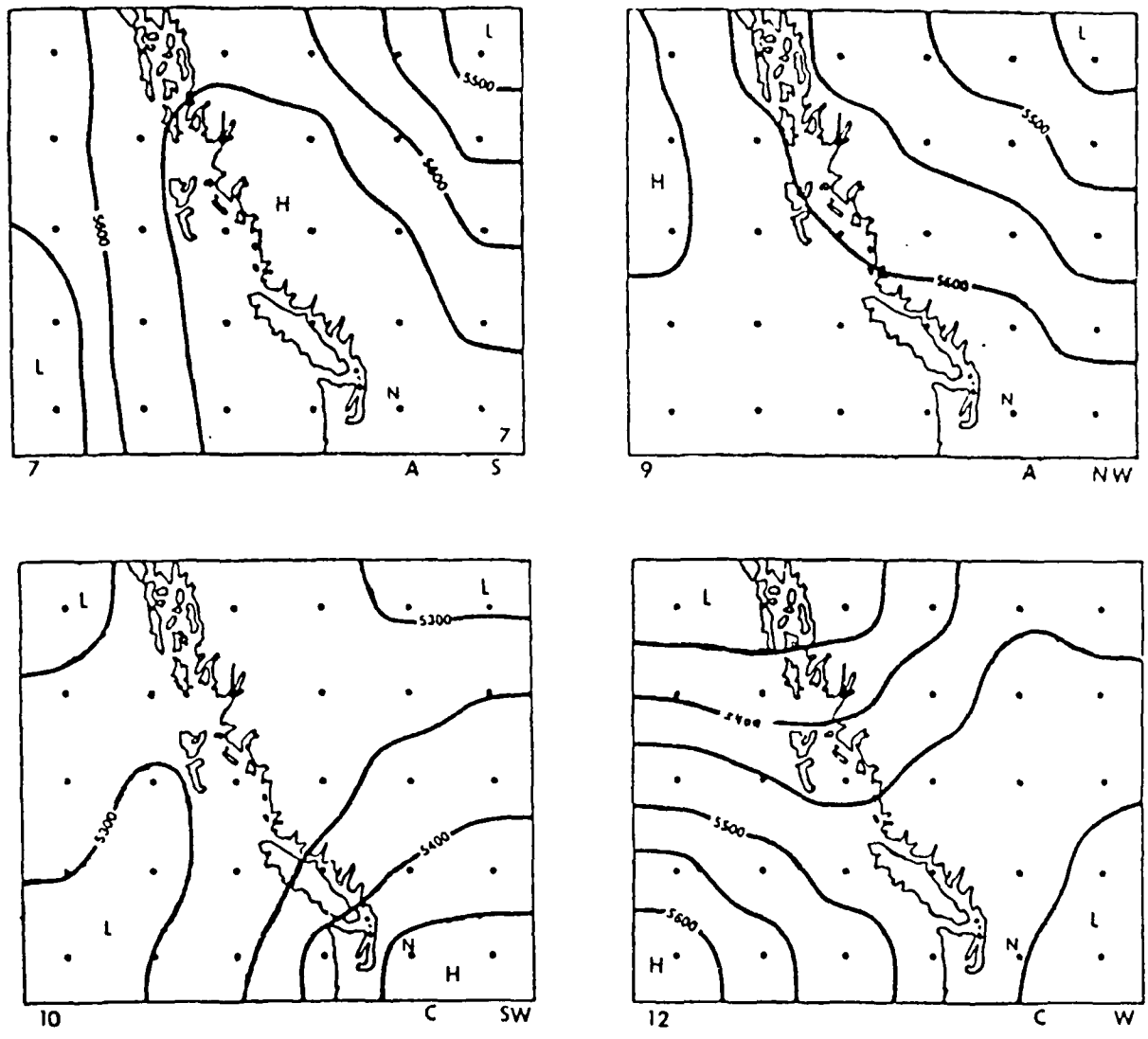

Figure 3. 500 mb pressure distribution maps used in classifying daily atmospheric circulation (Yarnal, 1984). These are four of the eighteen circulation types that account for 91% of all the days in the North Cacades. Circulation types are designated as anticyclonic(A), cyclonic (C) or intermediate (S). N=North Cascades, H=high pressure center, L=low pressure center.

circulation types. This task was completed in the Pacific Northwest for the 1982-1988 period, and 93% of the days could be classified into of the 18 circulation types (Fig. 3). The idea being that each circulation type would yield fairly specific weather conditions in the North Cascades and hence would have a predictable impact on North Cascade glacier mass balance. However, though the general climatic conditions for a given circulation type such as cool and wet or cool and dry, were seasonally consistent, the actual amount of precipitation or actual temperature proved to be to wide ranging for each circulation type to provide an accurate equation. Thus, atmospheric circulation records cannot yet be used to accurately predict North Cascade glacier mass balance. This conclusion is supported by Walters and Meier (in press), who noted that the primary changes in atmospheric circulation explain

62% of the annual variation in mass balance on Pacific Northwest glaciers. This is a correlation coefficient of 0.79 not bad, but far short of the 0.98 achieved using local weather records.

CONCLUSIONS

A method has been developed to efficiently monitor the mass balance of North Cascade glaciers with an accuracy of ±0.12-0.15 m/a. An equation to accurately predict the annual balance of North Cascade glaciers from climate records has also been developed. The mean error is ±0.09 m/a for North Cascade glaciers as a whole. The equation is not reliable for application to a specific glacier. From 1984 through 1989 the mean annual balance on North Cascade glaciers was -0.20 m/a. The cause of the negative mass balance is primarily due to the decrease in winter precipitation from the long term mean (Table 3).

The next step in this study is to test a model for predicting the annual mass balance for a single watershed, so as to improve forecasts of streamflow in glaciated drainage basins.

REFERENCES

Armstrong, R.A. 1989. Mass balance history of the Blue Glacier, Washington. In, Glacier Fluctuations and Climate Change, Edited by J. Oerlemans Kluwer Academic, London, 193-203.

Bazhev, A.B. 1986. Infiltration of meltwaters on temperate and cold glaciers. USSR Data of Glaciological Studies, 58: 165-170.

Krimmel, R.M. 1989. Mass balance and volume of South Cascade Glacier, Washington 1958-1985. In, Glacier Fluctuations and Climate Change, Edited by J. Oerlemans Kluwer Academic, London, 203-215.

Meier, M.F. and W.V. Tangborn 1965. Net budget and flow of the South Cascade Glacier, Washington. J. Glaciol., 5(41), 547-566.

Meier, M.F., Tangborn, W.V., Mayo, L.R. and Post, A. 1971. Ice and water balances at selected glaciers in the United States. Combined ice and water balances of Gulkana and Wolverine Glacier, Alaska and South Cascade Glacier, Washington, 1965 and 1966 hydrologic years. U.S. Geologivcal Survey Professional Paper 715-A.

Ostrem, G. and A. Stanley 1969. Glacier mass balance measurements.Canadian Department of Energy, Mines and Resources Norwegian Water Resources and Electricity Board.

Pelto, M.S. 1988. The annual balance of North Cascade, Washington Glaciers measured and predicted using an acitivity index method. Journal of Glaciology 34(117), 194-200.

Pelto, M.S. 1989. Time series analysis of mass balance and climate northwest North American Glaciers. IAHS publication no. 190 (Symp. on Glacier and Snowcover Variations, Baltimore, May, 1989) 6-11.

Pytte, R. 1969. Glacio-Hydrologiske Undersokelser i Norge 1968. Norges Vassdrages-og Elektrisitetsvesen, Rapport Nr. 69-1.

Tangborn, W.V. 1980. Two models for estimating climate-glacier relationships in the North Cascades, Washington, U.S.A. Journal of Glaciology 25(91), 3-21.

Walters, R. and M. Meier, in press. Variability of glacier mass balances in western North America. In, Aspects of Climate Variability in the Pacific and Western America's. AGU Monograph.

Yarnal, B. 1984. Relationship between synoptic scale atmospheric circulation and glacier mass balance in SW Canada during the IHD, 1965-1974. Journal of Glaciology, vol. 30, no. 105, p. 188-198.

The Role of Natural Flaws and Variability in Ice-Cover Fracture During River-Ice Break-Up

M.N. DEMUTH AND T.D. PROWSE

National Hydrology Research Institute
Environment Canada
Saskatoon, Saskatchewan S7N 3H5, Canada

INTRODUCTION

River-ice break-up can initiate if downstream forces exceed the resistance offered by the ice cover and its boundary support zones. Two general scenarios describe break-up: i) *thermal* break-up, characterized by low downstream forces and minimal ice-cover resistance owing to extensive ice and support deterioration; ii) *mechanical* break-up (or *dynamic*), involving the failure of more competent ice covers by the high forces associated with river waves. River waves are long-period, unsteady flow phenomena resulting from rapid run-off events, ice-jam releases and dam releases. The effect of river waves is to augment the downstream forces while inherent increases in stage can reduce the resistance offered by the cover support zones.

Prowse and Demuth (1989) categorized ice-cover failures based on observations made at a variety of river scales, hydraulic and cover conditions. *Global* and *Frontal* failure modes were identified with respect to the scale of deformation and the rate of failure. This classification, in part, attempts to emphasize the crucial effects of scale and deformation rate on the forces required to overcome ice-cover resistance. To date, the fracture characteristics of river-ice break-up, during spring run-off or wave transmission, have been described by numerous investigators. For example, physical models of large-scale transverse fracture due to wave-slope flexure (Billfalk, 1982; Beltaos, 1990) and horizontal flexure arising from planform shear-stress variation (Beltaos, 1990) have been proposed. Such models assume vertical and reach-wise homogeneity in the mechanical properties of the ice cover. More recently, Ferrick and Mulherin (1989) have characterized break-up as two distinct processes which generate failure and ice-cover movement depending on hydraulic conditions: i) *Support* break-up - large ice sheets will move downstream upon failure of the bank support zone (hinge cracks); ii) *Strength* break-up- where ice-cover fragmentation takes place at a smaller scale along a distinct "rubble" front while bank shear adequately resists large translations downstream.

Of significant influence in the characterization of resistance, is the heterogeneity of the ice cover. The degree and magnitude of this variability is intrinsic in determining the dominant ice failure process and thus can largely determine the forces necessary for the initiation and progression of break-up. It is proposed that the variability itself can, at extremes, be an intrinsic part of generating an ICE-Overthrust-Flexure-Fracture sequence (ICEOFF) leading to the non-simultaneous but progressive failure of distinct zones in the intact ice sheet (Fig. 1). ICEOFF has been observed at a variety of dimensional scales and levels of downstream forcing. It can occur when large sheets begin to converge on the downstream intact cover and through overthrusting cause further fracture downstream as well as fracturing the converging sheet into smaller plates.

Fig. 1 The ICEOFF process during break-up, Mackenzie River, N.W.T., Canada.

ICE RESISTANCE

The resistance of an ice cover encompasses its internal strength and the boundary states (thickness, lateral extent and support conditions) which influence its kinematic behaviour and mode of failure. Observations indicate that the variability of ice-cover composition and mechanical properties plays an important role in characterizing resistance. However, defining resistance is a difficult task given the dearth of concomitant observations detailing ice failure types and the accompanying level of downstream forcing. The body of river-ice strength data, particularly that detailing the pre-break-up deterioration and its large-scale spatial variability, are limited primarily to those of Ashton (1985), Bulatov (1970), Kozitsky and Bybin (1967) and more recently by Prowse *et al.* (1989, 1990).

The effect of scale and variability on ice resistance cannot be ig ored and efforts in the field of ice-structure interaction have begun to improve our understanding of large-scale ice failure. In a review addressing the perception of scale effect, Timco (1989) presents a comprehensive body of strength data and notes that their strength-scale characteristics are largely inconclusive. The principle question ultimately posed is whether the same failure modes exist, during small- to medium-scale laboratory and field testing, as in processes occurring at full-scale; and more specifically, what constitutes a flaw with respect to the evolution of failure?

Ice Cover Flaws and Variability

Flaws and variability in the context of the present discussion are limited to large-scale phenomena including: i) structural discontinuity in reaches comprised of a variety of structural ice forms, thicknesses and aerial extent, and ii) cracks or line failures resulting from thermal strain or previous ice failure (although important, micro-scale phenomena resulting in crack initiation and propagation are not discussed). The effect of these flaws may be to modify ice-cover confinement providing conditions which promote certain types of ice interaction and deformation; a common one is ice overthrust.

Structural Variability

Thermal and hydraulic freeze-up conditions strongly control the growth and distribution of ice types in the river system (Fig. 2). Types most commonly found to make up the competent portion of typical ice sheets include: i) primary and superimposed ice; ii) secondary ice, and iii) freeze-up jam/accumulation ice. Besides differing in their mechanical properties, their characteristic decay by radiation is also markedly different. For example, the decay of columnar ice structures can be significant under the influence of short-wave radiation and may result in a zone possessing little compressive or tensile strength whereas a cover having a granular white-ice surface is effectively insulated from short-wave radiation.

Extreme variations in ice thickness due to variable cover formation processes can result in localized zones of relatively thin ice. The strength of these zones can be further reduced by hydraulic erosion and surface ablation. Fragmented ice or rubble fields, produced during failure events at freeze-up or in advance of the main break-up, may provide a non-uniform line-failure possessing geometry likely to promote ice overthrust.

Fig. 2 Mackenzie River prior to break-up showing variability in ice-cover types.

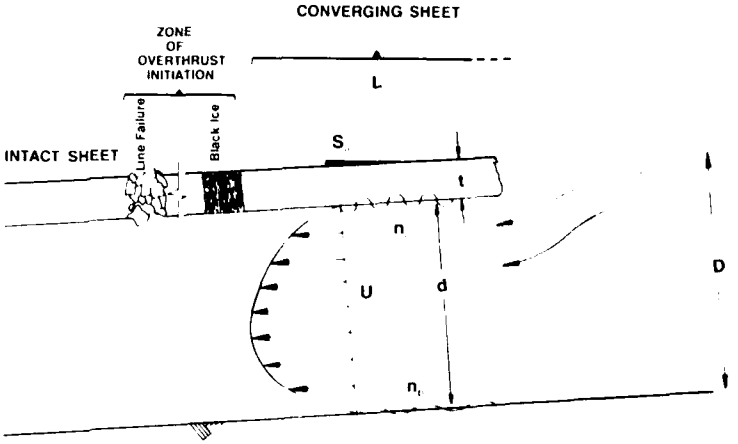

Fig. 3 A schematic of ice-cover convergence illustrating the hydro-mechanical forcing components.

Thermal Cracking

The process of thermal cracking is initiated if changes in ice temperatures induce sufficient strain. The degree to which thermal cracks become operative depends strongly on thermal conditions subsequent to their formation. In floating ice, thermal cracks may heal should infiltrating water refreeze. These flaws may re-manifest under certain thermal conditions such as radiation melt. Observations by the authors (unpublished) indicate that re-frozen thermal cracks in undeteriorated columnar ice samples subject to flexural loading, do not influence the flexural strength until warming and localized radiation melt re-manifested the flaw. This relatively uniform line-failure may have geometry likely to create a zone of ice overthrust.

OVERTHRUST KINEMATICS

It is proposed that the flaws described above, if appropriately established, could lead to an overthrust (Figs. 1,3). A zone of deteriorated black ice, for example, could fail under compressive forces and allow the upstream sheet to converge on the intact cover. In the ICEOFF scenario it is assumed that sufficient forces, due to vertical turbulence and brash-ice buoyancy, are imparted to the upstream sheet, to cause it, in most cases, to over ride the intact cover. Field observations suggest the tendency is to overthrust rather than to underthrust. As the converging sheet overthrusts the resulting vertical- and axial-end loads (Figs. 4,5) may fail the cover in flexure.

Overthrust Uplift and Submergence

The precise mechanism of overthrust is largely unknown except that it is a highly variable process which relies on the existence of some form of line failure or discontinuity, having the geometry to promote deformation in the vertical plane along the discontinuity (Fig. 3). Nevertheless, by equating the work done during an incremental overthrusting distance to the potential energy gained by the uplifting and submerging ice covers acting against gravity and

buoyancy respectively, it can be shown that the horizontal force $\Sigma F_h'$ (prime denotes per unit width) required is:

$$[1] \qquad \Sigma F_h' = \frac{\rho_i \, g \, t \, h_u \left[C + \frac{\rho_w}{\rho_i} - 1 \right]}{C + 1}$$

where ρ_i and ρ_w are the density of ice and water, g is the acceleration due to gravity, t is the ice thickness, h_u represents the height, above the hydrostatic water level (HWL), of the uplifted portion of the overthrust zone and C is the ratio of h_u to the depth below HWL attained by the submerged portion. For t = 1.0 m, $h_u \approx 1$ and $C \approx 1$, $\Sigma F_h' \approx 4.9$ kN·m^{-1}. Further details of this analysis can be found in Demuth and Prowse (1990).

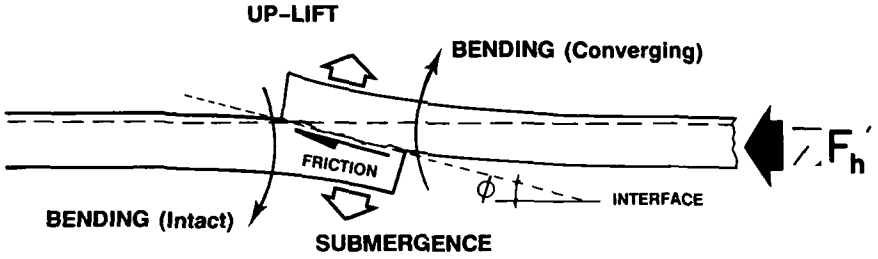

Fig. 4 The kinematic elements of ice overthrust.

Overthrust Flexural Failure

Flexural stresses, generated by the action of overthrust, can be described by considering the elastic deformation of an elastically-founded semi-infinite beam, subject to vertical- and axial-end loads. The differential equation governing the vertical deflection of such a beam is:

$$[2] \qquad EI \frac{d^4z}{dx^4} + N \frac{d^2z}{dx^2} + kz = 0$$

where E is the effective strain modulus for ice, N is the axial (compressive) load, k is the foundation stiffness ($\rho_w g \approx 10$ kN·m^{-3}) and I is the section modulus of the beam which is analogous to the plate rigidity $t^3/12(1-\nu^2)$ where ν is the Poisson ratio and z represents the vertical deflection at position x along the beam length. The effect of axial load N on the bending moment magnitude and distribution is shown in Fig. 5. Once overthrust has taken place, $N \rightarrow 0$, and the vertical overthrusting force at failure P_f' can be determined from:

$$[3] \qquad P_f' = -\frac{S_{tf}}{6} \cdot \left[\frac{3kt^5}{E(1-\nu^2)^3} \right]^{1/4} \cdot \frac{e^{\pi/4}}{\sin(\pi/4)}$$

where S_{tf} (MPa) is the tensile strength of ice as measured by flexural tests (see Demuth and Prowse, 1990; Mellor, 1986 for additional details). Substituting t = 1.0 m, E = 3 GPa, ν = 0.3 and taking pre-breakup values for S_{tf} in the range of 0.1 - 0.4 MPa (Prowse *et al.*, 1990; Mellor, 1986), P_f' ranges from approximately 3.1 kN·m^{-1} to 12.5 kN·m^{-1}.

For small overthrust slopes the $\Sigma F_h'$ necessary to impart P_f can be estimated from:

$$[4] \qquad \Sigma F_h' \approx \mu_k \cdot P_f'$$

where μ_k is the coefficient of kinetic friction. Taking μ_k = 0.3, we have, for the above ranges in tensile strength, $\Sigma F_h' \approx 0.9 \leftrightarrow 3.8$ kN·m^{-1}.

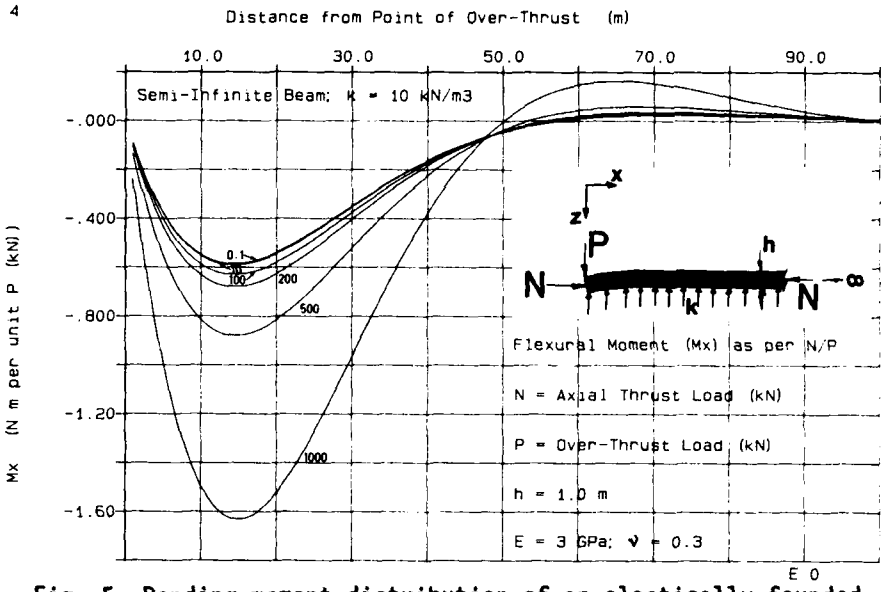

Fig. 5 Bending moment distribution of an elastically-founded beam subject to vertical- and axial-end loads.

There are a number of other related processes which can affect the transfer of forces during overthrust, whose relative importance are unknown. One example is ice roughness and its effect on the frictional resistance of the overthrust interface. Frictional resistance could increase where a zone of decayed crystals having columnar or needle-shaped structures is sheared and ploughed over as overthrust takes place. Water is often flooded on the surface due to turbulent wash or infiltration during the deflection of the intact cover; this tends to reduce the frictional resistance of the overthrust interface.

DOWNSTREAM FORCING

The above values for the required level of downstream forcing for uplift/submergence and subsequent flexural failure can be evaluated by considering the magnitude of downstream forces under typical break-up conditions. In a case study examining ICEOFF, Demuth and Prowse (1990) evaluated the role of individual ice-cover and waterway parameters and their effect on downstream forces (Table 1). Downstream forces are divided into two major categories: i) body force derived from the downstream component of the ice-cover weight (F_w); ii) hydrodynamic forces derived from leading-edge form-drag (F_t) and friction-drag (F_d), imparted to the ice cover by under-ice fluid flow (Fig. 3). These components are estimated using (Michel, 1978):

[5] $$F_w' = \rho_i \, t \, L \, S_o \, g$$

[6] $$F_t' = (1-d/D)^2 \, U^2 \, D \, \rho_w/2g$$

[7] $$F_d' = \rho_w \, d \, S_o \, n_i^{3/2} \, L \, g \, /2n_c^{3/2}$$

where L is the length of the converging ice-cover, S_o is the energy slope, d and D are the under-ice and upstream waterway depths, U is the mean under-ice velocity and n_i and n_c represent Manning's roughness coefficient for ice and the composite section.

The case study found that, under typical break-up conditions, the components of downstream forcing were of sufficient magnitude to precipitate ICEOFF. Notably, the magnitude of downstream forcing was several orders less than that required for simple elastic buckling. F_d and F_w are typically the greatest contributors, however F_t could play an important role if

U is high and when t/D increases significantly. Of pivotal importance is the role played by n_i and n_b and their obvious effect on F_d given any significant roughness variability through a reach.

Table 1
Hydro-Mechanical Forcing Magnitudes and Ice-Cover and Waterway Parameters

t	D	d	U	S_o	L	n_i	n_b	n_c	F_t'	F_d'	F_w'
1.0	5.0	4.08	3.0	0.001	100	0.028	0.028	0.028	0.08	2.00	0.90
1.0	5.0	4.08	3.0	0.001	100	0.028	0.140	0.095	0.08	0.32	0.90
1.0	5.0	4.08	3.0	0.001	100	0.028	0.006	0.019	0.08	3.58	0.90
1.0	5.0	4.08	3.0	0.001	100	0.056	0.011	0.038	0.08	3.57	0.90
1.0	5.0	4.08	3.0	0.001	1000	0.028	0.006	0.019	0.08	35.80	9.03
1.0	5.0	4.08	3.0	0.005	100	0.028	0.006	0.019	0.08	17.90	4.51
1.0	5.0	4.08	1.0	0.001	100	0.028	0.006	0.019	0.01	3.58	0.90
1.0	5.0	4.08	5.0	0.001	100	0.028	0.006	0.019	0.22	3.58	0.90
1.0	3.0	2.08	3.0	0.001	100	0.028	0.006	0.019	0.13	1.83	0.90
m	m	m	$m \cdot s^{-1}$	$m \cdot m^{-1}$	m	dmls			$kN \cdot m^{-1}$		

CONCLUSIONS

Estimates indicate that typical downstream forces during typical break-up conditions can be of sufficient order such that overthrust flexural failures are possible. Additional field data is required, describing the collective and relative magnitude of the downstream forcing with coincident observations of ice failure. The probability of an overthrust event occurring will depend largely upon the distribution and variability of ice structure and ice strength. Evidence suggests that typical river-ice covers exhibit considerable variability and possess flaws likely to promote ICEOFF. Observations of dynamic breakup indicate that knowledge of full-scale failure modes are important when applying ice strength data in an attempt to characterize the force-resistance balance.

LITERATURE CITED

Ashton, G.D. 1985. J. Energy Res. Tech. 107, 177-182.

Beltaos, S. 1990. Can. J. Civ. Eng. 17, 173-183.

Billfalk, L. 1982. USACRREL Report 82-3, 17 pp.

Bulatov, S.N. 1970. USACRREL Translation, IR 799, 120 pp.

Demuth, M.N. and T.D. Prowse 1990. NHRI Contribution No. CS-90026. Proc 1990 Northern Hydrology Symposium (submitted), 16 pp.

Ferrick, M.G., and N.D. Mulherin 1989. USACRREL Report 89-12, 21 pp.

Kozitsky, I.E. and E.A. Bybin 1967. DOE-NHRI Translation, 37 pp.

Mellor, M. 1986. in Geophysics of Sea Ice, Untersteiner ed., NATO ASI Series, 1196 pp.

Michel, B. 1978. in Ice Mechanics, 499 pp.

Prowse, T.D. and M.N. Demuth 1989. Proc 46th ESC, 237-241.

Prowse, T.D., M.N. Demuth and H.A.M. Chew 1989. NHRI No. CS-89053, J. Nordic Hydrology (in press).

Prowse, T.D., M.N. Demuth and H.A.M. Chew 1990. NHRI No. CS-89087, J. Hydr Res (in press).

Timco, G.W. 1989. Proc Workshop on Ice Properties, NRCC Tech Memorandum No. 144, 183-206.

The Lake Ontario Winter Storms Experiment (LOWS) and the Lake-Effect Snow Observation Network (LESON) Report for the 1989–1990 Snow Season

J.J. FERLITO, C. BEDFORD, T. PALMA AND S. OSBORNE

Galson Technical Services, Inc.
6601 Kirkville Road
East Syracuse, New York 13057, U.S.A.

R.B. SYKES, JR.

(Retired) State Univeristy of New York, Oswego
Oswego, New York 13126, U.S.A.

R. CAIAZZA

Niagara Mohawk Power Corporation
Environmental Affairs Department
Syracuse, New York 13202, U.S.A.

The 1989-90 snow season, especially dealing with lake-effect snow was the subject of The Lake Ontario Winter Storms (LOWS) experiment, sponsored Niagara Mohawk Power Corporation. The Central New York American Meteorological Societies Lake Effect Snow Observers Network (LESON) was invited to participate in the LOWS experiment at the request of Niagara Mohawk. Galson Technical Services, MesoWeather division was employed to operate this observer network.

The LOWS observer network expanded on the LESON network which measured snowfall the previous winter snow season (1988-89) to 40 observers. The observers were given a snowboard, yardstick, and a four inch diameter precipitation gauge. A meteorologist delivered, explained the use and sited these items at each observers location. When a snow event took place, the observers listed on an observation sheet, snowfall amounts, water equivalents, visibility, and comments they felt were important to the experiment. As a compliment to the observer network, 12 microbarographs and 4 weighing precipitation gauges were deployed at selected observer locations for the duration of the LOWS experiment.

This paper via the poster session presents the LOWS observer location maps, examples of snowfall amounts for specific events, and snowfall by contour mapping. The examples that follow cover selected LOWS and LESON snowfall events.

It is hoped that the LOWS experiment will continue in future winter seasons with additional co-sponsers to assist Niagara Mohawk.

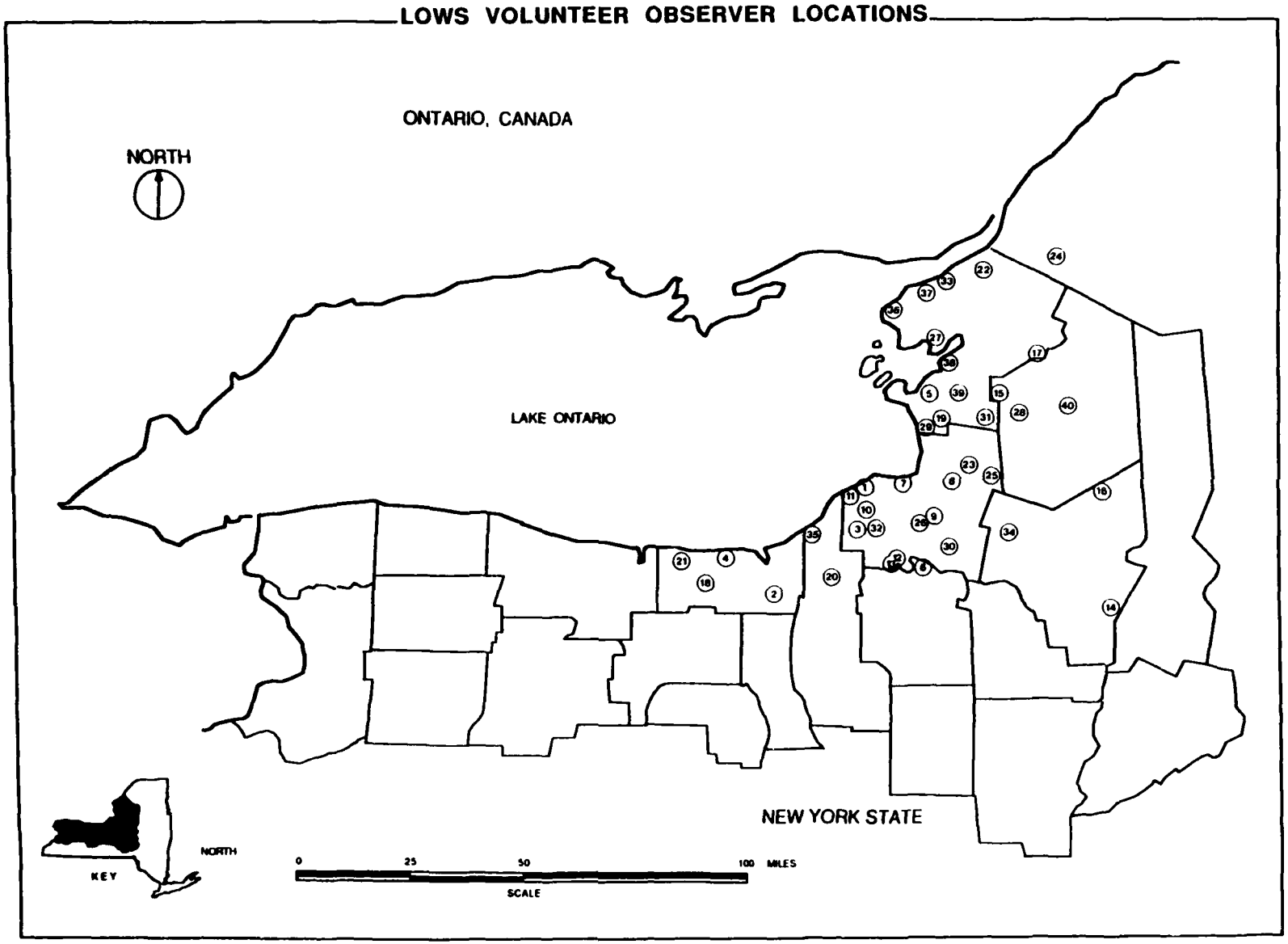

Map showing locations of LOWS volunteer snowfall observers.

LOWS EVENT NO. 1

LOCATION	JAN. 11,1990	JAN 12, 1990	JAN 13, 1990	JAN 14, 1990	EVENT NO. 1 TOTAL
1. OSWEGO	1.40	2.90	1.30	5.00	10.60
2. CLYDE	TRACE	2.50	4.25	0.25	7.00
3. DEXTERVILLE	0.00	5.50	8.75	1.75	16.00
4. SODUS	TRACE	2.00	4.95	0.00	6.95
5. HENDERSON	0.00	1.00	2.00	0.00	3.00
6. BREWERTON	0.00	3.70	0.80	0.00	4.50
7. ARTHUR	2.00	5.50	3.75	1.00	12.25
8. ALBION	0.00	6.50	6.25	0.25	13.00
9. HASTINGS	4.50	4.00	7.00	8.00	23.50
10. MINETTO		4.00	5.00	1.00	10.00
11. SW OSWEGO	0.00	0.60	5.00	4.70	10.30
12. PHOENIX	0.00	1.00	5.50	2.50	9.00
13. PHOENIX	0.00	2.75	1.05	1.95	5.75
14. UTICA	0.00	TRACE	1.90	2.50	4.40
15. BARNES CORNERS	12.00	7.00	8.00	0.00	27.00
16. BOONVILLE	5.00	3.00	0.50	0.00	8.50
17. W. CARTHAGE	0.00	6.75	4.50	0.00	11.25
18. MARION		1.00	3.50	0.25	4.75
19. MANNSVILLE	0.00	0.50	7.50	0.00	8.00
20. CATO	0.00	1.25	6.60	1.75	9.60
21. ONTARIO	0.00		4.00	1.00	5.00
22. PLESSIS	0.00	2.00			2.00
23. BENNETT BRIDGE	6.00	4.00	10.75	0.00	20.75
24. GOUVERNEUR	0.00	5.00	1.00	0.00	6.00
25. REDFIELD	0.00	12.75	2.25	0.00	15.00
26. PALERMO		7.00	5.00	9.00	21.00
27. CHAUMONT					
28. RECTORS CORNERS	6.00	28.00	4.00	3.00	41.00
29. SANDY POND (N)	0.00	13.25			13.25
30. CONSTANTIA	0.00	2.25	1.75	5.00	9.00
31. DIAMOND					18.50
32. FULTON	0.00	3.00	4.75	3.00	10.75
33. CLAYTON					1.00
34. CAMDEN	1.90	3.75	2.75	6.00	14.40
35. FAIR HAVEN	0.00	1.50	3.50	4.00	9.00
36. CAPE VINCENT					1.00
37. ST. LAWRENCE					N/A
39. SACKETTS HARBOR					N/A
39. ADAMS					N/A
40. LOWVILLE	TRACE	9.00	6.50	0.80	16.30

LOWS VOLUNTEER OBSERVER NETWORK

JAN. 11–14, 1990

SNOWFALL IN INCHES

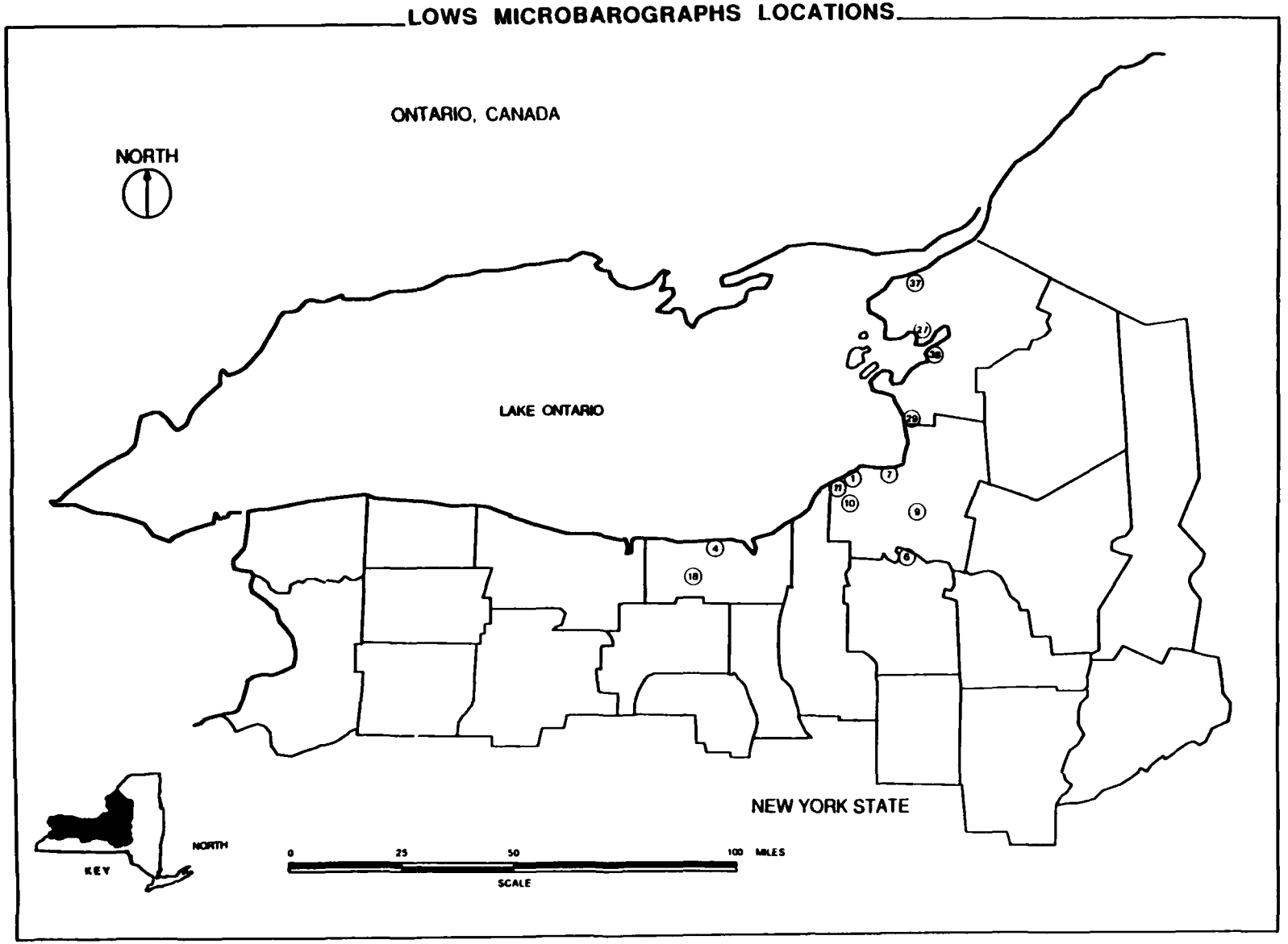

Map showing locations of LOWS analog microbarographs.

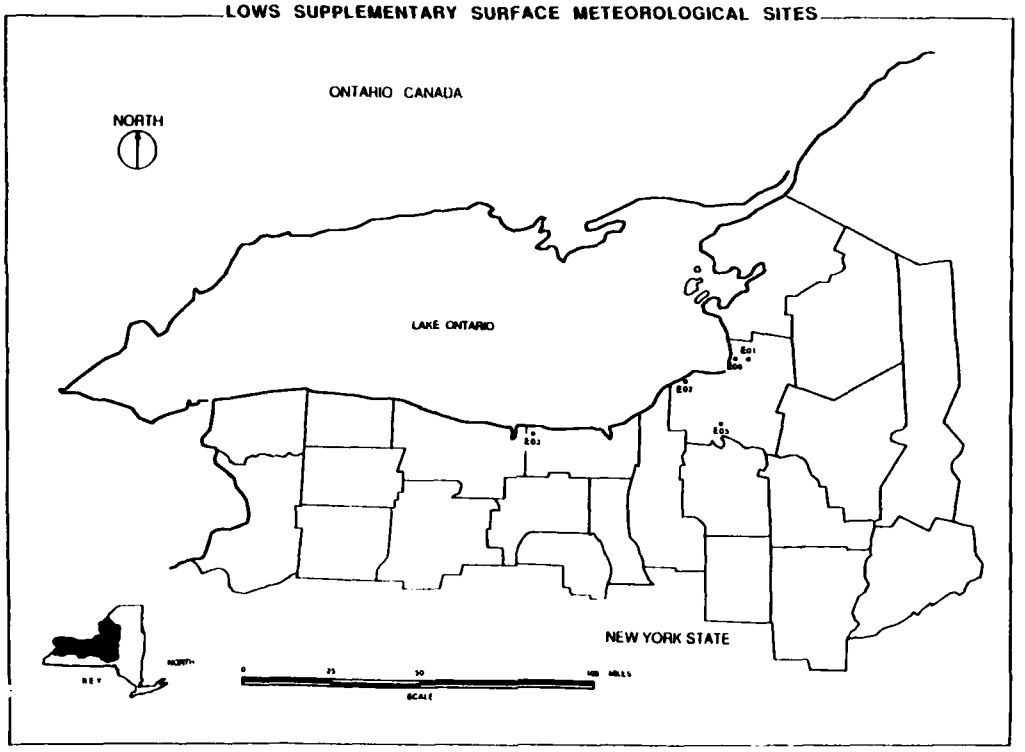

Map showing locations of LOWS supplementary surface meteorological sites

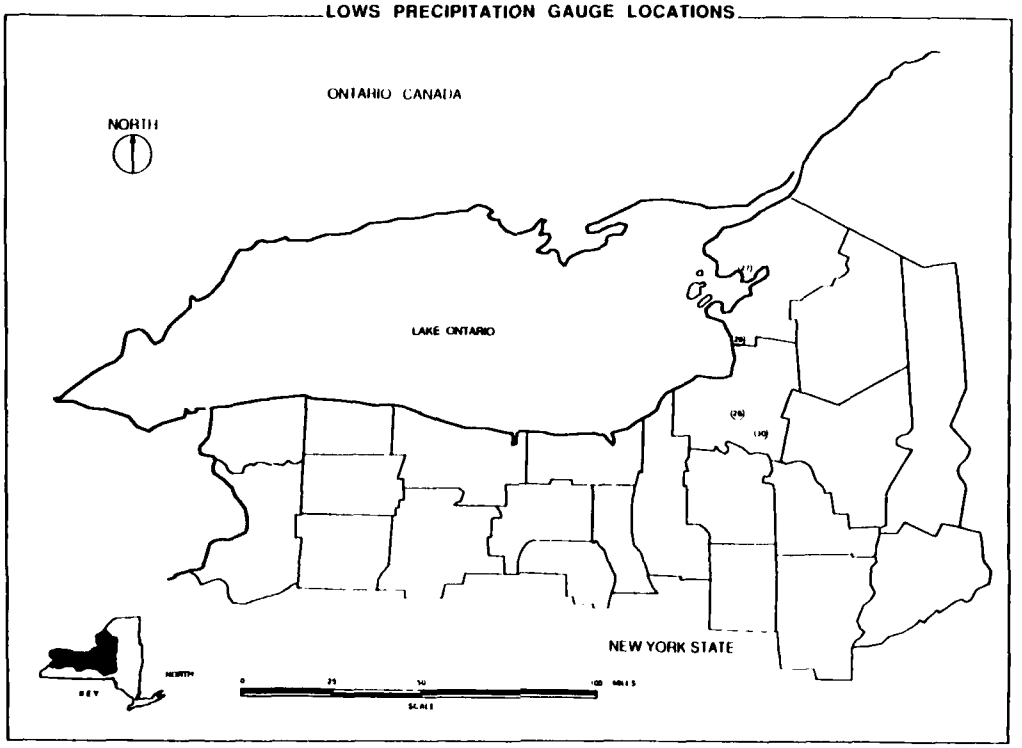

Map showing locations of LOWS precipitation gauges

LESON AND NWS LOCATIONS

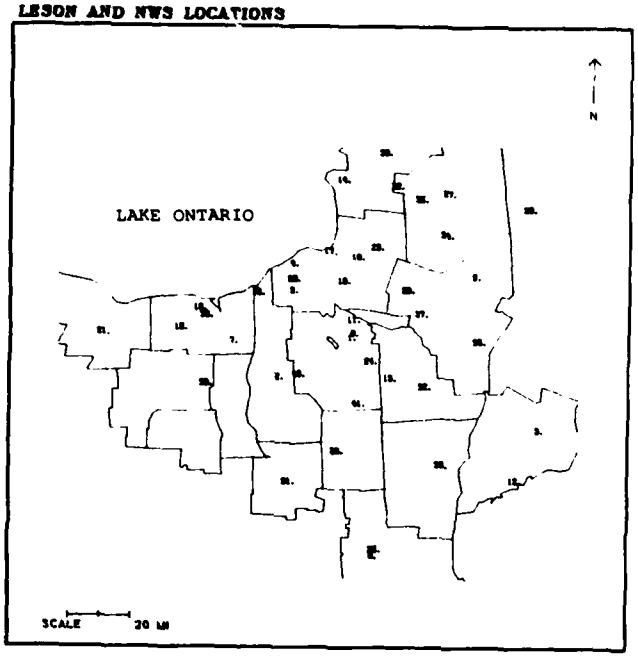

#	name:	location
1	NWS Syracuse - Dan Bartolf	North Syracuse
2	Robert J. Blanchard Sr.	Auburn
3	Harold Hollis	Cooperstown
4	John Ferlito	Oswego East
5	Harry Capron	Booneville
6	Jack Kaplan	North Syracuse
7	Gilbert Kinnetz	Clyde
8	NWS Binghamton- David Martin	Binghamton
9	V. Brien Mathews	Dexterville
10	Jack Matthys	Sodus
11	Ted Palma	Brewerton
12	SUNY - Oneonta	Oneonta
13	Bill Schmidt	Cazenovia
14	Marston Smith	Henderson
15	Fred Walker	Marion
16	Edgar Denton	Fair Haven
17	Alex Voninski	Arthur
18	Russ Berry	Albion
19	Jim Jones	Hastings
20	Al Stamm	Minetto
21	NWS Rochester	Rochester
22	Matt Macierowski	Barnes Corners
23	Bennett Bridge - Hydro	Bennett Bridge
24	Robert Golus	Manlius
25	NWS Bing	Binghamton
26	NWS Co-op	Cortland
27	NWS Co-op	Lowville
28	NWS Co-op	Old Forge
29	NWS Co-op	Camden
30	NWS Co-op	Sodus Center
31	NWS Co-op	Ithaca Cornell
32	NWS Co-op	Morrisville
33	NWS Co-op	Norwich
34	NWS Co-op	Highmarket
35	NWS Co-op	Rectors Corner
36	NWS Co-op	NY Mills (Utica3W)
37	NWS Co-op	Rome (GriffisAFB)
38	NWS Co-op	Watertown
39	NWS Co-op	Geneva (Research)
40	NWS Co-op	Skaneatles
41	NWS Co-op	Tully (AGWAY)

CENTRAL NEW YORK STATE

SNOWFALL NOVEMBER 1989

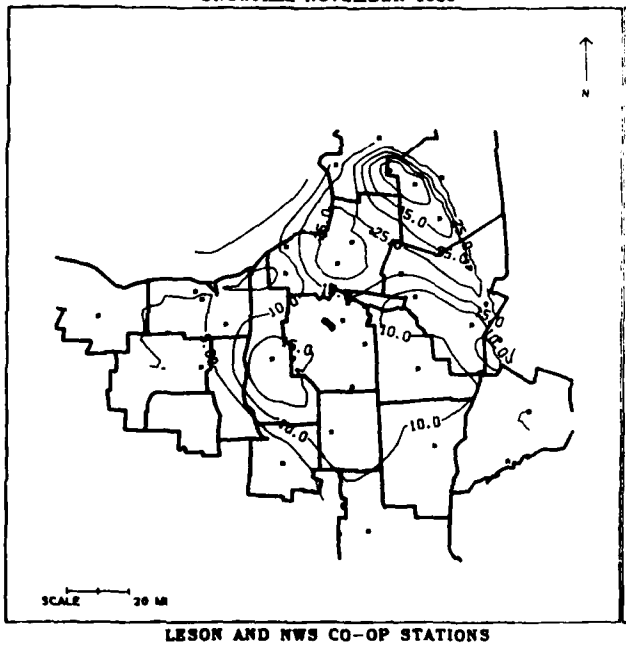

LESON AND NWS CO-OP STATIONS
NOVEMBER 1989
SNOWFALL IN INCHES

SNOWFALL DECEMBER 1989

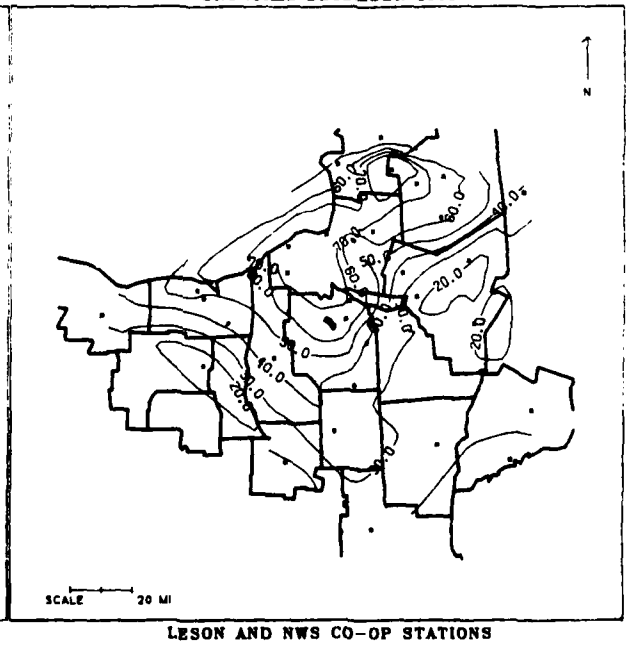

LESON AND NWS CO-OP STATIONS
DECEMBER 1989
SNOWFALL IN INCHES

Statewide Cooperative Snow Survey for Maine

M. LOISELLE

Maine Geological Survey
State House Station 22
Augusta, Maine 04333, U.S.A.

G. KEEZER

U.S. Geological Survey
26 Ganneston Drive
Augusta, Maine 04333, U.S.A.

Introduction

Estimates of water content in Maine's late winter and early spring snowpack provide valuable information to a number of Federal and State agencies and to private companies concerned with the management of Maine's surface water resources. This paper provides a brief history of the snow-survey program in Maine, describes the present statewide cooperative program, and provides some examples of the use of a geographic information system (GIS) for the analysis of snowpack data.

Annual snow surveys through 1987

Estimates of the water content of the snow cover have been made at selected sites in Maine for more than 70 years. Information on snow depth and equivalent water content has been collected by a number of operators of hydroelectric power plants and by the U.S. Geological Survey (USGS) in cooperation with the Maine Public Utilities Commission. In 1941, the USGS began a systematic annual compilation of all independently collected snow survey data and the preparation of an annual map showing lines of equal water content on March 1.

In 1972, Hayes compiled a summary map of snowpack data in Maine based on these systematic compilations for the period 1941 through 1965 (Hayes, 1972). This publication remains the only statewide data on the average water content and average density of the snowpack. In addition, the map shows the average date of the maximum water content of the snow in Maine, and the publication discusses how average density and water content of the snowpack varies over time.

Budget cuts at the Federal and State levels in the 1970s and early 1980s resulted in a significant reduction in the scope of the snowpack data collected by the USGS. Snow cover was not measured at many sites in the southern and central sections of the State. Annual maps of water content were prepared as before, but with reduced coverage over large areas of the State. It is likely that reductions in the snow survey program would have continued but for the flood of April, 1987.

The combination of warm temperatures in March (which produced a "ripe" snowpack near or at capacity with respect to water content), the saturated condition of the soils, and an intense low-pressure system that generated near-record amounts of precipitation in Maine's central highlands produced major flooding on many of Maine's rivers (Fontaine, 1987; Fontaine and Maloney, 1987). Damage from the flooding was estimated to ex-

ceed $100 million (Hasbrouck, 1987), and 14 of Maine's 16 counties were declared Federal disaster areas (Federal Emergency Management Agency, 1987).

Present statewide cooperative snow survey

As a result of the April 1987 flooding, increased State and Federal funding was appropriated to upgrade the USGS streamflow-gaging network, expand the annual snow survey network to reestablish statewide coverage, and provide for efficient communication of the results of the snow survey to concerned agencies and private companies.

The present snow survey program (1990) involves international, Federal, and State agencies and private companies (fig.1). These agencies include the St. John River Basin Cooperative Snow Survey, the USGS, the National Weather Service, the Maine Geological Survey and Maine Forest Service, hydroelectric power companies, and paper companies. The private power companies and paper companies collect snow cover data primarily in the headwater regions of Androscoggin, Kennebec, and Penobscot Rivers, and in the Sebago Lake watershed. Data for the St. John River Basin comes from a variety of sources through the St. John River Basin Commission. Data for the remaining part of the State (southern and midcoastal sections, the central highlands, and eastern Maine) are collected by the USGS and by the Maine Geological Survey and Maine Forest Service (which are in the Maine Department of Conservation).

Approximately 217 snow courses have been established in Maine and in adjacent parts of New Hampshire, New Brunswick and Quebec by the agencies listed above. Many of the sites Maine and New Hampshire are the same as those monitored by the USGS and others prior to the 1970s. In addition, new courses have been established to fill in areas on Hayes' 1972 map which was based on limited data, and to replace courses that were lost because of development. Present (1990) staffing levels allow data to be collected for 60 percent or more of these sites on or about February 1, March 1, March 15, and every 2 weeks from mid-March until the snow cover is completely melted (usually late April).

The program is coordinated by the USGS state office in Augusta, where the data are assembled and interpreted. The February 1 and March 1 survey dates are used primarily to train new observers, test communication channels, and coordinate with National Weather Service research efforts. Data from the March 15 survey are used to compile a map of snow cover water content and estimate the "ripeness" (or density) of the snowpack.

The data (in the form of contour maps of equivalent water content in the snow cover) are used primarily to help forecast the potential for floods on Maine's major rivers, estimate inflow to storage reservoirs, and plan long-term flow management. The Maine River Flow Advisory Committee, consisting of Federal, State, and private officials, meets in mid-March to evaluate the current streamflow and reservoir-storage conditions in the major river basins. After reviewing the available information, the Committee issues a press release that summarizes current statewide hydrologic conditions and reminds public officials and citizens that flooding can occur at any time if significant rainfall occurs over a short period. This press release is used by State and local officials in their emergency-response and flood-mitigation planning efforts.

Geographic information system analysis of snow survey data

Rapidly changing weather conditions can alter the condition of the snowpack substantially in in a very short time. Thus, the rapid analysis of snowpack data can increase the usefulness of the snow survey in forecasting snowmelt runoff and river stages. Use of a surface modeling software package to analyze snow survey data quickly and consistently is currently being explored.

The software package being used is the Triangulated Irregular Network (TIN) module of Environmental Research Systems Institute Arc-Info geographic information system (GIS) software. (Note: The use of specific trade names does not constitute endorsement by the U.S. Geological Survey.) On the basis of geographic coordinates and equivalent water contents measured on or about March 15 at sites in Maine and at adjacent locations in New Hampshire, New Brunswick, and Quebec, the software package constructs a three-dimensional surface

model composed of irregular triangles. Each vertex of a triangle represents a snow course with a measurement; the elevation of the vertex above the base datum represents the measured equivalent water content. Within any triangle defined by three measurement sites, the equivalent water content is computed by linear interpolation between the measured values at the vertices. Without any modification, the TIN software can produce three-dimensional perspective views of the snowpack water content.

A contouring package produces a smoothed contour map of equivalent water content from the TIN surface model. Any contour interval for the map may be selected, but using too small an interval produces a map with numerous small closed contours that represent individual snow courses, making interpretation of the final map difficult. Given the disparate sources of data and estimated accuracy of the snowpack-density measurements (and, therefore, the equivalent water content), a contour interval of 2 inches of equivalent water was selected (fig. 2).

Without refinement, the TIN-generated contour map cannot include orographic/topographic effects that can be incorporated into a hand-contoured map. Hayes (1972) discusses the difficulty in estimating snowpack water content at high elevations from his map. In addition, the data used to construct the map must be carefully screened prior to entry to remove questionable values. A comparison of contour maps produced by hand contouring and by the TIN surface model shows substantially more generalization in the hand-contoured map because of an informal averaging process that occurred while the hand contoured map was being produced. In this respect, TIN-generated contour map will produce more consistent and objective maps than hand-contouring methods. Also, once the snow course locations have been initially digitized, a finished contour map can be produced in less than an hour after the data are obtained from observers.

Quantitative estimates of total snowpack water content

GIS tools also can be used to make quantitative estimates of water content within a drainage basin or subbasin (such as a drainage area above a storage reservoir). These calculations take advantage of the inherent capability of GIS software to compute the area of an enclosed polygon.

After constructing an equivalent water-content contour map, the outline of the drainage basin (or subasin) is digitized and transformed into the same coordinate system as the water-content contour map. This basin outline is then combined with the contour map by a "clipping" function provided with the Arc-Info software; the resulting map "clips" the isopachs of equivalent water content at the basin boundaries, forming closed polygons bounded by the drainage-basin boundaries. The area of each closed contour is multiplied by the equivalent water content represented by the contour and summed to give the volume of water in the snowpack in the basin. These calculated volumes are useful both in forecasting flood potential and in flow management and water-resources planning.

Calculations in the Penobscot River basin based on the traditional and TIN-generated contour maps of snowpack for mid-March 1990 yielded storage volumes of 100 billion cubic feet and 106 billion cubic feet of equivalent water respectively. The 6 percent difference between these volumes probably is not significant given the errors in measurement and uncertainties in contouring the data. These volumes correspond to a basinwide average water content equivalent to 5.2 inches of precipitation.

Summary

Major flooding on Maine's rivers in April, 1987, generated renewed interest in obtaining accurate late-winter and early spring estimates of snowpack water content and condition. The present Statewide snow survey is a cooperative effort between international, Federal, and State agencies and private companies, coordinated by the USGS. Annual maps of equivalent water content in the snowpack on March 15 are reviewed by the State's River Flow Advisory Committee and are used by a number of agencies for forecasting flood potential, estimating inflow to storage reservoirs, and planning long-term flow management.

GIS has significant potential in the quantitative analysis of snow-survey data. In addition to providing a tool for the rapid preparation of objective and consistent contour maps on the basis of measured water contents, GIS tools can also be used to make quantitative estimates of total water content in the snowpack within a drainage basin or subbasin.

References

Federal Emergency Management Agency, 1987, Interagency hazard mitigation report: Federal Emergency Management Agency, Region I Hazard Mitigation Team, FEMA-788-DR-Maine, 29 p.

Fontaine, R.A., 1987, Flood of 1987 in Maine, Massachusetts, and New Hampshire: U.S. Geological Survey Open-File Report 87-460, 35 p.

Fontaine, R.A., and Maloney, T. J., 1987, Flood of April 1987 in Maine: U.S. Geological Survey, National Water Summary 1987 - Water Supply and Use: Selected Events: Water Supply Paper 2350, p. 41- 44

Hasbrouck, S., 1987, The flood of April 1987: University of Maine Land and Water Resources Center Natural Resources Highlight Special Report, 12 p.

Hayes, G.S., 1972, Average water content of snowpack in Maine: U.S. Geological Survey Hydrologic Investigations Atlas HA-452, 1 sheet, scale 1:1,000,000

Figure 1. Snowpack-measurement locations and source agencies

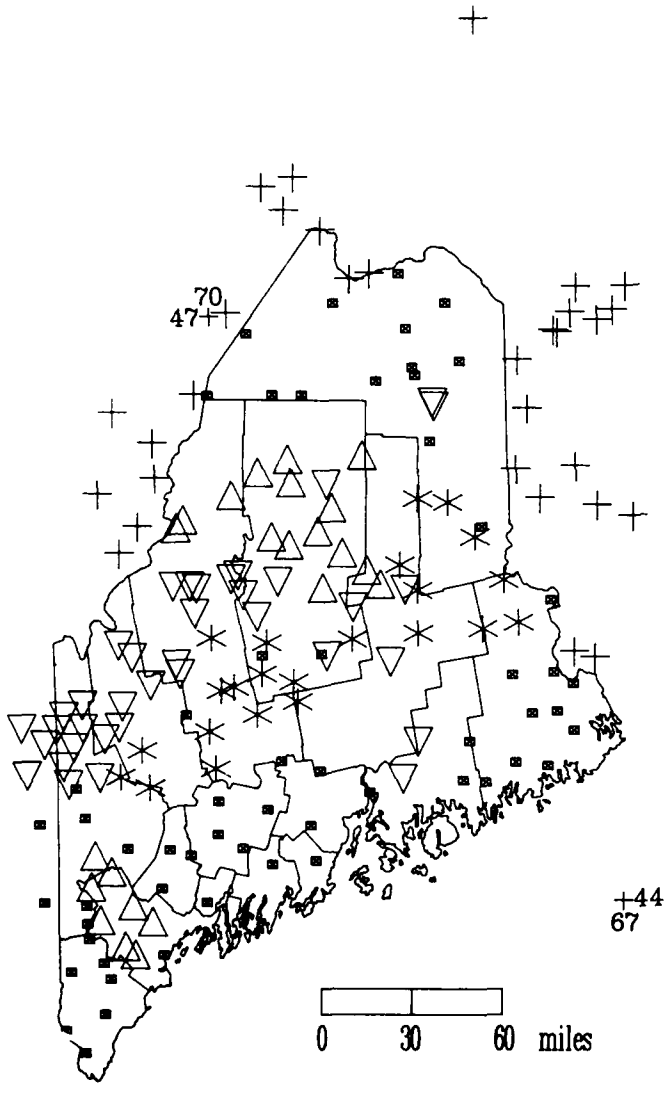

Explanation

- U.S. Geological Survey and National Weather Service
- St. John River Basin Cooperative Snow Survey (New Brunswick Electric Power Commission and Ministere de l'Environment du Quebec)
- Maine Geological Survey and Maine Forest Service
- Hydroelectric power companies (Union Water Power Company, Kennebec Water Power Company, Bangor Hydroelectric Company, and Maine Public Service Company)
- Paper companies (Great Northern Paper Company and S.D. Warren Company)

Figure 2. Comparison of hand-generated and TIN-generated snowpack contour maps. Contours based on measurements made on or about March 15, 1990.

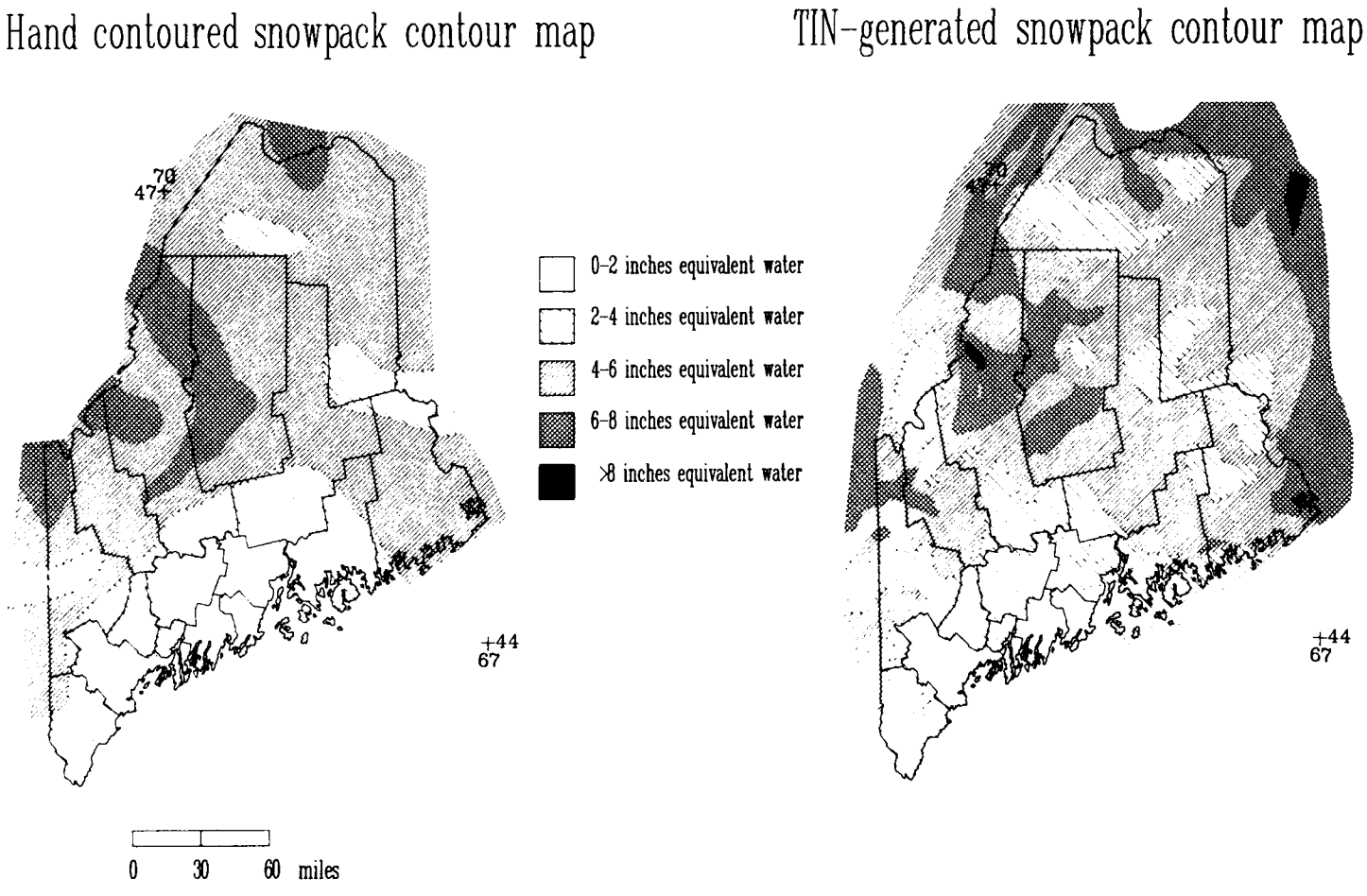

Morphological and Thermal Characteristics of Winter Nests of the Meadow Vole, *Microtus Pennsylvanicus*

R.L. ROBITAILLE AND G.M. COURTIN

Department of Biology
Laurentian University
Sudbury, Ontario P3E 2C6, Canada

INTRODUCTION

Mammals have evolved three distinct methods of surviving winter: one method is to migrate to a warmer climate, a second is to hibernate, and the third is to remain both winter active and to develop either physiological, or morphological or behavioural adaptations to cope with winter conditions. The meadow vole, *Microtus pennsylvanicus,* is an example of such a winter-active mammal.

The meadow vole lives in a system of surface runways and underground burrows, often nesting in the burrows during the summer. In winter, the meadow vole usually places its roughly spherical grass nest on the surface as long as there is snow cover (Whitaker, 1980). Wunder (1985) states that the meadow vole must allocate enough energy towards thermoregulation to maintain a constant body temperature of 38.4°C, and that energy allocated to one function generally cannot be used for another. Winter temperatures add an extra energy demand on the vole as it strives to maintain a constant body temperature. The nest of the vole provides an insulative barrier that reduces the amount of heat loss by the vole to the environment.

Our research group has observed high mortality rates in meadow voles owing to conditions of wet snow and rain that alternated with extreme cold when the snow pack is shallow. It was noted that in all cases of mortality the nesting material was saturated.

The present work was an attempt to expand on our previous research (Kalliomaki,1985 and Hillis, 1988) by examining some of the morphological characteristics of meadow vole nests such as: 1. the study of nesting material length and how it changes over a period of time; 2. a study of heat loss through a dry, a humid, and a saturated nest built by 1, 2 or 3 voles; 3. to establish a relationship between nests built in a controlled environment and nests built under an established snow cover.

METHODS

Caged voles at a density of 1, 2, and 3 voles, respectively, were provided with dry grass *ad libitum* as nest-building material for a period of three days. The effects of time on the type of nest produced was determined by collecting the nest either after 3 days, or 7 days or 16 days and measuring the length of fifty randomly-collected pieces of grass from various areas of the nest.

The thermal characteristics of the nests were obtained as follows: a surrogate vole was constructed by skinning a dead vole and replacing the body with a rubber balloon. Two lengths of latex tubing and a thermocouple were sealed into the mouth of the balloon with silicone cement. Water was

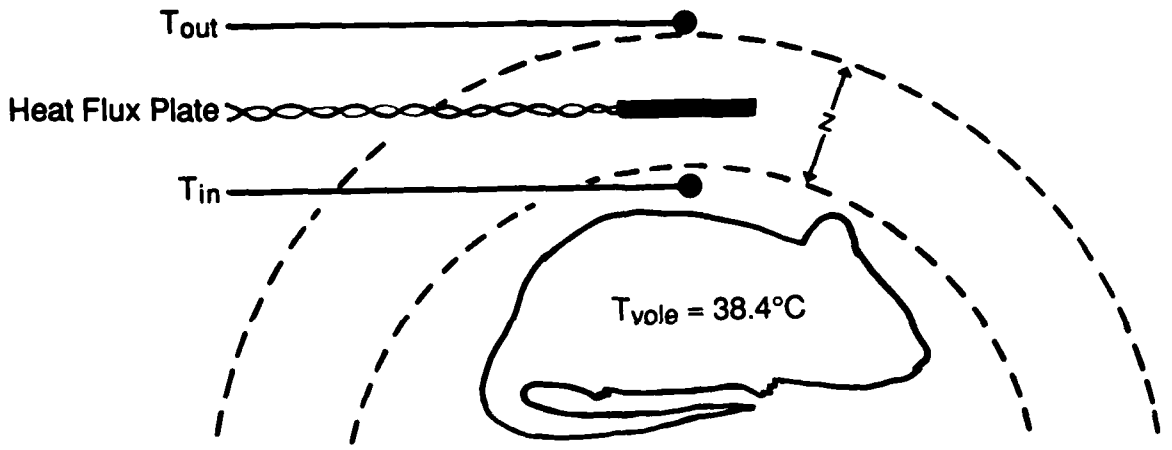

Fig. 1. Schematic to show the method of measurement of thermal conductivity of meadow vole nests. A heat flux plate was inserted into the wall of the nest equidistance from the inner surface and the outer surface of the nest. The temperature gradient was measured with two 22-gauge copper-constantan thermocouples; one was placed on the outer surface (T_{out}) of the nest and the other the inner surface (T_{in}) of the nest, above and below the flux plate. The distance (z) between the two thermocouples was measured. The surrogate vole's core temperature (T_{vole}) was kept at 38.4 ± 1°C.

circulated through the balloon via the tubing at the core temperature of a live vole (38.4°C) and the thermocouple used to monitor the temperature inside the balloon.

The surrogate vole was placed inside a nest with the ambient air temperature outside the nest at 0°C. The inputs from all required sensors were recorded using a Campbell 21X datalogger. Thermal conductivity and cooling rate were determined for nests built by 1, 2, and 3 voles, respectively under both dry and humid conditions. Thermal conductivity was calculated using a form of the Fourier heat-transfer equation:

$$Q = -k' \, dT/dz$$

where Q = heat flux (mv), k' = thermal conductivity (W/m/K), and dT/dz = mean temperature gradient (K/m). The sensor placement are shown in Fig. 1.

Three cages which contained 1, 2, and 3 voles, respectively, were prepared by inserting the maximum amount of grass possible through the cage bars. The cages were placed at ground level under an established snowpack for a period of three days. The thermal conductivity of each nest under humid and saturated conditions was determined as previously described.

RESULTS

A two-way analysis of variance showed that there was no interaction between time (3 days under snow; 7 days and 16 days under controlled conditions) and density (1, 2, and 3 voles) with respect to grass length of the nesting material. A one-way analysis of variance showed that there was a significant difference between grass length with respect to meadow vole numbers per nest and between grass length with respect to number of days given to build the nest. The mean grass length of nesting material was greatest for a nest built by 1 vole over three days under the snow and was shortest in a nest built by 3 voles under the same conditions (Fig. 2). The same trend was observed for nests built in 7 days and 16 days under controlled conditions.

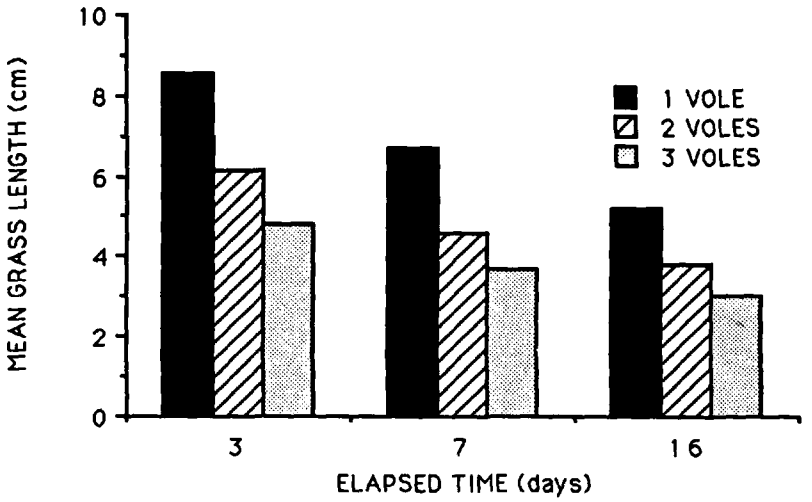

Fig. 2. Changes in mean grass length over time (days) with respect to the number of female meadow voles involved in the nest construction.

The thermal conductivity varied from 0.053 W/m/K to 0.07 W/m/K. No pattern may be deduced from the data either with respect to number of voles or the condition of the nesting material (dry or humid) (Fig. 3).

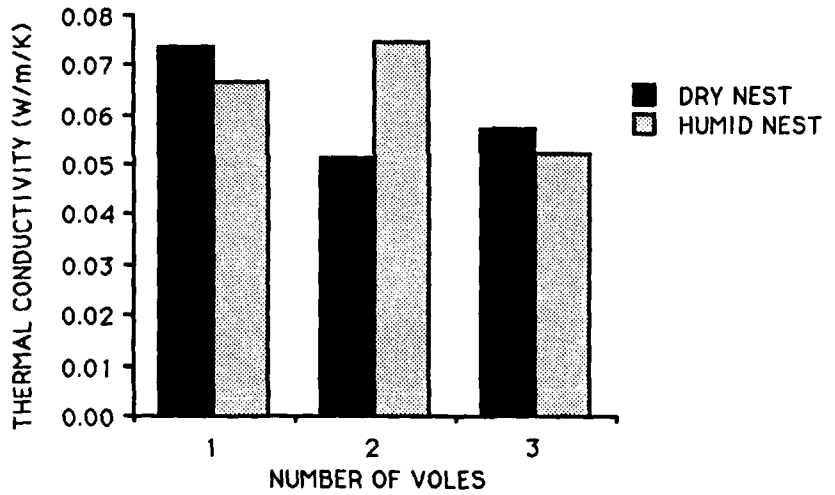

Fig. 3. Changes in mean thermal conductivity (W/m/K) with respect to both a dry nest and a humid nest in a controlled environment.

A relationship exists between the number of voles involved in the construction of the nest and the amount of time it takes the inner nest to cool. For both dry and humid nests the trend was towards an increased rate of cooling with an increase in vole numbers (Fig. 4). The slight decrease in cooling rate for 3 voles cannot be explained.

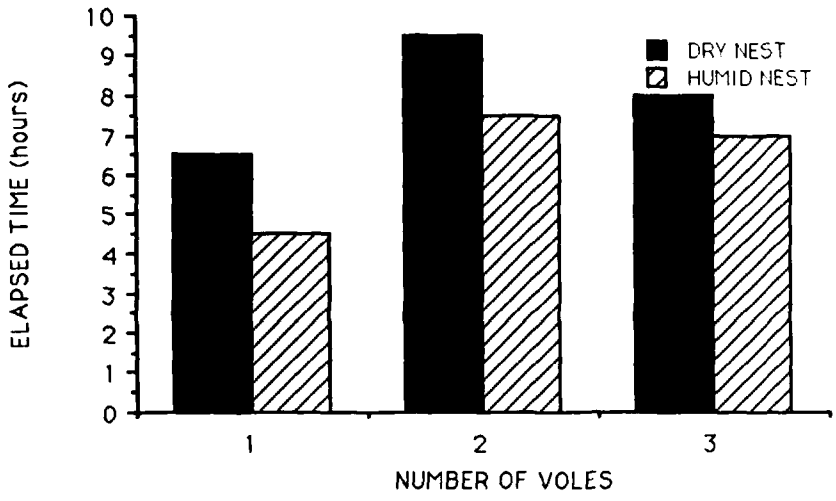

Fig. 4. Elapsed time to reach ambient air temperature for the surrogate vole core which was initially at 38.4°C with the heating source turned off. Solid bars = dry vole in a dry nest; hatched bars = dry vole in a humid nest.

The thermal conductivity value of a nest built by 3 voles in seven days in a controlled environment increased as the nest and the fur of the surrogate vole got wetter (Fig. 5). The thermal conductivity of a nest built in the snow in 3 days by 3 voles also increased as the nest and as the fur of the surrogate vole got wetter (Fig. 5). The dry surrogate vole in a dry nest took 14 hours to reach ambient cooler temperature. But within a wet nest the surrogate vole reached ambient temperature within 2 hours.

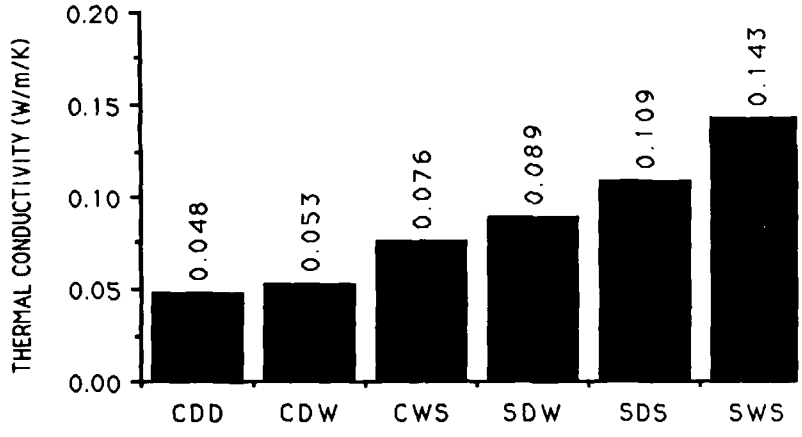

Fig. 5. Changes in mean thermal conductivity (W/m/K) of a nest built by 3 voles in seven days in a controlled environment and a nest built by 3 voles in 3 days under an established snow pack. CDD: controlled chamber; dry fur and dry nest; CDW: controlled chamber; dry fur and saturated nest; CWS: controlled chamber; wet fur and saturated nest; SDW: snow nest; dry fur and humid nest; SDS: snow nest; dry fur and saturated nest; SWS: snow nest; wet fur and saturated nest

DISCUSSION

It was observed that there was a pattern to the distribution of grass lengths used to form the nest. The longer nesting material formed the dome and the shorter, finer material formed the walls and the foundation of the nest. In most cases all the grass presented to the voles was cut and the excess littered the bottom of the cage. This length distribution suggests that there is an optimal grass length and an optimal amount of grass used to build a nest. There is a logarithmic relationship between grass length and time which demonstrates that the collected grass is quickly cut, then, over time, it is slowly modified to a desired length. The slope of the curves show that a nest built by 3 voles is more quickly comminuted than a nest built by 1 vole. These curves could signify that the chances of voles surviving a lethal drop in temperature when there is no snow cover increases with the number of voles involved in the construction of the nest.

The condition of the nest also plays a role in the nest's capacity to retain heat. If the nest is not completely saturated it still provides an adequate barrier from the environment and this may be biologically significant to the meadow vole. Heat loss by the vole to the interior of the nest must play a role in keeping the inner wall of the nest dry. The more voles huddle in the nest, the warmer the nest, and the drier the inner wall. This should increase the chances of vole survival during cold, rainy days when there is no snow cover. Stark (1963) studied nests built by Microtus californicus and stated that the inner surface of the nest was much drier than the external surface, the moisture being held in the grass fibres. It appeared that the hygroscopic properties of the nesting material protected the interior from excessive moisture. Stark (1963) also noted that old, abandoned nests were sometimes completely soaked.

When conditions are unfavourable, small mammals find it advantageous to form communal nests. Heat loss by conduction or convection varies in direct proportion to the amount of surface area exposed, huddling reduces the exposed surface area by at least a third, and heat loss, therefore, is reduced by an equal amount (Marchand, 1987). Huddling, therefore, lengthens the cooling period and increases the vole's chances of surviving when both the animal's fur and the nest are wet. When conditions are unfavourable, voles that huddle should have a better chance of survival than a lone vole in a nest built by itself.

I suggest that meadow voles may depend on well insulated nests to help maintain homeothermy. A nest reduces a vole's heat loss to a cold environment. Meadow voles are most vulnerable to death by hypothermia when they are in a saturated nest with no access to a drier area or to drier nesting material. This could explain why others in our laboratory have observed high mortality in their own experimental work.

In conclusion, my results demonstrate that there is a significant difference between the length of the nesting material used in the construction of the nest with respect to the number of voles involved in the building of the nest and the time given to build the nest. On the surface there seems to be no difference in thermal conductivity values between the nests but it should be stated that thermal conductivity values are relative, and not absolute, values because one cannot be sure of perfect contact between the nesting material and the heat flux plate. The differences in cooling rate emphasis the importance as to whether the nesting material is saturated or dry. Further work is needed for a complete understanding of how heat is dispersed through the nest and how this heat loss affects the meadow vole.

LITERATURE CITED

HILLIS, T.L., G.M. COURTIN. 1988. Subnivean nest temperatures and diurnal activity patterns in the meadow vole, *Microtus pennsylvanicus*. Proceedings of the Ontario Ecology and Ethology Colloquium, April 17-19, Univ. of Western, Ont.

KALLIOMAKI, N.M., G.M. COURTIN, F.V. CLULOW. 1985. Thermal Index and Thermal Conductivity of Snow and Their Relationship to Winter Survival of the Meadow Vole, *Microtus pennsylvanicus*. Proceedings of the Eastern Snow Conference, Vol. 29, 41st Annual Meeting, Washington, D.C., June 7-8, 1984.

MARCHAND, P.J. 1987. Life in the Cold; An Introduction to Winter Ecology. Univ. press of New England, Hanover and London. pp. 93-125.

STARK, H.E. 1963. Nesting Habits of the California Vole, *Microtus californicus,* and Microclimatic Factors Affecting its Nests.Ecology, Vol 44(4):663-669.

WHITAKER, J.O. 1980. The Audubon Society Field Guide to North American Mammals. Alfred A. Knopf, Inc , New York. pp.495 and 496.

WUNDER, B.A.,1985. Energetics And Thermoregulation in Biology of New World Microtus. Robert H. Tamarin.(ed), Special Publication No 8, The American Society of Mammalogists, pp 812-839.

Honor Student Paper:

A Comparison of Meltwater Discharge From a Debris-Free and a Debris-Covered Glacier, Canadian Rocky Mountains

L.E. MATTSON

University of Waterloo
Waterloo, Ontario N2L 3G1, Canada

INTRODUCTION

A common characteristic linking most glacial meltwater forecasting models is that they have been developed from glaciers exhibiting relatively "clean" surfaces. In reality, however, a significant portion of the world's glaciers contain either a partial or complete debris cover which masks their ablation zones. It is hypothesized that this debris cover can significantly influence the surficial ablation process, thereby altering the discharge characteristics of their meltwater streams.

PURPOSE

The purpose of this poster paper is to test this hypothesis by comparing and contrasting the surficial ablation and the meltwater discharge characteristics of a debris free glacier and a debris covered glacier.

OBJECTIVES

1) To prove that a debris cover on a glacier's surface does exert a significant influence on ablation;
2) To illustrate that the two basins are similar in all respects with the exception of a debris cover; and
3) To illustrate how meltwater discharge patterns differ between debris-free and debris-covered glaciers.

STUDY SITES

The two basins chosen for this study are the Athabasca (52° 11' N, 117° 15' W) and the Dome (52° 12' N 117° 17' W), both of which are located in the Columbia Icefield (Figure 1). These adjacent basins contain the streams which form the headwaters of the Sunwapta River which, in turn, flows via the Athabasca, Slave, and Mackenzie Rivers to the Arctic Ocean. The hypsometric curves for the two basins are illustrated in Figure 2. A list of the morphometric, morphologic, and dynamic characteristics of the Dome and Athabasca Glaciers is given in Table 1. The extensive debris cover is the most evident characteristic which differentiates the Dome from the Athabasca Glacier. The debris cover extends over the entire glacier surface from the terminus to a point 625 m up-glacier (Figure 1). From this point on, to a distance of 3.5 km, the debris cover dominates the surface of the glacier with a tendency decrease in thickness from the lateral margins (0.5 m thick) to the center axis of the glacier (0.0 m thick). Field observations indicate that debris sources include: snow and ice avalanches, high frequency-low magnitude rockfall, and the emergence of englacial debris.

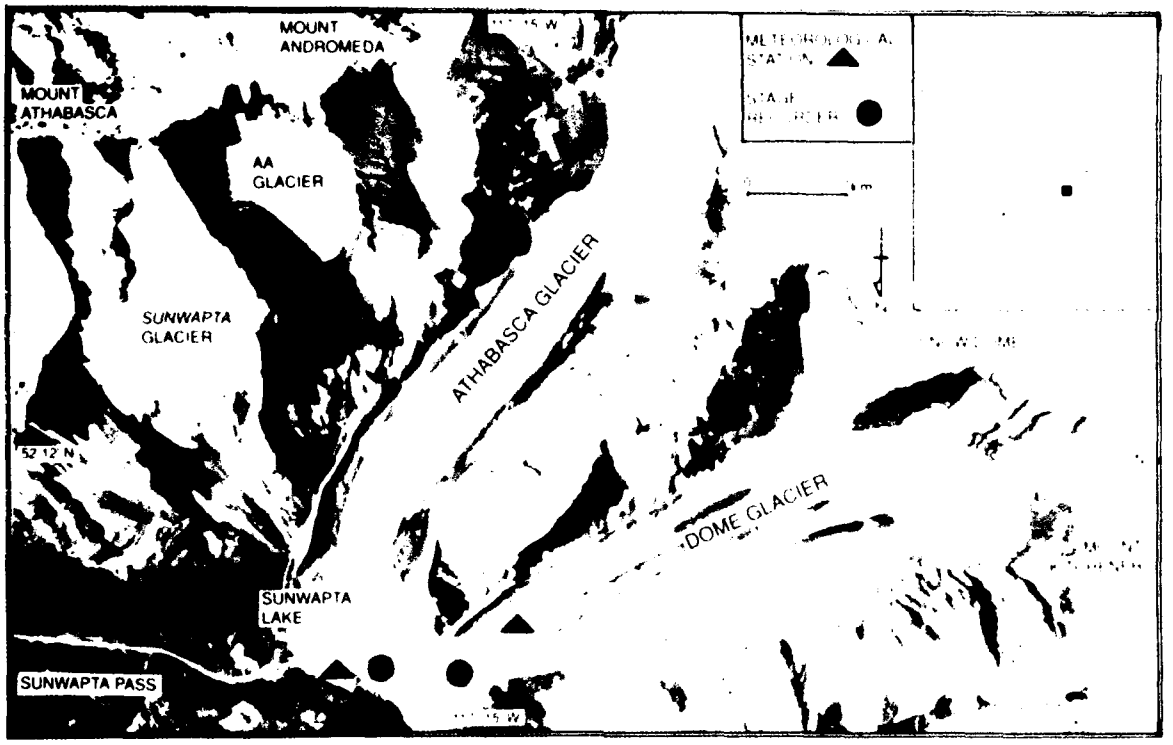

Figure 1: STUDY SITES. The Athabasca Basin covers an area of roughly 28 km^2. Of this, about 65 % or 18 km^2 is covered by glacial ice. The Sunwapta, the AA, and the Andromeda Glaciers cover an area of about 3.7 km^2. The remaining 14.3 km^2 of ice cover is accounted for by the Athabasca Glacier. The Dome Basin covers an area of about 15 km^2 and of this about 68 % or 10 km^2 is ice. There is a single cirque glacier associated with the Dome Basin known as the Saddle Dome Glacier which covers an area of 0.25 km^2. The remaining 9.75 km^2 of ice cover is accounted for by the Dome Glacier.

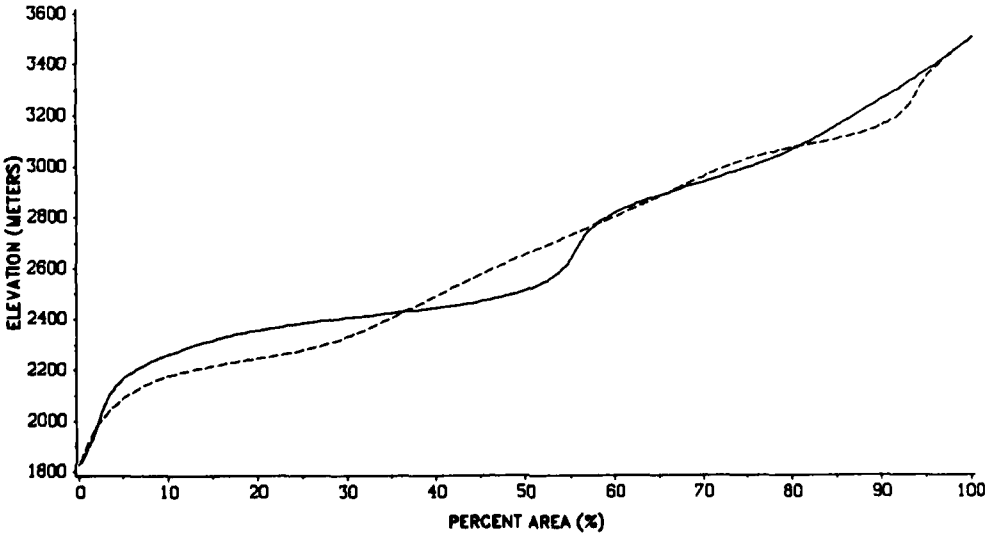

Figure 2: HYPSOMETRIC CURVES. This figure illustrates the similarity of the area to altitude relationship between the two study basins.

Table 1

Morphologic, morphometric, and dynamic characteristics of the Dome and Athabasca Glaciers.

ATTRIBUTE	DOME	ATHABASCA
GLACIER LENGTH (M)	8.5	5.4
MAXIMUM ELEVATION (M A.S.L.)	3460	3460
TERMINUS ELEVATION (M A.S.L.)	2000	2000
ALTITUDINAL RANGE (M)	1460	1460
AVERAGE GRADIENT	1:6	1:4
FIRN LINE ELEVATION (M A.S.L.)	2500	2500
AREA OF ACCUMULATION ZONE (KM^2)	8.3	4.9
AREA OF ABLATION ZONE (KM^2)	6.0	5.5
ICE THICKNESS AT BASE OF ICEFALL (M) *	300	---
VELOCITY AT BASE OF ICEFALL (M YR^{-1}) **	75	35
YEAR OF MAXIMUM HOLOCENE EXTENT ***	1843	1846
RATE OF RETREAT (1721-1953) (M YR^{-1}) ****	4.7	4.7
RATE OF RETREAT (1938-1960) (M YR^{-1})	28	19

* KITE AND REID, 1977
** PATERSON AND SAVAGE, 1963
*** LUCKMAN, 1988
**** DEATON, 1975

DATA COLLECTION

Meltwater discharge was monitored between July 11 and August 23, 1989 for the Dome Basin with the use of a continuous recording stage recorder while discharge data for the Athabasca Basin were derived from previously collected surface water surveys undertaken by Environment Canada at the Sunwapta River gauging station (Figure 1). Meteorological measurements commenced on July 11, 1989 at a standard meteorological station situated at the terminus of the Dome Glacier (Figure 1). Specific variables measured included: continuous relative humidity and air temperature, precipitation type and amount, as well as incident shortwave solar radiation. Daily maximum and minimum air temperatures and precipitation data were also derived from a meteorological station at the Columbia Icefield Information Center (Figure 1). Ablation was monitored on a daily basis through a simple ablation stake network located on the Dome Glacier.

OBSERVATIONS

1. Figure 3 illustrates the relationship between debris-cover thickness and surficial ablation. Past a threshold thickness of approximately 2.0 cm, ablation rates decreased in comparison to "clean" glacier surfaces. It was found that the greatest mean ablation rate (9.5 cm day^{-1}) occurred beneath a debris cover of about 1.0 cm. Those areas with less than 1.0 cm of debris exhibited relatively lower ablation rates. The mean daily ablation rate for a "clean" ice surface was about 7.0 cm day^{-1} compared to a rate of 1.0 cm day^{-1} for ice beneath 39.0 cm of debris.

2. A combination of topographic map analysis, air photo interpretation, reference literature review and field observations reveal that the Dome and Athabasca Basins are relatively similar with respect to their morphological characteristics. These include: size, orientation, slope, altitudinal range and percentage ice cover. Table 1 also indicates that the Dome and Athabasca Glaciers display relatively similar characteristics with respect to their morphology (slopes, lengths, and widths), morphometry (areas and ice depths), and dynamics (ice flow velocities and past rates of retreat).

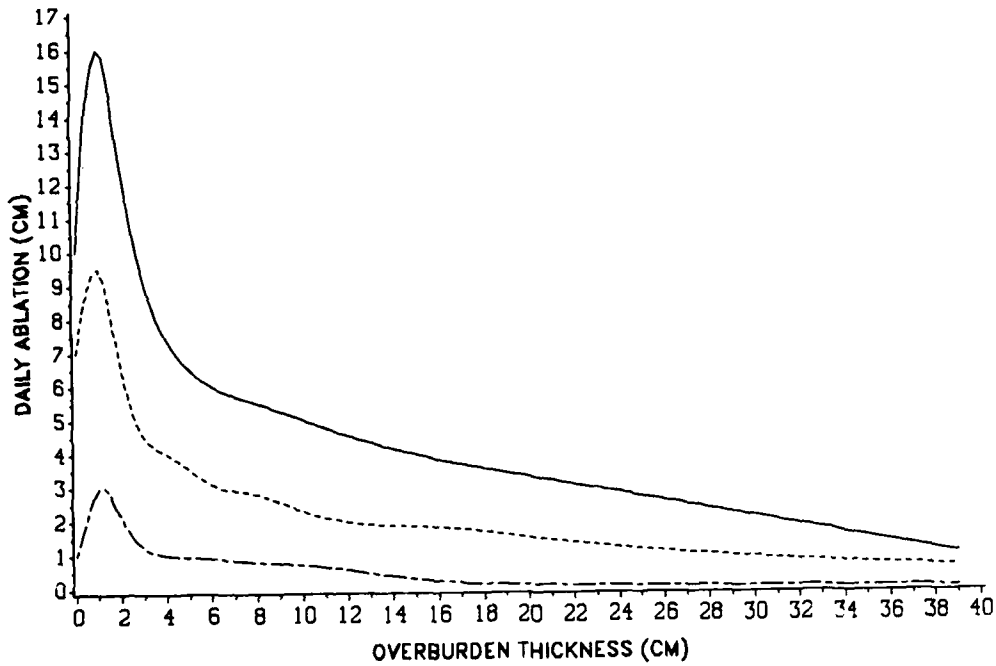

Figure 9: ABLATION VS. DEBRIS THICKNESS. Relationship of mean, maximum, and minimum daily ablation to debris cover thickness for the Dome glacier.

3. Meteorological data derived from the Dome site was relatively similar to that collected at the information center. The mean seasonal maximum air temperature for the Athabasca basin was 17.0 ° C. while that for the Dome was 13.0 ° C.; a difference of 4.0 C. ° The higher values for the Athabasca basin can possibly be explained by the fact that the meteorological station was located in the proglacial zone while that for the Dome was located on the surface of the glacier. The mean seasonal minimum temperature for the Athabasca Glacier was 4.5 ° C. while that for the Dome was 4.3 ° C.; a difference of only 0.2 C °. The similarity in values is most likely a result of cold air drainage off of the icefield during late evening hours. In total, 128.8 mm. of rain fell in the Dome basin compared to 116.6 mm. in the Athabasca, a difference of only 12.2 mm. or 10 %.

4. The seasonal discharge pattern of the Sunwapta and Dome Rivers is characterized by a series of oscillating waves which matched each other in form and amplitude. It is evident that the quantities of water released by both basins is in the same order of magnitude. The mean seasonal discharge for the Athabasca Basin was 5.6 m^3 s^{-1} resulting in a total seasonal discharge of 20,321,280 m^3. The mean seasonal discharge for the Dome Basin was 4.8 m^3 s^{-1} resulting in a total seasonal discharge of 17,418,240 m^3; almost three million cubic meters (14 %) less than that of the Athabasca. The mean daily maximum discharge for the Athabasca Basin was 8.9 m^3 s^{-1} which converts to a daily total of 768,960 m^3. The mean daily maximum discharge for the Dome Basin was 7.0 m^3 s^{-1} which converts to 604,800 m^3. Differences between the two basins for mean daily maximum discharge was 164,160 m^3 in favor of the Athabasca Basin.

5. At the seasonal scale the fluctuations of discharge in both rivers varied uniformly in duration from 4 to 12 days. These general trends in discharge were mainly a function of changes in regional weather conditions. Over the short term, however, the form of each individual wave did not always corresponded with that of the other for the same time period. There are, in fact, short periods which exhibit opposite trends in discharge. For example, on August 03 (215 Julian days) the discharge of the Dome River experienced an increase of 0.26 m^3 s^{-1} while the Sunwapta River experienced a decrease of 2.87 m^3 s^{-1}. Field observations reveal that this anomaly can be explained by a rain storm tracking over one basin as opposed to over both.

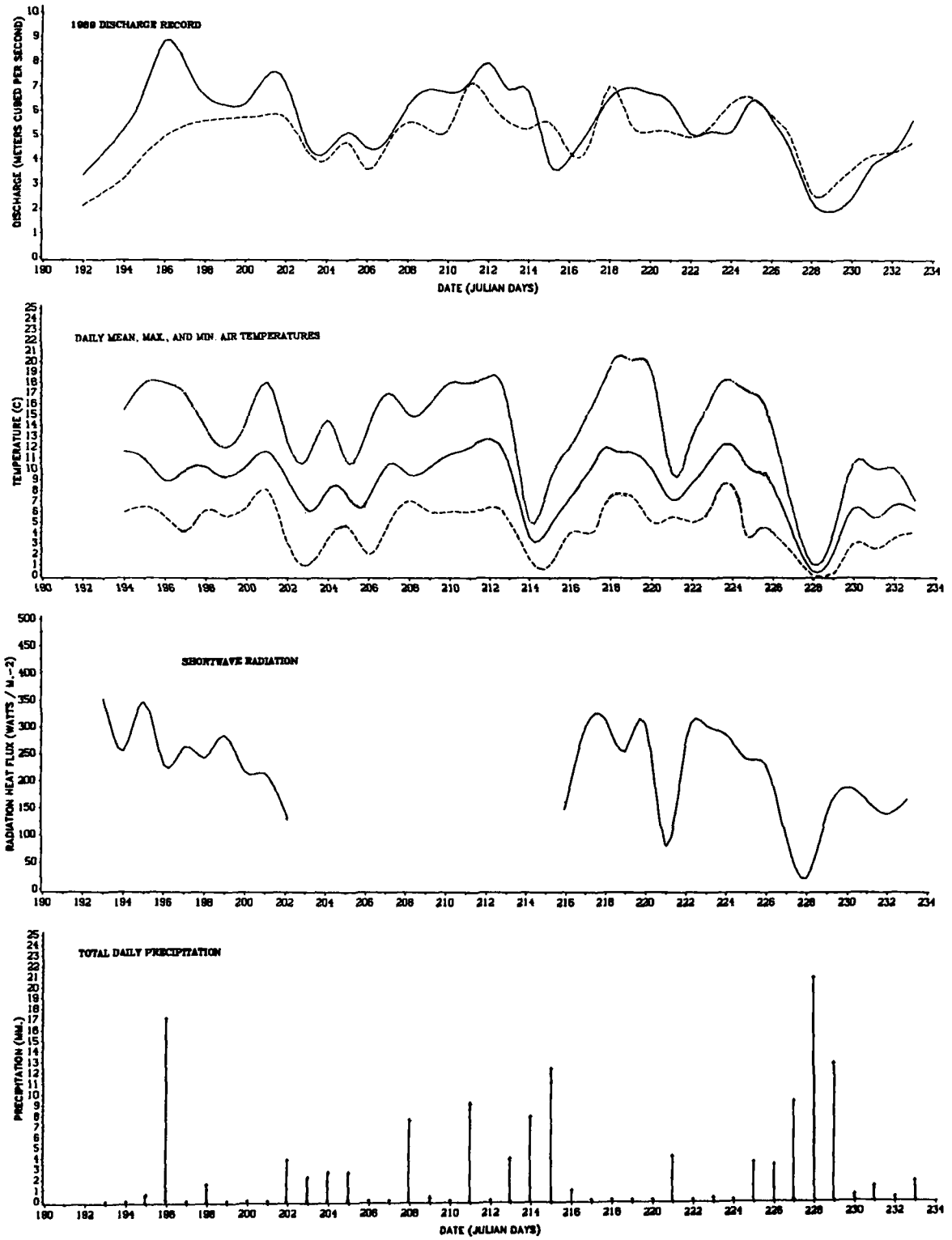

Figure 4: FIELD OBSERVATIONS. Meteorological conditions and meltwater discharge hydrographs for the Dome and Athabasca Basins for the period between July 11 to August 21, 1989 (191 - 233 Julian Days).

6. Analysis indicates that air temperature parameters, daily maximum for the Athabasca and daily minimum for the Dome, present the strongest positive correlations to discharge of all meteorological variables. A weak negative relationship also exists between discharge and precipitation which is surprising considering that precipitation acts as an input to the basin's hydrological cycle. It is assumed that this relationship is the result of some other related factor such as cloud cover.

CONCLUSIONS

The relationship between debris-cover thickness and ablation can be explained in terms of the surficial radiant energy exchanges in conjunction with the storage and transfer of energy within the debris cover. A debris cover equal to or greater than 1.0 cm in thickness will significantly decrease the albedo of the surface thus increasing the amount of absorbed shortwave radiation. Those areas with less than 1.0 cm of debris exhibit less ablation due to higher reflectivity caused by partial ice coverage. However, the debris-cover also acts as a medium through which the energy must be transferred in order to ablate underlying ice. Not all of the energy entering the debris cover reaches the ice. A portion of it is used to increase the internal temperature of the debris cover thus converting it into a state of storage. An increase in debris cover thickness results in an increase in stored energy which, in turn, results in less energy available for ablation. Once the threshold thickness is surpassed, a greater amount of energy is lost to storage than is gained through the increase in absorption.

It can safely be stated that a debris-cover does exert a significant influence on the ablation process at the micro-scale, however, this is not evident at the basin scale. The similarity in shape between the discharge hydrographs indicates that the driving forces behind the production of meltwater are the same for both types of glaciers. There is no indication that debris cover causes a lag or any other related phenomenon on a diurnal basis. The 14 % difference in the volume of discharge released between the two basins is relatively constant and can be explained by the fact that the ablation zones within the Athabasca Basin occupy an area 15 % larger than that of the Dome's. The hypothesis, however, should not be prematurely rejected due to the fact that the Dome Glacier may be an exception where by increased ablation in thin debris-covered areas is counterbalanced by the decreased ablation in thickly covered areas. Further research on other debris covered glaciers is necessary to fully test this hypothesis.

ACKNOWLEDGMENTS

The author acknowledges the field assistance of Dr. J. S.Gardner, Keith Carr, and Philip Friend and the reviewing of the completed paper by Ingrid Bajewsky. Stream discharge data for the Sunwapta River was provided by Environment Canada. The research was financed by an operating grant from The Natural Sciences and Engineering Research Council of Canada to Dr. J. S. Gardner.

REFERENCES

Deaton, G.H. (1975) Glaciers of the Canadian Rocky Mountains. In *Mountain glaciers of the Northern Hemisphere*, Vol. 1. W.O. Field (ed.), Amer. Geo. Soc., Dept. of Exploration and Field Research and the U.S. Army Cold Regions Research and Engineering Laboratory.

Environment Canada (1990) *Surface Water Data, Alberta, 1989.* Inland Waters Directorate, Water Resources Branch, Water Survey of Canada, Canada.

Kite, G.W. and Reid, L.A. (1977) Volumetric change of the Athabasca Glacier over the last 100 years. In *J. of Hydrology*, 32: 279-294.

Luckman, B.H. (1988) Dating the moraines and recession of Athabasca and Dome Glaciers, Alberta, Canada. In *Arctic and Alpine Research*, Vol. 20, no.1: 40-54.

Paterson, N.S.B. and Savage, J.C. (1963) Geometry and movement of the Athabasca Glacier. In *J. of Geophysical Research*, 68: 4513-4520.

Honor Student Paper:

Palatability of Winter Browse in The Snowshoe Hare (*Lepus americanus*) Herbivore Species Interactions

S.S. PAQUETTE

Department of Biology
Laurentian University
Sudbury, Ontario P3E 2C6, Canada

ABSTRACT

The major constraint upon winter survival of the snowshoe hare is shortage of food. Ether-extractable resins contained in plants seem to play a prominent role in determining the palatability of a given species. Cafetaria-style experiments conducted revealed a significant difference in that white birch was more readily eaten than trembling aspen (higher resin). In the mammalian herbivory study, the significant difference in percent consumption was due to the lateral sprouts produced following browsing by hare as compared to the differently browsed basal sprouts. Further investigation of these different sprouts offered in terms of resin levels are still in progress. Rhoades (1985) mentions that maybe the evolution of a mechanism to recognize the salivary factors of the particular herbivore by the plant would allocate less to growth and more to defense following an attack. Experiments are in progress to understand better this potential salivary relationship.

INTRODUCTION

In northern latitudes, the availability of food in most habitats is lowest in winter. This lack of food, therefore, presents a crucial barrier for the snowshoe hare (*Lepus americanus*) to obtain high quality winter browse. In the fall, winter and spring, certain plants, by virtue of their specific life form and functions, will influence the movements and ranges of snowshoe hare (Bider, 1961). Moreover, the main abiotic parameters namely, wind, light and snow play independent restrictive roles in the winter movements of the snowshoe hare. For the most part winter movement seems to be determined by necessity.

The most widespread predator deterrent of plants is what might be termed "chemical warfare" (Pianka, 1983). Plants contain a vast array of secondary compounds and have distinct seasonal patterns both with respect to growth and to carbon and nutrient allocation. These are plant characteristics that have important implications for palatability and resistance to herbivores. Forage selection patterns are largely the result of avoidance of plant tissues that contain high concentrations of secondary chemical constituents that are antagonistic to vertebrate herbivore fitness.

Given a choice, hares consistently prefer mature growth forms over intermediate and juvenile growth forms. The preferred food supply of snowshoe hare consists of the early- and mid-successional deciduous trees and shrubs. Some of the trees include: a) *Betula papyrifera* ssp. *humilis* (Alaska paper birch), b) *Populus tremuloides* (quaking aspen), c) *Populus balsamifera L.* ssp. *balsamifera* (balsam poplar), d) *Alnus crispa* ssp. *crispa* (green alder) and e) *Salix alaxensis* ssp. *longistylis* (feltleaf willow) (Bryant, 1981). Snowshoe hare clip twigs (diameter <4mm) and also strip or gnaw the bark which characteristically will have large toothmarks and a shaggy appearance.

Survival of various species of trees and shrubs are differentially influenced by barking pressure. Barking is heavier on species in open-grown places than in dense stands. Browsing takes place over a longer period of the year than barking. The localized distribution of high browsing and barking intensity seems to be governed mainly by the successional stages of the vegetation (de Vos, 1964). Hares switch from a diet of herbaceous vegetation to browsing woody vegetation with the arrival of the first frost. This activity reduces plant vigor and also stimulates increased branching of twigs. Girdling results in death because there is complete removal of the cambial layer and growth of adventitious sprouts.

There is an extreme flexibility with respect to chemical defense in the browse. The advantage of this is that energy rich substances, such as resins, appear to be produced after severe browsing whereas, when there is little browsing, the carbons are allocated to growth of the plant.

The present research project focusses on allelochemics in relation to palatability for the snowshoe hare (*Lepus americanus*). Browsing in relation to timing in the season, use of allelochemics and the effects of other herbivore activities was studied. The main objective of this study then was to assess what balance exist between the damage brought about by hare browsing and the plant's defensive response in relation to palatability. In order to determine this, the following hypotheses were tested:

1. Does the browsing product from different herbivores (beaver, hare, human and forest tent caterpillars) affect the plant in such a way as to affect the browsing activity of the snowshoe hare?
2. Is mechanical clipping of available browse of equal effectiveness to browsing, in terms of how the plant responds?
3. Does the snowshoe hare's browsing timing represent a crucial factor in the timing of plant response?

METHODS

Site selection

The sample area chosen for collection of browse was the Lake Laurentian Conservation Area in Sudbury, Ontario (Lat 46° 27' 30" N; Long 80° 56' 30" W.) Both white birch (*Betula papyrifera* Marsh.) and trembling aspen (*Populus tremuloides* Michx.) were selected as they were found to be abundant and the most frequently browsed. The overall experimental feeding site for all these twig collections was located in an area, 12 km west of Sudbury, Ontario, where hares were both abundant and active. Sampling was performed as follows:
a) To study the effects of different herbivores, four sites were selected in the summer of 1988 in order to mark trees defoliated by caterpillars and undefoliated trees. In the winter of 1988-1989, three other sites were selected in the Conservation Area which included browsing by hares, beavers and mechanical clipping by humans.
b) To examine the effects of mechanical clipping versus browsing by hares, another site was chosen at Wanup (34 km SE of Sudbury, Ontario) for a year-long study.

Experimental design

The experimental layout for the cafeteria-style experiment was six individually separated rectangular areas (4X2 m each) that were each sub-divided into eight compartments. Randomly placed bundles of twigs were left to be freely browsed by the snowshoe hares for 7 days.

Collection of samples

For every collection, twigs utilized had a diameter of < 4 mm which is usually considered to be the preferred size by snowshoe hare (Reichardt, *et al.*, 1984).

Samples collected for the forest tent caterpillar study consisted of 12 trembling aspen and 12 white birch trees. Six trees of each species had suffered

severe defoliation whereas the remainder had not been attacked and were used as controls. A twig (<4mm) bundle and a control bundle (to determine the degree of dessication) for each tree was fastened together and presented to the hares, upright, to mimic a shrub. Selection of twigs was done in such a way as to achieve optimal similiarity between the bundles.

Samples collected from beaver, hare and human activity consisted of white birch, which were either cut by beavers, mechanically clipped by pruning shears, or browsed upon by snowshoe hares. Every collection consisted of basal sprouts except for the lateral sprouts that had grown in response to browsing by snowshoe hare.

At the Wanup site, three different areas of white birch (diameter up to about 6cm) were chosen and enclosed using chicken wire fence. The fenced-in areas had been previously either severely browsed by snowshoe hare, or, as far as could be determined, had never been browsed at all by hares. The latter trees were fenced either following mechanical clipping with pruning shears or left untouched to be used as a control. Lastly, one area of heavy hare activity was left unfenced. The following winter, 1989-1990, bundles of twigs from each of the three fenced-in area and the unfenced area were prepared using the regrowth of each of the trees.

Chemical analysis

All samples were analysed for the extractable resin content following the method of Chapin *et al.* (1985). This ether-extractable fraction is a complex of waxes and secondary metabolites that have been shown to be repellent to mammalian herbivores (Bryant, 1981).

RESULTS AND DISCUSSION

Effect of insect herbivory

In the present study on insect herbivory, there was no significant difference ($P<0.05$) in consumption by snowshoe hare of the bundles of twigs prepared from trees that had been defoliated by forest tent caterpillar the previous summer, from the undefoliated controls (Fig 1). There was a significant ($P<0.05$) species difference, however with white birch being selected over trembling aspen irrespective of insect defoliation (Fig 1). It is assumed, therefore, that damage brought about by the forest tent caterpillar was confined to the tree foliage and not to the twigs. Other studies, however, seem to indicate that larvae grew poorly on foliage from trees defoliated in the previous year (Haukioja and Neuvonen, 1985). Samples of the twig bundles that remained following browsing were analyzed for resin content. The levels of resin were higher in the trembling aspen as compared to the white birch (Fig 1). There was no significant difference ($P<0.05$) between resin levels of the

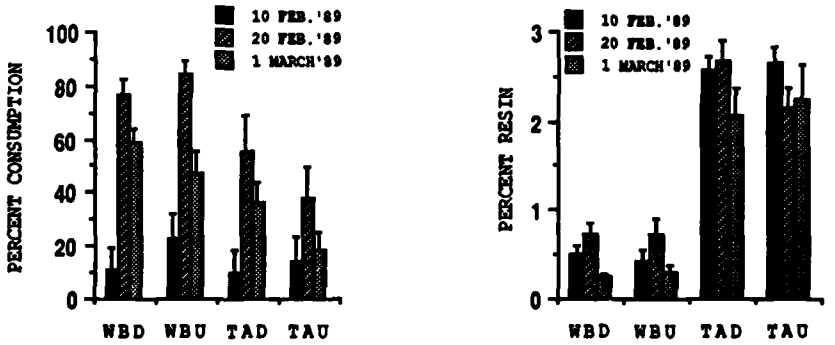

Fig. 1 Percent consumption (n=6) of, and percent resin (n=18) in, twig bundles of white birch and trembling aspen, whose leaves had been attacked by forest tent caterpillar. WBD=white birch defoliated; WBU=white birch undefoliated; TAD=trembling aspen defoliated; TAU=trembling aspen undefoliated

undefoliated and defoliated twigs of each respective study species. The weight loss of the control bundles owing to dessication was negligible. Levels of resin and the percentage of twigs eaten seem to indicate that as the level of resin rises, the degree of browsing decreases (Fig 1).

Effect of mammalian herbivory

Percent consumption was significantly different ($P<0.05$) for all categories of mammalian herbivory for the first two runs (March '89; Dec-Jan '90)(Fig 2). The difference was due to the hare browsed lateral sprouts which were totally consumed as compared to the other choices. The last run (Feb '90) showed no significant difference ($P<0.05$) for all categories (Fig 2). Resin levels for the first run was not significantly different ($P<0.05$) for basal sprouts produced from large beaver-cut stumps, lateral sprouts following hare browsing and the mechanically-clipped basal sprouts, but was different for the basal sprouts that initiated from small and medium sized beaver-cut stumps (Fig 2). Again, the percent consumption and the level of resin are in agreement with the experiment on insect herbivory in that twigs with elevated resin levels were less browsed. Control bundle weight loss owing to dessication was also negligible. Data for the second (Dec-Jan '90) and third (Feb '90) runs are as yet unavailable owing to analytical equipment failure.

In the mammalian herbivore study, beavers seem to react to palatability in a similar fashion to that of the snowshoe hare. Basey *et al.* (1988) state that when the juvenile form of aspen is uncommon in an area (ie. low levels of previous beaver activity) the beavers choose aspen by size following what is known as the optimal foraging model. On the other hand, when beavers are abundant they select large diameter trees that are more likely to have a low concentration of a specific phenolic compound. Thus in conducting this experiment, the sprouts presented to the hares had previously been rejected by beaver as being of low palatability (Fig 2). The data seem to indicate that there is a difference in taste preference because the hares browsed these twigs. The lateral sprouts from a hare-browsed tree were preferred by the hare and contained little resin (Fig 2). This finding indicates that the lateral sprouts do not have the same chemical defense strategy as the adventitious shoots which deter hares readily. The resin content determination of this same series of twigs is incomplete.

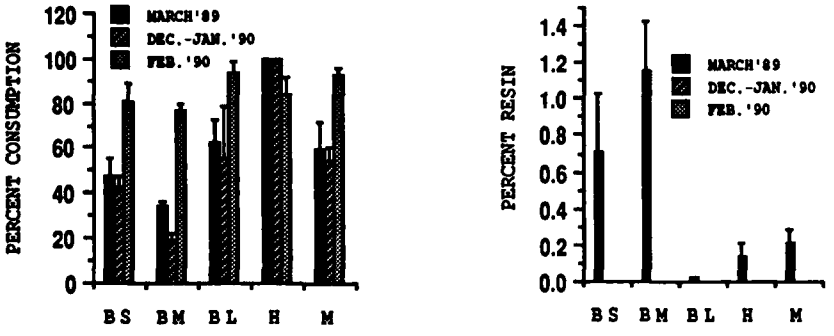

Fig. 2 Percent consumption (n=3) of, and percent resin (n=9) in, twig bundles of white birch previously browsed by beavers or hare or subjected to mechanical clipping. Basal sprouts from: BS=small, beaver browsed stump (<3cm); BM=medium, beaver browsed stump (3-5cm); BL=large, beaver browsed stump (>5-6cm); M=mechanically clipped trees; and Lateral sprouts from: H=hare browsed trees

Effect of browsing technique

Percent consumption differences were only detected between the unfenced trees (Hare) and the fenced control, and between the unfenced trees and the mechanically

clipped trees (Fig 3). Mechanical clipping does not affect palatability to the same extent as browsing by hares which indicates an allelochemic response in trees that have been naturally browsed. If this is true, the effect is long-lived because hare-browsed trees that were fenced in the spring of 1989 showed no difference in palatability from trees which hares had been able to browse as they wished (Fig 3). Further analysis of twig resin levels will be investigated to support the second and third hypotheses.

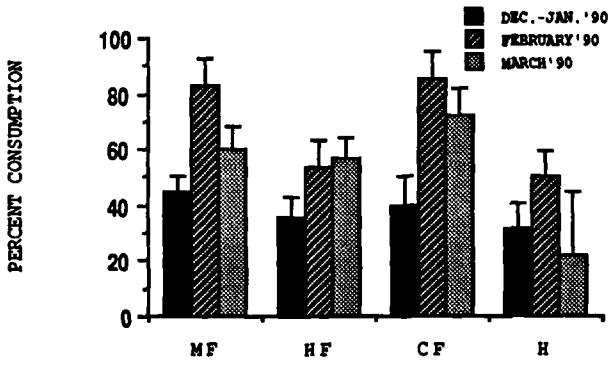

Fig. 3 Percent consumption by snowshoe hare of twig bundles of white birch (n=3). Fenced off: MF=mechanically clipped; HF=hare browsed; CF=control; Unfenced: H=hare browsed

CONCLUSIONS

Over the years the strong selection pressures imposed by populations of herbivores have affected the vegetation that forms part of their environment through many different mechanisms. Important factors include seasonal climatic conditions, the location of herbivore and plant, both spatially and temporally, and changes in the respective population densities. Plant species with their inherent genetic potential are subject to predictable, systematic and directional pressures from herbivores which participate with them "in a continual evolutionary dance" (Levin, 1976).

It is recognized that juvenile-form woody plants express traits associated with low palatability to browsing mammals (Schaffalitzky de Muckadell, 1962). It is also observed that herbivores such as the snowshoe hare do not feed on all different parts of a plant but only specific ones (Bryant *et al.*, 1983).

Hares clearly are able to select preferentially the browse that they eat both in terms of species and degree of palatability. The resin content in a given food species seems to play a critical role in the selection of browse by hares. Data collected support other reports in the literature; namely, that species that contain low levels of resin are preferred over those with high resin contents. Other mammalian and insect herbivores do not seem to affect hares directly but actually contribute (in the case of beaver) to an increase in browse availability. The effects of hare saliva on browsed twigs will be confirmed further after more resin analyses have been performed.

Snowshoe hares definitely play a vital role in the adaptive history of plant species and, in return, allelochemics allow for palatability levels to change. To ensure the survival of both snowshoe hares and the plants that they eat, this evolution is continuous.

ACKNOWLEDGEMENTS

The present study was funded through a grant from the Laurentian University Research Fund to supervisor G.M. Courtin and an Ontario Graduate Scholarship to the author. The assistance of R. Robitaille and B. Evans with preparation of the manuscript was much appreciated. I acknowledge gratefully the assistance of G.M. Courtin for his supervision of the research.

LITERATURE CITED

Basey, J.M., S.H. Jenkins and P.E. Busher. 1988. Optimal central-place foraging by beavers: tree-size selection in relation to defensive chemicals of quaking aspen. Oecologia 76:278-282.

Bider, J.R.. 1961. An ecological study of the hare *Lepus americanus*. Can. J. of Zool. 39:81-103.

Bryant, J.P.. 1981. Phytochemical deterrence of snowshoe hare browsing by adventitious shoots of four Alaskan trees. Science 213:889-890.

Bryant, J.P., G.D. Wieland, P.B. Reichardt, V.E. Lewis and M.C. McCarthy. 1983. Pinosylvin methyl ether deters snowshoe hare feeding on green alder. Science 222:1023-1025.

Chapin, F. Stuart III, J.P.Bryant and J.F.Fox. 1985. Lack of induced chemical defense in juvenile Alaskan woody plants in response to simulated browsing. Oecologia 67(4):457-459.

de Vos, A.. 1964. Food utilization of snowshoe hares on Manitoulin Island, Ontario. J. of For. 62:238-244.

Haukioja, E. and S.Neuvonen. 1985. Induced long-term resistance of birch foliage against defoliators: defensive or incidental? Ecology 66(4):1303-1308.

Levin, D.A.. 1976. The chemical defenses of plants to pathogens and herbivores. Ann. Rev. Ecol. Syst. 7:121-159.

Pianka, E.R.. 1983. Evolutionary Ecology 3rd ed.. Harper and Row Publ.. New York. 416 pp.

Reichardt, P.B., J.P. Bryant, T.P. Clausen and G.D. Wieland. 1984. Defence of winter-dormant Alaska paper birch against snowshoe haress. Oecologia 65:58-69.

Rhoades, D.F. 1985. Offensive-defensive interactions between herbivores and plants: their relevance in herbivore population dynamics and ecological theory. Am. Nat. 125(2):205-238.

Schaffalitzky de Muckadell, M. 1962. Environmental factors in developmental stages of trees. Pages 289-298 in T.T. Kozlowski, editor. Tree growth. Ronald, New York, New York, USA.

SNO-FOO AWARD

TO ERR IS HUMAN, TO FORGET IT WOULD BE DIVINE

This award is to be presented to an individual or group of individuals, for having committed or having been associated with an outstanding "blooper" during the year prior to the annual meeting.

To be considered for this award, the nominee must be a member in good standing of the Eastern Snow Conference.

This award is to be presented and accepted in a manner which is considered to be "in good taste." No one person or organization will be eligible to qualify for this award more than once. Nominations will be accepted by the ESC Equipment Committee. The decision of the committee is final.

SNO-FOO 1990—Kersi Davar

Kersi is certainly a good sport and a fine example of a teacher who is dedicated to work with our young men and women. It is not often that our group gets a wonderful chance to poke fun at one of our most respected members and mentors.

Professor Davar in his eagerness to attend our conference in Bangor, Maine, submitted a payment of two times the actual amount due. We were not privy to his mathematical wizardry or confusion, but we cannot excuse the error. However, his student went on to present the winning paper and won the coveted Wiesnet medal. This award may not be quite so coveted, but it certainly was a one-two punch for the University of New Brunswick. Kersi in his reckless generosity, placed the icing on the cake.

Please be advised that Professor Davar was so enthralled with the Sno-Foo Award and the trophy that he refused to return it to me for safekeeping until next year. Therefore, be it herewith known to all concerned that Professor Davar will return the trophy for its disposition to the next recipient. Enjoy and savor the trophy, Kersi.

Stan Zeccolo